A Novel Fibre Composite System to Investigate Tenocyte Metabolism Under Physiological and Pathological Loading Conditions.

Dharmesh Patel

Submitted in partial fulfilment of the requirements of the Degree of Doctor of Philosophy

Supervisor: Dr Hazel Screen

Queen Mary, University of London
School of Engineering and Materials Science

December 2015

An Arthritis Research UK supported project

Statement of Originality

I, Dharmesh Patel, confirm that the research included within this thesis is my own work or that where it has been carried out in collaboration with, or supported by others, that this is duly acknowledged below and my contribution indicated. Previously published material is also acknowledged below.

I attest that I have exercised reasonable care to ensure that the work is original, and does not to the best of my knowledge break any UK law, infringe any third party's copyright or other Intellectual Property Right, or contain any confidential material.

I accept that the College has the right to use plagiarism detection software to check the electronic version of the thesis.

I confirm that this thesis has not been previously submitted for the award of a degree by this or any other university.

Signature: D. Patel

Date: 07/12/2015

Acknowledgments

I would like to thank my supervisor, Hazel Screen, for her guidance and faith in my abilities. I could not have asked for a more dedicated supervisor, whose support has allowed me to develop as a researcher. Her enthusiasm, depth of knowledge and ability to stay on top of things despite her busy schedule never ceases to amaze me. She is an inspiration.

I would also like to thank Arthritis Research UK for funding this research project and thank all the collaborators involved. Thank you Graham Riley and Eleanor Jones, University of East Anglia, UK, for your guidance and assistance in performing gene expression analysis. Thank you Stephanie Bryant, University of Colorado Boulder, USA, for allowing me to visit and use your facilities, and thank you to all your graduate students for making me feel welcome during my time there.

I would also like to acknowledge all my friends and colleagues at Queen Mary, University of London, who made every day at Queen Mary an enjoyable experience. I would particularly like to thank Mahentha Krishnamoorthy for her constant encouragement and lending an ear during those hard times in the project. A big thank you also goes to all my friends not at Queen Mary, who have been understanding and supportive during my absence in the world outside the PhD, thank you for keeping me sane!

Finally I would like to dedicate this thesis to my mother for her constant love and support. I am forever grateful.

ABSTRACT

Tendons are crucial for locomotion, transferring forces from muscle to bone. They are subjected to high forces, and possess highly specialised hierarchical structures to function efficiently. Tendinopathies are debilitating tendon disorders common in both athletes and non-athletes. The unclear aetiology of tendinopathies has led to limited, generalised treatment, with poor regenerative outcomes for patients. Tendinopathies are thought to be instigated by changes in the local cellular environment, with tendon overuse generating matrix microdamage, which increases cellular shear. Shear is potentially an important mechanotransduction cue, but no mechanism is available to investigate this directly.

To address this need, a fibre composite system based on polyethylene glycol (PEG) was developed, consisting of cell seeded PEG-peptide fibres encapsulated in a PEG matrix. Composites were developed to mimic the cell mechanical environment in tendons, creating shear-tension ratios equivalent to those seen physiologically (40% of applied strain transferred to the fibres; the remaining 60% as fibre shearing within the matrix). High shear-low tension (~25% tension, ~75% shear) and low shear-high tension (~60% tension, ~40% shear) environments were also developed to investigate non-physiological conditions.

Broad spectrum gene expression analysis was performed to determine how different shear-tension ratios affect the behaviour of tenocytes derived from healthy and tendinopathic human tendons. Tendinopathic tenocytes appeared more mechano-sensitive than healthy tenocytes (shear-tension mediated changes in versican, IL-8, TIMP-3, MMP-3 and MMP-13 expression) and showed a distinct basal profile similar to that observed in tendinopathic tissue (lower MMP-3 and higher MMP-13 expression). Further investigation with bovine tenocytes found changing the cell attachment peptide in fibres from RGD to DGEA increased the sensitivity of tenocytes to the local shear-tension environment (shear-mediated changes in scleraxis, MMP-2 and COL-3 expression). This suggests tenocytes are more responsive when attached to collagen-like materials, and consequently that specific integrins are involved in sensing the local shear-tension environment.

Table of Contents

List of Tables

List of Figures

List of Abbreviations

18S	18S Ribosomal Ribonucleic Acid
ACAN	Aggrecan
ADAM	A Disintegrin and Metalloproteinase
ADAMTS	A Disintegrin and Metalloproteinase with Thrombospondin Motifs
AMCA	7-aminocoumarin
ANOVA	Analysis of Variance
BFGF	Basic Fibroblast Growth Factor
BGN	Biglycan
BSA	Bovine serum albumin
CDET	Common digital extensor tendon
CDI	1-1'-Carbonyl Diimidazole
cDNA	copy-Deoxyribonucleic Acid
COL-11A1	Collagen Type XI, Alpha 1
COL-12A1	Collagen Type XII, Alpha 1
COL-14A1	Collagen Type XIV, Alpha 1
COL-1A1	Collagen Type I, Alpha 1
COL-2A1	Collagen Type II, Alpha 1
COL-3A1	Collagen Type III, Alpha 1
COL-4A1	Collagen Type IV, Alpha 1
COL-5A1	Collagen Type V, Alpha 1
COL-6A1	Collagen Type VI, Alpha 1
COL-9A1	Collagen Type IX, Alpha 1

COMP	Cartilage Oligomeric Matrix Protein
COX-2	Cyclooxygenase-2
CS	Chondroitin Sulphate
DAPI	4',6-diamidino-2-phenylindole
DCN	Decorin
DEPC	Diethylpyrocarbonate
DET	Digital extensor tendon
DGEA	Aspartic Acid-Glycine-Glutamic Acid-Alanine
DI	Deionized
DMEM	Dulbecco's Modified Eagle Medium
DMEM-G	Dulbecco's Modified Eagle Medium with GlutaMAX
DMSO	Dimethyl Sulfoxide
DNA	Deoxyribonucleic Acid
DS	Dermatan Sulphate
DSC	N,N'-Dissucinimidyl Carbonate
ECM	Extracellular Matrix
EGF	Epidermal Growth Factor
FACIT	Fibril associated collagen with interrupted triple helices
FAM	Carboxyfluorescein
FBS	Fetal Bovine Serum
FITC	Fluorescein isothiocyanate
FMOD	Fibromodulin
FN-1	Fibronectin
GAG	Glycosaminoglycan
GAPDH	Glyceraldehyde 3-phosphate dehydrogenase

GFOGER	Glycine-Phenylalanine-Hydroxyproline-Glycine-Glutamic Acid-Arginine
HEPES	4-(2-hydroxyethyl)-1-piperazineethanesulfonic acid
IFM	Interfascicular Matrix
IGF	Insulin-like Growth Factor
IGFBP	Insulin-like Growth Factor-Binding Protein
IL	Interleukin
iNOS	Inducible Nitric Oxide Synthase
ITGA	Integrin Alpha
KS	Keratan Sulphate
LAMA-1	Laminin
MA	Methacrylic Anhydride
MACIT	Membrane associated collagen with interrupted triple helices
MMP	Matrix Metalloproteinase
MOPS	3-(N-morpholino)propanesulfonic acid
Multiplexin	Multiple triple helix domain and interruptions
MW	Molecular Weight
NHS	N-Hydroxysuccinimide
NMR	Nuclear Magnetic Resonance
NOS	Nitric Oxide Synthase
NTC	Non-template Control
OPA	O-Phthalaldehyde
PBS	Phosphate buffered saline
PCR	Polymerase Chain Reaction
PDGF	Platelet Derived Growth Factor

PDMS	Polydimethylsiloxane
PEG	poly(ethylene glycol)
PEGDM	Poly(ethylene glycol dimethacrylate)
PEO	poly(ethylene oxide)
PG	Proteoglycans
PGA	Polyglycolic acid
PHEMA	poly(2-hydroxyethyl methacrylate)
PI	Photoinitiator
PICP	Procollagen I C-terminal Propeptide
PLA	Polylactic acid
PLGA	Poly(lactic-co-glycolic acid)
PRG-4	Proteoglycan 4, also known as Lubricin
PTT	Posterior Tibialis Tendon
RER	Rough Endoplasmic Reticulum
RGD	Arginine-Glycine-Aspartic Acid
RNA	Ribonucleic Acid
RT	Room temperature (~20°C)
RT-qPCR	Real Time Quantitative Reverse Transcription Polymerase Chain Reaction
SCS	Standard Curve Stock
SCX	Scleraxis
SDFT	Superficial digital flexor tendon
SEM	Scanning Electron Microscopy
TAMRA	Carboxytetramethyl Rhodamine
TEGDM	Tetraethylene glycol dimethacrylate

TGFβ	Transforming Growth Factor Beta
TIMP	Tissue Inhibitor of Metalloproteinase
TLDA	TaqMan Low Density Array
TND	Tenomodulin
TNF-α	Tumor Necrosis Factor Alpha
TOP-1	Topoisomerase
TSC	Tendon Progenitor Stem Cell
Tukey's HSD	Tukey's Honest Significant Difference
UTS	Ultimate tensile strength
UV	Ultra Violet
VCAN	Versican
YRGDS	Tyrosine-Arginine-Glycine-Aspartic Acid-Serine

Chapter 1: Literature Review

1.1 Tendon Composition and Structure

Tendons play a key role in the locomotion; they function to transmit forces from muscle to bone allowing the production of movement about joints. Consequently tendons are used in everyday activities, being exerted more so in athletic sports where high forces are generated frequently. Tendons are able to function under these high tensile loads due to a specialised hierarchical structure which also contributes to a unique cellular environment.

Tendons are essentially comprised of collagen, proteoglycans, cells and water, with water contributing ~70% of weight in a human tendon (Elliott, 1965). Collagen provides 75-90% of the total tendon dry weight (Bernard-Beaubois et al., 1997; Kjaer, 2004; Schulze-Tanzil et al., 2004) and more than 95% of the collagen present in tendons is type I (other types include III, V, VI, IX and XI). Other proteins present include fibronectin and elastin, with the latter being 1-2% of the total dry weight (Elliott, 1965; O'Brien, 1997).

The hierarchical structure of tendons is summarised in Figure 1. At the nano-scale, collagen is comprised of three polypeptide α-chains of repeating Glycine-X-Y units (where X and Y are usually amino acids proline and hydroxyproline) intertwined into a triple helix, creating collagen molecules approximately 300nm in length. Closely packed collagen molecules overlap and form inter-molecular crosslinks at the C terminus of one molecule and N terminus of the other, with the assembled structure known as collagen fibrils. This method of crosslinking also creates a staggered arrangement of the molecules which results in collagen fibrils having visible microscopic bands every 67nm (D-periodicity of 67nm) (Baselt et al., 1993; Jozsa and Kannus,

1997; Kadler et al., 1996; Kannus, 2000; Silver et al., 2003). This forms the basic structural unit of collagen found in tissues.

The terminology for the higher structural levels of the tendon hierarchy varies through literature. For this review, multiple collagen fibrils aligned parallel and grouped together are termed collagen fibres, primary bundles of fibres are referred to as subfascicles, secondary fibre bundles are termed fascicles and finally tertiary fibre bundles are called fascicle bundles (Figure 1). In human tendons, the diameter of subfascicles range from 15µm to 400 µm while fascicles vary from 150µm to 1000µm, both depending on the type of tendon (Jozsa and Kannus, 1997; Silver et al., 2003).

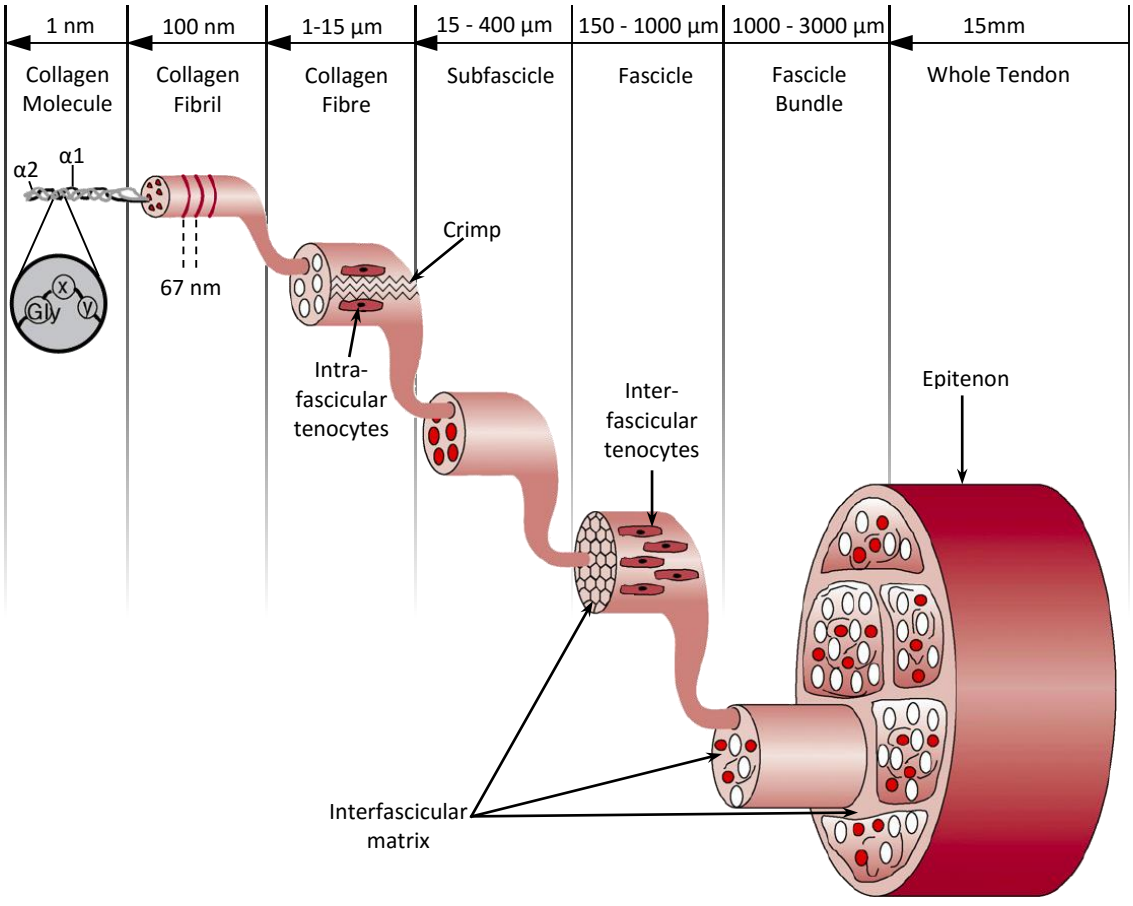

Figure 1: Hierarchical structure of a typical tendon starting from the repeating amino acid chain up to the macroscopic tendon unit. (Image adapted from Liu et al. (2008) and information collated from Franchi et al. (2007b); Jozsa and Kannus (1997); Silver et al. (2003)).

The orientation of collagen fibres allows efficient transmission of force, and as such fibres have been seen to exhibit a number of arrangements in different tendons to optimise mechanics. In most tendons collagen is predominantly aligned parallel to the axis of loading (Jozsa and Kannus, 1997; Kannus, 2000). Collagen fibres also display structures known as crimps which are visible as jagged sinusoidal like patterns extending along the length of fascicles (Figure 2). Crimps are thought to be a result of the tertiary structure of collagen fibres, possibly being maintained by the presence of elastin fibres, and exhibit a periodicity of 10-100µm (Freed and Doehring, 2005). The degree of crimping also differs from tendon to tendon with studies suggesting crimp angle could be dependent on the amount of tensile load the tendon has to bear (Jarvinen et al., 2004). A structural study by Magnusson et al. (2002) found that the angle of crimps in human Achilles tendons, both intact and ruptured, were between 35° to 37°. Ultrastructure analysis of collagen fibril crimping have shown that fibrils possess a left handed helical twist termed fibrillar crimps (Figure 2A) (Franchi et al., 2007a; Franchi et al., 2010).

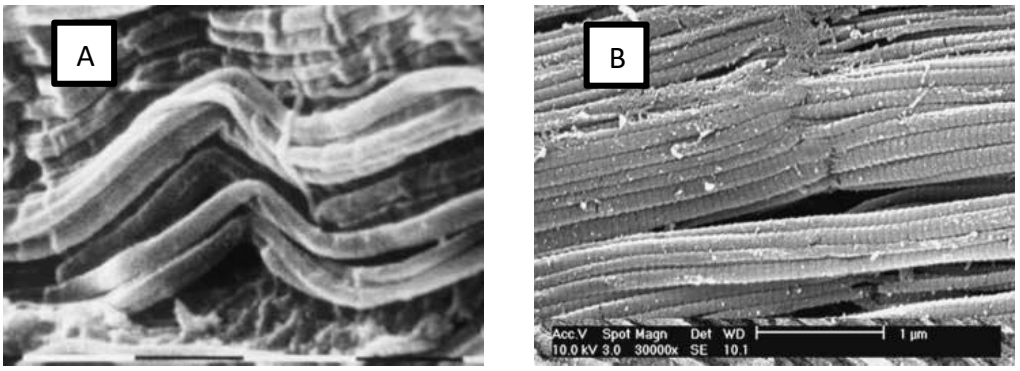

Figure 2: Scanning electron microscopy (SEM) of collagen fibril crimp structures in rat Achilles tendons. A) Relaxed tendon sectioned longitudinally showing both crimp pattern and fibrillar crimps. B) Stretched tendon showing straightened fibrils. Scale bar = 1 µm (Franchi et al., 2007a).

The high viscosity of tendon extracellular matrix (ECM) is thought to be primarily due to the proteoglycan (PG) content. PGs surround collagen fibrils and fibres, providing structural support, lubrication and spacing of collagen fibres which is essential for gliding and cross-tissue interactions (Sharma and Maffulli, 2005). Gliding at fascicle and intra-fascicle levels allows

contour flexibility and transmission of tension when tendons move over joints with varying angles of inclination (Benjamin et al., 2008). PGs present in tendons include small-leucine rich proteoglycans (SLRPs) decorin, biglycan, lumican and fibromodulin, along with larger PGs lubricin, aggrecan and versican. Common proteoglycans found in tendons and their roles are summarised in Table 1. Decorin, biglycan, fibromodulin and lumican have all been associated with the regulation of collagen type I fibrillogenesis (Birk et al., 1995; Dunkman et al., 2013; Jepsen et al., 2002; Schonherr, 1995; Yoon and Halper, 2005). The binding of SLRPs, such as decorin, to collagen fibrils has also been suggested as a mechanism for transferring stress between fibres, as the glycosaminoglycan (GAG) side chains of decorin are known to connect from one decorin molecule to another on an adjacent collagen fibril (Reese et al., 2013). Models have consequently proposed that tendon overload results in the breakage of connecting GAG chains and thus altered tendon mechanics (Redaelli et al., 2003; Vesentini et al., 2005).

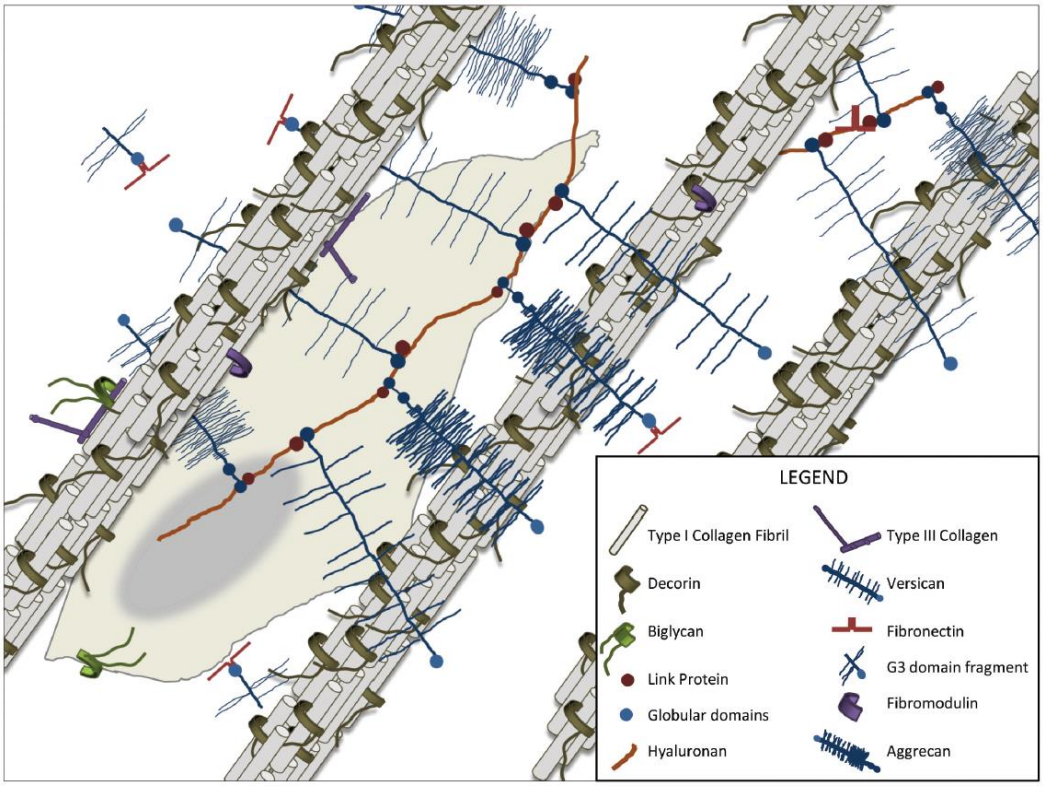

Figure 3: Schematic of collagen type I fibril, proteoglycan and other matrix protein interaction in tendons (Parkinson et al., 2011).

The content and distribution of ECM components has recently been shown to differ through the levels of the tendon hierarchy. For example, the inter-fascicular matrix (IFM), which is the ECM between fascicles, has been noted to contain specific localised components such as elastin, lubricin and versican (Thorpe et al., 2013a), with lubricin being particularly localised to the interface between collagen fibre bundles and the ECM (Sun et al., 2006).

Table 1: Summary of PG structures and functions relevant in tendons. CS = chondroitin sulfate, DS = dermatan sulfate, KS = Keratan sulfate. (Information adapted from (Yoon and Halper, 2005) with added content as indicated).

Name	Core Protein Size (kDa)	GAG Chain type	Location in Tendons	Suggested Roles
Decorin	36[1]	CS/DS[1]	Bound to fibrillar collagen. Also binds to TGFβ and EGFR[1].	Inhibits collagen fibrillogenesis[1], stress transfer between fibres[2].
Biglycan	38[1]	CS/DS[1]	Bound to fibrillar collagen. Not found in avian species[1].	Involved in fibrillogenesis[1].
Fibromodulin	42[1]	KS[1]	Bound to fibrillar collagen[1].	Facilitates collagen fibril maturation[1].
Lumican	38[1]	KS[1]	Bound to fibrillar collagen[1].	Inhibits size of collagen fibrils[1].
Lubricin	117-150[3,4]	CS/KS[5,6]	Found on the tendon surface, surrounding collagen bundles and localised to the IFM[5,6,7,8].	Lubrication - reduces friction coefficient[5,6,7].
Aggrecan	220[1]	CS/KS[1]	Linked to hyaluronan. Low levels found in tensional parts of tendon and high levels in compressed regions[1].	Provides structural support[1].
Versican	265-370[1]	CS/DS[1]	Linked to hyaluronan. Low levels found in tensional parts of tendons and slightly higher levels in compressed regions. Localised to the IFM[8,9].	Provides structural support[1].

1) Iozzo and Murdoch (1996), 2) Reese et al. (2013), 3) Abubacker et al. (2013), 4) Steele et al. (2013), 5) Juneja and Veillette (2013), 6) Schumacher et al. (1994), 7) Sun et al. (2006), 8) Thorpe et al. (2013a), 9) Reese et al. (2013).

Specialised cells found in tendons are known as tenocytes and contribute approximately 90-95% of the cellular elements, with the remainder including chondrocytes, synovial cells and vascular cells (Jozsa and Kannus, 1997). Tenocytes are situated on the surface of collagen fibres, leading to their arrangement in rows parallel to the fibres. Tenocytes are also situated between fascicles in the IFM. These interfascicular tenocytes are more prolific and have a rounder morphology compared to intrafascicular tenocytes. There is currently significant interest in their phenotype and potential role in tendon homeostasis (Clegg et al., 2007; Richardson et al., 2007; Spiesz et al., 2015; Thorpe et al., 2015a). Tendon progenitor stem cells (TSCs) have also been suggested to reside in tendons, with studies identifying populations in rabbit, mouse and human tendon tissue (Bi et al., 2007; de Mos et al., 2007; Zhang and Wang, 2010a; Zhang and Wang, 2013; Zhang and Wang, 2010b). Characterisation of tenocytes has found intracellular type I, III and V collagen within the cytoplasm, with type I collagen preferentially distributed around the nuclei. Type III collagen was also found distributed closer to the cell membrane and type V found in a fibrillary and vesicular form (Figure 4) (Gungormus and Kolankaya, 2008).

Tendons typically appear white due to the low degree of vascularisation but they contain small thin-walled blood vessels. Some tendons, particularly those around bony prominences, are also known to have entirely avascular regions (Benjamin et al., 2008). Fibrous and synovial sheaths surround tendons, particularly those of the hand and feet, providing a friction reducing tunnel, to improve function over curved or longer distances. This is alternatively achieved (to a lesser degree) via a loose layer of connective tissue, often referred to as the paratenon, on tendons such as the Achilles tendon, where distinct synovial sheaths are not present (Jozsa and Kannus, 1997).

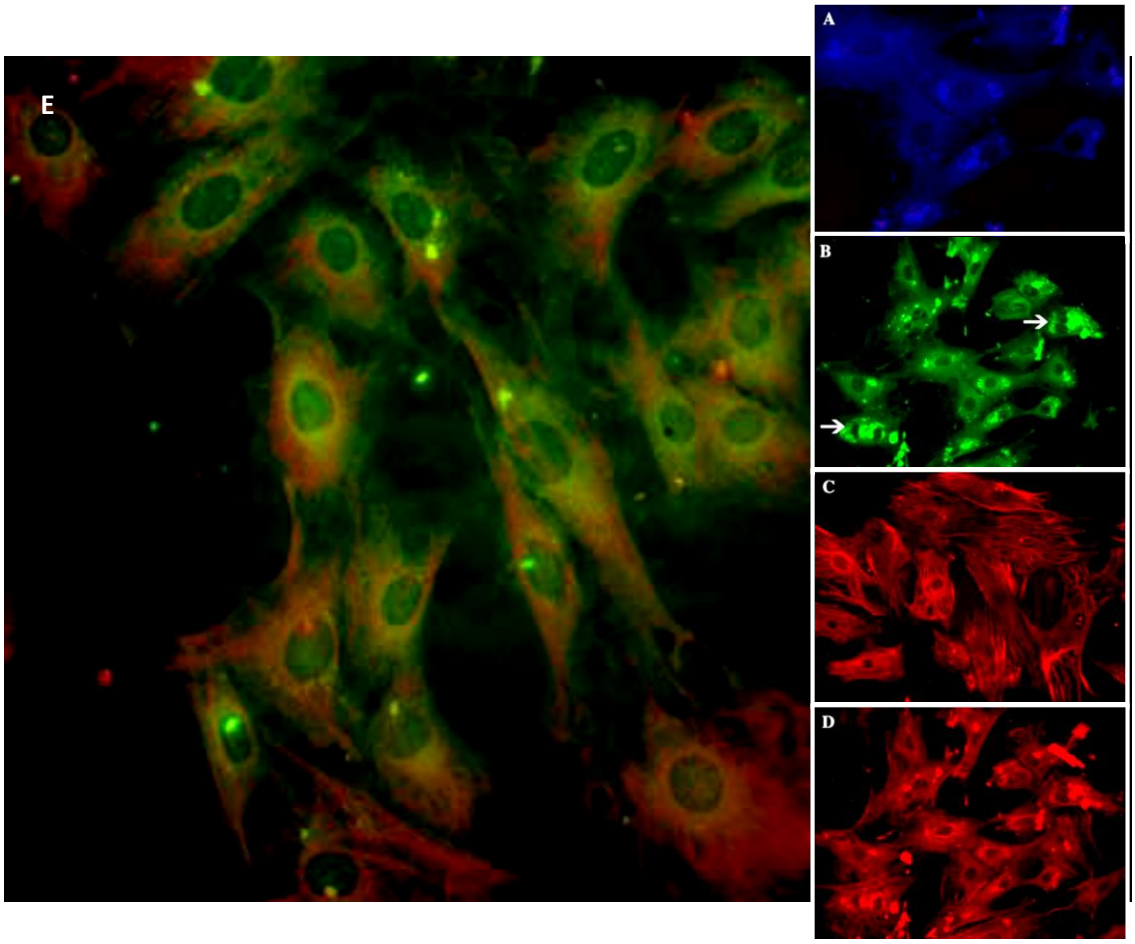

Figure 4: Tri-colour immunofluorescence images of rat Achilles tenocytes in a high density culture system; A) collagen type I, B) collagen type III, C) collagen type V (fibrillar) and D) collagen type V (vesicular) antibody stained tenocytes after 3 weeks in a high density culture system (x80 magnification). E) Composite immunofluorescence image of tenocytes incubated for 7 weeks (4 weeks in monolayer and 3 weeks in a high density culture system) which showed positive staining for type I (blue, AMCA), type III (green, FITC) and type V collagen molecules (red, Texas Red fluorochrome) (x120 magnification). White arrows in B) indicate brighter collagen type III staining in tenocytes which are proliferating. (Adapted from Gungormus and Kolankaya (2008)).

1.2 Function and Properties

The tendon matrix, arranged in multiple hierarchical levels, provides a versatile structure allowing tendons to optimise their mechanics to function effectively. The strains tendons are exposed to varies, depending on functional demand and location. Two general categories exist to describe tendons based on their function; positional tendons which function to transmit forces from muscle to bone, and energy storing tendons which in addition to transferring forces, also store and release energy during locomotion to improve efficiency (Birch, 2007; Lichtwark and Wilson, 2005).

The presence of PGs within tendon IFM and fascicular matrix contributes towards the viscoelastic properties of tendons; PGs are hydrophilic and also form bonds between collagen fibrils both longitudinally and transversely (Cribb and Scott, 1995). The exact mechanism providing tendons with the ability to stretch and recover large strains is unclear. Energy storing tendons can stretch further than others, and also appear to recoil more elastically, returning over 90% of the energy they store (Benjamin et al., 2008). The content of elastin is low at 1-2% of the dry mass of tendons, thus the aforementioned properties are a result of multiple interactions. Figure 5 shows the typical stress-strain curve of a tendon when stretched, with characteristic regions demonstrating the complexity of tendon extensibility. The first distinct feature is a toe region associated with crimps. Crimp structures are seen to straighten when load is initially applied and can revert back to the original crimped state upon the removal of load. Due to the number of crimps present in a tendon and their angles, the accumulation of their small reversible extensions generates a significant effect, requiring strains of up to 1.8% to fully straighten (Franchi et al., 2007a; Sasaki and Odajima, 1996a; Screen et al., 2003). The straightening and alignment of fibres along with fascicle rotation also contribute to this toe region (Screen et al., 2003; Thorpe et al., 2013b). The resulting non-linear extension results in high strains with low loads, hence the toe region allows deformation with limited direct collagen

loading, ensuring minimal fibrous tissue damage and also functioning to facilitate shock absorbance (Franchi et al., 2007a).

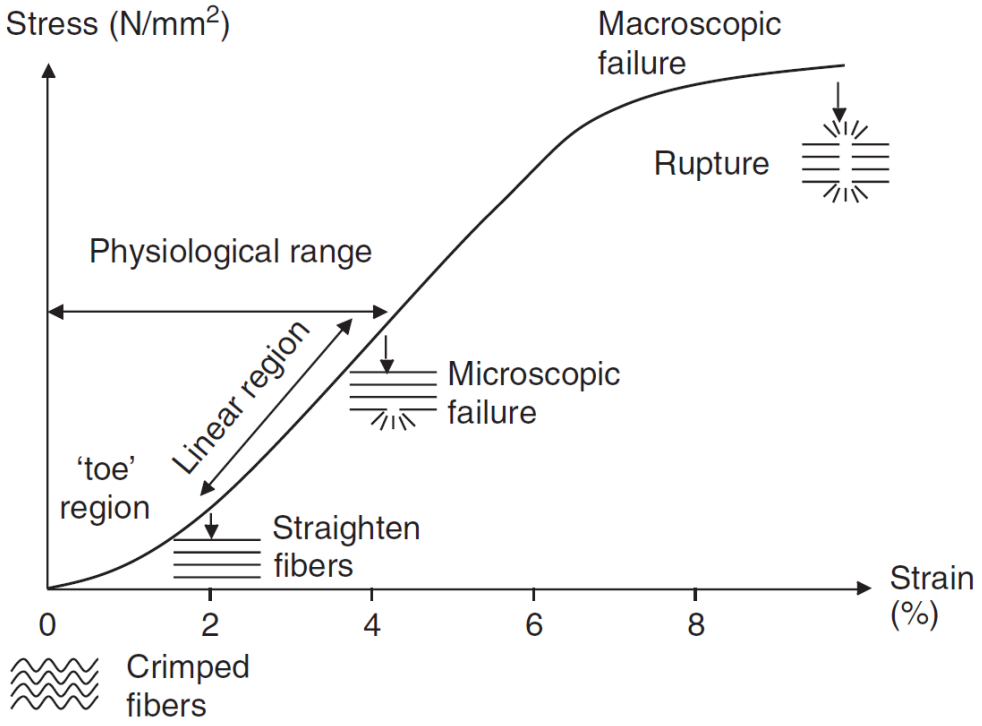

Figure 5: Typical tendon stress-strain curve showing an initial toe region where crimp straightening and fibre alignment occur, then a broadly linear region consisting of fibre extension, fibre sliding and fascicle sliding, followed by microdamage and eventually tendon rupture. (Adapted from Wang (2006)).

Once crimps have straightened and fibres have aligned, further load application results in a quasi-linear region of stress and strain. The collagen fibres within tendons have been observed to stretch, however the extent of fibre extension is seen to be less than that of the whole tendon (Fratzl et al., 1997; Rigozzi et al., 2013; Sasaki and Odajima, 1996a; Shepherd et al., 2014; Thorpe et al., 2013c). Physiologically, the fibres in tendon are seen to stretch by approximately 40% of the applied strain (Shepherd et al., 2014). Consequently, the extensibility of tendons past the toe region is due to a combination of fibre extension, fibre sliding (Figure 6) and fascicle sliding facilitated by the IFM (Cheng and Screen, 2007; Screen et al., 2003; Thorpe et al., 2015b). Even further application of load past the linear region surpasses the tendons extensibility mechanisms and results in microdamage of fibres and eventually complete tendon rupture.

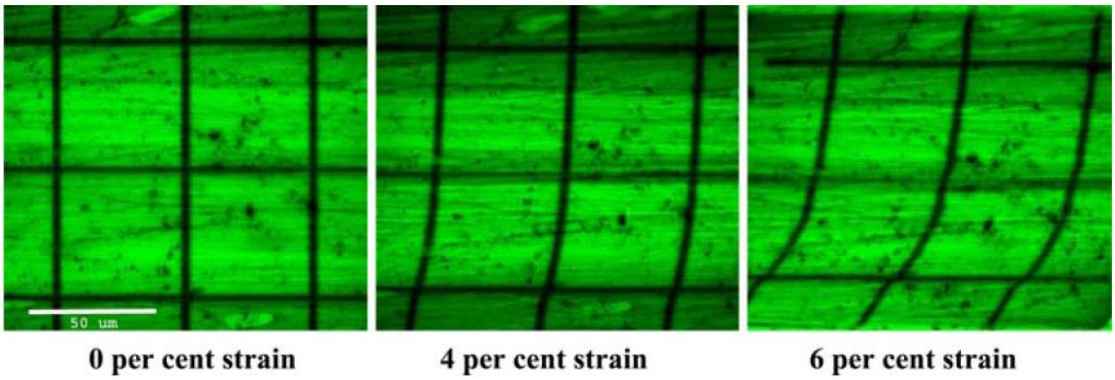

Figure 6: Wistar rat tail tendons stained with a strain grid and then stretched under a confocal microscope using a specialised strain rig. Images show grid distortion under increasing strains, indicating fibre sliding (adapted from Cheng and Screen, 2007).

Due to their function, energy storing tendons often experience high strains. For example, the human Achilles tendon is an energy storing tendon which sees average peak strains up to 4.6% whilst walking, 5.8% when running and 8.3% during one-legged hopping (Lichtwark and Wilson, 2005; Lichtwark and Wilson, 2006). Similarly, the equine superficial digital flexor tendon (SDFT) experiences strains of up to 16% during galloping (Dowling et al., 2000). Comparison of the equine SDFT and positional common digital extensor tendon (CDET) found the capacity for fascicle sliding was greater in energy storing tendons. This has been attributed to differences in the IFM, with energy storing tendons possessing specialised IFM to provide greater extensibility (Thorpe et al., 2012). The fascicles within the SDFT tendon have also been observed to exhibit a helical substructure (Figure 7), which is absent in the CDET, suggesting more efficient energy storage in the SDFT through a spring-like mechanism (Thorpe et al., 2013b; Thorpe et al., 2014). Consequently, energy storing tendons are more elastic than positional tendons and have a higher fatigue resistance to function efficiently at larger strains (Thorpe et al., 2015b). The combination of the described mechanisms to allow tendon extensibility, in both energy storing and positional tendons, result in a complex intra-tendon environment during loading, consisting of both tension and shear.

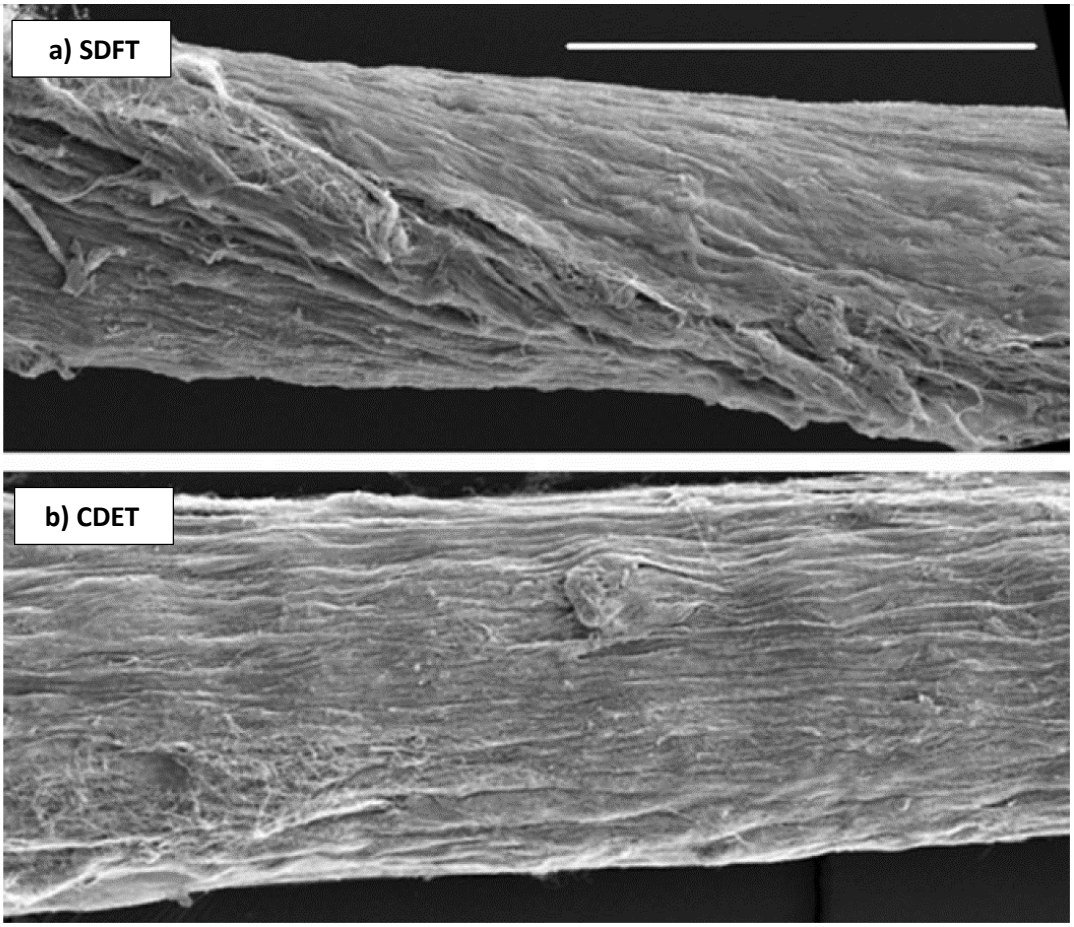

Figure 7: Scanning electron microscope image of a) an equine energy storing tendon, SDFT, and b) an equine positional tendon, CDET. Scale bar = 200 µm. A helical substructure is observed in the SDFT fascicle which is absent in the CDET fascicle. This structure is consequently implicated as a specialisation of energy storing tendons, acting as a spring-like mechanism to store energy. (Adapted from Thorpe et al. (2015c)).

The stiffness of tendons varies depending on location, age and physical activity, for example the equine energy storing tendon SDFT has been seen to be less stiff than the positional CDET (Thorpe et al., 2012). The Young's modulus of the tendon associated with the medial gastrocnemius muscle in humans has been found to be between 0.28-1.16 GPa *in vivo* (Kubo et al., 2002; Maganaris and Paul, 2002), while the human Achilles has a modulus between 0.67-1.07 GPa *in vivo* (Lichtwark and Wilson, 2005), and the human patellar tendon a modulus of 2GPa *in vitro* (Svensson et al., 2012). Svensson et al. (2012) also characterised the modulus of isolated collagen fibrils, finding a value of 2.8GPa. The modulus of tendon derived individual collagen molecules has been seen to range from 3-9 GPa (Sasaki and Odajima, 1996b).

Therefore the tendon hierarchy can be seen to be a compromise between the mechanical properties of collagen and the flexibility and extensibility needed to function efficiently at a given anatomical location. Ageing has been associated with changes in tendon properties; the bulk properties of equine tendons and their fascicles remained unchanged with increasing age, however the stiffness of the IFM increased with ageing, accompanied by reduced fascicle sliding (Thorpe et al., 2013c). Consequently, it has been proposed that ageing alters the extensibility mechanisms in tendons, with increased IFM stiffness resulting in less fascicle sliding and more fascicle extension. This higher strain transfer to fascicles could subsequently increase the risk of microdamage, potentially predisposing older tendons to injury (Thorpe et al., 2015c; Thorpe et al., 2013c).

1.3 Tendinopathy

The term tendinopathy is used to cover a range of tendon injuries, including those referred to as tendinitis (pain accompanied with inflammation) and tendinosis (pain without inflammation). Sporting activities generate high forces repeatedly and therefore it is not surprising that the yearly incidence of tendinopathies in sports are high; of all Achilles tendinopathies 24-64% are seen in runners, 23% of adolescent basketball players see patellar tendinopathy and 69% of young elite swimmers have supraspinatus tendinopathy (Cook et al., 2000; Sein et al., 2010; Sorensen et al., 2007; Woo et al., 2007). However, tendinopathies are not isolated to sporting activities, as a sample of the general Dutch population has shown a 2.35% incidence of Achilles tendinopathy in an entirely sedentary population, and rotator cuff tendinopathies, especially the supraspinatus, are common in the elderly (de Jonge et al., 2011; Woo et al., 2007).

There are many factors associated with tendinopathy, both intrinsic and extrinsic. Intrinsic factors include age, gender, anatomical variations, biomechanics and systemic diseases, while extrinsic factors include profession, sports, training errors, repetitive physical load and abnormal movement (Rees et al., 2006; Riley, 2004; Seitz et al., 2011).

The causes and mechanisms behind tendinopathies are not fully understood, with the role of inflammation often debated and tendon overuse usually attributed as a primary factor (Arnoczky et al., 2007; Arnoczky et al., 2002b; Dakin et al., 2014; Fredberg and Stengaard-Pedersen, 2008; Fung et al., 2010; Khan et al., 1999; Rees et al., 2013). Tendon overuse can lead to microdamage throughout the matrix, disrupting the matrix organisation and changing cell-matrix interactions. The disrupted tendon matrix is theorised by some to cause under stimulation of tenocytes, with studies showing increased collagenase expression when cells are stress deprived (Arnoczky et al., 2007). On the other hand some researchers think over-stimulation is a factor instead; an *in vitro* study by Zhang and Wang (2010b) found cells within

tendons changed their phenotype when stretched, differentiating towards adipocytes, chondrocytes and osteoblasts, whereas lower strain percentages maintained the tenocyte phenotype (Zhang and Wang, 2010b). In both cases the altered interactions are said to eventually contribute to further tendon degradation.

Although the aetiology is unclear and debated, most researchers agree tendinopathies are a degenerative pathological process, usually thought to be a failed response in tendon healing (Arnoczky et al., 2007; Cook et al., 2004; Magnan et al., 2014; Reinking, 2012; Scott and Bahr, 2009; Shearn et al., 2011).

1.3.1 Tendinopathy Features and Changes

Painful human tendons show a number of abnormal signs, such as increased cellularity, rounded cells, disrupted fibrillar structure and reduced preferential cell orientation (Figure 8), while ruptured tendons generally show reduced cellularity and loss of fibrillar structure (Busch et al., 2013; Jones et al., 2006). Characterisation of ruptured Achilles tendons have found the tissue to be more severely degenerated than tendinopathic Achilles tendons, implying that tendinopathies may increase the susceptibility to further tendon injury (Tallon et al., 2001b).

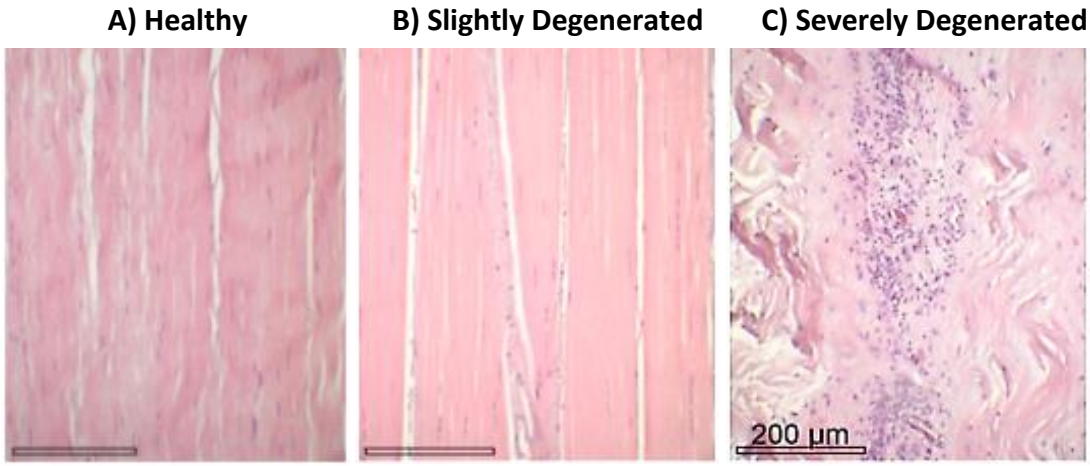

Figure 8: Comparison of healthy (A), slightly (B) and severely degenerated (C) human finger tendon after haematoxylin and eosin staining. Collagen fibres are stained pink and cells are stained violet. Slightly degenerated tendon (B) looks similar to healthy tendon (A), with minor differences such as looser tissue surrounding fascicles in the slightly degenerated tendon. Severely degenerated tendon (C) exhibits more significant changes such as irregular collagen arrangement, high cellularity and neovascularisation. (Adapted from Busch et al. (2013)).

Hyper cellularity and increased vascularisation have been used to identify tendinopathic tissue (Fu et al., 2002; Khan et al., 1999), with the equivalent of 3 weeks overuse exercise exhibiting these changes in *in vivo* models (Andersson et al., 2011). Interestingly, the same *in vivo* model also found endogenous neuropeptide production increased after 1 week of overuse activity, indicating that neuropeptide production precedes tendon damage and proposing a link with tendinopathy (Backman et al., 2011). Neurovascularisation was also seen to occur in damaged or ruptured tendons, which then disappeared with healing, suggesting the neuropeptides produced were directed towards the neurovascularised sites. Acetylcholine, another neuron associated substance, has been shown to increase tenocyte proliferation upon addition to culture, while the tenocytes themselves were found to produce and release enzymes associated with acetylcholine synthesis (Fong et al., 2013).

Comparison of healthy and tendinopathic tendons has found that diseased tendons exhibit increased PG content (Riley, 2008), with the pathological posterior tibialis tendon (PTT) showing higher collagen type I, collagen type III, aggrecan, biglycan, MMP-2 and MMP-13 and reduced MMP-3 and ADAMTS-5 gene expression compared with healthy PTT (Corps et al., 2012). The ratio of collagen type III to collagen type I has also been shown to increase when characterised in injured rotator cuff tendons (Riley et al., 1994b). ADAMTS-4 gene expression is higher in ruptured Achilles tendon (Corps et al., 2008) as is decorin expression, while painful Achilles tendons have shown a significant increase in aggrecan and biglycan gene expression when compared to healthy Achilles tendons (Corps et al., 2006). Lower versican (Corps et al., 2004) and MMP-3 gene expression has been observed in tendinopathic Achilles tendons whereas collagen type I, type III and Tenascin-C gene expression were larger (Ireland et al., 2001). Tendinopathy has also shown increased MMP-1, procollagen type I and reduced TIMP-1 through immunolabelling of tendinopathic and healthy patellar tendons (Fu et al., 2002). Lower MMP-3 activity and higher MMP-1 activity was similarly seen in tendinopathic supraspinatus tendon compared to a healthy controls (Riley et al., 2002). A number of differences were

identified in human Achilles tendons by Jones et al. (2006), including lower MMP-3 and TIMP-3 expression and elevated ADAM-1 and MMP-11 in both ruptured and painful tendons compared to healthy tendons. Increased ADAMTS-4, MMP-1, MMP-14 and TIMP-1 was also reported in ruptured tendons (Jones et al., 2006). IL-6 expression levels have also been shown to differ in Achilles tendinopathy and patellar tendinopathy, showing dependence on both the tendon location and tendinopathy type (Legerlotz et al., 2012).

The function of nitric oxide (NO) has also been explored in tendons. Nitric oxide synthase (NOS) gene expression has been found to increase in rat rotator cuff tendons after overuse, suggesting a role in the development of tendinopathies (Szomor et al., 2006). Interestingly, in human tenocytes derived from ruptured rotator cuff tissue, NO has also been found to regulate collagen synthesis, with increased NO availability up-regulating synthesis, while inhibition of inducible NOS (iNOS) down-regulates synthesis (Xia et al., 2006). More holistically, elevated NO levels have been proposed to alter the balance between the anabolic and degenerative catabolic response in tendons, as NO is also involved in the activation of MMPs and TGFβ (Scott and Bahr, 2009; Szomor et al., 2006; Xia et al., 2006).

Recent research has also suggested that some individuals may be genetically prone to developing tendinopathies, with polymorphisms in ECM related genes COL-5A1, TIMP-2 and ADAMTS-14 being associated with Achilles tendinopathy (Abrahams et al., 2013; El Khoury et al., 2013; Morrey et al., 2013).

The schematic in Figure 9 briefly summarises potential mechanisms involved in developing tendinopathies as described by Shearn et al. (2011). It is clear that the pathology, although initiated by various means, ultimately results in altered cellular metabolism and subsequently ECM changes, such as decreased collagen fibril diameters and increased collagen III gene expression and content (Corps et al., 2012; Pingel et al., 2014), eventually leading to the

symptoms associated with tendinopathies. A summary of these tendinopathic changes is also presented in Table 13 towards the end of this chapter.

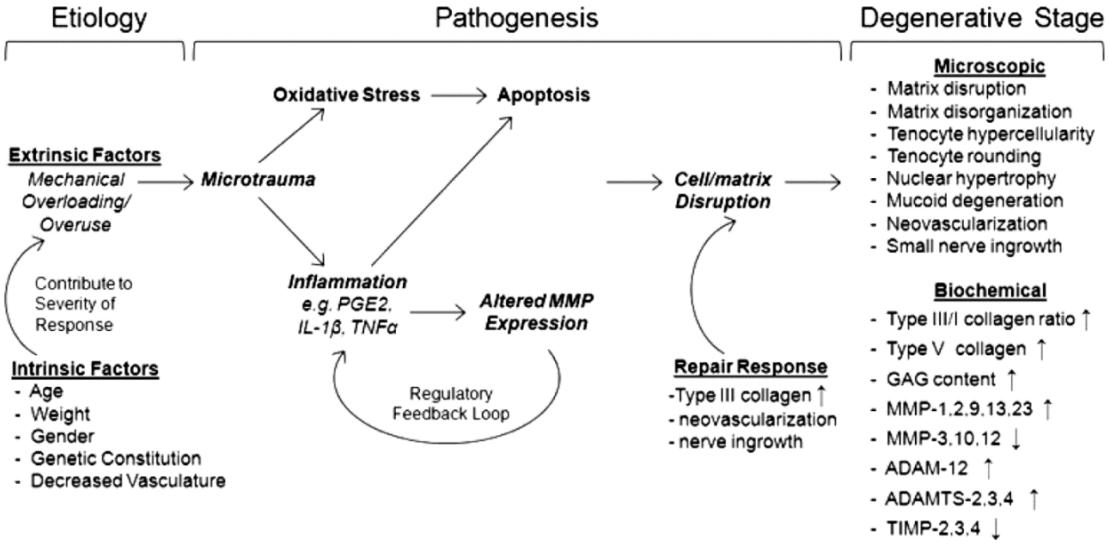

Figure 9: Schematic indicating possible mechanisms for degenerative tendinopathy (Shearn et al., 2011).

1.3.2 Tendinopathy Treatment

The consequences of tendinopathies vary depending on the site and degree of symptoms; they can range from simple swelling and slight pain to complete immobilisation of the affected area. As the exact mechanisms leading to tendinopathies are not known, treatment is delivered progressively depending on the symptoms shown and the extent of disability. Treatment first attempts to reduce inflammation and pain, followed by the restoration of flexibility and function. This can be attempted in many ways, usually starting with rest and use of non-steroidal anti-inflammatory drugs which, upon failure, are then followed by physical therapy, corticosteroid injections, deep ultrasound therapy or muscle stimulation (Cucurulo et al., 2009; Metzl et al., 2008; Speed, 2001; Woo et al., 2007).

The treatments suggested differ from clinician to clinician but ultimately do not resolve the underlying problem. For example, eccentric exercises commonly used to reduce pain in chronic Achilles tendinopathy have been shown to fail in completely eliminating pain after a 5 year

follow-up, with 60.3% of patients still exhibiting pain to some degree (de Vos et al., 2007; van der Plas et al., 2012).

Corticosteroid injections are typically used to treat inflammation. However inflammation does not occur in all tendinopathies, and any inflammation is usually related to the healing process, thus this approach may not be ideal (Speed, 2001). Corticosteroid injections have also been linked to adverse side effects such as inhibiting collagen synthesis, reducing tendon mass, reducing biomechanical integrity and overall delaying of tendon healing, which is why use is cautioned with tendons (Speed, 2001; Woo et al., 2007). Other injection therapies for tendinopathies include: sclerosing injections where agents (such as polidocanol) are used to reduce vascular and neural ingrowth to reduce pain; platelet rich plasma injections which potentially introduce necessary growth factors directly into the pathological site; and autologous blood injections to induce healing (Hoksrud and Bahr, 2011).

If it is deemed necessary, surgical repair is utilised for treatment (Cucurulo et al., 2009; Khan et al., 1999; Nixon et al., 2012). This involves excision of the tendinopathic area and is termed a tenotomy. Tenotomies can be performed in a variety of ways including openly exposing the tendon or percutaneously along the longitudinal axis and either with or without paratenon stripping (Cucurulo et al., 2009; Tallon et al., 2001a). Patients treated surgically for Achilles tendinopathies using these methods have reported success rates of more than 70%, although later complications are not uncommon (Roche and Calder, 2013; Tallon et al., 2001a).The physical act of performing surgery on tissue is known to produce a strong healing response, therefore it is difficult to differentiate between the effects of the surgical procedure and the healing response itself (Woo et al., 2007).

It is evident that effective tendinopathy treatments are lacking, particularly due to the absence of pathology understanding, resulting in pain reducing therapies taking dominance rather than rectification.

1.4 Tenocyte Behaviour

Tenocytes maintain the ECM by producing the main components such as collagen type I and PGs, and are responsible for collagen assembly and turnover. To better understand tendinopathy development, an understanding of tenocyte behaviour during physiological function is necessary. The structure of tendons, as described earlier, provides a complex and mechanically stimulating cellular environment. As tenocytes reside both on the collagen fibres and between fascicles in the IFM, tenocytes are exposed to both tension and shear during tendon loading. Many studies have looked into characterising tenocyte behaviour to elucidate the mechanisms of mechanotransduction and the loading conditions which could promote anabolic and catabolic states.

1.4.1 Mechanotransduction Mechanisms

The use of mechanical stimulants, such as shear pressure, to alter cell behaviour is considered a mechanotransduction pathway. Mechanotransduction is defined as a series of dynamic processes that allow cells to convert biomechanical stimuli into biochemical activity (Kamkin and Kiseleva, 2008). The process of mechanotransduction can be divided into four distinct stages; force transmission, mechanotransduction, signal propagation and cellular response (Atala et al., 2008). Force transmission requires the application of a force to the tissue or ECM which can then be detected and converted into a local stimuli, i.e. deformation of the ECM, changes in hydrostatic pressure and other structural changes to the local cell environment. The local stimuli is then detected by the cell as a deformation, where integrins, ion channels and other receptors on the cell surface act as sensors and convert the local stimuli into intracellular signals (Atala et al., 2008; Schwartz, 2010). Signal propagation can then occur as the intracellular signal produced travels through the cell and ultimately results in a cellular response.

Integrins are key transmembrane receptors involved in mechanotransduction as these are used by cells to adhere to a substrate surface, thus sensing mechanical changes. They possess a

heterodimer structure, with 24 possible combinations from 18 α- and 8 β-subunits in mammals (Arnaout et al., 2007). The extracellular portion of integrins binds to a variety of ligands depending on the combination of subunits, while the intracellular portion binds to the cytoskeleton. This bridging across the cell membrane results in the ability of cells to react bidirectionally (Figure 10), thus allowing cells to adhere, migrate, grow and differentiate (Arnaout et al., 2007; Qin et al., 2004). Integrin activation and cytoskeleton attachment is achieved through actin-binding proteins such as talin, α-actinin and filamin at the cytoplasmic tail end (intracellular portion), which additionally recruits F-actin localised to focal adhesion points (Giannone et al., 2003; Liu et al., 2000; Schwartz, 2010). At the transmembrane region (extracellular portion) multiple ligands can bind to a given α-β combination, and equally different α-β combinations can bind to the same ligand (Campbell and Humphries, 2011). For example the proteins laminin and collagen can both attach to integrins α1β1 and α2β1, or fibronectin which is recognised by α2β1, α3β1, α4β1, α4β7, α5β1, α8β1, αvβ1, αvβ3, αvβ5, αvβ6, αvβ8 and αIIbβ3 although with different affinities (Askari et al., 2009; Campbell and Humphries, 2011; Plow et al., 2000). Thus the rearrangement, recruitment and remodelling of integrins and the cytoskeleton in response to mechanical changes show that these structures are heavily involved in mechanotransduction pathways (Chiquet, 1999; Schwartz, 2010).

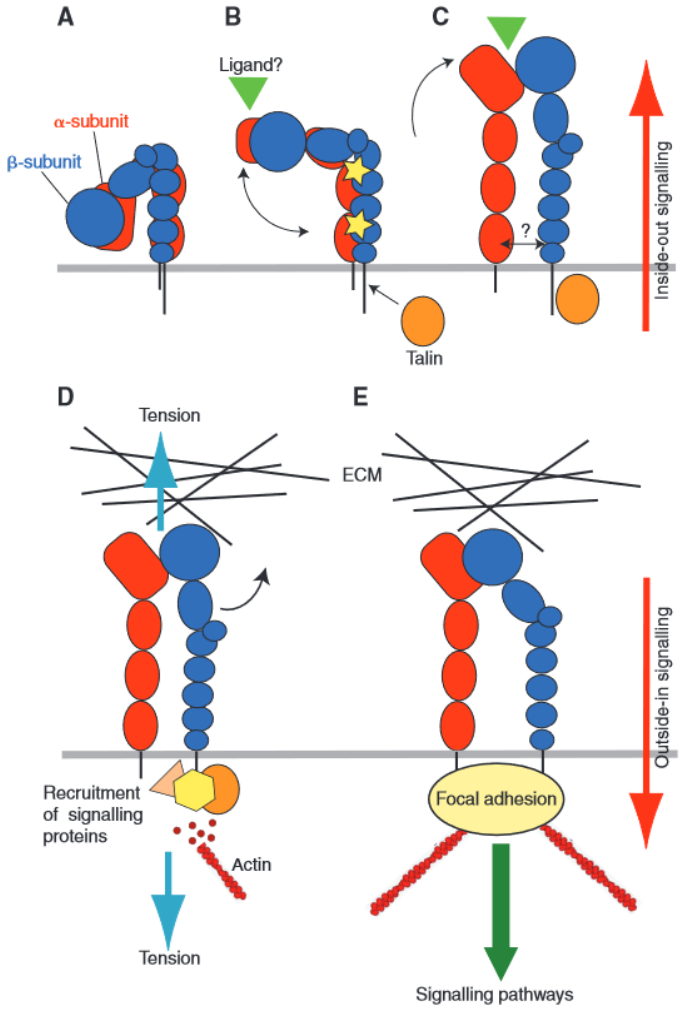

Figure 10: Model of integrin conformational changes and bidirectional signalling. Integrins in A) Inactive, B) primed and C) ligand bound state, while D) and E) show formation of focal adhesion points through external force (Askari et al., 2009).

Direct deformation of the nucleus has also been implicated in mechanotransduction; the presence of nuclear actin, lamins and lamin-binding transmembrane proteins, all of which contribute to connections between the cytoskeleton and the nucleus, provide a mechanism for mechanotransduction (Dahl et al., 2008). This connection was also explored by Arnoczky et al. (2002a) wherein tenocytes within rat tail tendons were observed during loading and found to show a correlation between applied strain and nuclear deformation.

Mechanotransduction is critical to homeostasis in tendons. However, injuries and changes in tendon properties can result in an altered cellular environment, and thus produce an altered mechanotransduction signal.

1.4.2 ECM Turnover

As collagen is the most abundant ECM protein present in tendons, collagen synthesis can be correlated with tendon ECM synthesis. Collagen synthesis starts with polypeptide α-chain (pre-procollagen) mRNA transcription within the cell nucleus like other cellular proteins. The mRNA moves into the cytoplasm where it is translated by ribosomes, producing the N-terminus of the pre-procollagen chain first. This portion is recognised by the rough endoplasmic reticulum (RER), allowing the pre-procollagen chain to be directed into the RER itself as the ribosome completes translation (Ishikawa and Bachinger, 2013). Different genes code for the different types of procollagen chains, with 3 procollagen chains needed to form a procollagen molecule and a number of different chain combinations possible (known collagen types and their chain combinations are listed in Table 2 to Table 6). When a combination of 3 procollagen chains are present in the RER, the chains are aligned and stabilised through disulphide bonds and glycosylated, resulting in a procollagen molecule with a characteristic triple helix. The procollagen molecules are then transported extracellularly via the Golgi apparatus where procollagen N-proteinase and procollagen C-proteinase (also known as propeptidases) cleave the N- and C- terminus, respectively, resulting in collagen molecules (tropocollagen) with the ability to aggregate and covalently crosslink to form collagen fibrils. The propeptidases are therefore vital in collagen synthesis as they are necessary to process procollagen into tropocollagen molecules (Canty and Kadler, 2002; Gelse, 2003; Kadler et al., 1996).

With the collagen biosynthesis processed detailed, it is evident the gene expression of pre-procollagen chains can be used to determine which collagen type a cell is promoting for synthesis. The mRNA transcription and subsequent translation by ribosomes is similar for other proteins, thus gene expression investigation can also be used to monitor other proteins promoted for synthesis.

Matrix metalloproteinases (MMPs) are key enzymes involved in the degradation, and thus remodelling, of the ECM. They are similar to ADAM (a disintegrin and metalloproteinase) and ADAMTS (a disintegrin and metalloproteinase with thrombospondin motif) in structure, with all three protease types characterised by a catalytic Zn^{2+} domain and a hydrophobic cleft of variable depth (Klein and Bischoff, 2011; Nagase et al., 2006). In addition to ECM processing, these proteases are also involved with the release of membrane bound cytokines, growth factors and chemokines (Klein and Bischoff, 2011; Visse and Nagase, 2003).

There are over 20 distinct MMPs identified in humans, each having different substrate specificity (summarised in Tables 7 to 10). MMPs have traditionally been categorised as collagenases, gelatinases, stromelysins or matrilysins (Visse and Nagase, 2003). However, this classification is often considered a hindrance in portraying their function, as each MMP can process multiple substrates, with different substrates indicating different roles. An example of this is depicted in Figure 11 where the multiple downstream effects of MMP-2 are reviewed (Butler and Overall, 2009; Butler, 2000; McCawley and Matrisian, 2001).

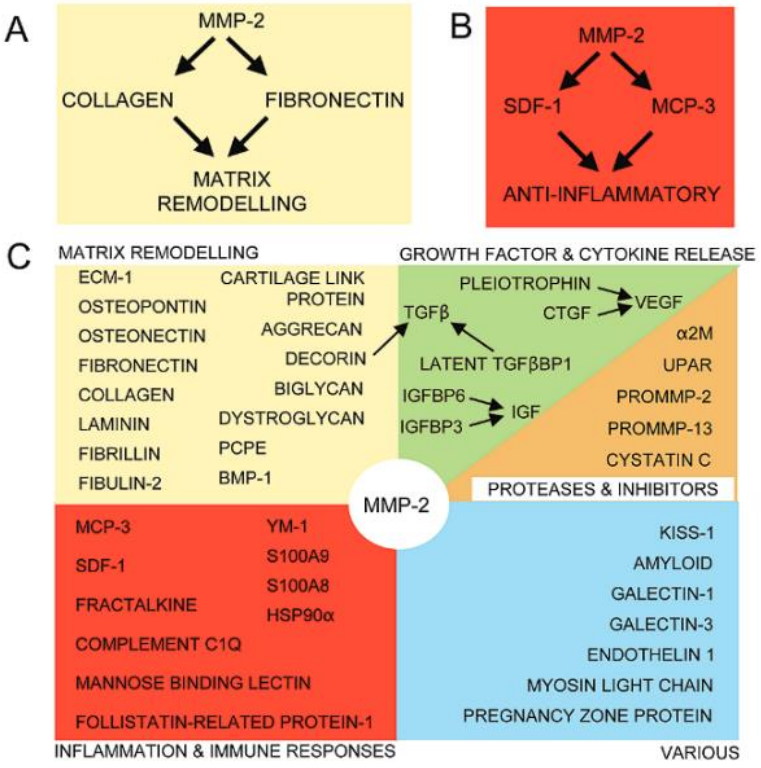

Figure 11: Schematic summarising the variety of MMP-2 interactions. A) and b) demonstrate the role at any given time is dependent on the substrate upon which it is acting, while C) summarises which substrates are linked to which roles (Adapted from Butler and Overall (2009)).

MMPs can be regulated in 4 ways: gene expression, compartmentalisation, activation and inhibition. Transcription control and post-transcription modification via mRNA stability and microRNA constitutes regulation at the gene expression level. MMPs are synthesised as pre-proenzymes, released as proenzymes and therefore MMP activation from proMMPs is another key method for regulation (Chung et al., 2004; Nagase et al., 2006). MMP activation is achieved by removal of a propeptide-domain, which otherwise blocks and prevents interactions by the Zn^{+} ion, and can be achieved through proteinases such as trypsin and other MMPs, or chemicals such as thiol-modifying agents, detergents and reactive oxygen species (Klein and Bischoff, 2011; Loffek et al., 2011; Nagase et al., 2006; Sela-Passwell et al., 2010). This is usually a stepwise process, whereby once part of the obstructing propeptide is removed, the remaining portion likely becomes unstable and is removed via partially activated MMPs or other MMPs (Visse and Nagase, 2003). For example, MMP-3 has been shown to be involved in the activation of MMP-1 and MMP-13 (Klein and Bischoff, 2011). Compartmentalisation of secreted MMPs to pericellular zones creates a focused response and thus localises their release, in addition to providing a store for quick release (Loffek et al., 2011). Finally, there are 4 tissue inhibitors of metalloproteinases (TIMPs), each of which functions to obstruct MMP activity. This is achieved by directly blocking the substrate recognition site, via chelation of the Zn^{+} ion with the TIMP N-terminal in a 1:1 molar ratio – typically described as the wedge shaped TIMP molecule slotting into and occupying the active MMP site (Nagase et al., 2006). Alterations which detrimentally affect the chelating ability of TIMPS inactivate their MMP inhibition (Sela-Passwell et al., 2010). TIMPs have a broad specificity resulting in each TIMP being able to inhibit a wide variety of MMPs, with all four collectively covering the known MMPs (Klein and Bischoff, 2011; Sharabi et al., 2014).

MMP-1, MMP-8, and MMP-13 have typically been considered collagenases in humans, along with the membrane type MMP-1 (also known as MMP-14). This is due to their ability to initiate degradation in fibrillar collagens, arising from their hemopexin prodomain, which locally

unwinds the structure of collagen such that the catalytic Zn^+ domain can cleave collagen into ¾ and ¼ fragments (Chung et al., 2004; Nagase et al., 2006; Sarkar et al., 2012). Once broken, other MMPs can also recognise the fragments as substrates and aid degradation further. Although MMP-1, MMP-8 and MMP-13 can all cleave collagen type I, II and III, their substrate specificity differs. MMP-1 is seen to preferentially cleave collagen type III, MMP-8 preferentially cleaves collagen type I and MMP-13 preferentially cleaves collagen type II (Howes et al., 2014; Manka et al., 2012; Mitchell et al., 1996; Ricard-Blum, 2011).

Gelatinases MMP-2 and MMP-9, as the names suggests, digest gelatins. This includes degraded collagens (i.e. compromised triple helix) and laminin (Visse and Nagase, 2003). Thus their activity extends to fibrillar collagens once they have been processed by the aforementioned collagenolytic MMPs. Controversially, MMP-2 has been demonstrated to cleave fibrillar collagens into ¾ and ¼ fragments similar to MMP-1 (Aimes and Quigley, 1995; Patterson et al., 2001) and stated to do so in reviews (Klein and Bischoff, 2011; Nagase et al., 2006; Visse and Nagase, 2003). However, this is hotly debated, with opponents suggesting that the collagen used in this study was not native, and damage to the triple helix facilitated degradation by MMP-2 (Seltzer and Eisen, 1999). This is also reinforced by a further study where MMP-2 had no collagenolytic effect on triple helical type I collagen unlike MMP-1 and MMP-14 (MT-MMP-1) (Ohuchi et al., 1997). However a subsequent study showed that, although MMP-2 possesses a hemopexin domain, it can bind to native collagen type I using its fibronectin like domain and could possess weak collagenolytic behaviour towards fibrillar collagen type I (Tam et al., 2004). A more recent study took extra care to source intact collagen type I which could form its native triple helical structure when gelled and found MMP-2 unable to accomplish any digestion while MMP-1 did (Christiansen et al., 2007).

There are 19 human ADAMTS which are generally similar to MMPs in that they are secreted as proenzymes, inhibited by TIMPs with varying affinities and digest numerous substrates, many

of which are currently unidentified or of unknown function (Porter et al., 2005). A list of ADAMTS, their structure and known substrates are shown in Table 11 and Table 12. One key difference between MMPs and ADAMTS is the ability for the latter to bind to the ECM (Porter et al., 2005). Some ADAMTS, notably ADAMTS-2, ADAMTS-3 and ADAMTS14, act as procollagen peptidases, thus are involved in the regulation of collagen fibril synthesis.

Table 2: Summary of Collagen structures, and their involvement in tendinopathies and response to loading. (Information from Ricard-Blum (2011) and Shoulders and Raines (2009) unless stated otherwise). Part 1 of 5.

Type	Individual Chain Structures	Chain Arrangements	Formation type and Associations	Changes with Loading or Tendinopathy
I	α1[I]:  α2[I]: 	$\alpha1[I]_3$ $\alpha1[I]_2.\alpha2[I]$	-Fibrillar -The homotrimer $\alpha1[I]_3$ is resistant to all MMP collagenases and found in foetal tissue, fibrosis and cancerous cells (16).	Increased in tendinopathy (3,11,12). Increased expression in pathological PTT (9). Increased expression with loading (4,7,8,14,15). Increased content with loading (5,8).
II	α1[II]: 	$\alpha1[II]_3$	-Fibrillar	
III	α1[III]: 	$\alpha1[III]_3$	-Fibrillar -Forms heterotypic fibrils with collagen type I	Increased in tendinopathy (3,10,11). Increased expression in pathological PTT (9). Increased collagen content with loading (5,8). Increased expression with loading (6,15).
IV	α1[IV] and α2[IV]:  α3[IV], α4[IV], α5[IV] and α6[IV]: 	$\alpha1[IV]_2.\alpha2[IV]$ $\alpha3[IV].\alpha4[IV].\alpha5[IV]$ $\alpha5[IV]_2.\alpha6[IV]$	-Network	

Key:

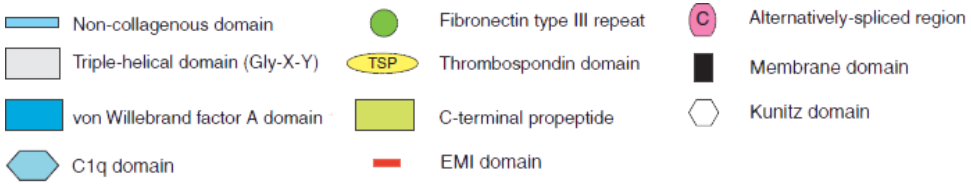

Collagen formation types:

FACIT – *Fibril associated collagen with interrupted triple helices.*
MACIT – *Membrane associated collagen with interrupted triple helices.*
Multiplexin – *Multiple triple helix domains and interruptions.*

1 = Corps et al., 2008. 2 = Jones et al., 2006. 3 = Riley, G., 2008. 4 = Jones et al., 2013. 5 = Maeda et al., 2007. 6 = Maeda et al., 2009. 7 = Legerlotz et al., 2013. 8 = Huisman et al., 2014. 9 = Corps et al., 2012. 10 = Riley et al., 1994. 11 = Ireland et al., 2001. 12 = Fu et al., 2002. 13 = Riley et al., 2002. 14 = Zhang and Wang, 2010. 15 = Sun et al., 2010. 16 = Han et al., 2010. 17 = Canty and Kadler, 2005. 18 = Fitzgerald et al., 2008. 19 = Wu and Eyre, 1995.

Table 3: Summary of Collagen structures, and their involvement in tendinopathies and response to loading. (Information from Ricard-Blum (2011) and Shoulders and Raines (2009) unless stated otherwise). Part 2 of 5.

Type	Individual Chain Structures	Chain Arrangements	Formation type and Associations	Changes with Loading or Tendinopathy
V	α1[V]:  α2[V]:  α3[V]:  	$\alpha1[V]_3$ $\alpha1[V]_2.\alpha2[V]$ α1[V]2.α4[V] α1[V].α2[V].α3[V] α1[XI].α1[V].α3[XI]	-Fibrillar -Isoform exists with type XI chain. -Forms heterotypic fibrils with collagen type I (17).	Increased with long term loading (15).
VI	α1[VI]:  α2[VI]:  α3[VI]:  α4[VI]:  α5[VI]:  α6[VI]: 	α1[VI].α2[VI].α3[VI] α1[VI].α2[VI].α4[VI]	-Network -Other chains include α4[VI], α5[VI] and α6[VI] (18).	Increased expression in both degenerate and ruptured human Achilles tendon (11).
VII	α1[VII]: 	$\alpha1[VII]_3$ $\alpha1[VII]_2.\alpha2[VII]$	-Anchoring fibril	

Key:

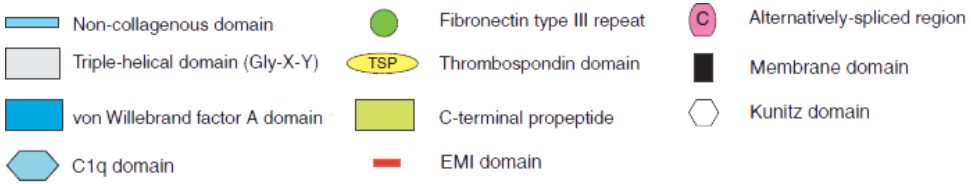

Collagen formation types:

FACIT – *Fibril associated collagen with interrupted triple helices.*
MACIT – *Membrane associated collagen with interrupted triple helices.*
Multiplexin – *Multiple triple helix domains and interruptions.*

1 = Corps et al., 2008. 2 = Jones et al., 2006. 3 = Riley, G., 2008. 4 = Jones et al., 2013. 5 = Maeda et al., 2007. 6 = Maeda et al., 2009. 7 = Legerlotz et al., 2013. 8 = Huisman et al., 2014. 9 = Corps et al., 2012. 10 = Riley et al., 1994. 11 = Ireland et al., 2001. 12 = Fu et al., 2002. 13 = Riley et al., 2002. 14 = Zhang and Wang, 2010. 15 = Sun et al., 2010. 16 = Han et al., 2010. 17 = Canty and Kadler, 2005. 18 = Fitzgerald et al., 2008. 19 = Wu and Eyre, 1995.

Table 4: Summary of Collagen structures, and their involvement in tendinopathies and response to loading. (Information from Ricard-Blum (2011) and Shoulders and Raines (2009) unless stated otherwise). Part 3 of 5.

Type	Individual Chain Structures	Chain Arrangements	Formation type and Associations	Changes with Loading or Tendinopathy
VIII	α1[VIII]:  α2[VIII]: 	$\alpha1[VIII]_3$ $\alpha2[VIII]_3$ $\alpha1[VIII]_2.\alpha2[VIII]$ $\alpha1[VIII].\alpha2[VIII]_2$	-Network	Increased expression in both degenerate and ruptured human Achilles tendon (11).
IX	α1[IX]:  α2[IX]:  α3[IX]: 	$\alpha1[IX].\alpha2[IX].\alpha3[IX]$	-FACIT -Associated with collagen type II fibrils (17).	
X	α1[X]: 	$\alpha1[X]_3$	-Network	
XI	α1[XI]:  α2[XI]: 	$\alpha1[XI].\alpha2[XI].\alpha3[XI]$ $\alpha1[XI].\alpha1[V].\alpha3[XI]$	-Fibrillar -Isoform with collagen type V chain exists. -Forms heterotypic fibrils with collagen type II (17). -The α3[XI] chain is the same sequence as α1[II], however post-translation modifications and cross linking differ (19).	

Key:

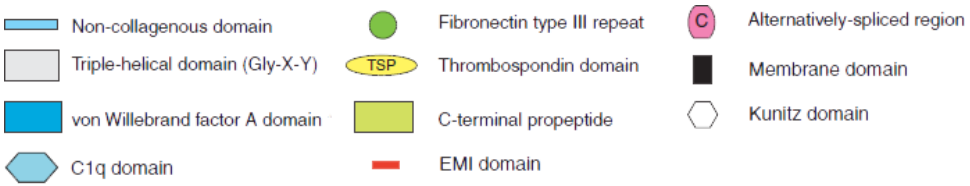

Collagen formation types:

FACIT – *Fibril associated collagen with interrupted triple helices.*
MACIT – *Membrane associated collagen with interrupted triple helices.*
Multiplexin – *Multiple triple helix domains and interruptions.*

1 = Corps et al., 2008. 2 = Jones et al., 2006. 3 = Riley, G., 2008. 4 = Jones et al., 2013. 5 = Maeda et al., 2007. 6 = Maeda et al., 2009. 7 = Legerlotz et al., 2013. 8 = Huisman et al., 2014. 9 = Corps et al., 2012. 10 = Riley et al., 1994. 11 = Ireland et al., 2001. 12 = Fu et al., 2002. 13 = Riley et al., 2002. 14 = Zhang and Wang, 2010. 15 = Sun et al., 2010. 16 = Han et al., 2010. 17 = Canty and Kadler, 2005. 18 = Fitzgerald et al., 2008. 19 = Wu and Eyre, 1995.

Table 5: Summary of Collagen structures, and their involvement in tendinopathies and response to loading. (Information from Ricard-Blum (2011) and Shoulders and Raines (2009) unless stated otherwise). Part 4 of 5.

Type	Individual Chain Structures	Chain Arrangements	Formation type and Associations	Changes with Loading or Tendinopathy
XII	α1[XII]: 	$\alpha1[XII]_3$	-FACIT	Increased with long term loading (15).
XIII	α1[XIII]: 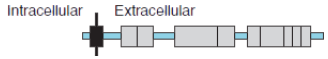	$\alpha1[XIII]_3$	-MACIT	
XIV	α1[XIV]: 	$\alpha1[XIV]_3$	-FACIT	
XV	α1[XV]: 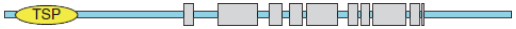	$\alpha1[XV]_3$	-Multiplexin	
XVI	α1[XVI]: 	$\alpha1[XVI]_3$	-FACIT	Increased expression in both degenerate and ruptured human Achilles tendon (11).
XVII	α1[XVII]: 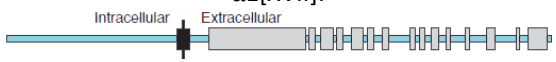	$\alpha1[XVII]_3$	-MACIT	
XVIII	α1[XVIII]: 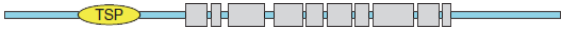	$\alpha1[XVIII]_3$	-Multiplexin	
XIX	α1[XIX]: 	$\alpha1[XIX]_3$	-FACIT	
XX	α1[XX]: 	$\alpha1[XX]_3$	-FACIT	

Key:

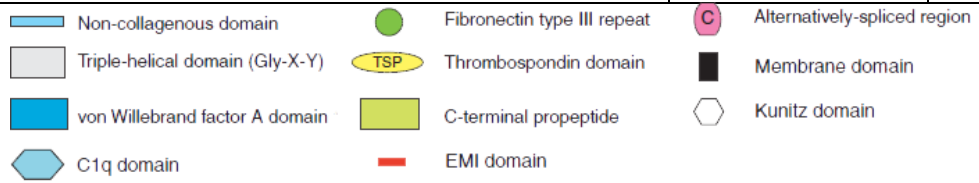

Collagen formation types:

FACIT – *Fibril associated collagen with interrupted triple helices.*
MACIT – *Membrane associated collagen with interrupted triple helices.*
Multiplexin – *Multiple triple helix domains and interruptions.*

1 = Corps et al., 2008. 2 = Jones et al., 2006. 3 = Riley, G., 2008. 4 = Jones et al., 2013. 5 = Maeda et al., 2007. 6 = Maeda et al., 2009. 7 = Legerlotz et al., 2013. 8 = Huisman et al., 2014. 9 = Corps et al., 2012. 10 = Riley et al., 1994. 11 = Ireland et al., 2001. 12 = Fu et al., 2002. 13 = Riley et al., 2002. 14 = Zhang and Wang, 2010. 15 = Sun et al., 2010. 16 = Han et al., 2010. 17 = Canty and Kadler, 2005. 18 = Fitzgerald et al., 2008. 19 = Wu and Eyre, 1995.

Table 6: Summary of Collagen structures, and their involvement in tendinopathies and response to loading. (Information from Ricard-Blum (2011) and Shoulders and Raines (2009) unless stated otherwise). Part 5 of 5.

Type	Individual Chain Structures	Chain Arrangements	Formation type and Associations	Changes with Loading or Tendinopathy
XXI	α1[XXI]: 	α1[XXI]$_3$	-FACIT	
XXII	α1[XXII]: 	α1[XXII]$_3$	-FACIT	
XXIII	α1[XXIII]: 	α1[XXIII]$_3$	-MACIT	
XXIV	α1[XXIV]: 	α1[XXIV]$_3$	-Fibrillar	
XXV	α1[XXV]: 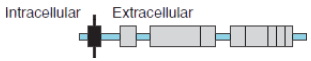	α1[XXV]$_3$	-MACIT	
XXVI	α1[XXVI]: 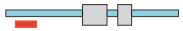	α1[XXVI]$_3$	-FACIT	
XXVII	α1[XXVII]: 	α1[XXVII]$_3$	-Fibrillar	
XXVIII	α1[XXVIII]: 	α1[XXVIII]$_3$	-Multiplexin	

Key:

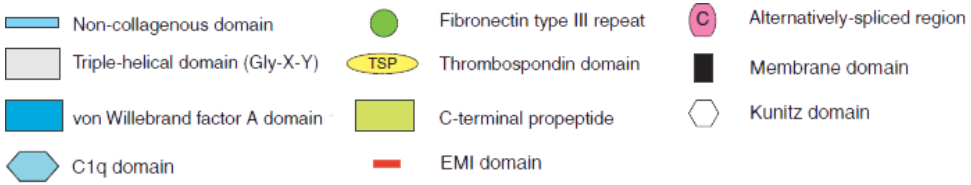

Collagen formation types:

FACIT – *Fibril associated collagen with interrupted triple helices.*
MACIT – *Membrane associated collagen with interrupted triple helices.*
Multiplexin – *Multiple triple helix domains and interruptions.*

1 = Corps et al., 2008. 2 = Jones et al., 2006. 3 = Riley, G., 2008. 4 = Jones et al., 2013. 5 = Maeda et al., 2007. 6 = Maeda et al., 2009. 7 = Legerlotz et al., 2013. 8 = Huisman et al., 2014. 9 = Corps et al., 2012. 10 = Riley et al., 1994. 11 = Ireland et al., 2001. 12 = Fu et al., 2002. 13 = Riley et al., 2002. 14 = Zhang and Wang, 2010. 15 = Sun et al., 2010. 16 = Han et al., 2010. 17 = Canty and Kadler, 2005. 18 = Fitzgerald et al., 2008. 19 = Wu and Eyre, 1995.

Table 7: Summary of Human matrix metalloproteinases, and their involvement in tendinopathies and response to loading. (Information collated from reviews Klein and Bischoff (2011), McCawley and Matrisian (2001) and Nagase et al. (2006) unless indicated. Schematics of structures from Loffek et al. (2011). Part 1 of 4.

Name *(Traditional Name)*	General Structure	Known Substrates	Changes with Loading or Tendinopathy
MMP-1 *(Collagenase-1)*	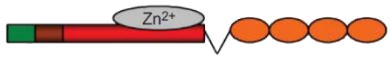	Collagen types I, II, III, VII, VIII, X and XI, gelatin, vitronectin, α_2-macroglobulin, fibronectin, IL-1β, aggrecan, versican, perlecan, nidogen, serpins, Tenascin-C, IGFBP-3, IGFBP-5, Pro-MMP-1, Pro-MMP-2 and Pro-MMP-9.	Increased expression in ruptured human Achilles tendon (2). Increased in tendinopathy (3,12). Reduced expression with loading (4). Increased in ruptured human tendons (13).
MMP-2 *(Gelatinase-A)*	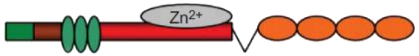	Collagen types I, III, IV, V, VII, X and XI, and gelatin, aggrecan, tenascin, decorin, substance P, fibronectin, laminin, IL-1β, elastin, vitronectin, Pro-MMP-1, Pro-MMP-2 and Pro-MMP-13.	Increased in tendinopathy (3). Increased expression in pathological PTT (9). Increased expression in both degenerate and ruptured human Achilles tendon (11). Increased with long term loading (15).
MMP-3 *(Stromelysin-1)*	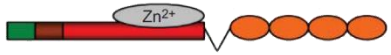	Collagen types III, IV, V, IX, X and XI, gelatin, aggrecan, elastin, vitronectin, α_2-macroglobulin, tenascin, decorin, fibronectin, laminin, E-cadherin, plasminogen, perlecan, IL-1β, laminin, Pro-MMP-1, Pro-MMP-3, Pro-MMP-7, Pro-MMP8, Pro-MMP-9 and Pro-MMP-13.	Reduced expression in both pathological (2,11) and ruptured human Achilles tendon (2). Reduced expression in pathological PTT (9). Increased in ruptured human tendons (13). Reduced in tendinopathy (3). Reduced expression with loading (4,15).

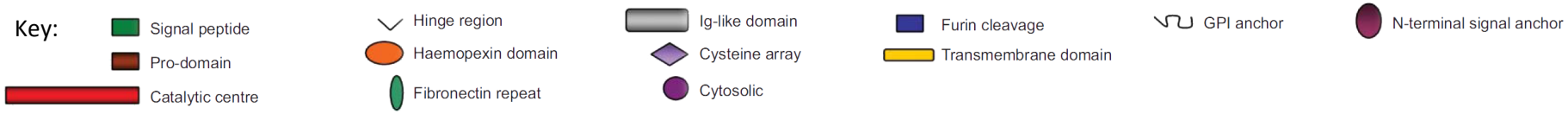

1 = Corps et al., 2008. 2 = Jones et al., 2006. 3 = Riley, G., 2008. 4 = Jones et al., 2013. 5 = Maeda et al., 2007. 6 = Maeda et al., 2009. 7 = Legerlotz et al., 2013. 8 = Huisman et al., 2014. 9 = Corps et al., 2012. 10 = Riley et al., 1994. 11 = Ireland et al., 2001. 12 = Fu et al., 2002. 13 = Riley et al., 2002. 14 = Zhang and Wang, 2010. 15 = Sun et al., 2010. 16 = Han et al., 2010. 17 = Canty and Kadler, 2005. 18 = Fitzgerald et al., 2008. 19 = Wu and Eyre, 1995.

Table 8: Summary of Human matrix metalloproteinases, and their involvement in tendinopathies and response to loading. (Information collated from reviews Klein and Bischoff (2011), McCawley and Matrisian (2001) and Nagase et al. (2006) unless indicated. Schematics of structures from Loffek et al. (2011). Part 2 of 4.

Name *(Traditional Name)*	General Structure	Known Substrates	Changes with Loading or Tendinopathy
MMP-7 *(Matrilysin-1)*		Collagen types III, IV, V, IX, X and XI, gelatin, aggrecan, tenascin, fibronectin, plasminogen, decorin, E-cadherin, gelatin, laminin, elastin, tenascin, TNF-α, IGFBP, Pro-ADAM-28, Pro-MMP-1, Pro-MMP-2, Pro-MMP-7 and Pro-MMP9.	Reduced expression in ruptured human Achilles tendon (2).
MMP-8 *(Collagenase-2)*	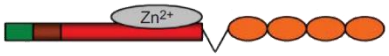	Collagen types I, II, III, VII and X, gelatin, tenascin, aggrecan and Pro-MMP-8.	
MMP-9 *(Gelatinase-B)*	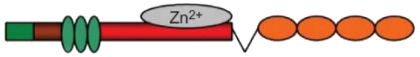	Collagen types IV, V, VII, XI and XIV, elastin, aggrecan, decorin, laminin, Plasminogen, IL-1β, IL-8 and TGF-β.	Increased expression in ruptured human Achilles tendon (2,11).
MMP-10 *(Stromelysin-2)*	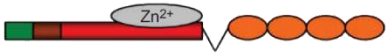	Collagen types III, IV, V, IX, X and XI, gelatin, fibronectin, vitronectin, elastin, tenascin, aggrecan, laminin, Pro-MMP-1, Pro-MMP7, Pro-MMP-8, Pro-MMP-9 and Pro-MMP-10.	Reduced expression in painful human Achilles tendon (2). Reduced in tendinopathy (3). Increased expression with loading (4).
MMP-11 *(Stromelysin-3)*	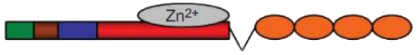	Collagen type VI, gelatin, fibronectin, laminin, aggrecan and IGFBP-1.	Increased expression in both painful and ruptured Human Achilles Tendons (2). Reduced expression with loading (4).
MMP-12 *(Macrophage Elastase)*	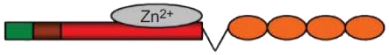	Collagen type IV, elastin, gelatin, fibronectin, laminin, vitronectin, aggrecan and plasminogen.	Increased expression in painful human Achilles tendon (2). Reduced in tendinopathy (3).

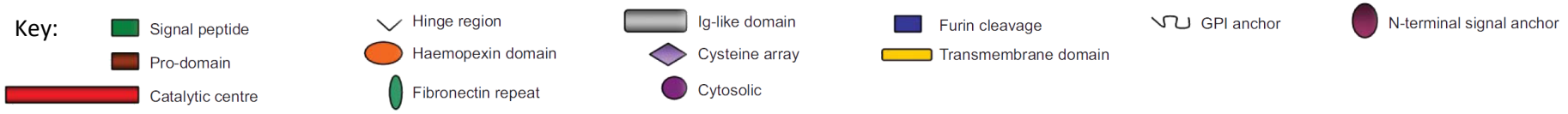

1 = Corps et al., 2008. 2 = Jones et al., 2006. 3 = Riley, G., 2008. 4 = Jones et al., 2013. 5 = Maeda et al., 2007. 6 = Maeda et al., 2009. 7 = Legerlotz et al., 2013. 8 = Huisman et al., 2014. 9 = Corps et al., 2012. 10 = Riley et al., 1994. 11 = Ireland et al., 2001. 12 = Fu et al., 2002. 13 = Riley et al., 2002. 14 = Zhang and Wang, 2010. 15 = Sun et al., 2010. 16 = Han et al., 2010. 17 = Canty and Kadler, 2005. 18 = Fitzgerald et al., 2008. 19 = Wu and Eyre, 1995.

Table 9: Summary of Human matrix metalloproteinases, and their involvement in tendinopathies and response to loading. (Information collated from reviews Klein and Bischoff (2011), McCawley and Matrisian (2001) and Nagase et al. (2006) unless indicated. Schematics of structures from Loffek et al. (2011). Part 3 of 4.

Name *(Traditional Name)*	General Structure	Known Substrates	Changes with Loading or Tendinopathy
MMP-13 *(Collagenase-3)*	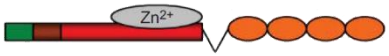	Collagen Types I, II, III, IV, VII, IX, X and XIV, gelatin, aggrecan, perlecan, biglycan, tenascin-C, fibrinogen, IGF-I, IGF-II, PDGF, BFGF, TGF-β1, IL-1, IL-6, TNF-α, Pro-MMP-9 and Pro-MMP-13.	Reduced expression with loading (4,6,15). Increased expression in pathological PTT (9).
MMP-14 *(MT1-MMP)*		Collagen types I, II and III, gelatin, CD44, laminin, fibronectin, vitronectin, tenascin, nidogen, aggrecan, fibrin, fibrinogen, E-cadherin, N-cadherin, integrins, proteoglycans, Pro-MMP-2, Pro-MMP-8 and Pro-MMP-13.	Increased expression in ruptured human Achilles tendon (2,11) and degenerate human Achilles tendon (11). Reduced with long term loading (15).
MMP-15 *(MT2-MMP)*		Laminin, fibronectin, tenascin, aggrecan, perlecan and Pro-MMP-2.	
MMP-16 *(MT3-MMP)*		Aggrecan and Pro-MMP-2.	Increased expression in painful human Achilles tendon (2).
MMP-17 *(MT4-MMP)*		Fibrin, fibrinogen, gelatin, TNF-α, Pro-MMP-2 and Pro-ADAMTS-4.	Reduced expression with loading (4).
MMP-19 *(RASI)*	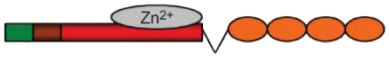	Collagen type IV, gelatin, tenascin-C, fibronectin, COMP, aggrecan and laminin.	Increased expression ruptured human Achilles tendon (2).
MMP-20 *(Enamelysin)*	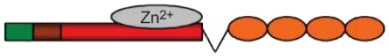	Aggrecan, COMP and amelogenin.	

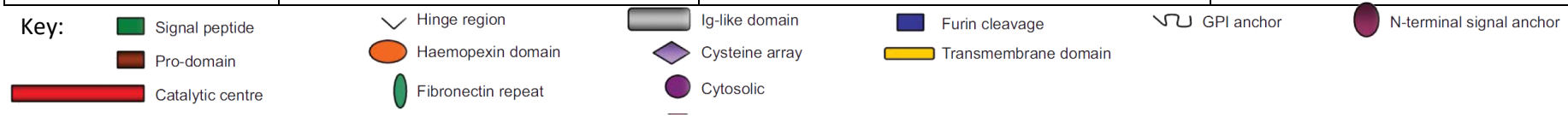

1 = Corps et al., 2008. 2 = Jones et al., 2006. 3 = Riley, G., 2008. 4 = Jones et al., 2013. 5 = Maeda et al., 2007. 6 = Maeda et al., 2009. 7 = Legerlotz et al., 2013. 8 = Huisman et al., 2014. 9 = Corps et al., 2012. 10 = Riley et al., 1994. 11 = Ireland et al., 2001. 12 = Fu et al., 2002. 13 = Riley et al., 2002. 14 = Zhang and Wang, 2010. 15 = Sun et al., 2010. 16 = Han et al., 2010. 17 = Canty and Kadler, 2005. 18 = Fitzgerald et al., 2008. 19 = Wu and Eyre, 1995.

Table 10: Summary of Human matrix metalloproteinases, and their involvement in tendinopathies and response to loading. (Information collated from reviews Klein and Bischoff (2011), McCawley and Matrisian (2001) and Nagase et al. (2006) unless indicated. Schematics of structures from Loffek et al. (2011). Part 4 of 4.

Name *(Traditional Name)*	General Structure	Known Substrates	Changes with Loading or Tendinopathy
MMP-23 *(Femalysin)*	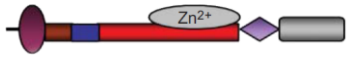	Gelatin and Pro-MMP-23.	Increased expression in painful human Achilles tendon (2). Increased in tendinopathy (3). Increased expression in pathological PTT (9).
MMP-24 *(MT5-MMP)*		Gelatin, fibronectin, vitronectin, aggrecan and Pro-MMP-2.	Reduced expression in ruptured human Achilles tendon (2). Increased expression with loading (4).
MMP-25 *(MT6-MMP)*		Collagen type IV, fibrin, fibrinogen, fibronectin, proteoglycans, TNF-α and Pro-MMP-2.	Increased expression in ruptured human Achilles tendon (2).
MMP-26 *(Matrilysin-2)*		Collagen type IV, fibronectin, fibrinogen, gelatin, aggrecan, tenascin and Pro-MMP-9.	
MMP-27	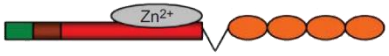	Unknown	Reduced expression in painful human Achilles tendon (2). Reduced in tendinopathy (3).
MMP-28 *(Epilysin)*	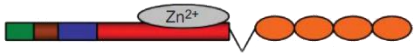	Unknown	Reduced expression in ruptured human Achilles tendon (2).

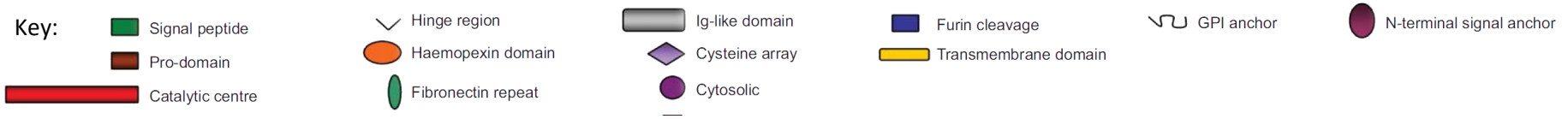

1 = Corps et al., 2008. 2 = Jones et al., 2006. 3 = Riley, G., 2008. 4 = Jones et al., 2013. 5 = Maeda et al., 2007. 6 = Maeda et al., 2009. 7 = Legerlotz et al., 2013. 8 = Huisman et al., 2014. 9 = Corps et al., 2012. 10 = Riley et al., 1994. 11 = Ireland et al., 2001. 12 = Fu et al., 2002. 13 = Riley et al., 2002. 14 = Zhang and Wang, 2010. 15 = Sun et al., 2010. 16 = Han et al., 2010. 17 = Canty and Kadler, 2005. 18 = Fitzgerald et al., 2008. 19 = Wu and Eyre, 1995.

Table 11: Summary of the structure and substrates of the ADAMTS family, and their relevance in tendinopathies and response to loading. (Information from Lin and Liu (2009) and Porter et al. (2005) unless stated otherwise). Part 1 of 2.

Name *(Other Names)*	Structure	Known Substrates	Changes with Loading or Tendinopathy
ADAMTS-1 *(Aggrecanase-3)*		Aggrecan and versican	
ADAMTS-2 *(Procollagen I N-proteinase)*		Procollagen I, II and III N-propeptides	Higher expression in painful human Achilles tendon (2). Increased in tendinopathy (3). Increased expression with loading (4).
ADAMTS-3		Procollagen II N-propeptide	Higher expression in painful human Achilles tendon (2). Increased in tendinopathy (3).
ADAMTS-4 *(Aggrecanase-1)*		Aggrecan, brevican, versican, decorin, fibromodulin and COMP	Higher expression in ruptured human Achilles tendon (1,2). Increased expression with loading (4).
ADAMTS-5 *(Aggrecanase-2)*		Aggrecan and brevican	Lower expression in painful human Achilles tendon (2). Reduced in tendinopathy (3). Reduced expression in pathological PTT (9). Increased expression with loading (4).
ADAMTS-6	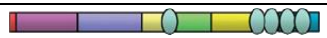		Increased expression with loading (4).
ADAMTS-7		COMP, α_2-macroglobulin	Lower expression in ruptured human Achilles tendon (2).
ADAMTS-8		Aggrecan and Versican	
ADAMTS-9		Aggrecan and Versican	

Key:

1 = Corps et al., 2008. 2 = Jones et al., 2006. 3 = Riley, G., 2008. 4 = Jones et al., 2013. 5 = Maeda et al., 2007. 6 = Maeda et al., 2009. 7 = Legerlotz et al., 2013. 8 = Huisman et al., 2014. 9 = Corps et al., 2012. 10 = Riley et al., 1994. 11 = Ireland et al., 2001. 12 = Fu et al., 2002. 13 = Riley et al., 2002. 14 = Zhang and Wang, 2010. 15 = Sun et al., 2010. 16 = Han et al., 2010. 17 = Canty and Kadler, 2005. 18 = Fitzgerald et al., 2008. 19 = Wu and Eyre, 1995.

Table 12: Summary of the structure and substrates of the ADAMTS family, and their relevance in tendinopathies and response to loading. (Information from Lin and Liu (2009) and Porter et al. (2005) unless stated otherwise). Part 2 of 2.

Name *(Other Names)*	Structure	Known Substrates	Changes with Loading or Tendinopathy
ADAMTS-10			Increased expression with loading (4).
ADAMTS-12		Aggrecan, COMP and α_2-macroglobulin	
ADAMTS-13		Von Willebrand factor	
ADAMTS-14		Procollagen I and II N-propeptides	Increased expression with loading (4).
ADAMTS-15		Aggrecan	
ADAMTS-16		α_2-macroglobulin	Increased expression with loading (4).
ADAMTS-17			
ADAMTS-18			
ADAMTS-19		Aggrecan	
ADAMTS-20	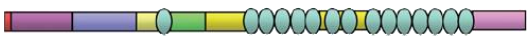	Aggrecan	

Key:

- Signal peptide
- Pro domain
- Metalloproteinase domain
- Disintegrin domain
- Thrombospondin type I motif
- Cysteine-rich domain
- Protease and lacunin motif
- *Gon-I*-like motif
- Cubilin motif
- Spacer region
- Mucin-like domain

1 = Corps et al., 2008. 2 = Jones et al., 2006. 3 = Riley, G., 2008. 4 = Jones et al., 2013. 5 = Maeda et al., 2007. 6 = Maeda et al., 2009. 7 = Legerlotz et al., 2013. 8 = Huisman et al., 2014. 9 = Corps et al., 2012. 10 = Riley et al., 1994. 11 = Ireland et al., 2001. 12 = Fu et al., 2002. 13 = Riley et al., 2002. 14 = Zhang and Wang, 2010. 15 = Sun et al., 2010. 16 = Han et al., 2010. 17 = Canty and Kadler, 2005. 18 = Fitzgerald et al., 2008. 19 = Wu and Eyre, 1995.

1.4.3 Tenocyte Response to Loading

Tendons, as a result of mechanotransduction, respond to mechanical stimuli by changing their structure, composition and mechanical properties (Wang, 2006). Given the content of collagen type I in tendons and its structural importance, collagen synthesis rates following exercise has been explored in tendons in an attempt to understand the relationship between anabolic and catabolic triggers. An *in vitro* study by Maeda et al. (2007) showed that the duration of the time that a rat tail tendon undergoes cyclic loading affects the synthesis of collagen by tenocytes within. Tendons which experienced 86400 cycles had increased collagen production compared to those which underwent 600 cycles (Maeda et al., 2007). Similar results were obtained by another study, (Goodman et al., 2004), which observed collagen production changes were dependant on age and loads experienced, with more collagen produced in immature tendon samples. A study by Miller et al. (2005) investigated collagen synthesis in human tendons after 1 hr of one-legged kicking exercise and found fractional protein synthesis to increase after 6 hours, peak at 24 hours and remain elevated after 72 hours (Miller et al., 2005). This is similar to the previous experiment by Langberg et al. (1999) where a decrease in Procollagen I C-terminal peptide (PICP), a collagen type I synthesis marker, was seen during the initial rest period after acute exercise, followed by an increase to more than the basal amount after 72 hours (Langberg et al., 1999). It is likely that during the first 24-36 hours post-acute exercise net collagen degradation occurs, however in the subsequent 24-36 hours net collagen synthesis follows (Figure 12) (Magnusson et al., 2010).

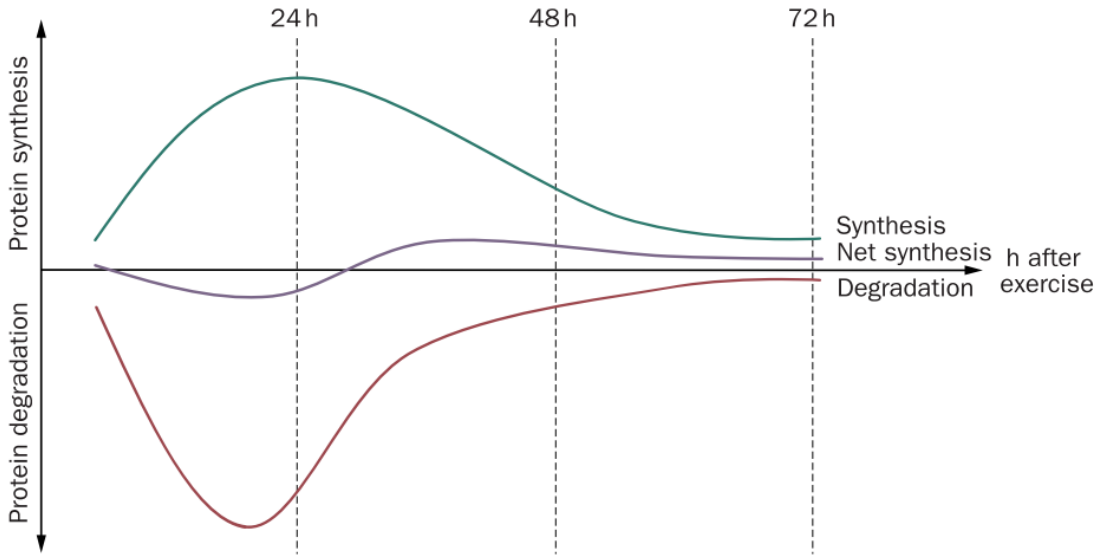

Figure 12: Representative graph of collagen synthesis and degradation up to 72 hours after a bout of acute exercise in humans. (Adapted from Magnusson et al. (2010)).

The collagen synthesis-degradation timeline highlights the potential importance of rest in tendon health as continuous exercise will lead to further degradation and less synthesis (Magnusson et al., 2010; Reinking, 2012). This is further fortified by studies like Huisman et al. (2014) where including resting periods in loading studies increased collagen synthesis. In this study tenocytes digested from healthy human hamstring tendons were cultured onto type I collagen coated membranes and loaded at 0.1Hz to an average applied strain of 3-5% using the Flexcell system. Loading bouts of either 100 or 1000 cycles with 10s rest between bouts showed more collagen type I gene expression and more pro-collagen type I protein than continuous loading alone (Huisman et al., 2014). Similarly, Scott et al. (2011), saw increased tenocyte proliferation with rest periods inserted between loading bouts (Scott et al., 2011).

TGFβ-1 has been associated with collagen synthesis in tendons, being capable of directly inducing collagen type I and collagen type III expression (Heinemeier and Kjaer, 2011). The role of TGFβ-1 has more specifically been implicated in the mechanotransduction signalling pathway of human tenocytes as the addition of TGFβ-1 seems to invoke a similar gene expression response to that created by the application of strain (Jones et al., 2013). This was particularly

evident with ADAMTS-5 where combining both loading and TGFβ supplementation increased expression more than loading alone. A previous study by Goodman et al. (2004), interestingly found the effect of TGFβ differed depending on the type of equine tendon the tenocytes were sourced from, i.e. from the energy storing SDFT or the positional CDET. The cultured mature CDET tenocytes showed increased proline incorporation and up-regulation of type I and type III collagen proteins with the addition of TGFβ-1 whereas the mature SDFT tenocytes only showed increased proline incorporation with the addition of TGFβ-1 (Goodman et al., 2004). Further studies using TGFβ inducible early gene (TIEG) knockout mice found that after tendon damage collagen type I expression was initially reduced in the knockout relative to the wild type, however expression became similar after 3 days (Tsubone et al., 2006). Therefore, although TGFβ is found to be related to collagen and the mechanotransduction signalling pathway, its involvement in tenocyte behaviour is still unclear.

Scleraxis expression is often used as an indicator for the tenocyte phenotype (Busch et al., 2013; Fong et al., 2013; Morita et al., 2013; Qiu et al., 2013; Schulze-Tanzil et al., 2004; Scott et al., 2011; Wagenhauser et al., 2012) and may be required for embryonic tendon differentiation (Schweitzer et al., 2001), although its specificity to tendons has been questioned (Benjamin et al., 2008; Scott et al., 2011). Other proposed tendon markers include tenomodulin, tenascin-C and Mohawk (James et al., 2008; Scott et al., 2011). Scleraxis has been reported to regulate collagen type I expression (Fong et al., 2013; Lejard et al., 2007), and knocking down scleraxis in tenocytes within collagen gels has shown reduced collagen density, while applying load maintains scleraxis expression (Scott et al., 2011) or causes up-regulation (Huisman et al., 2014).

Fatigue testing of tendon fascicles has shown microdamage and altered fascicle micromechanics (Thorpe et al., 2014). Studies replicating fatigue loading with rat patellar tendons have observed an up-regulation of collagen type III and collagen type V expression and down-regulation of collagen type I expression, which in combination signifies a possible

catabolic response (Andarawis-Puri and Flatow, 2011; Sun et al., 2010). Bovine and equine tendon fascicles tested with *in vitro* overload models have shown inflammatory markers IL-6 and COX-2 are expressed by tenocytes post loading, along with up-regulation of MMP-13 (Spiesz et al., 2015; Thorpe et al., 2015a). IL-6 has also been suggested to regulate TGFβ activity in a dose dependent manner (Zhang et al., 2005) and possess other roles in addition to both pro- and anti-inflammatory functions (Heinemeier and Kjaer, 2011; Scheller et al., 2011). Bovine tenocytes have been seen to increase IL-6 expression (Langberg et al., 2002; Legerlotz et al., 2013) while IL-6 itself has seen to stimulate collagen synthesis (Andersen et al., 2011).

Studies such as Jones et al. (2013) have focused on metalloproteinase expression in tenocytes as a response to loading, to identify instigators for anabolic or catabolic behaviours and those involved in tendinopathies. In a collagen gel system with human tenocytes, 5% cyclic strain down-regulated MMP-1 and MMP-13 gene expression after 24 hours loading while COL-1A1 was up-regulated (Jones et al., 2013). Tenocytes seeded on stiffer substrates have also been shown to down-regulate MMP-1 gene expression although no change in collagen type I expression was observed (Maeda et al., 2013a). Increase in collagen type 1 expression has been seen when loading fascicles from bovine extensor tendons (Legerlotz et al., 2013) and human tenocytes in a flexcell system (Huisman et al., 2014). Collagen type III expression has been seen to increase with cyclic loading of rat tail fascicles for 6 hours, up regulation of MMP-3 if loaded for 10 minutes and down regulation of MMP-13 if loaded continually for up to 24 hours (Maeda et al., 2009). Other studies have seen very little to no change with loading but could likely be attributed to differences in methods (Steiner et al., 2012).

The changes with loading and chemical stimuli discussed in this section, along with changes seen in tendinopathies, are summarised in Table 13. This information emphasises the complexity of interactions and uncertainty of roles of gene expression and protein level changes

observed during tendon loading. Therefore there is a need for further systematic investigation of tenocyte behaviour under physiological conditions to better understand these changes.

Table 13: Summary of changes seen due to tendinopathy, loading or chemical stimuli.

Tendinopathy	Loading		Chemical Stimulus
	In Vivo	*In Vitro*	
Cellularity increased [1,2,3,4] Matrix degeneration [1,2,3,4] Neovascularisation [1,2,3,4] Collagen type I increased [5,6,10] Collagen type III increased [5,12] Aggrecan increased [5,6] Biglycan increased [5,6] MMP-2 increased [5,6] MMP-13 increased [5,6] MMP-3 decreased [5,6] ADAMTS-5 decreased [5,6] Versican decreased [7] Tenascin-C increased [8] MMP-1 increased [3] TIMP-1 decreased [3] TIMP-3 decreased [9] ADAM-1 increased [9] MMP-11 increased [9] IL-6 increased [10] NO increased [11]	Collagen synthesis increased [13] Collagen type I increased [14] Collagen type III increased [18,19] Collagen type V increased [18,19]	Proliferation increased [17] Collagen synthesis increased [16,30] Collagen type I increased [15,16,22,23] Collagen type III increased [16,24] IL-6 increased [20,21,29] COX-2 increased [20,21] MMP-1 decreased [22] MMP-13 decreased [22,24] MMP-3 increased [24] Scleraxis increased [15,17]	Effect of NO: Increased collagen synthesis [25] Effect of TGFβ: Increased collagen type I [16,26], collagen type II [16,26], ADAMTS-5 [22], and cell proliferation [16]. Collagen synthesis also initially decreased [27]. Effect of IL-6: Increased collagen synthesis [28]

1) Busch et al. (2013), 2) Tallon et al. (2001b), 3) Fu et al. (2002), 4) Khan et al. (1999), 5) Corps et al. (2012), 6) Corps et al. (2006), 7) Corps et al. (2004), 8) Ireland et al. (2001), 9) Jones et al. (2006), 10) Legerlotz et al. (2012), 11) Szomor et al. (2006), 12) Riley et al. (1994b), 13) Miller et al. (2005), 14) Langberg et al. (1999), 15) Huisman et al. (2014), 16) Goodman et al. (2004), 17) Scott et al. (2011), 18) Sun et al. (2010), 19) Andarawis-Puri and Flatow (2011), 20) Spiesz et al. (2015), 21) Thorpe et al. (2015a), 22) Jones et al. (2013), 23) Legerlotz et al. (2013), 24) Maeda et al. (2009), 25) Xia et al. (2006), 26) Yang et al. (2004), 27) Tsubone et al. (2006), 28) Andersen et al. (2011), 29) Langberg et al. (2002), 30) Maeda et al. (2007).

1.5 Platforms for Tenocyte Study

The behaviour of tenocytes in response to loading and chemical stimuli discussed in the previous section were investigated by researchers using a number of different *in vitro* and *in vivo* systems. This in itself has been one of the underlying problems in characterising tenocyte behaviour under physiological conditions and is discussed here.

One common *in vitro* platform currently used is the Flexcell system. This commercial system combines a flexible membrane and a vacuum to provide a means for applying tension to cells (depicted in Figure 13). Flexcell culture plates, custom 6 well plates containing flexible bottom membranes, are first coated with a protein of choice. This is usually collagen type I in the case of Flexcell studies performed with tenocytes (Arnoczky et al., 2002b; Backman et al., 2011; Goodman et al., 2004; Huisman et al., 2014). Plates can be seeded with cells and positioned on top of loading posts (Figure 13a). Strain is applied via a programmable computer controlled vacuum under the cell seeded membranes. Generating a vacuum stretches and pulls the membrane down around the loading post, which in turn strains the cells attached to the membrane surface. Cyclic loading can be performed by modulating the vacuum to release and re-stretch the membrane. The mode of strain can be changed depending on the shape of the loading post; an equibiaxial strain can be applied using round posts or a largely uniaxial strain can be applied using rectangular (Arctangle®) loading posts.

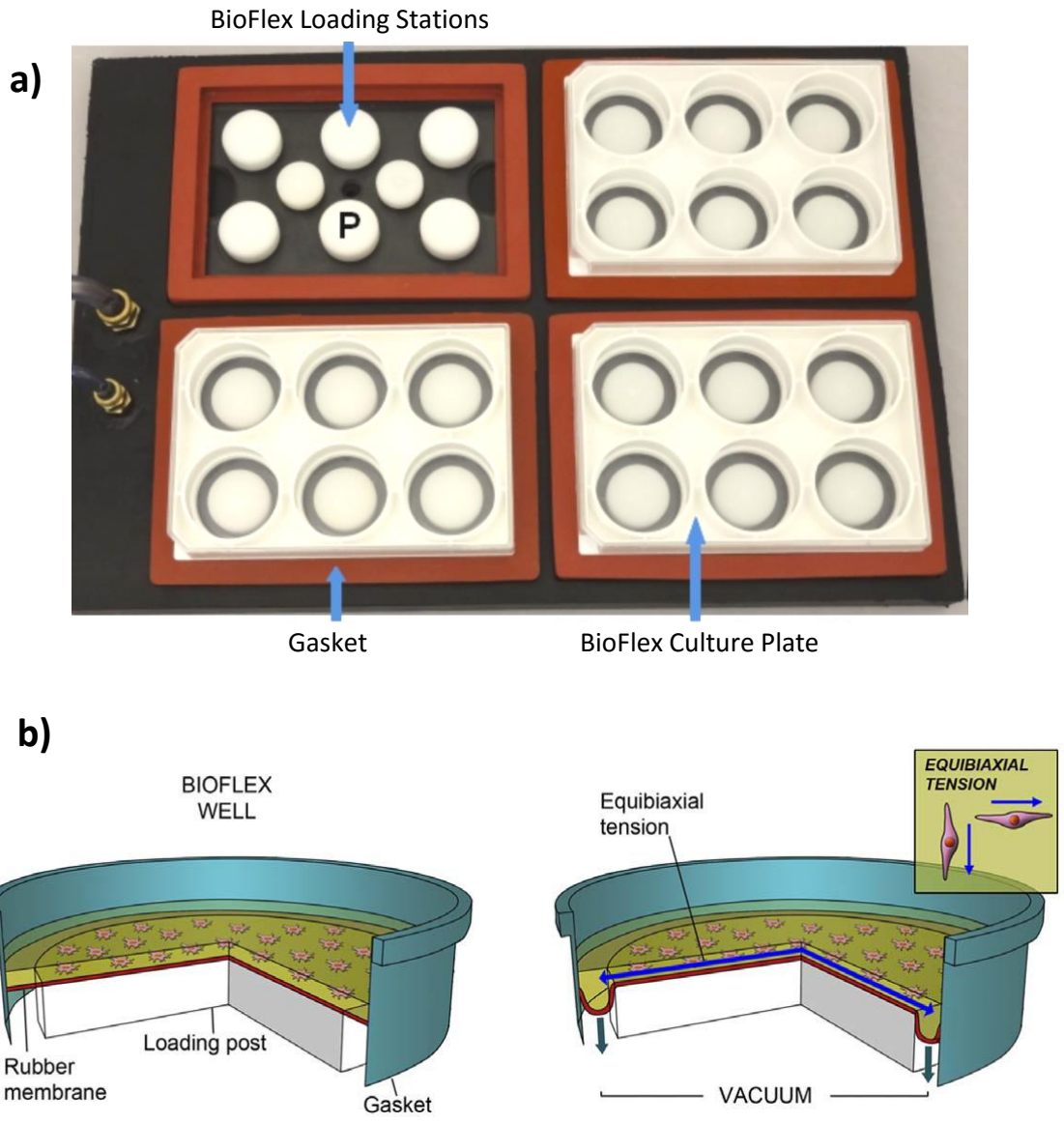

Figure 13: a) Flexcell system components including loading posts and custom culture plates with flexible membrane bases. b) Equibiaxial strain is applied to cells by controlling a vacuum which stretches the cell seeded membrane around a circular loading post. Uniaxial strain is applied by using rectangular (Arctangle®) loading posts. (Adapted from Frazer et al. (2009) and Backman et al. (2011)).

Although the Flexcell system is highly controllable and conditions reproducible, one obvious problem with this method is the limitation to a 2D mechanical environment. As cells are essentially a monolayer on the surface of the membranes, only strain is experienced by cells while shear is completely absent. Consequently, the cellular environment becomes significantly different to the 3D cellular environment of tendons, leading to reduced suitability of such systems in tendon research.

Indeed, due to the above limitation, a more 3D environment has been incorporated into the Flexcell system through the use of collagen gels on the surface of the membrane (schematic shown in Figure 14). Collagen constructs are fabricated within moulds in a 6 well plate. The mould is placed under the membrane and a vacuum applied to pull the membrane into the mould. A solution of collagen and cells can then be injected into the depression created and polymerised to form a 3D collagen gel. The vacuum is then released and the mould replaced with a loading post to allow strain application to the construct as described previously.

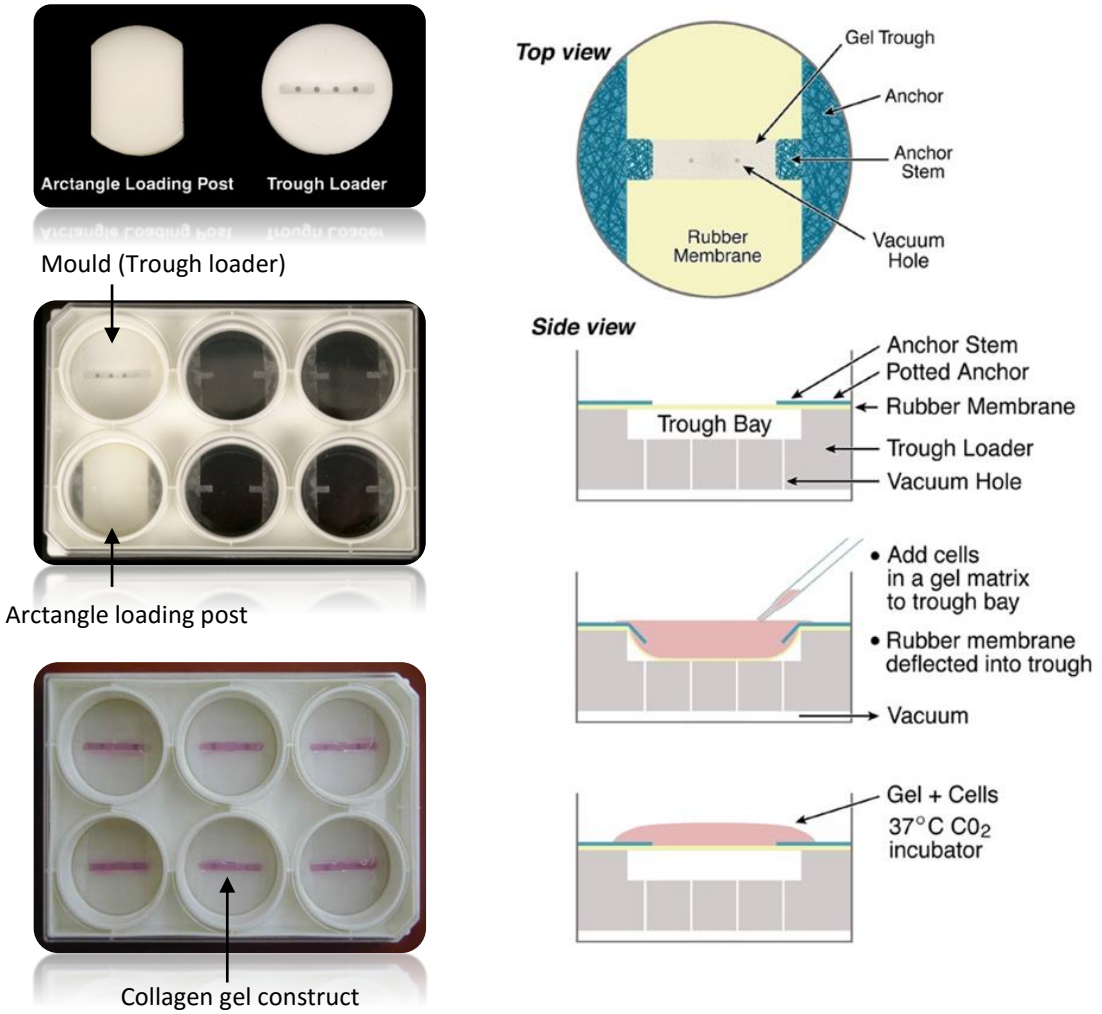

Figure 14: Flexcell system for 3D collagen gels (Tissue Train® Culture System). A trough loader is used as a mould around which the flexible membrane can be pulled. The collagen and cell solution is then added to the trough bay created, which can then be polymerised to create a collagen gel anchored into the Flexcell system. Uniaxial loading is then performed using the Arctangle® loading post. (Adapted from Banes et al. (2009)).

This system has been used in tendon related research (Garvin et al., 2003; Jones et al., 2013). However, although a 3D cellular environment is created, it is not necessarily the same as that found in tendons due to the nature of collagen gels produced. The properties of simple collagen gels made *in vitro*, such as fibril diameter, length and density can be altered by changing parameters such as gelation temperature, collagen concentration and solution pH (Yang et al., 2009; Yang et al., 2010). However, collagen fibres made in this manner still remain randomly orientated and thus present cells with a microenvironment starkly different to that found in tendons. Although some degree of fibre orientation can be induced through strain application (Vader et al., 2009), the lack of controlled fibre orientation in simple collagen gels leads to varying levels of tension transferred to cells during loading and an uncontrolled cellular shear environment.

The application of controlled shear has been achieved in some studies through the use of fluid shear. Maeda et al. (2013b) developed a system to apply controllable amounts of shear and tension to tenocytes (Figure 15). The system applied tension to a flexible cell seeded microgrooved membrane, with the microgrooves present to keep cells isolated in rows. Fluid was then moved across the surface of the cells at a controlled speed, with both tension and fluid flow applied in a uniaxial direction. However, this system was aimed at investigating interstitial fluid flow (Maeda et al., 2013b) and hence does not replicate the physiological shear generated by the movement of collagen fibres and fascicles in tendons.

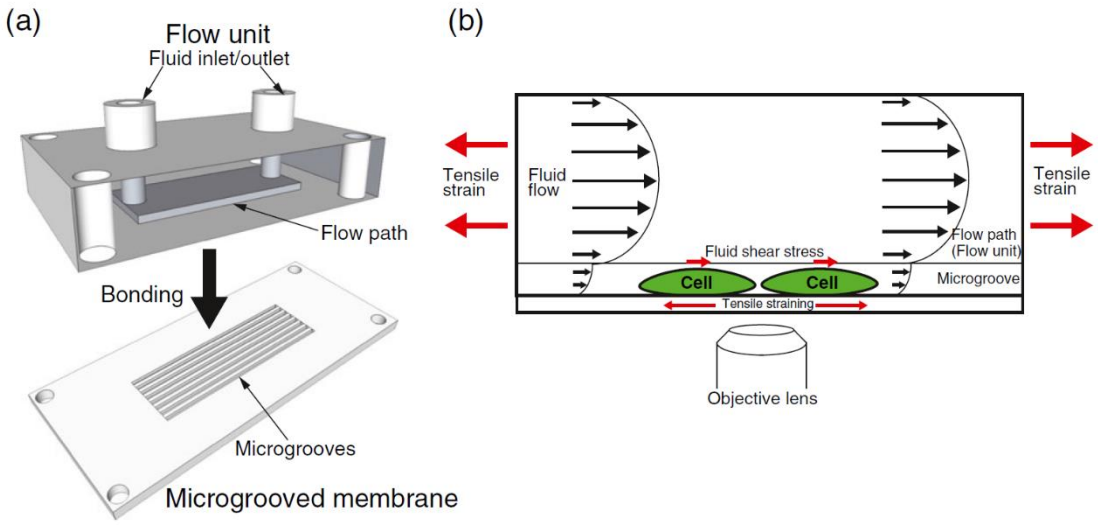

Figure 15: Tension and fluid shear strain system developed by Maeda et al., (2013). a) A Cell seeded microgroove membrane is placed within a concealed flow chamber. b) Fluid shear is created through moving medium from the inlet to the outlet, and cyclic strain is simultaneously created through stretching the membrane. (Adapted from Maeda et al. (2013b)).

Explants and *in vivo* models have been used in studies as an alternative to *in vitro* systems, overcoming the inability of current *in vitro* systems to appropriately recreate the physiological cellular environment in terms of tension and shear. For example, Fung et al. (2010) and Andarawis-Puri and Flatow (2011) employed a rat model (Figure 16) to investigate fatigue damage response in rat patellar tendons. However, although having the correct physiological environment, there are many difficulties with such systems. Firstly, it is extremely difficult to translate such methods into human models with ethical approval. The use of biological tissue also causes challenges as natural variations in structure and composition cannot be accounted for, reducing the reproducibility of experiments. Moreover, the use of biological tissue limits the amount of control a researcher has on the shear condition; the tissue provides the physiological tendon environment but the extent of cellular shear cannot be altered easily. Consequently the effect of varying magnitudes of shear on cellular behaviour cannot be investigated methodically. Other systemic changes also make it almost impossible to unravel exactly how the cells respond to a certain load condition.

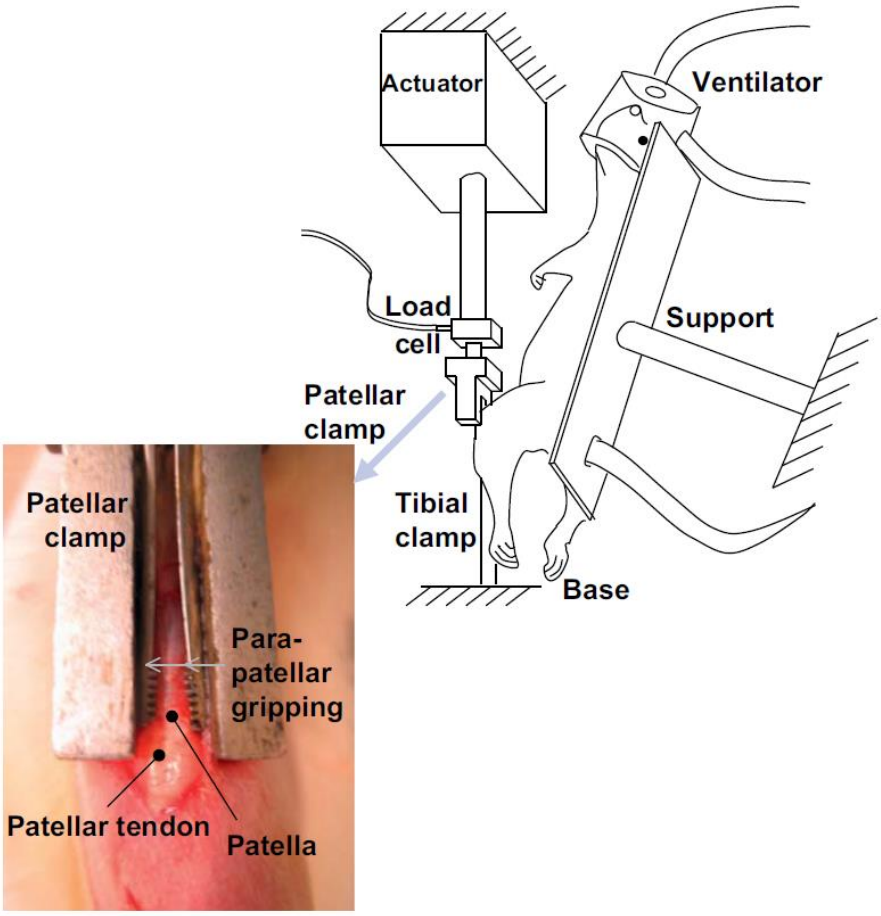

Figure 16: *In vivo* model used to fatigue load rat patellar tendons. The patellar tendons of anesthetised rats are connected to a load cell while the tibia is connected to a fixed clamp. (Adapted from Fung et al. (2010)).

Overall, there is currently no sufficiently controlled *in vitro* environment in which the cell response to precise, known levels of shear and tension can be investigated. The primary aim of this project was to address this need and provide a platform from which a host of physiologically representative mechanobiology questions can be addressed. Specifically, by developing a system more representative of physiological tendon conditions and with the ability to control the amount of tension and shear, tenocyte behaviour can be investigated more closely in a reproducible manner, helping to better understand the aetiology of tendinopathy.Aim, Objectives and Hypothesis

1.6 Project aim, objectives and hypothesis

1.6.1 Aim

To develop a system able to create and tightly control cellular shear-tension ratios, allowing the investigation of shear-tension ratio effects on tenocyte gene expression, particularly genes related to matrix turnover.

1.6.2 Objectives

- Create a system capable of controlling cellular shear and tension.
- Confirm the system can incorporate and maintain viable cells.
- Characterise the micromechanics and gross mechanics of the system to establish the range of shear-tension ratios producible.
- Ensure local mechanisms can recapitulate the physiological shear-tension ratio found in tendons (~40% of the applied strain transferred to fibre strain), as well as non-physiological high tension and high shear conditions.
- Test the effects of the shear-tension ratios on tenocyte gene expression.

1.6.3 Global Hypothesis

It is hypothesised that the shear-tension ratio is a mechanical cue sensed by tenocytes, involved in regulating tenocyte gene expression. Shear-tension ratios above and below those found physiologically in tendons will affect matrix related gene expression in tenocytes, and play a role in tendon homeostasis and tendinopathy development.

Chapter 2: Fibre Composite System Development

This chapter will focus on the development of the fibre composite system used to expose cells to both shear and tension. First some conventional materials used with cells will be briefly reviewed to provide context for the materials adapted in this study. This is followed by the concept of fibre composites, a review of a fibre composite system previously published and finally its further development into a functional system.

2.1 Biocompatible Materials

A simple method to narrow down potential materials for use with cells is to focus in on materials typically used for tissue engineering associated scaffolds as these have already been identified as biocompatible, avoiding material derived toxic effects. Scaffolds are defined as structures that provide mechanical support in addition to promoting cellular infiltration (O'Brien, 2011).

Materials currently used for scaffolds range from synthetic to naturally available degradable and non-degradable materials which can be used in vivo and in vitro. Materials currently used in clinical treatments tend to be resorbable as non-resorbable scaffolds lead to poor clinical performance (Ma and Elisseeff, 2005).

In addition to mechanical and chemical stimuli, cellular activity is also affected by the material surface. Hence, although a material may have the required gross mechanical properties, if the surface does not provide the relevant surface to promote cellular activity or provides incorrect strains at cellular level then the material becomes inadequate. This problem can in some cases

be addressed through surface modification which can be achieved through protein coating, peptide attachment, micro-patterning, or plasma (glow discharge) treatment.

There are two main categories of scaffold materials; natural and polymers. Both materials have their individual advantages and disadvantages due to the way they can be produced and their components, some of which will now be reviewed.

2.1.1 Natural Materials

The purpose of this section is to provide a feel for some natural materials available and their advantages and disadvantages. Hence a full materials review is not provided and only the two most commonly used natural scaffolds are discussed: a distinctive form of extracellular matrix (ECM) and different forms of collagen.

Extracellular Matrix (ECM)

The extracellular matrix (ECM) is the material surrounding cells and is frequently used for tissue engineering in altered states. ECM typically consists of fibrillar proteins (mainly collagen and fibronectin), GAGs, and glycoproteins. A common form of ECM used as a scaffold is decellularised xenogeneic ECM. This form is typically used for skin grafts and has very good biocompatibility since the cellular antigens are removed in the decellularising process, thus eliminating a foreign body response (De Boer et al., 2008). ECM also degrades over time and due to its composition can also be resorbed by the body. The rate of degradation varies depending on the presence of chemical cross links, with fewer cross links resulting in quicker degradation.

An ECM scaffold is prepared by decellularising the matrix through a combination of mechanical, physical and enzymatic processes and results in the removal of cellular and nuclear material (De Boer et al., 2008). Although ECM can be available with many different mechanical properties,

their load bearing capabilities are inadequate when it comes to replicating tendon function and therefore one layer of ECM is not enough for any purpose which is mechanically demanding. One solution for this inadequacy is through the use of multiple layers of ECM which is achieved by laminating hydrated sheets of the ECM under a vacuum (Badylak et al., 2005).

Another problem associated with using ECM or other natural materials in cellular studies is the remodelling capability of the material. ECM is considered a dynamic material as cells are able to extensively remodel it, consequently causing changes to the mechanical properties of the ECM over time (Gattazzo et al., 2014). This is beneficial for tissue engineering approaches as cells can help recreate the target tissue composition and structure, however this aspect also means the mechanical conditions of experimental samples cannot be kept constant for mechanotransduction studies, making the use of ECM for such studies unsuitable.

Collagen gels and sponges

The close arrangement of the polypeptide chains and the helices in collagen give rise to high tensile strength of collagen networks as stated previously in Chapter 1.

Collagen matrices have been used extensively in medical applications such as wound dressing and artificial skin due to the minimal inflammatory and antigenic response by the body. However the clinical applications of these matrices have been limited, due to their relatively low mechanical properties, fast degradation and the risk of viral infection when implanted into the human body (De Boer et al., 2008). Although there are disadvantages in using collagen, there are many collagen scaffolds still being used.

Collagen platforms are limited in their manufacturing methods due to the low thermal stability resulting from the proteins. Hence they cannot be processed via melt-based techniques and rely on solvent based techniques. One common form of collagen used is gel. Collagen gels do not have a pre-defined shape due to their high water content and therefore can be made into

any desired shape by using a mould. This allows them to provide a flexible environment and allows the possibility for the encapsulation of isolated cells. Due to their gel nature and non-orientated collagen fibres they are usually applied in conditions where initial mechanical function is not a requirement (Dumitriu, 2001), hence are commonly used in drug and cell delivery. This is done by mixing the required chemicals or cells with the gel which can then be either injected or implanted into the intended tissue site. The gels allow the steady release of encapsulated contents (the drugs or cells) through degradation. The release rate is therefore directly proportional to the degradation rate and requires the structure of the collagen gels to be customised to attain suitable degradation rates.

Sponges are another form of collagen with better mechanical stability, hence are often applied in more mechanically demanding situations. Collagen sponges have been seen to promote collagen production by cells (Ma and Elisseeff, 2005). One factor which affects cell growth and migration is the pore size. The pore sizes are regulated by controlling the manufacture techniques, such as freeze-drying, or by the degree of cross linking. Similarly the mechanical properties have also been seen to improve if the cross linking is conducted in a de-hydrothermal process (Lewandrowski et al., 2002). Generally, an increase in the intermolecular cross links results in an increased degradation time, since the collagen becomes less vulnerable to enzymatic attack, and also reduces the absorption capacity of water and increases its tensile strength (Lanza et al., 2000).

Both collagen sponges and gels have been used in a wide variety of scaffolds for various applications including cardiovascular valves, bone, cartilage, skin and periodontal ligaments connected to teeth (guided tissue regeneration). For these different applications, different methods are needed when processing the collagen. This is another advantage of collagen based systems as there are many side groups such as carboxylic, amino and hydroxylic groups, which consequently result in a wide range of possible chemical modifications. The processing of

collagen for the situations stated above include freeze-drying, with crosslinking occurring by thermal-dehydration, or by crosslinkers such as hexamethylenediisocyanate, carbodiimides and 1,6-diisocyanatohexane, gelation at various temperatures and solvent evaporation.

Although natural materials are biocompatible and used in some medical applications as described above, the mechanical properties are generally poor for load bearing situations. For the composite system specifically, there is a need for a material where its mechanical properties can be altered and are homogenous. This is a problem for the natural materials described, with collagen gels known to have problems with reproducibility and homogeneity (Plant et al., 2009). Additionally, optical transparency of the material is a beneficial aspect not provided by either ECM or collagen based gels. A transparent system would allow characterisation and investigation of cells encapsulated within, thus providing extra versatility for the system where future studies can investigate cell loading in conjunction with morphological changes or explore load mediated pathways such as calcium signalling (Wall and Banes, 2005). In summary, the limited fabrication options alongside the mechanical malleability and inhomogeneity in common natural materials leave them unsuitable for the current application.

2.1.2 Synthetic Polymers

Similar to the Natural Materials section, the purpose of this section is to touch on advantages and disadvantages of some synthetic polymers. Hence a full materials review is not provided, but a few common polymers reviewed.

Synthetic polymers are commonly used as scaffold materials due to their ease of fabrication and reproducibility compared to natural materials, which is especially valuable when scaffolds are made in large scales.

Poly (lactic-co-glycolic acid) (PLGA)

Poly (lactic-co-glycolic acid) (PLGA) is a commonly used biodegradable copolymer with good biocompatibility and biodegradability. The degradation rate of PLGA can be controlled by altering the content ratio of polyglycolic and polylactic acid (PGA and PLA) and hence allows the possibility to create PLGA for specific applications. The rate control mechanism is mainly due to the methyl group in PLA making it more hydrophobic than PGA and hence more resistant to hydrolytic attack; hence a higher ratio of PLA results in a slower rate of degradation (Laurencin and Nair, 2008). The properties of PLGA also differ depending on composition, but they typically possess a Young's modulus between 2-7 GPa (De Boer et al., 2008).

Although the control of degradation is beneficial in PLGA, it also surfaces as a disadvantage due to the nature of the resulting products. Lactic and glycolic acids are released when PLGA is hydrolysed; acids also present in metabolic pathways. The bulk degradation of PLGA results in the deposition of large quantities of both acids and causes the immune system to respond with local inflammation (De Boer et al., 2008). Another disadvantage of PLGA scaffolds is the low cellular adhesion. This is once again partly due to the hydrophobic nature of PLA which causes the surface of PLGA to also be hydrophobic and hence does not promote cell attachment. However, there are methods to overcome this in the form of surface treatments which are discussed later.

There are different ways to produce a PLGA scaffold such as using a mould or through the use of computer controlled micropositioner systems. Both these methods have been used in the construction of microfabricated scaffolds (Vozzi et al., 2002). The micropositioner with micro-syringe deposition method can be used with a number of different polymers and utilises a three axis micropositioner connected to a computer. A micro-syringe provides an extremely fine tip and hence the whole computer based system can achieve a precision of about 0.1 µm. The second method uses 'soft lithography' approaches. A poly-dimethylsiloxane (PDMS) mould is

soaked in a PLGA solution, put in a vacuum to allow the PLGA to displace any air present and then exposed to UV light (Vozzi et al., 2002). Both methods produce usable PLGA scaffolds but approach the problem differently. The micro-syringe method produces scaffolds with high precision and the procedure allows the production of exact duplicate scaffolds. However, with the use of a machine and computer designed scaffolds, this method becomes expensive and takes time to produce large batches. The second micro mould technique has the advantage of creating a mould quickly which can be used repeatedly for a faster turnover as compared to the previous method. However, with the increase in speed and decrease in cost, there is a loss in accuracy; the scaffolds produced will not be exactly the same as the mould or to the next/previous scaffold produced.

Poly (2-hydroxyethylmethacrylate) (PHEMA)

Poly (2-hydroxyethylmethacrylate) (PHEMA) is a thermoset hydrogel with good biocompatibility which has been used in a variety of medical applications in the past. PHEMA is also a non-degradable material and hence it cannot be broken down by the mechanisms of hydrolysis (even in the presence of strong acids and alkali) or by enzymatic activity (Schiraldi et al., 2004). However, through the use of different crosslinkers, such as those based on divinyl-functionalised acetal, it is possible to produce degradable PHEMA (Bulmus et al., 2007). Although PHEMA is considered biologically inert, it is still permeable to metabolites meaning it can be used to serve many roles, thus leading to it popularity as a biomaterial.

The synthesis and polymerisation of PHEMA was first conducted in the early 1960's by Otto Wichterie and Drahoslav Lim which was followed by great interest and many experiments. One of the more successful uses of PHEMA is in contact lenses, with the first commercial contact lenses being sold in 1971 by Bausch and Lomb (De Boer et al., 2008). PHEMA is still currently being used in some contact lenses with its success due to the transparent nature of the hydrogel and its permeability.

The properties of PHEMA gels can change depending on how they are prepared, the polymer volume fraction and the temperature. For example, if HEMA monomers are polymerised in a waterless environment, the resulting PHEMA has a glassy look and hardness comparable to that of bone (Filmon et al., 2002), whereas if the PHEMA is swollen in water they become softer depending on the water content and can have an opaque appearance (De Boer et al., 2008). The first PHEMA scaffolds which used this opaque variant were termed 'sponges' and were seen to allow cells to penetrate into their pores. They also had the added advantage of withstanding autoclaving and the ability to be formed into different shapes (ideal for soft tissue replacements). Clinical trials were conducted where PHEMA variants were used as a breast implant material. However, the scaffolds were found to undergo calcification in long term in vivo environments preventing further development in this area (De Boer et al., 2008).

The effect of cross linking agents in PHEMA polymerisation have been explored previously by studies such as that by Mabilleau et al. (2006). It was seen that the Young's modulus of hydrated PHEMA can vary from 1.83 ± 0.07 MPa to 18.03 ± 1.36 MPa while the dehydrated state gave a Young's modulus ranging from 696.44 ± 5.55 MPa to 923.77 ± 5.00 MPa. These samples were prepared using benzoyl peroxide as the initiator, adding ascorbic acid as an accelerator and heating to 50°C for 2 hours (Mabilleau et al., 2006). There are a few methods to polymerise and make PHEMA scaffolds along with many choices of cross linkers. These cross linkers include ethylene glycol dimethacrylate, 3-oxapentamethylene dimethacrylate, 2,3-dihydroxytetramethylene or trimethylolpropane trimethacrylate (Salamone, 1996).

One method to prepare PHEMA is phase separation. Thermally induced phase separation (TIPS) has been used in tissue engineering to produce many scaffolds including those consisting of PHEMA. This technique uses the lowering of the temperature to reduce the solubility of the polymer and hence produce the scaffolds. There are two types of TIPS which are known as liquid-liquid phase and solid-liquid phase separation.

The liquid-liquid phase method is a result of the heated homogenous polymer solution separating into two polymer concentrations, high and low, as it cools. These two regions result in different structures with the high concentration area crystallising to create dense foams while the less concentrated region forms a highly porous material. The result of varying concentrations can be seen in Figure 17. The solid-liquid phase technique is similar to the aforementioned phase separation method except it is used when the freezing point of the polymer is higher than the liquid-liquid phase separation temperature, and hence the polymer solidifies whilst in the homogenous state when the temperature is lowered (Ma and Elisseeff, 2005).

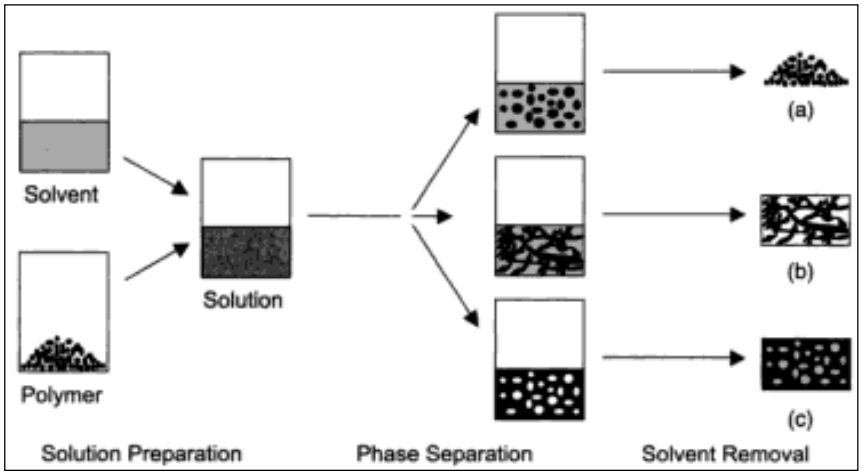

Figure 17: Illustration of the resulting three fabrication types with phase separation. a) Powder. b) Continuous networks. c) Foam with closed pore. (Adapted from Ma and Elisseeff (2005)).

Another method to polymerise HEMA is by photopolymerisation. There are three requirements in photopolymerisation; electromagnetic radiation, chromophore-containing photoinitiators and monomers containing groups such as styrene, acrylate or methacrylate (vinyl groups) (Wnek and Bowlin, 2004). Specific wavelengths of visible light (400-800nm) and ultraviolet light (190-400nm) can be used in the polymerisation, with the required wavelength depending on the photoinitiator used. The role of the photoinitiator is to create reactive free radicals to initiate the polymerisation of the monomers. As light is needed, this method requires

transparent moulds/surfaces in the fabrication process to allow light to pass through with sufficient intensity.

The mechanical properties of PHEMA can be customised to be suited for different applications with different structural requirements (e.g. requirements differ when used in contact lenses and bone scaffolds). The different methods described for manufacturing PHEMA based materials also provides a degree of manufacture flexibility. For example, if any toxic or unwanted side effects are encountered due to the additives, a different method for production can be used.

Poly (ethylene glycol) (PEG)

Poly-(ethylene glycol) (PEG), also known as Poly-(ethylene oxide) (PEO), is another commonly used hydrogel and consists of two hydroxyl group terminals. PEG is readily soluble in water and many organic solvents, and the hydrophilic nature of PEG has commonly led to its use as a dehydrating agent in studies (Rigozzi et al., 2013). The end groups of PEG can be easily modified allowing the possibility for many synthetic reactions such as acryloyl chloride or methacryloyl chloride with triethylamine to produce photoreactive vinyl group (Ifkovits and Burdick, 2007).The properties of PEG itself differ depending on its molecular weight. For example, the compressive modulus is seen to be around 34.2 $\pm$ 3.3 kPa for 4600 g/mol PEG where as a molecular weight of 10000 g/mol reduces the compressive modulus to 18.6 $\pm$ 2.4 kPa (Ostroha, 2006).

Two common techniques to produce cross linked PEG networks are chemical cross linking and radiation cross linking (Ratner and Bryant, 2004). Chemical cross linking can be achieved using the hydroxyl groups present. For example, PEG can be mixed with a triol and a diisocyanate to produce the polymers in a dehydrated state. Catalysts such as tin can also be used for the cross linking process but the toxic affects need to be taken into account when considering this

method for biological use (Harris, 1992). Radiation cross linking is a method which produces water swollen polymers and is a preferred technique as the addition of potentially toxic cross linking agents are not required.

PEG is usually used in producing polymer blends or copolymers. This is done to increase the hydrophilicity, biocompatibility or softness of the resulting material. These hydrogels have very different properties depending on the type of blend made. For example, poly (propylene fumerate-co-ethylene glycol) has been used for cardiovascular applications but, with further modifications using pore forming agents and cell adhesive ligands, the resulting porous scaffold can be used for bone tissue engineering. Degradable PEG based polymers can also be produced similar to oligo (polyethylene glycol) fumerate which has been used in guided tissue regeneration (Ratner and Bryant, 2004).

Many different PEG based hydrogels can be made, and its extensive use in cell based applications ensures PEG is viewed as a versatile material in the medical field especially since it can be used to alter biocompatibility of other materials (i.e. through PEG coating), allows nutrient diffusion and has a wide range of possible chemical modifications including the coupling of proteins and peptides (Leslie-Barbick et al., 2009; Roberts et al., 2002).

In summary, the customisable chemistry and mechanical properties of synthetic polymers provide an advantage over natural based materials. The synthetic materials can also be made with varying degrees of optical transparency which many natural materials lack. The biocompatibility benefit of natural materials can be matched with some synthetic polymers as described above, therefore overall some synthetic polymers, such as PHEMA and PEG, are ideal versatile materials which can be used in the fibre composite system.

2.2 Fibre Composite Concept

A composite material is known as a "material made by dispersing particles of one or more materials in another" (Piggott, 2002), hence forming a continuous network. Although the properties of the individual materials involved in a composite material remain unchanged, in some instances the overall material property may be considerably different. Composites can be characterised into two main categories; Particulate Composites and Fibrous Composites. The mechanical properties of fibrous composites tend to be better than particulate composites due to their long fibre like components and some polymer-fibre composites are known to have stiffness and strength equivalent to metals (Ratner and Bryant, 2004). The different types of classifications and sub-classifications are illustrated below in Figure 18.

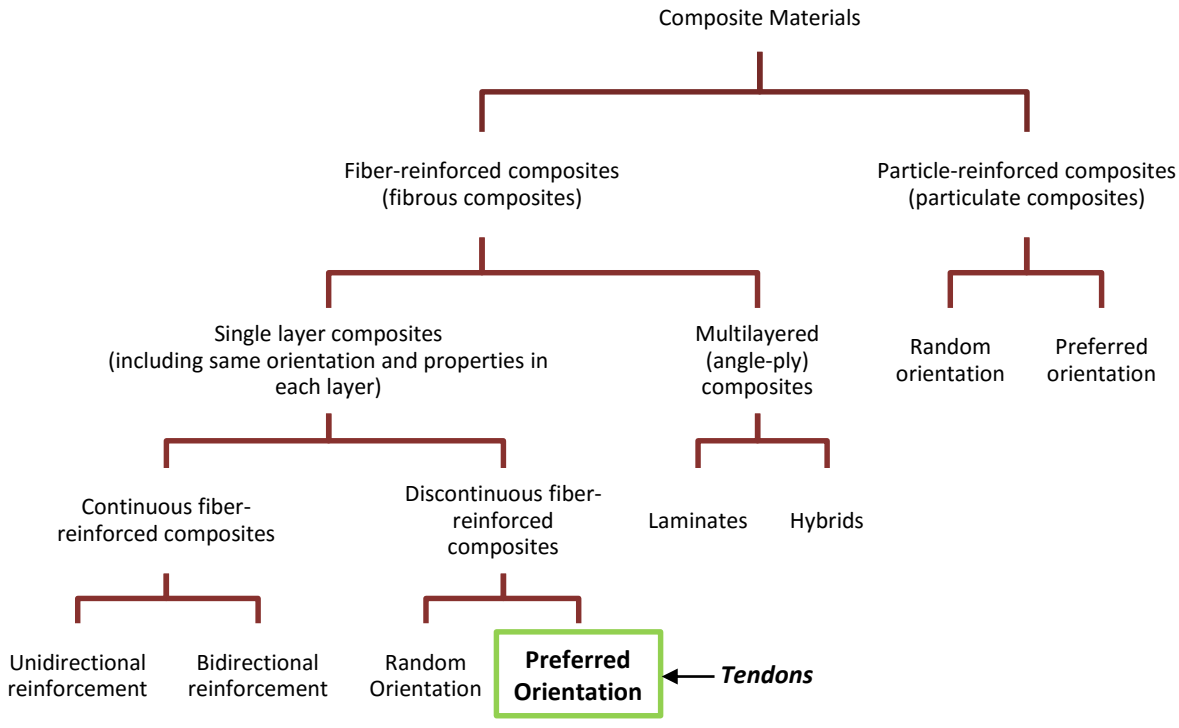

Figure 18: The different classifications of composite materials with the branch best describing tendons indicated in green. ***(Adapted from Ratner and Bryant (2004)).***

Tendons can be classified as a composite material at the molecular and micro-structural level (Ratner and Bryant, 2004). More specifically, tendons can be described as natural multilevel fibre composites classified as a fibre-reinforced composite with discontinuous fibres in a preferred orientation (Figure 18). Therefore an ideal way to imitate their behaviour is by the use of such fibre composites.

2.2.1 The effect of Fibre Orientation

The organisation of the collagen fibres and their bonds (both inter and intramolecular), play a vital role in providing the known tensile strength of tendons. The effect of fibre organisation is also seen in fibrous composite constructs.

The theoretical curve in Figure 19 for the Young's modulus in composites depends on the angle (θ) at which the fibres are orientated with respect to the direction of load - the difference between the principle fibre direction and the stress direction.

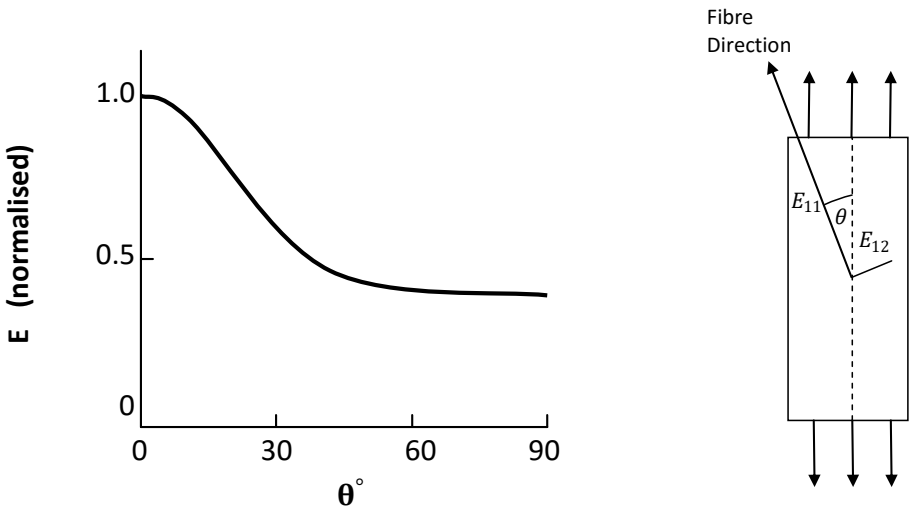

Figure 19: Graph and schematic drawing showing the effect of fibre orientation. The graph shows the change in Young's modulus against the angle θ, while the diagram depicts how θ is measured. (Adapted from Hancox (1981)).

It can be seen that as the fibre orientation changes, the Young's modulus exhibited by the material also changes, with the peak modulus occurring when both the load and fibre orientation are in the same direction. Hence the material property can be customised through the orientation of the fibres and the effect of the orientation on the Young's modulus can be modelled using the related equations (Hancox, 1981).

The actual forces on the individual fibres can be found using the simple stress relationship:

$$\sigma = \frac{F}{A}$$

Where σ is stress, F is force and A is cross sectional area. This can be simplified for fibres such that;

$$\sigma = \frac{F}{\pi r^2} \quad \text{or} \quad F = \pi r^2 \sigma$$

2.2.2 The Shear Lag Model

There are two common models used to estimate the shear stresses within fibre composite materials. The first model was derived by Cox (1952) and is known as the shear lag model. This model assumes that the load applied to the construct is transferred from the matrix to the short fibres by shear (Soboyejo, 2002). This model also assumes that the displacement in a fibre in the composite material is proportional to the displacement in the fibre and the matrix of the material. The longitudinal Young's modulus is therefore given by the equation (when it is assumed that the stresses at the end of the fibres are zero, $\sigma_0 = 0$);

$$E_c = V_f E_f \left[1 - \frac{\tanh\left(\frac{\beta l}{2}\right)}{\left(\frac{\beta l}{2}\right)}\right] + E_m V_m$$

Where:

E_c = Modulus of elasticity of composite

E_f = Modulus of elasticity of fibre

E_m = Modulus of elasticity of matrix

l = Length of fibre

V_f = Fibre Volume fraction $\left(\text{Where } V_f = \frac{A_f}{A_c} \right)$

V_m = Matrix Volume fraction $\left(\text{Where } V_m = \frac{A_m}{A_c} \right)$

Also;

$$\beta = \frac{G_m 2\pi}{E_f A_f \ln(R/R_f)}$$

Where:

G_m = Shear modulus of the matrix

R = The mean separation of the fibres

R_f = Radius of the fibres

The shear lag model, whilst a simple model of fibre behaviour and used to model tendons (Ahmadzadeh et al., 2013), has been hypothesised to not produce accurate stress distributions, and hence other methods could be used to provide alternative modelling (Lee and Suh, 2006).

2.2.3 The Tyson Critical Length

To load short uniaxial fibres embedded within a matrix to their maximum strength, the matrix must be able to sustain the shear deformation. When short fibres are subjected to tensile stress, stress build up occurs at the edges of the fibres and, if the fibre is long enough, plateaus to a constant maximal value (Hancox, 1981). This is demonstrated in figure 10 where three different fibre lengths are compared and once the fibre length reaches a critical value, the normal stress reaches its maximum value.

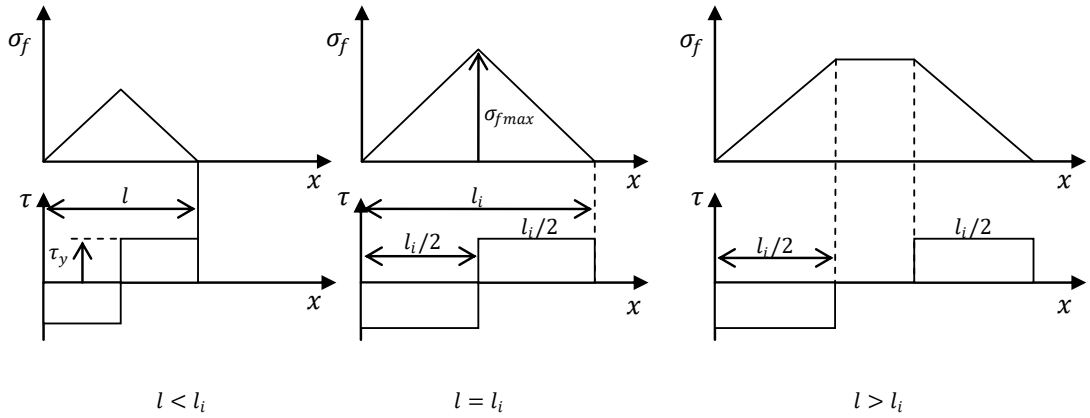

Figure 20: Graphs comparing the stress distribution against three distinct different fibre lengths using the Tyson model. Where $l_i = l_c = \text{critical length}$ and x denotes the fibre length. (Adapted from Lee and Suh (2006)).

If the fibres are shorter than this critical length the fibre will fail due to its inability to withstand the shear and not due to fracturing as the fibres will not reach their fracture stress. The equation for the critical length is given as:

$$l_c = \frac{D\sigma}{2\tau} = \frac{R\sigma}{\tau}$$

Where:

l_c = Critical length

D = Fibre diameter

R = Fibre radius

σ_f =Tensile stress on fibre

τ = Shear stress

This leads to a simple force balance described using the formula;

$$\tau = \sigma_f \frac{R}{4l_c}$$

Where:

τ = Shear stress on fibre

σ_f = Tensile stress on Fibre

The critical length and fibre strain depend on the fibre stiffness and shear strength of the interface between the matrix and the fibres, two parameters which can be manipulated to alter the local mechanics of the composite.

2.3 Fibre Composite Development

The hierarchical structure of tendons, with multiple fibres making up fascicles and fascicles grouped together to make tendons, creates a complex cellular environment. When a tendon is stretched the fibres within both stretch and slide (Rigozzi et al., 2013; Sasaki and Odajima, 1996a; Shepherd et al., 2014; Thorpe et al., 2013b). Studies have found the fibres to stretch by approximately 40% of the applied strain in physiological tendons (Shepherd et al., 2014). This consequently creates both tension and shear for the cells within tendons. The purpose of developing a fibre composite system is to be able to reproduce this cellular shear and tension environment seen in tendons. Achieving this would allow tenocyte mechanotransduction studies under tightly controlled reproducible conditions. Studies targeted for investigation using this system include the matrix related gene expression of tenocytes, derived from both healthy and tendinopathic tissue, and the gene expression changes in response to different shear/tension ratios. This will help address the implications of shear in tendon matrix turnover and tendinopathy.

The requirements for such a system primarily include the ability to both create and control cellular shear and tension ratios. Without being able to control this, the effects of varying magnitudes of shear and tension, including physiological equivalents, cannot be investigated and compared. The system must be able to support the incorporation of cells and maintain their viability. Subsequently, the system must also be able to permit diffusion of nutrients and other solutes from encompassing media. This aspect also provides versatility to the system, allowing use in future studies where response to additives such as growth factors can be investigated. Similarly, optical clarity of the system is another requirement providing a more useful system as encapsulated cells and components can be imaged and monitored easily.

The first fibre composite system designed for exposing cells to shear and tension was initially developed by Screen et al. (2010). This system was based on two hydrogels; poly (2-

hydroxyethyl methacrylate) (PHEMA) and poly (ethylene glycol dimethacrylate) (PEGDM). To manufacture the composites, fibres of PHEMA were made using a photopolymerisable solution consisting of 80% 2-hydroxyethyl methacrylate (HEMA), 2 mol % tetraethylene glycol dimethacrylate (TEGDM) and 1.5% Irgacure 651 (a photoinitiator) in ethylene glycol and water (1:1.33). This solution was injected into a mould and exposed to UV light (~4 mW cm^{-2} of 365nm wavelength light) to produce fibres averaging 2.80 mm in length and 0.36 mm in diameter when swollen. Collagen was then immobilised on the surface of these fibres via the use of the coupling agent 1,1'-carbonyl diimidazole (CDI) which creates carbamate groups able to react with amines present in collagen. This process essentially changes the fibre surface to promote cell attachment. These fibres were then seeded with cells and encapsulated in a PEG matrix made by mixing 10 wt% PEGDM with 0.05% Irgacure 2959 (a photoinitiator) and polymerising under UV light (365nm wavelength at ~4 mW cm-2).

The study by Screen et al. (2010) characterising this composite without cells found mechanical properties of the system could be customised through altering the fabrication process: increasing the time PHEMA fibres were left to dry and soak in PEG solution prior to polymerisation resulted in higher moduli and ultimate tensile strength (UTS). This study also demonstrated cell attachment onto collagen type I coated PHEMA fibres. A comparison of fibroblasts in the composite under loading to that in 2D culture and unorganised 3D encapsulation showed a significant increase in collagen type I gene expression in the composite.

Although the properties of the individual components of the above system could be customised and cellular shear created, a couple of significant limitations were present. The first was the system using fibre 'drying' as a method to change micromechanics: a combination of drying PHEMA fibres and leaving them to soak in PEG was required to increase the extent of matrix integration into fibres, which in turn changed the composite micromechanical properties and consequently the shear/tension ratio. However, the process of drying fibres would kill the cells

attached to the surface of the fibre. Thus, the only viable composite type created by this system would be one where the fibres are not dried, resulting in only one composite type: a high shear-low tension environment. The second problem seen with this system was an observation of the composite fragility seen personally by Dr Screen and Dr Bryant. Composites were seen to readily tear at the fibre/matrix interface once the fibres were coated in collagen, indicating a poor matrix-fibre interface.

Therefore further development of the above fibre composite system was performed to address these limitations and achieve the desired system as described at the beginning of this section.

2.3.1 Characterising Collagen Coupling via 1-1'-Carbonyl Diimidazole (CDI)

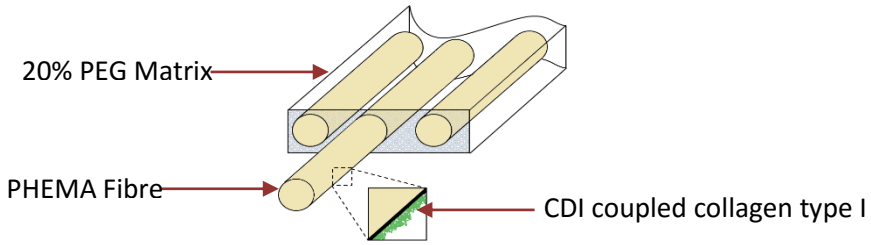

The system described by Screen et al. (2010) was used as the basis for development. The limited feasible shear/tension properties produced by this system were first addressed by using an additional PHEMA fibre stiffness. This was done by using 65% PHEMA, resulting in less stiff fibres compared to the original 80% PHEMA. A less stiff fibre would theoretically stretch more than a stiff fibre when the composite is stretched and consequently result in less matrix sliding against it. Further characterisation of the matrix-fibre interface was also performed to determine the cause of the weak interface following collagen immobilisation. Collagen immobilisation is performed in two stages, first PHEMA modification via CDI (CDI reaction), then coating with collagen type I (collagen coating), with the contribution of either to the interface weakness unknown. Therefore both steps involved in collagen immobilisation were investigated to determine their individual effect on the extent of matrix-fibre integration.

Experimental Overview

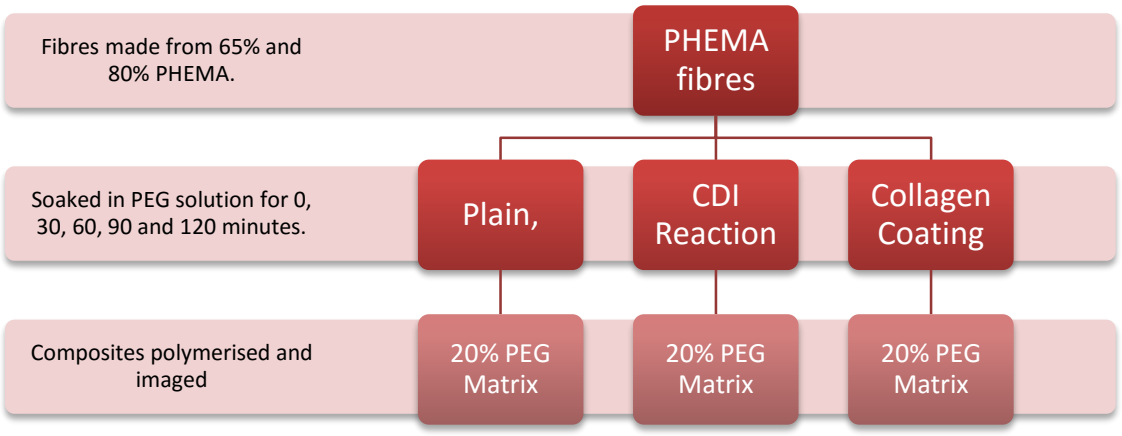

Figure 21: Flow diagram for studying the effect of CDI coupling and collagen coating on the matrix-fibre interface.

Methods

Note 1: Procedures performed at room temperature (RT) unless stated otherwise.

Note 2: Further details of all chemicals used, including supplier details, are present in Table 35 and Table 36, in Appendix B: Chemicals and Materials List.

PHEMA Fibre Production

Fibres of two degrees of stiffness were made by preparing pre-polymer solutions of 65% and 80% PHEMA. The pre-polymer solutions were made by combining 2 mol% TEGDM and 1.5% w/v Irgacure 651 in ethylene glycol and deionised water (1:1.33) with either 80% v/v HEMA for an 80% PHEMA solution or 65% v/v HEMA for a 65% PHEMA solution. This was done in 5 mL vials and the solution vortexed to ensure the Irgacure 651 was fully dissolved. The solutions were then labelled fluorescently by adding 0.1% w/w fluorescein methacrylate. This entire solution was wrapped in foil to protect from light and stored at 4°C.

The pre-polymer solutions were polymerised into fibres by using Teflon moulds containing holes of 0.3 mm diameter and 4 mm length (Figure 22). The outer mould edges were first lightly smeared with silicon grease and placed on top of a glass slide (75 mm x 25 mm x 1 mm) to create a liquid tight seal. The PHEMA pre-polymer solution was then pipetted into the holes and another glass slide placed on top once full. Bulldog clips were used to hold the glass slides and mould together. The solution was then polymerised by placing under 365nm UV light (~4 mW/cm^2) and leaving for 10 minutes with the entire assembled mould turned over after the first 5 minutes to ensure the UV light penetrated and polymerised the whole fibre. Resulting fibres were termed 65% or 80% PHEMA.

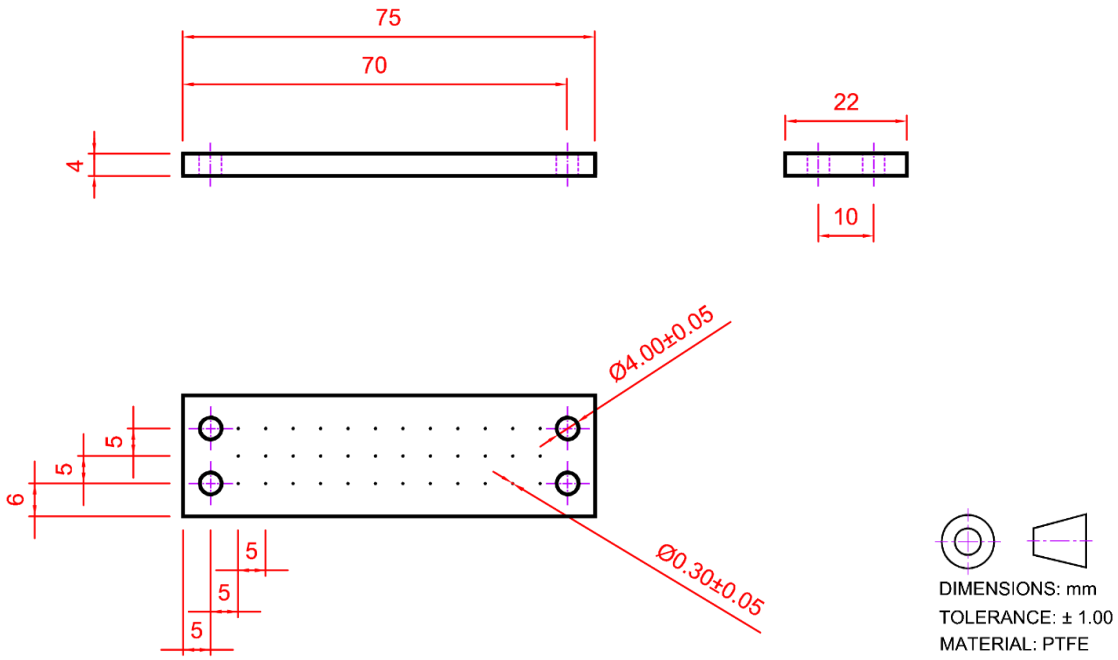

Figure 22: CAD drawing of Teflon mould used for creating fibres. Mould contains 36 holes of 0.3 mm diameter and 4 mm length.

Once polymerised, fibres were extracted from the mould by peeling away the glass slides. Most fibres remained attached to the bottom of the glass slide and could be cut away at the base. The fibres remaining in the mould were retrieved using a thin wire (diameter <0.3 mm) to push them out of the holes. The PHEMA fibres were stored in 70% ethanol until ready for the fibre treatment stage.

Fibre Treatment

To assess the stages involved in collagen immobilisation PHEMA fibres were either kept plain (i.e. untreated), coupled with CDI (stage 1) or coupled with CDI and coated with collagen (stage 2).

Fibres to be reacted with CDI were stored in 50% methanol and 50% water for at least 1 hour, after which they were transferred into clean vials with 70% ethanol and left for a minimum of 2 hours. Vials containing fibres were covered with parafilm which was perforated using a syringe

needle to allow the ethanol to evaporate. These vials were placed in a vacuum oven to speed up the drying process. Once dried, vials were transferred into a sterile hood with the integrated UV lights on to sterilise the fibres. From this point forward the fibres were treated as sterile. After 30 minutes the parafilm was removed and the vial half filled with 100% dry acetone. With the lids placed back on, the vials were sonicated for 30 minutes after which the dry acetone was replaced while in a sterile hood and then re-sonicated. This sonicated rinse process was done for a total 3 times.

Acetone was removed from the vials after the final rinse and the fibres left to air dry in a sterile hood. A 20 mM CDI acetone solution was created and added to the vial containing fibres and left to react for 5 minutes on an orbital shaker. The CDI solution was removed following the reaction and 3 more sonicated rinses were performed with acetone. After the third rinse the acetone was removed, fibres left to air dry for 1 minute and then stored in phosphate buffered saline (PBS) at 4°C. These fibres were labelled as 'CDI reacted'.

For collagen coated fibres a 0.3 mg/mL sterile collagen solution was made by mixing Type I rat tail collagen with a sodium bicarbonate buffer, prepared by mixing sodium bicarbonate in deionised water and adjusting the pH to 10.4. Taking CDI reacted fibres after their final sonicated rinse and air drying, rather than transferring to PBS, 2 mL of the prepared collagen solution was added to each vial. This was left for 48 hours at 4°C on an orbital shaker after which the fibres were rinsed in PBS, labelled as 'Collagen coated' and stored in cold PBS at 4°C.

Matrix PEGDM Solution

The procedure for making a stock quantity of PEGDM can be summarised as two procedures; methacrylation followed by purification.

Methacrylation consisted of weighing a known quantity of 3000 molecular weight polyethylene glycol (PEG) in a microwaveable 20 mL glass vial and adding trace amounts of hydroquinone. This was microwaved for 5 minutes at 400W and left to cool for another 5 minutes. Depending on the quantity of PEG weighed, a 10 fold molar excess of methacrylic anhydride was added, the vial purged with argon and then briefly vortexed to mix the solution. This was microwaved for a total of 10 minutes at 400W, with a cooling period of 10 minutes after the first 5 minutes.

Following methacrylation, polyethylene glycol dimethacrylate (PEGDM) was precipitated and purified to remove reaction by-products and unreacted methacrylic acid. First the vials were left to cool for at least 30 minutes after methacrylation. The supernatant liquid was removed and enough dichloromethane added to each vial to dissolve the PEGDM (~25% w/v). The PEGDM was then precipitated in cold diethyl ether (10:1 v/v to dichloromethane used) and the solution kept moving using a magnetic stir bar and plate. Using a vacuum flask, pump, Buchner funnel and Whatman Grade 1 filter paper the solution was filtered and collected in a beaker shielded from light. The collected PEGDM was re-dissolved in dichloromethane and re-precipitated in diethyl ether to further purify the product; a process repeated a total of 3 times. After the final collection, the PEGDM was protected from light and left to air dry for a few days. The percentage methacrylation was confirmed by performing 1H nuclear magnetic resonance (NMR) spectroscopy.

For the composite matrix a 20% PEGDM solution was made by first preparing a stock solution of the photoinitiator Irgacure 2959 at 0.006 g/mL in PBS. This solution was left in a water bath at 37°C for a week until the photoinitiator had fully dissolved. A mixture of 20% w/v PEGDM, 0.05% w/v Irgacure 2959 and PBS was then prepared in a 5 mL vial and vortexed until the PEGDM had dissolved. This solution was labelled fluorescently by adding 0.02% w/w Rhodamine methacrylate and protected from light.

Composite Production

Composites were made by surrounding the different types of PHEMA fibres in PEG solution and then polymerised to make the final composites.

For initial studies of the integration of PEG into PHEMA fibres, simple cylindrical moulds for the PEG solution were adapted by trimming the ends off 1 mL syringes (Figure 23). The fibres were placed in these trimmed syringes and 100 µL 20% PEGDM solution pipetted in slowly to submerge fibres without bubbles. Two fibres were present in each syringe and left to soak in this solution for 0, 30, 60, 90 or 120 minutes before proceeding to the polymerisation step. When ready for polymerisation, filled syringes were placed under 365nm UV light at 4mW/cm^2 for 10 minutes after which they were collected and rinsed in PBS. 6 repeats were made of each test condition.

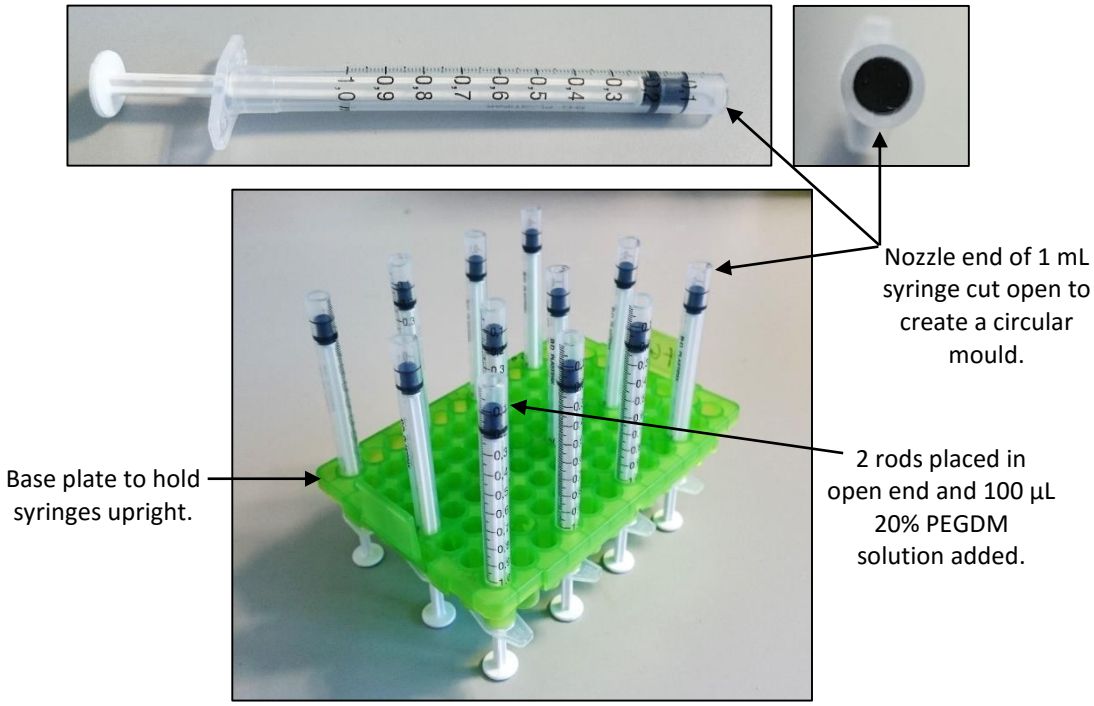

Figure 23: Circular moulds. 1 mL syringes were cut at the nozzle end and used as moulds for cylindrical composites. A pipette tip holder from a 200 µL pipette box was used as a base plate to hold multiple trimmed syringes vertical.

Confocal Imaging and Analysis

Composites were imaged via confocal microscopy and the fluorescent fibres and matrix excited using Argon and He-Ne lasers. The extent of fibre-matrix integration was calculated by measuring the distance Rhodamine labelled PEG matrix (red) was present past the boundaries of the fluorescein labelled PHEMA fibres (green) using ImageJ. Two PHEMA fibres were analysed in each composite, with three measurements taken on either side of each fibre. Thus each gel provided 6 measurements. An example of the measurements is shown in Figure 24.

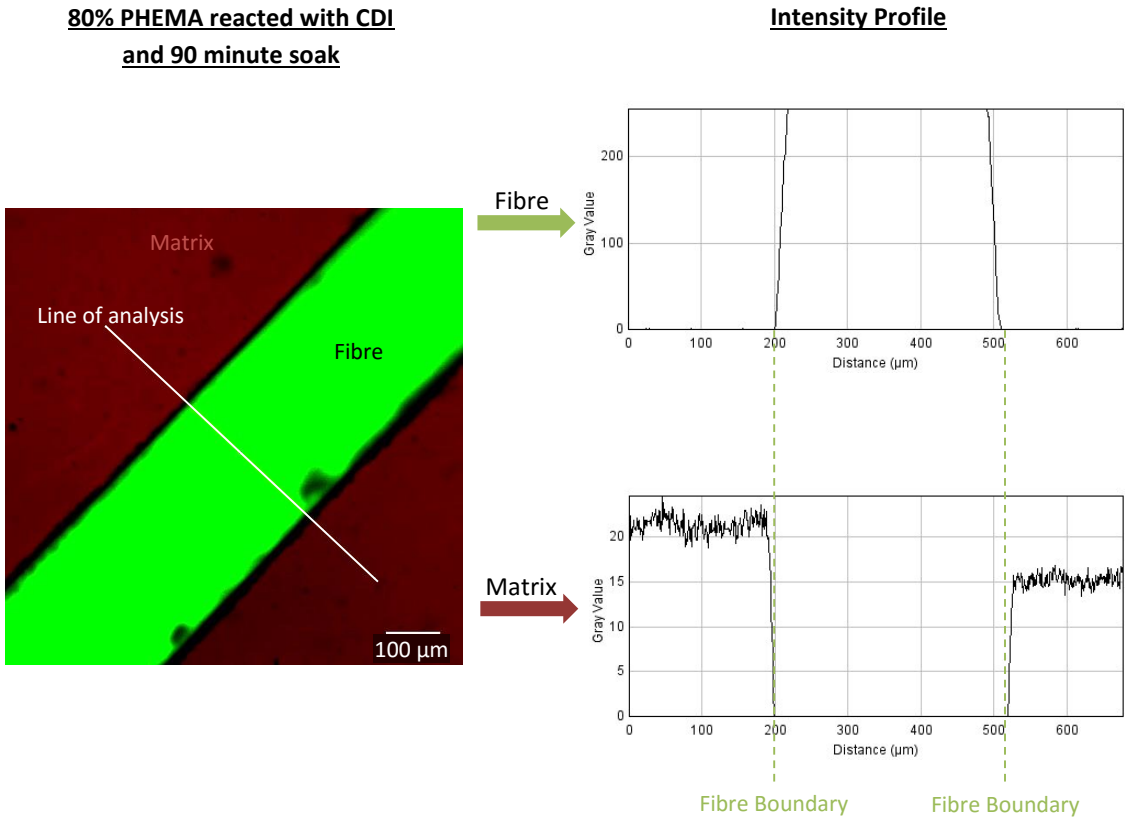

Figure 24: Example of image analysis method performed on a composite with 80% PHEMA fibre reacted with CDI and 90 min soak. Intensity profiles are plot along 3 lines running across the fibre (only one line shown) for the red (matrix) and green (fibre) channels separately. The green channel is used to define the boundaries of the fibre. The distance the red fluorescence is seen past these boundaries, i.e. interpenetration into the fibre, is measured and taken as the integration distance.

Results

Figure 25 shows a positive trend between soak time and interpenetration distance for plain 65% and 80% PHEMA fibres. Both percentages of PHEMA fibres show no difference in integration when soaked for 0 and 30 minutes, with the average integration distance being 74.4 µm and 86.2 µm for 80% PHEMA and 72.7 µm and 86.2 µm for 65% PHEMA, respectively. However at 60, 90 and 120 minutes a significant difference ($p<0.05$) is seen between the two fibre types suggesting these longer soak times can be used to adjust the matrix-fibre interface.

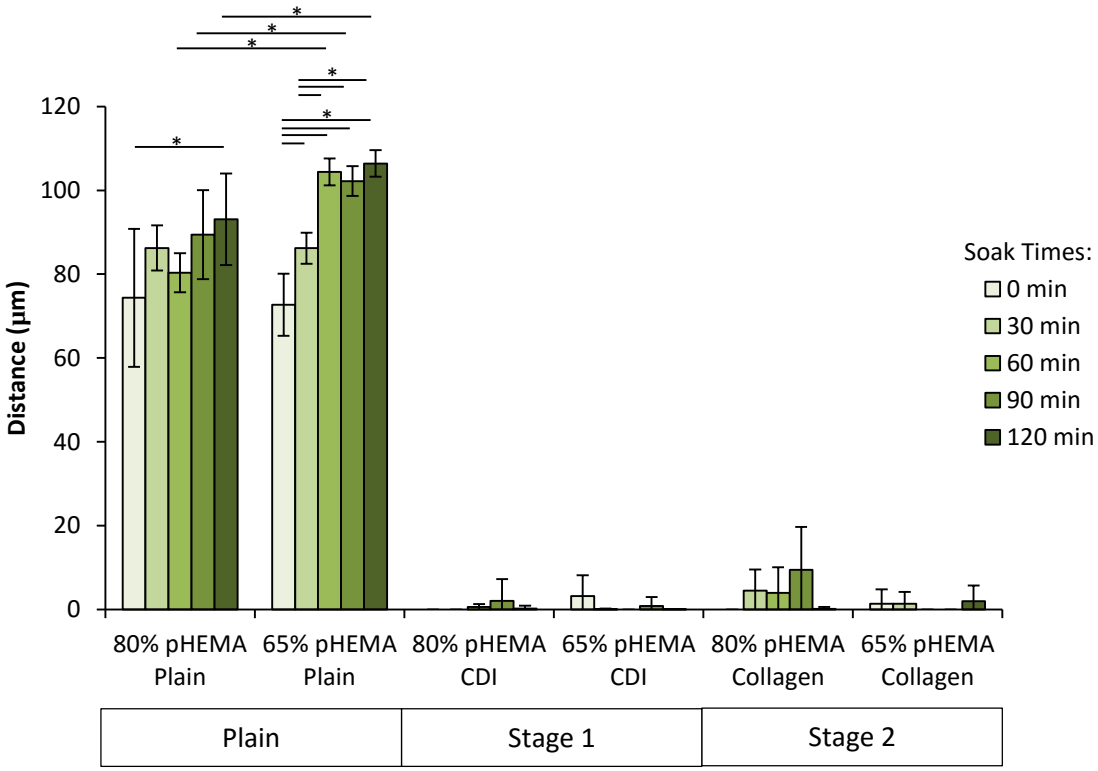

Figure 25: Summary of average PEG integration into 65% and 80% PHEMA fibres in composites as either plain untreated fibres (Plain), CDI reacted fibres (Stage 1) and collagen coated fibres (Stage 2) (n = 6). Increasing soak time can be seen to increase the integration distance for 65% PHEMA fibres. However, after reacting PHEMA fibres with CDI, integration is significantly inhibited. * = P<0.05.

Figure 25 also demonstrates that performing the CDI reaction on PHEMA fibres results in a significant decrease in integration of the matrix into the fibres. Since collagen coating requires the CDI reaction it was not surprising that the collagen coated fibres also exhibited little to no integration.

Discussion and Conclusion

The system originally described by Screen et al. (2010) was limited in the ability to generate varying shear/tension ratios and was found to have fragile a matrix-fibre interface following collagen immobilisation. The data obtained after further characterising these PHEMA/PEG composites provides an insight into the matrix-fibre interface, specifically that changes to the permeability of the PHEMA occur during the stages involved in coating fibres with collagen. It was found performing the CDI reaction on PHEMA fibres significantly prevented the PEG matrix from penetrating into the fibres (Figure 25). This also meant reacting fibres with type I collagen resulted in little matrix-fibre integration as the CDI reaction was a prerequisite. Therefore the fragile composites observed by Dr Screen and Dr Bryant, where composites readily tore at the matrix-fibre interface, can be attributed to this weak interface. It was noted that fibres post CDI reaction appeared more rigid when handled than those not reacted. As a result it is thought that CDI cross links with itself during the reaction to form a layer on the surface of PHEMA fibres, thus restricting the integration of PEG matrix. This is reinforced by the fact that hydroxyl groups activated with CDI, i.e. the intermediate state, can react with neighbouring hydroxyl groups while still maintaining reactivity towards amines (Everaerts et al., 2007; Hermanson, 2008). As such, although matrix integration is not seen, the fibres retained their amine reactivity allowing successful collagen type I coating and, consequently, cell attachment (Screen et al., 2010).

The matrix-fibre interface is an important aspect of the composite as this allows bulk strain to be transferred to the fibres. Without integration it is not possible to control this interface and therefore only a high shear cellular environment can be created. This makes this system unsuitable for exploring the effects of different tension and shear ratios on cellular metabolism. Hence, it was necessary to find an alternative method to achieve this goal.

2.3.2 N,N'-Dissucinimidyl Carbonate (DSC) and Collagen System

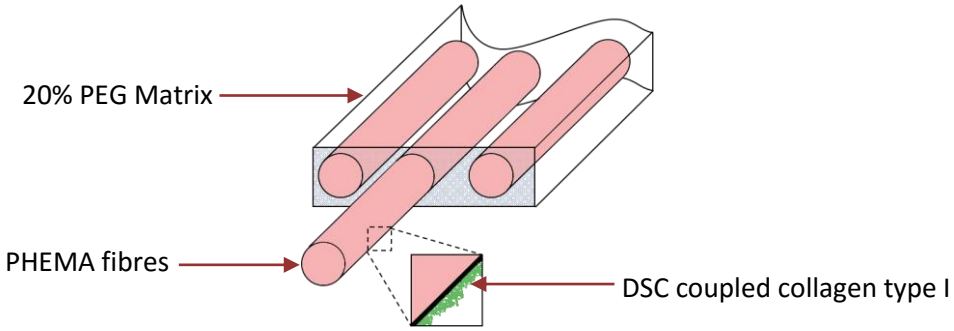

Following the results from the CDI integration experiment, an alternative coupling agent was investigated to allow collagen to be conjugated with PHEMA. The requirement once again was to have a reaction modifying the hydroxyl group of PHEMA and allowing addition of contacting amines.

N,N'-Discuccinimidyl Carbonate (DSC) is a cross linking agent which contains N-hydroxysuccinimidyl (NHS) esters and has been widely used for the conjugation of peptides (Huang et al., 2002; Huang et al., 2001; Lahiri et al., 1999; Miron and Wilchek, 1993). Similar to the CDI method, DSC can be used to convert hydroxyl groups into amine reactive groups. Therefore this can be used with PHEMA as an alternative method to produce collagen coated fibres for the fibre composite system.

2.3.2.1. DSC Protocol Optimisation

Experimental Overview

Adapting the protocol from Hermanson (2008), a method optimised for use with PHEMA fibres was established. The method is similar to that in the previous section using CDI where the plain PHEMA fibres are first reacted with the coupling agent (DSC) and then reacted with collagen (stages summarised in Figure 26).

Previous observations with the CDI method found cracks running along the length of some fibres and therefore an additional objective was introduced to reduce the extent of cracking through different preparation methods. To reduce fibre cracking the necessity of drying fibres within the protocol (Stage 1) was evaluated in addition to the effectiveness of 'graded' solutions when transferring fibres to acetone. The analysis compared direct transfer to acetone with a graded transfer (Stage 2) as outlined below:

i. Ethanol : Water (50:50)
ii. Ethanol : Water : Acetone (33:33:33)
iii. Water : Acetone (50:50)
iv. Water : Acetone (25:75)
v. Acetone (100%)

Fibres in all groups were then reacted with DSC, a coupling agent which introduces NHS esters into PHEMA fibres (Stage 3), and then collagen coated (Stage 4) for the final comparison, giving 4 treatment groups as outlined in Table 14. Collagen conjugated fibres were analysed via Raman Spectroscopy to check for the presence of collagen and the success of the reaction.

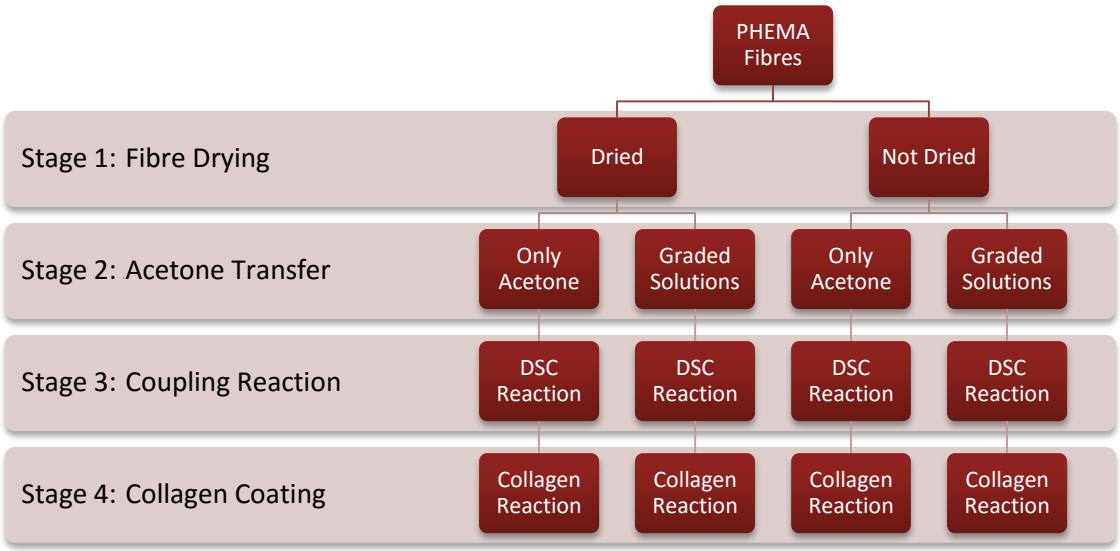

Figure 26: Flow diagram detailing the stages involved in achieving collagen coated PHEMA fibres via DSC. The four protocol variables are dried fibres straight to acetone (DFSA), dried fibres through graded solutions (DFGS), non-dried fibres straight to acetone (NDSA) and non-dried fibres through graded solutions (NDGS).

Methods

Note: Procedures performed at room temperature (RT) unless stated otherwise.

Note 2: Further details of all chemicals used, including supplier details, are present in Table 35 and Table 36, in Appendix B: Chemicals and Materials List.

PHEMA Fibre Preparation

80% PHEMA fibres were prepared as described in the previous section and stored in 70% ethanol. Enough fibres were made for all 4 of the procedures shown in Table 14. 10 plain 80% PHEMA fibres were taken and set aside as non-modified controls.

Table 14: Summary of variations and abbreviations of protocols tested.

Condition	Abbrev.	Dried	Acetone Transfer	No. Fibres	Dry Weight (g)
Dried fibres straight to acetone	DFSA	Yes	Acetone only	91	0.033
Dried fibres in graded solutions	DFGS	Yes	Acetone only	98	0.038
'Not dried' fibres straight to acetone	NDSA	No	Graded	100	0.039
'Not dried' fibres in graded solutions	NDGS	No	Graded	95	0.037

Considering the groups with dried fibres, the ethanol was removed from the glass vials containing sterile fibres designated as DFGS and DFSA and fibres left to air dry for 10 minutes in a sterile hood. These were then placed in a lyophiliser for 2 hours to completely dry. Non-dried fibres, NDSA and NDGS, remained in 70% ethanol. NDSA and DFSA were then immediately immersed in 100% dry acetone and three 30 minute sonicated rinses performed, with the solution being replaced after each sonication. NDGS and DFGS were transferred through graded solutions, with three 30 minute sonicated rinses performed with each solution. After the final rinse all fibres types were kept in 100% dry acetone.

NHS Ester Addition via N,N'-Discuccinimidyl Carbonate (DSC)

NHS ester addition was performed by creating two solutions of molar concentrations 6 times that of HEMA (i.e. using dry weight from Table 14); 6x DSC in 10 mL dry acetone and 6x 4-(dimethylamino) pyridine catalyst in 10 mL dry acetone.

When ready, acetone was removed from the fibre vials and the 6mmol DSC solution added with a magnetic stir bar to keep the mixture stirring. The catalyst solution was then slowly poured in. The magnetic stir bars were then removed and the vials left on a shaker for 6 hours.

After the reaction the solutions were removed and fibres rinsed by performing three 30 minute sonicated rinses with dry acetone. 20 fibres were taken from each vial at this point to perform Raman spectroscopy in the 'post reaction' state.

Collagen Immobilisation

12 mL of a cold sterile 0.3 mg/mL collagen reaction solution was made using 3 mg/mL stock rat tail type I collagen solution and a sodium bicarbonate buffer prepared to pH 10.4. The dry acetone was removed from all fibres and 3 mL of this collagen solution was added to each vial and left to react overnight on a shaker at 4°C. These fibres were then stored in PBS and labelled as 'collagen coated'. 10 collagen coated fibres from each protocol were allocated for Raman spectroscopy analysis.

Results

Visual assessment of PHEMA fibres in each of the 4 treatment groups, looking for signs of cracking, showed drying had little effect on crack formation (Table 15). Fibres transferred through different graded solutions, DFGS and NDGS, appeared to be more prone to cracks. PHEMA fibres that weren't dried and transferred straight into acetone, NDSA, produced no visible cracking probably due to the least amount of 'processing' and handling.

Table 15: Summary of the visual assessment of fibres in each of the 4 treatment groups, alongside the unreacted PHEMA control fibres. The number of separate distinct cracks were counted on each fibre and then averaged by the total number of fibres counted to produce the data for each fibre type and the standard deviation (SD) (n=6 for all fibre types).

Protocol Type	Average No. Cracks	SD
Control	0.0	0.0
NDSA	0.0	0.0
NDGS	0.8	0.8
DFSA	0.3	0.5
DFGS	1.5	1.0

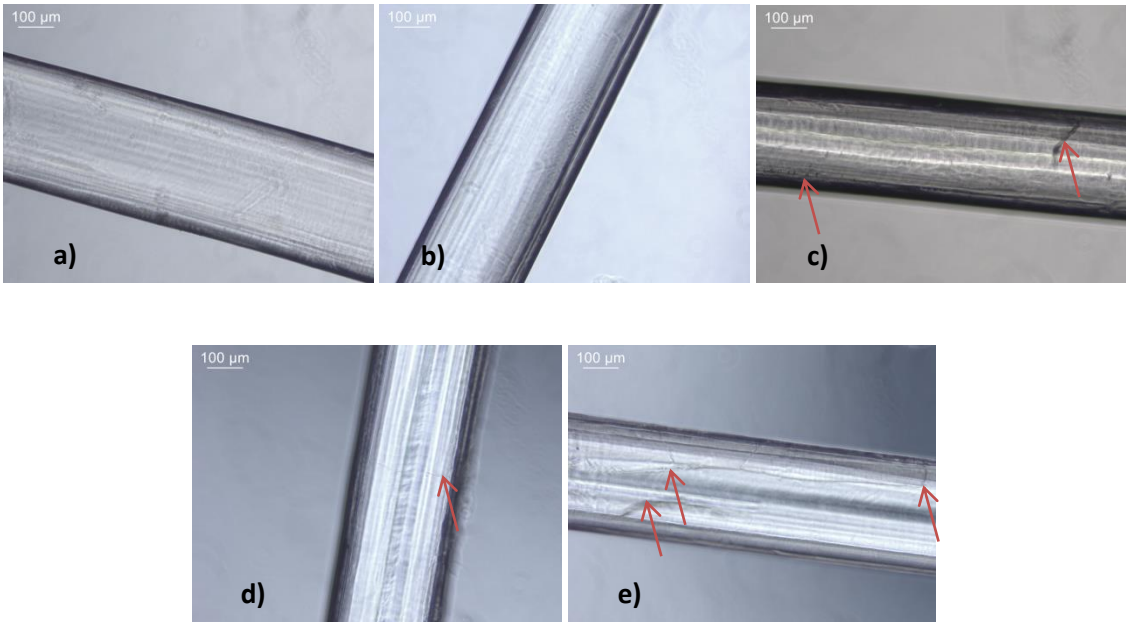

Figure 27: Representative bright-field microscopy images at x10 magnification of a) a plain fibre (control), b) NDSA fibre, c) NDGS fibre, d) DFSA fibre and e) DFGS fibre. Locations of cracks indicated by red arrows. Fibres that underwent the NDSA protocol showed the least amount of fibre cracking once processed.

Raman spectroscopy was performed at the three stages of the protocol; unreacted PHEMA fibres (control), post NHS addition reaction for each protocol version and post collagen coating. Results were consistent between repeats and therefore it was possible to show a reliable representative spectra for each condition. Figure 28 shows that the spectra for all 4 treatment groups (DFSA, DFGS, NDSA and NDGS) post NHS addition were the same in relation to peak locations. This provides confidence in the different protocol versions having little or no effect on the NHS addition reaction. Subsequently, comparisons with plain PHEMA fibres and collagen coated fibres were carried out using only the spectrum produced from NDSA as this condition also reduced cracking, therefore being the ideal protocol for further experiments.

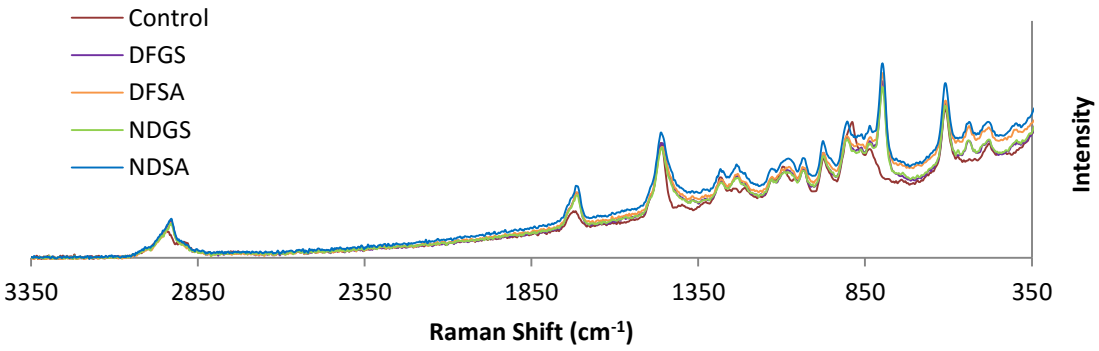

Figure 28: Comparison of representative Raman spectra of DFSA, DFGS, NDSA and NDGS treatment groups post NHS addition. All protocols can be seen to have the same spectral profile, thus all methods create the same modifications.

Raman spectroscopy showed there were a few distinct changes after NHS ester addition to PHEMA fibres (Figure 29); notably a large peak appears at 797 cm^{-1} along with additional small peaks at 395 cm^{-1}, 535 cm^{-1} and 1230 cm^{-1}. Peak shifts were also seen from 1105 cm^{-1} to 1080 cm^{-1}, 1720 cm^{-1} to 1710 cm^{-1} and 2945 cm^{-1} to 2935 cm^{-1}. Peak shifts and widening between 1700-1800 cm^{-1} have been linked to changes in NHS ester formation (Deckert et al., 2004). Following collagen coating some peaks disappear such that they resume the same appearance as that of the control spectrum. This is particularly noticeable with the peaks at 797 cm^{-1} and 535 cm^{-1} which are associated with nitrogen-carbon rings (Carcamo et al., 2012; Krishnakumar and Balachandran, 2004).

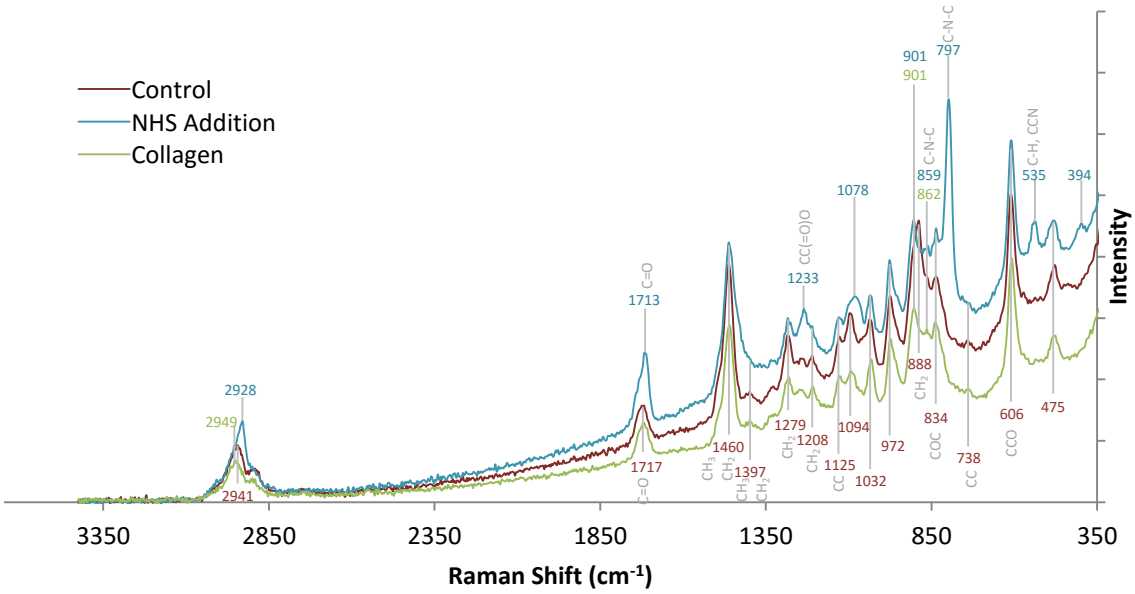

Figure 29: Raman Spectra for plain PHEMA (control), PHEMA after DSC reaction ('NHS addition') and after collagen coating (Collagen). Graph intensity separated for each spectra to allow easier comparison of peaks. Red numbers indicate peaks found in the control samples, blue indicates peaks which change with NHS addition and green indicate changes with collagen addition. Possible peak assignments were identified from literature and indicated as grey text (Carcamo et al., 2012; Krishnakumar and Balachandran, 2004; Mabilleau et al., 2008; Movasaghi et al., 2007; Qin et al., 2006; Taddei et al., 2005).

Discussion and Conclusion

As the original method for creating collagen coated fibres presented a problem with matrix-fibre integration, an alternative method for coating PHEMA fibres with collagen was explored. This new method used DSC to couple collagen type I to PHEMA fibres. The results from 4 different DSC reaction protocols found that drying PHEMA fibres was not a necessary step and fibres can be transferred straight to 100% dry acetone from 70% ethanol with no discernible cracks. Transferring fibres gradually from ethanol to acetone was attempted to try reduce the rate of swelling, however this method increased crack prevalence. This is likely due to increased handling and the need for better optimisation in the order and ratio of graded solutions. As drying and graded solutions are not needed, the ideal protocol is also the shortest and simplest.

Raman Spectroscopy analysis of the hydrogel found peaks similar to other studies which examined PHEMA based polymers, with peaks at 1275 cm^{-1}, 1205 cm^{-1}, 1088 cm^{-1}, 1026 cm^{-1}, 896 cm^{-1} and 830 cm^{-1} (Mabilleau et al., 2008; Taddei et al., 2005), thus providing a reliable control spectrum. Comparisons of the chemical structure of PHEMA fibres at the three stages involved in collagen immobilisation showed distinct new peaks after NHS ester addition (Figure 29). These additional and changed peaks are attributed to the change in structure, namely the addition of a nitrogen-carbon ring, which also brings additional C=O species. Since the spectra are similar for all 4 protocols (DFSA, DFGS, NDSA, NDGS), it can be concluded that drying fibres or using graded solutions during fibre rinses does not affect the NHS reaction.

Performing the collagen reaction is seen to change the Raman spectra of the specimens again; however, the resulting spectra appear almost identical to the control spectrum, particularly the loss of peaks 797 cm^{-1} and 535 cm^{-1}, and minor changes at 1320 cm^{-1}, 901 cm^{-1}, 862 cm^{-1} and 367 cm^{-1}. This change is not surprising as any unreacted NHS activated hydroxyl groups will revert back to the original hydroxyl state through hydrolysis, while collagen reacted hydroxyls will also lose the additional nitrogen-carbon ring (Hermanson, 2008), thus giving a similar bulk structure to normal PHEMA. The Raman spectrum for collagen has been documented previously (Carcamo et al., 2012; Sun et al., 2008). It was not possible to distinguish these peaks in the spectra obtained for collagen coated fibres. However, as the collagen is essentially confined to a monolayer on the surface of the fibre, there will be a very small amount present, making it difficult to distinguish any small collagen peaks amongst the overshadowing hydrogel peaks.

2.3.2.2. Cell attachment

Experimental Overview

In order to establish if collagen coating had been successful, an alternative assessment method was required, and cell attachment to the fibres was investigated. The method outlined by Screen et al. (2010) was adapted for use with the new collagen coating method. Plain, DSC reacted and collagen coated fibres were covered with cells and the extent of cell attachment was compared between the groups to determine whether collagen coating was successful.

Additionally, the effect of agitating cells during fibre seeded was investigated to determine the optimal conditions for seeding, exploring whether keeping fibres static or allowing fibre movement and rotation increased cell coverage. Static seeding of fibres was compared to agitation using either a roller or a shaker for up to 48 hours after an initial 24 hours static culture (Figure 30).

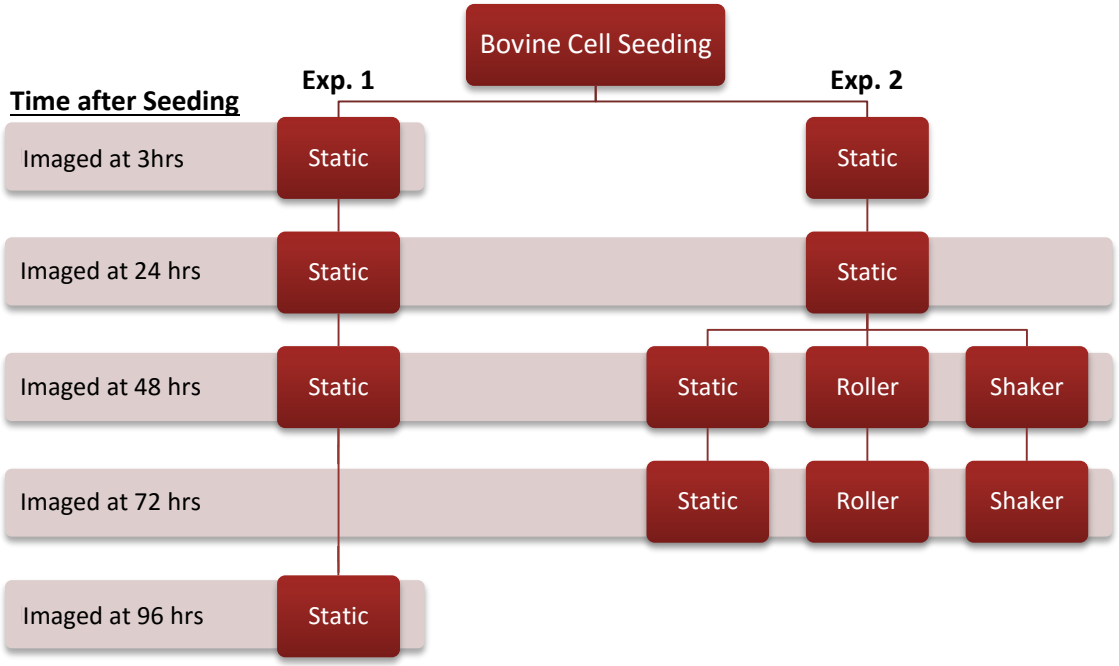

Figure 30: Flow diagram detailing the variables and time points investigated for optimising cell seeding. The diagram represents two experiments, one looking at static culture for up to 96 hours, and the other looking at agitation for up to 48 hours using either a roller or a shaker after the initial 24 hours static culture.

Method

Note 1: Procedures performed at room temperature (RT) unless stated otherwise.

Note 2: Further details of all chemicals used, including supplier details, are present in Table 35 and Table 36, in Appendix B: Chemicals and Materials List.

Bovine Tenocyte Explant Culture

Fresh surplus bovine joints were obtained from the local abattoir, from which digital extensor tendon (DET) explants were used to culture bovine tenocytes. Briefly, small sections of DET were cut and collected in sterile conditions, taking care to remove as much tendon sheath as possible. Central portions of these sections were then extracted to further eliminate the possibility of tendon sheath culture and diced into smaller pieces of ~3mm^3. A tissue culture treated 6 well plate was filled with 3 diced pieces per well, each submerged in a small drop of 50% fetal bovine serum (FBS) culture medium (medium components detailed in Table 16). This was incubated for 48 hours at 37°C with 5% CO_2, after which an additional 1mL of culture medium was added, taking care not to detach the explants from the culture plate surface. After a further 2 days of incubation, 0.5 mL of the medium was replaced with fresh medium, an activity repeated every 3 days. At the end of the second week the explants were removed and media in all wells changed to culture medium containing 10% FBS. The medium was then changed every 2-3 days and cells left to proliferate until the wells were 70-80% confluent, at which stage the cells were trypsinised using 1mL 1X Trypsin-EDTA and seeded into T25 flasks labelled as passage 1 (P1). The cells were then grown, repeating the trypsinisation and seeding process when confluent, until the cells reached P3 and spare cells frozen down until needed. Note: every increase in P indicates splitting of cells from 1 culture flask into two flasks (i.e. a doubling of area).

Cells were frozen by re-suspending cells in media containing 5% dimethyl sulfoxide (DMSO) and no FBS at 1 million cells/mL and transferring 1 mL of this solution into cryovials. The vials were

then placed in an isopropyl bath and moved in to a -80°C freezer for 24 hours after which they were transferred into the cryobank until needed.

Table 16: Bovine Tenocyte culture medium components and quantity

Component	50% FBS Medium	10% FBS Medium
Dulbecco's Modified Eagle Medium (DMEM) with low glucose	100 mL	500 mL
Fetal Bovine Serum	50 mL	50 mL
HEPES (1M)	2 mL	10 mL
L-Glutamine (200mM)	1 mL	5 mL
Penicillin/Streptomycin (10000U/10mg per mL)	1 mL	5 mL
Non-essential amino acids	1 mL	5 mL

Cell Seeding

For the first part of the experiment which focused on looking at cell attachment over time in static culture, plain PHEMA (80%), DSC reacted and Collagen coated fibres were produced using the NDSA protocol as described in section 151.2490538.0. Bovine primary tenocytes, P3, were resuscitated by retrieving a cell vial from the cryobank and briefly opening in a sterile hood to release pressure. The vial cap was then closed firmly and thawed quickly by dipping in a 37°C water bath for 2-3 minutes. Once completely thawed the cell suspension in the vial (1 mL) was transferred into 10 mL of 10% FBS media. This was then centrifuged as 2000rpm for 5 minutes, after which the media was aspirated and the cell pellet re-suspended in 5 mL 10% FBS media (Table 16). A T150 flask was filled with 20 mL 10% FBS media and the 5 mL cell suspension was added. This was then incubated at 37°C and 5% CO_2. The cells were grown and passaged until P5 before use.

The fibres were transferred into a 24 well plate using sterile forceps. A total of 3 wells were used, with the different types of fibres kept in separate wells and each well containing 152 fibres with 1 mL 10% FBS media. This was temporarily placed in an incubator to warm up and displace the ethanol while the cells were prepared for seeding.

Cells were harvested from flasks by first rinsing with warmed sterile PBS and then adding 4 mL Trypsin-EDTA (1X concentration). This was left in the incubator for ~5 minutes. Once the cells detached, the cell/trypsin solution was transferred into a 50 mL conical tube containing 10 mL 10% FBS media. The tube was then centrifuged at 2000 rpm for 5 minutes to pellet the cells. Once centrifuged, the supernatant was aspirated and fresh 10% FBS media was added (5 mL) to re-suspend the cells. The cells were then counted using a haemocytometer and trypan blue; 15 µL cell suspension was mixed with 15 µL trypan blue (dilution factor 2), 10 µL of stained cells pipetted into haemocytometer on either side (total 20 µL), cells in the 4 corner grids on each side counted (total 8 sub-grids counted), and the total cell number determined by averaging the count and multiplying by the dilution factor (2), haemocytometer volume factor (10000) and total cell suspension volume (5 mL). The cell suspension was then diluted with 10% FBS media to make a solution of ~4 million cells/2.5 mL. The well plate containing fibres was retrieved from the incubator and the media aspirated carefully using a 250 µL pipette to avoid discarding any fibres. Fibres were covered with 2.5 mL of the cell suspension (~4 million cells) slowly, and the plates were incubated for the cells to attach for 3 hours. Fibres were then transferred into a 6 well plate containing 10% FBS media using sterile forceps and cell attachment inspected at 3, 24, 48, and 96 hours of culture using Calcein AM (n=6 per time point).

A second experiment investigated agitation within the protocol (static, roller or shaker) for effectively seeding cells. An additional set of plain 50% PHEMA fibres, DSC modified fibres and Collagen coated fibres (n = 100 per group) were prepared and seeded with ~4 million cells per well as just described. After the initial 24 hours static culture, the fibres were placed into their respective modified culture conditions for up to 48 hours and imaged as described (Figure 30). Fibres (n=3) were taken for analysis after the initial 24hrs of static culture, and then additionally at 48 hours and 72 hours after spending the additional time in their secondary seeding condition.

Florescent Cell Staining

Cells for Exp. 1 were visualized by adding 5 µM Calcein AM and incubating fibres at 37°C for 30 minutes. These were then imaged via a Perkin-Elmer spinning disk confocal microscope at the designated time points (3, 24, 48 and 96 hours, n=6 per time point).

The cells on fibres in Exp. 2 were imaged at 24 and 48 hours post seeding (n=3). Images were taken on a Leica SP2 confocal microscope after fixing samples in 4% paraformaldehyde for 30 minutes, permeabilising cells with 0.1% Triton-X100 for 4 minutes and then staining with Phalloidin (Alexa Fluor 488) diluted 1:40 in PBS with 1% bovine serum albumin (BSA) for 30 minutes at room temperature.

In both experiments, an estimate of cell coverage was calculated using ImageJ (*National Institutes of Health*, Abramoff (2004)) to measure the area of the fibre fluorescently covered with cells as a percentage of the total fibre area.

Results

Figure 31 reviews the data from Experiment 1 in which static culture of cells on plain PHEMA fibres and fibres after the DSC and collagen reactions were compared. As expected, there was no cell attachment on plain fibres. However, cell attachment after treatment indicates the successful coating of fibres. It can be seen that DSC reacted fibres which are not coated with collagen still allowed cell attachment, although to a lower extent. It was also notable that these cells remained more spherical in appearance with increasing culture time, suggesting cells were less well attached. In collagen coated and DSC reacted fibres the density of attached cells appeared to reduce after the initial 24 hours.

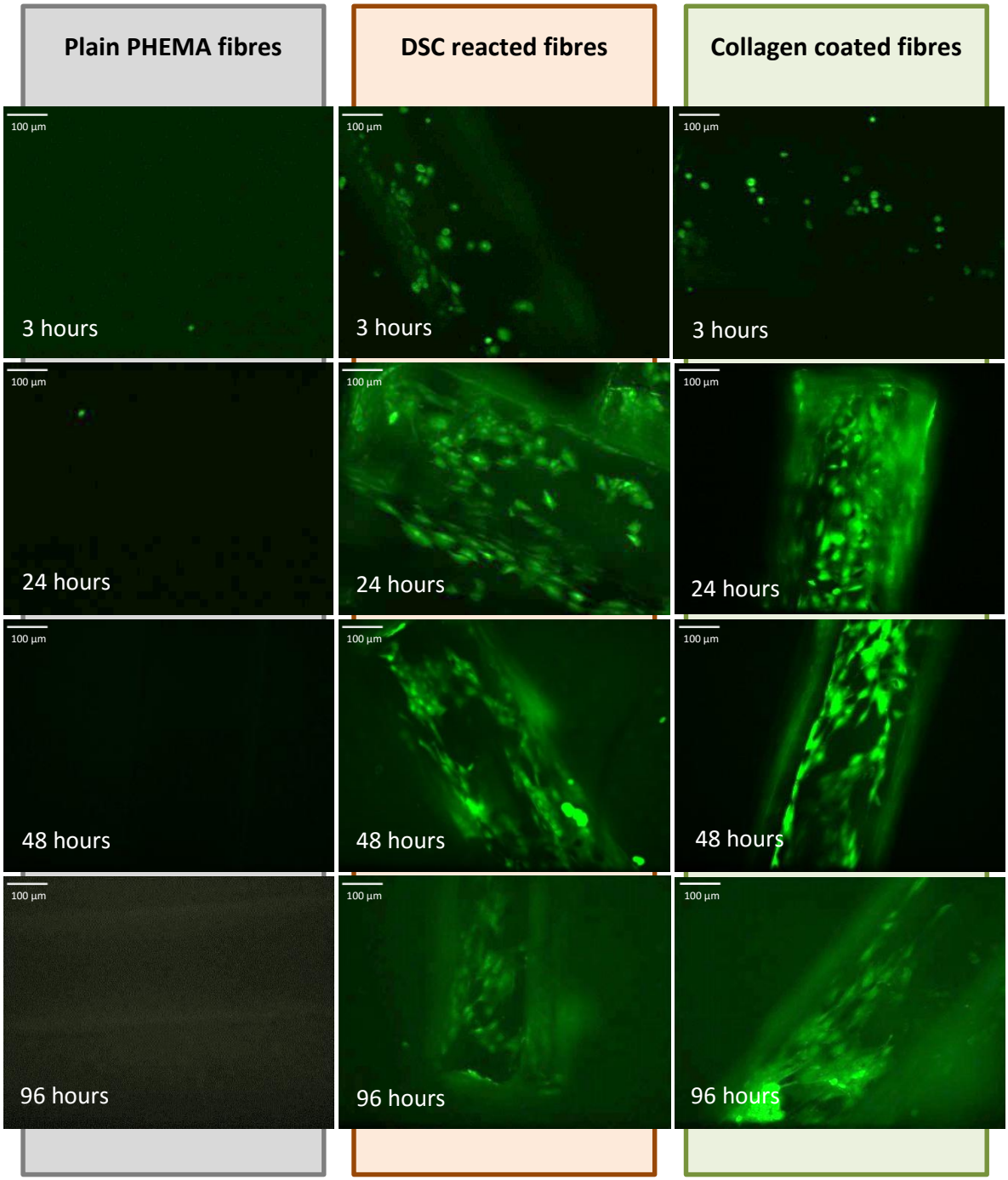

Figure 31: Representative images from Experiment 1 comparing plain, DSC reacted and collagen coated fibres after 3, 24, 48 and 96 hours static seeding. Calcein AM dye used and images taken using Perkin-Elmer at X10 magnification. Both DSC reacted and collagen coated fibres allowed cell attachment unlike plain PHEMA rods. The DSC reacted fibres, although not coated with collagen, still allowed cell attachment due to proteins in the culture medium binding to reactive NHS esters. However, DSC reacted fibres generally showed less cell attachment and more spherical cells compared to collagen coated fibres.

Agitating the well plates for as little as 24 hours resulted in cells detaching from fibres in all cases (Figure 32). An estimate of the percentage cell coverage in some samples (n=6 for static and n=3 for other methods) in Figure 33 confirms static culture for 24 hours as the optimal cell seeding method.

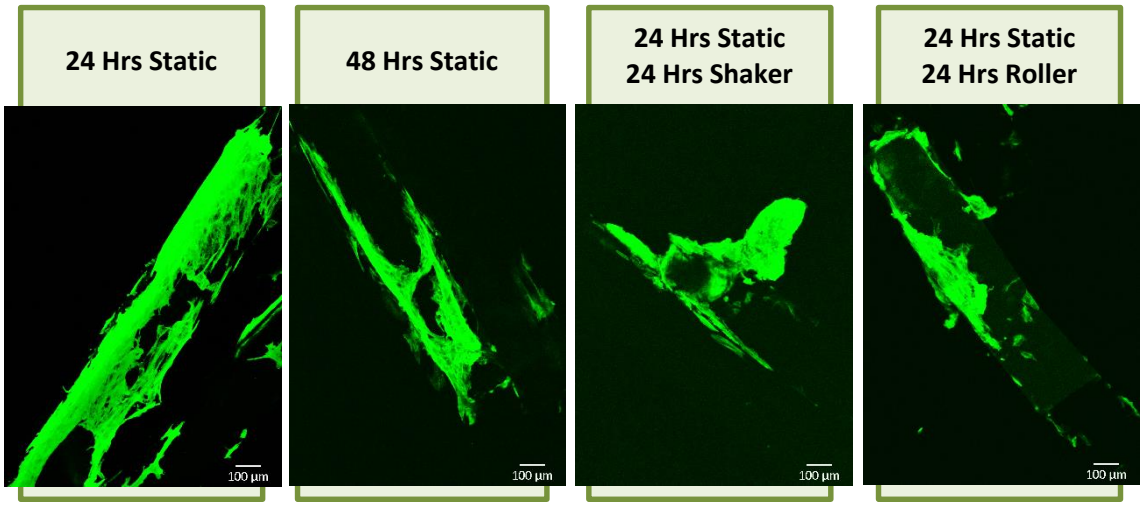

Figure 32: Representative images of collagen coated fibres after 24 hours static culture; 48 hours static culture; 24 hours static culture and 24 hours agitation on a shaker; and 24 hours static culture and 24 hours agitation on a roller. Cells were stained with Phalloidin (Alexa Fluor 488) and imaged using a Perkin-Elmer spinning disk confocal microscope at X10. 24 hours static culture is observed as the superior cell attachment protocol

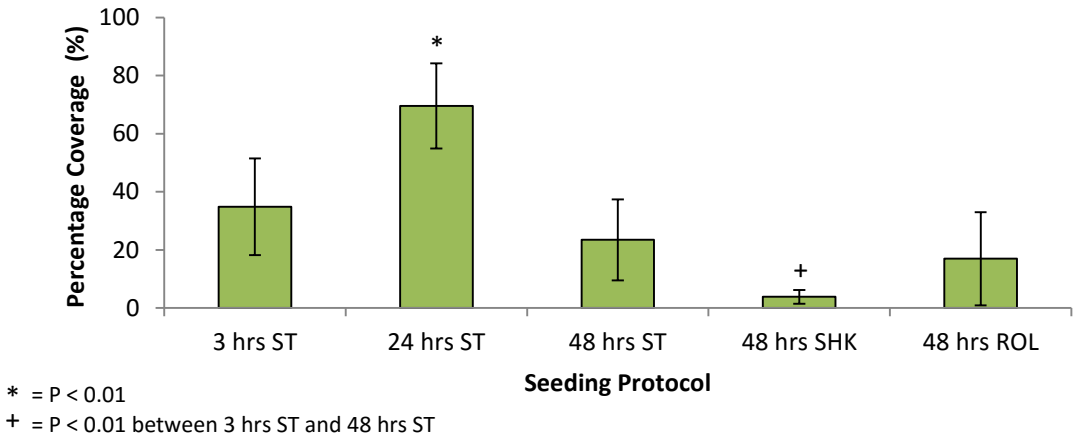

Figure 33: Percentage cell coverage calculated over half the fibre surface (surface closest to microscope lens), calculated as fluorescent area relative to the total fibre area (n=3). ST = static, SHK = shaker and ROL = roller. Note: Although cells were seen to encompass the entire fibre surface, only the top half of fibres were analysed due to fluorescence obstruction. Therefore the % coverage over the visible half of the fibre was doubled to provide an estimate of overall coverage.

Discussion and Conclusion

In order to determine if collagen had attached to fibres using the DSC-collagen modification process, the ability of cells to attach to the fibre surface was addressed; tenocytes should not attach to plain PHEMA while collagen coated fibres would allow attachment. It was established that bovine tenocytes did indeed attach to treated fibres in comparison to plain PHEMA fibres, demonstrating the collagen attachment protocols were successful. However, Figure 31 showed that DSC reacted fibres, although not coated with collagen, still allowed some cell attachment. This can be attributed to the NHS esters still being reactive when culture medium (containing serum) is present and thus any protein within the medium would be immobilised and create a potential site for cell attachment. The cells attached to DSC reacted fibres without collagen appeared more spherical in appearance, suggesting they had not attached as well as to collagen coated fibres.

The results in Figure 32 and Figure 33 show 24 hours static culture as the most suitable condition for cell attachment, reaching an average of 75% fibre coverage. Any agitation of fibres knocked cells off. After 24 hours, regardless of culture condition, there was a significant decrease in cell coverage as cells migrated away from fibres again. 75% coverage is an ideal starting point for studies using the fibre composite; there must be areas of the fibre without cells to enable integration of surrounding PEG into the PHEMA fibre for appropriate composite mechanics. However, if cellular coverage is too high, integration will be limited and result in a weak composite. 75% coverage provides sufficient fibre surface area for integration whilst ensuring total cell numbers are sufficient for later gene expression techniques.

As no cell attachment is seen with plain PHEMA fibres, it can be concluded that fibre modification and collagen coating can be achieved with DSC and the described techniques. Using a culture period of 24 hours allows a quick, simple and repeatable seeding protocol to carry forward in studies.

2.3.2.3. Matrix-Fibre Integration

With the protocol for collagen immobilisation using the coupling agent DSC established and cell attachment confirmed, investigation of the extent of matrix-fibre integration was attempted using the same method as detailed in Section 2.3.1. The PEG matrix and PHEMA fibres were labelled fluorescently with Rhodamine methacrylate and fluorescein methacrylate respectively and soak times of 0, 30, 60, 90 and 120 used when making composites.

Methods

Note 1: Procedures performed at room temperature (RT) unless stated otherwise.

Note 2: Further details of all chemicals used, including supplier details, are present in Table 35 and Table 36, in Appendix B: Chemicals and Materials List.

The integration of the matrix into fibres was investigated using a similar method to that described in section 2.3.1. Fluorescent pre-polymer solutions of 65% and 80% PHEMA were first prepared. The pre-polymer solutions were made by combining either 65% v/v HEMA or 80% HEMA with 2 mol% TEGDM and 1.5% w/v Irgacure 651 in ethylene glycol and deionised water (1:1.33). This was done in 5 mL vials and vortexed to ensure Irgacure 651 was fully dissolved. The solutions were then labelled green fluorescently by adding 0.1% w/w fluorescein methacrylate. The vial was then protected from light by wrapping in foil and stored at 4°C.

Both pre-polymer solutions were polymerised into fibres using the Teflon moulds described previously containing holes of 0.3 mm diameter and 4 mm in length. The mould edges were lightly covered with silicon grease and placed on top of a glass slide (75 mm x 25 mm x 1 mm). The PHEMA pre-polymer solution was then pipetted into the holes with another glass slide placed on top and secured with bulldog clips. The solution was polymerised by placing the entire mould under UV light (365 nm, ~4mW/cm2) for 10 minutes, with the entire mould being turned

over after the first 5 minutes. This was done for the 65% and 80% PHEMA solutions separately. Fibres were extracted from the mould and stored in 70% ethanol until ready for the fibre treatment stage.

A 20% PEG solution for the composite matrix was made by mixing 20% w/v PEGDM, 0.05% w/v Irgacure 2959 and PBS in a 5 mL vial. This was fluorescently labelled by adding 0.02% w/w Rhodamine methacrylate.

Composite cylinders were made as described previously, placing 2 fibres into a trimmed 1 mL syringe and filling with 100 µL 20% PEG matrix solution (shown previously in Figure 23). The designated soak time was waited and then composites polymerised under UV light (~4mW/cm2) for 10 minutes. Soak times were 0, 30, 60, 90 and 120 minutes. Three gels were made for each time point, with 2 fibres encapsulated per gel (total fibre n=6 per time point). The polymerised composites were then washed in PBS over 2 hours, with the PBS changed every 30 minutes, to remove excess dye.

The composites were imaged by confocal microscopy as described in section 2.3.1. Images were analysed via ImageJ, plotting fluorescence profiles across 6 spots on each fibre for 3 composites for each soak group as described previously (total n for measurements = 36 per group). The distance the matrix had penetrated past the fibre edge, i.e. the distance the matrix fluorescence was seen inside the fibre, was used as the integration distance.

Results

The integration of matrix into plain 65% and 80% PHEMA fibres was seen to increase as the soak time was increased (Figure 34). Unfortunately, similar to the matrix-fibre integration patterns seen after the CDI reaction, the DSC reaction also significantly restricted integration of the matrix into the fibres. The consequences were particularly evident in images where the fibres had pulled away from the matrix (Figure 35). It was noted that PHEMA fibres and other larger PHEMA specimens tested separately exhibited an increase in stiffness post the DSC reaction. Thus crosslinking on the surface of PHEMA fibres could have occurred similar to that seen in the CDI method. Studies have seen similar unintended non-specific crosslinking from DSC coupling agents where binding occurs with non-amine functional groups, such as hydroxyls, or multiple side chains on proteins (Everaerts et al., 2007; Lane et al., 2011).

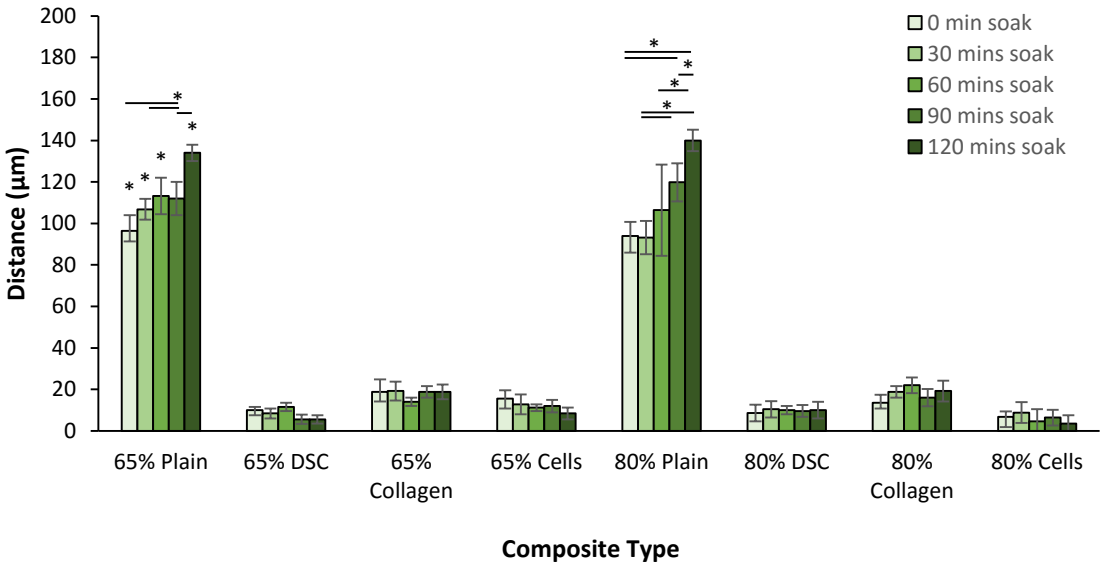

Figure 34: Summary of matrix integration in fibres after the different stages of PHEMA modification and fibre soak times of up to 120 minutes (fibre n=6). Data shown as average distance PEG matrix present past the boundaries of PHEMA fibres, and error bars represent standard deviation. 'Plain' = plain PHEMA fibres, 'DSC' = DSC reacted fibres, 'Collagen' = collagen coated fibres, and 'Cells' = cell seeded fibres. Plain 65% and 80% PHEMA fibres allow matrix integration, which also increases with soak time. However, modification with DSC, and consequently collagen coating and cell coating, limited the extent of integration dramatically. * = P<0.05.

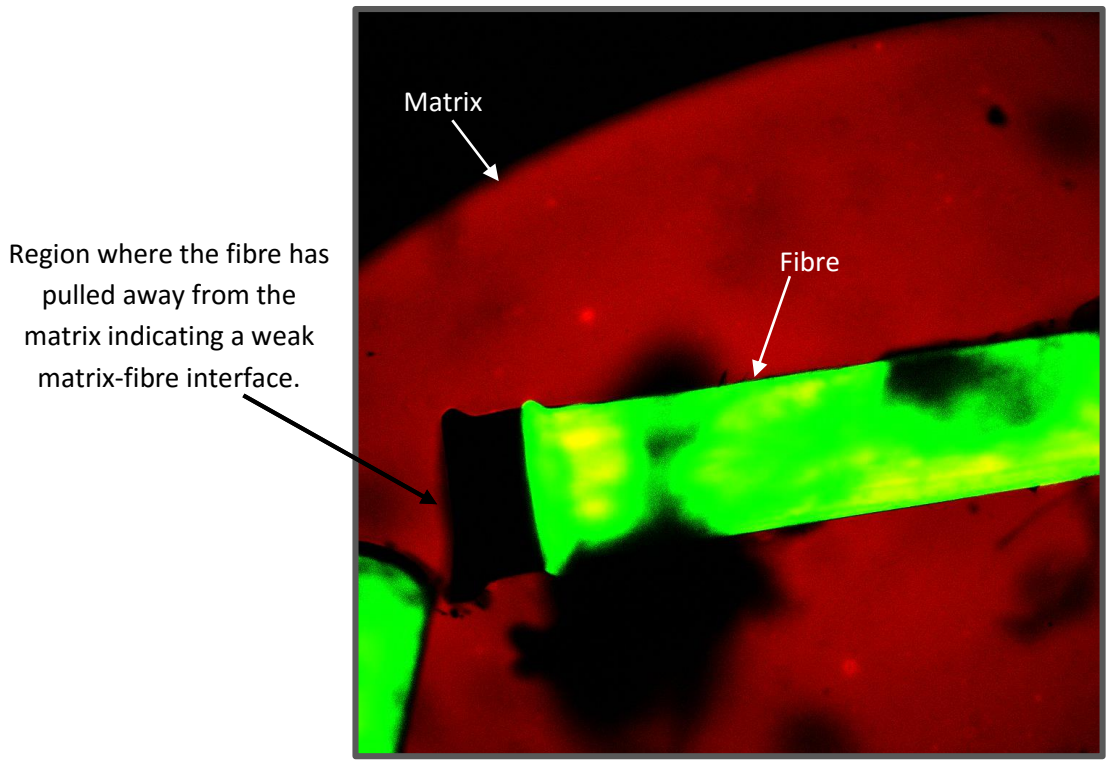

Figure 35: Confocal image of composite made from collagen coated 65% PHEMA fibres in 20% PEG matrix after 150 min soak period. Matrix labelled fluorescently red with Rhodamine methacrylate and fibres labelled green with fluorescein methacrylate. Note a complete lack of matrix-fibre integration indicated by the separation of the fibres from the matrix.

Discussion and Conclusion

After successfully coating PHEMA fibres with collagen type I, the matrix-fibre interface was characterised once fibres were incorporated in a 20% PEG matrix. The matrix-fibre integration distance was measured as the distance the matrix (labelled red fluorescently) had penetrated past the edge of the fibres (labelled green fluorescently). This integration was found to be lacking following the NHS addition reaction with PHEMA fibres. Consequently both collagen coated and cell covered fibres also showed little or no PEG integration as NHS modification is required to achieve both. The consequences of this lack of integration can also be seen in Figure 35 where a collagen fibre has pulled away from the PEG matrix. As stated previously, the lack of matrix-fibre integration is undesirable due to the inability in providing different cell shear-tension environments; if there is no matrix-fibre integration, the only cellular shear/tension

environment producible is one of high shear as the matrix will slide against the fibres and not transfer tension when the composite is stretched.

Both methods used to functionalise PHEMA to enable cell attachment altered the chemistry such that no integration was possible. Since these coupling reactions are the source of the problem, it was decided to move away from this method and introduce a new system.

2.3.3 PEG-Peptide System

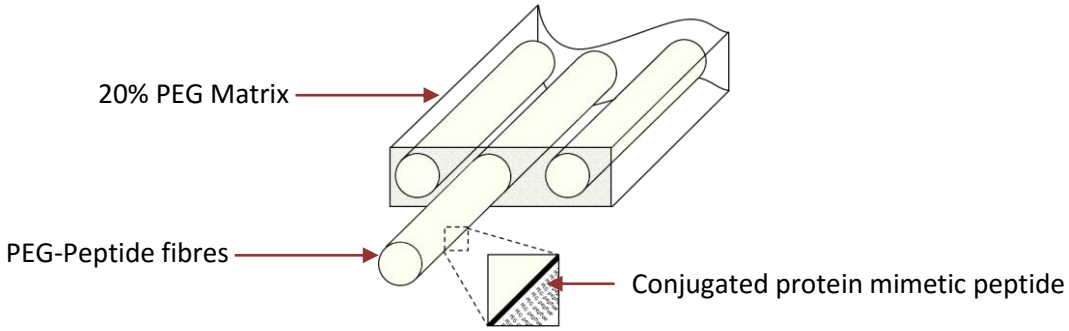

As described previously, PEG is a versatile material due to the large number of modifications and conjugations that can be performed. One such conjugation is that of peptides to enable cell attachment via acrylate reactive groups. This modification of PEG differs to the coupling reaction needed to modify PHEMA, as peptide sequences are directly incorporated into the PEG network during polymerisation and therefore eliminates the secondary crosslinking problem seen in previous attempts at making fibres for the composite.

Any primary amine containing peptide sequence can be used and conjugated with PEG, however for the fibre composite system, one which mimics the attachment site found in proteins is required to allow cell attachment on the otherwise bioinert PEG. A common cell attachment peptide used in studies is Arg-Gly-Asp (RGD) (DeLong et al., 2005; Dettin et al., 2009; Lynn et al., 2011; Steinmetz and Bryant, 2011; Yang et al., 2005). Although this sequence is commonly associated with the attachment site found on fibronectin, it is also present in many other protein cell adhesive sites including vitronectin, fibrinogen, laminin, and tenascin (Ruoslahti, 1996). RGD is also found in collagen type I, however it is only accessible once the collagen is partially degraded and hence not the intended motif for cell attachment in this case (Taubenberger et al., 2010). A number of integrins bind to RGD; α5β1, α8β1, αVβ1, αVβ3, αVβ5, αVβ6, αVβ8 and αIIbβ3 (Ruoslahti, 1996).

Collagen type I mimetic peptides have been identified and characterised by their ability to be recognised by the β1 integrins; α1β1, α2β1, α3β1, α10β1 or α11β1 (Luo and Tong, 2011;

Taubenberger et al., 2010). Gly-Phe-Hydroxyproline-Gly-Glu-Asp (GFOGER) is a sequence found on the α1 chain of collagen type I and known to bind to integrin α2β1 (Knight et al., 2000). The shortest collagen type I mimetic peptide sequence is Asp-Gly-Glu-Ala (DGEA) and binds to α2β1 integrin (Mizuno et al., 2000). Such peptides haves been used in studies looking for either alternatives to RGD (Culpepper et al., 2010; Weber et al., 2007) or to enhance surfaces with collagen specific motifs (Blewitt and Willits, 2007; Connelly et al., 2011; Culpepper et al., 2010; Hennessy et al., 2009; Wojtowicz et al., 2010).

DGEA, as it is one of the shortest collagen type I mimetic peptides, and YRGDS as it has been used extensively in PEG based hydrogels, with the RGDS variant having better cell attachment activity than RGD (Hirano et al., 1993), were selected for investigation as potential alternative materials to PHEMA within the fibre composite system.

Experimental Overview

The peptides were incorporated into PEG by first combining commercially available acrylate-PEG-NHS monomers with either DGEA or YRGDS to create acrylate-PEG-DGEA or acrylate-PEG-YRGDS monomers, respectively. These were then added to a solution of PEGDM. The monomers contained an acrylate group, the same crosslinking chemistry used in PEGDM, becoming incorporated into the PEG network when the solution was polymerised.

Conjugation of DGEA and YRGDS to acrylate-PEG-NHS monomers was first characterised, after which fibre composites made using the two peptide types were characterised in terms of cell attachment, gross mechanics and micromechanics (Figure 36).

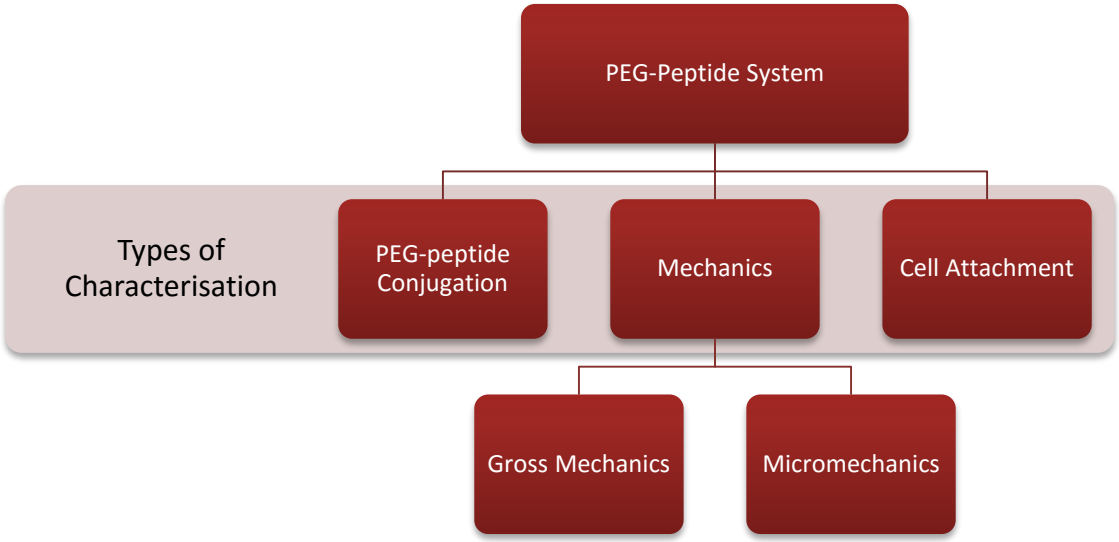

Figure 36: Flow diagram summarising different aspects of characterisations performed.

Methods

Note 1: PEG-YRGDS fibres are referred to as PEG-RGD fibres from here onwards.

Note 2: Procedures performed at room temperature (RT) unless stated otherwise.

Note 3: Further details of all chemicals used, including supplier details, are present in Table 35 and Table 36, in Appendix B: Chemicals and Materials List.

PEG-Peptide Synthesis

PEGDM was synthesised as described previously (section 2.3.1). YRGDS and DGEA were purchased from Genscript, USA, using their custom peptide synthesis service. Both YRGDS and DGEA were conjugated to PEG using the same technique, therefore both are referred to as 'peptide' unless specific steps unique to either sequence were required.

Sufficient sodium bicarbonate buffer, pH 8.4, was first prepared and the desired quantity of peptide weighed in a micro-centrifuge tube (40mg YRGDS or 30mg DGEA). A 20mL amber vial was filled with 9mL buffer while a further 1 mL of buffer was added to the peptide in the micro-centrifuge tube. The peptide solution was mixed and then transferred to the amber vial (total

solution now 10mL) along with a magnetic stir bar. A sample of this solution (66uL) and a sample of the buffer (1500uL) were taken, labelled as 'pre-reaction' and stored at 4°C to perform a conjugation assay later.

Commercially available acrylate-PEG-NHS monomers were used to create acrylate-PEG-peptide monomers. The quantity of Acrylate-PEG-NHS was first calculated to ensure the final mix had a peptide excess of 10%:

For 40mg YRGDS:

YRGDS MW = 596.59

Acrylate-PEG-NHS MW = 3500

40mg YRGDS:

$$n = \frac{40 \div 1000}{596.59} = 6.705 \times 10^{-5}\ mol$$

10% excess:

$$6.705 \times 10^{-5} \div 110 \times 100 = 6.095 \times 10^{-5}\ mol$$

Therefore, mass of acrylate-PEG-NHS needed:

$$6.095 \times 10^{-5} \times 3500 \times 1000 = 213.3mg$$

For 30mg DGEA:

YRGDS MW = 390.35

Acrylate-PEG-NHS MW = 3500

30mg YRGDS:

$$n = \frac{30 \div 1000}{390.35} = 7.69 \times 10^{-5}\ mol$$

10% excess:

$$7.69 \times 10^{-5} \div 110 \times 100 = 6.99 \times 10^{-5}\ mol$$

Therefore, mass of acrylate-PEG-NHS needed:

$$6.99 \times 10^{-5} \times 3500 \times 1000 = 244.54mg$$

With the quantity calculated, the acrylate-PEG-NHS bottle (stored at -20°C) was quickly brought to room temperature and the calculated amount weighed. The bottle was then purged with nitrogen and returned to the -20°C freezer. The weighed Acrylate-PEG-NHS was added to peptide containing amber vial and left to react for 2 hours on a stir plate protected from light.

30 minutes before the end of the reaction, dialysis membranes (molecular weight cut off 500-1000 daltons) were cut and rinsed in deionised water, and the bottom ends of the dialysis membranes were folded and secured with dialysis clips to prevent liquid from leaking out of the membranes. At the end of the reaction period, a sample of solution (130 µL) was taken, labelled as 'post-reaction' and stored at 4°C for the conjugation assay performed later. The remaining reacted peptide solution was pipetted into the dialysis membrane tube and the opening folded and secured with another set of dialysis clips. The filled membranes were left in a 1 L beaker containing deionised water, with the water changed every 30 minutes for at least 4 hours after which they were left overnight. Amber vials were half filled with the solutions from the membranes and placed in the -80°C freezer for 2 hours. These were then lyophilised for 2 days and the final product weighed.

Conjugation Assay

A conjugation assay was performed with the samples taken from the PEG-peptide synthesis to confirm the peptide had attached to the acrylate-PEG-NHS monomers.

The conjugation assay used Fluoraldehyde O-phthalaldehyde (OPA) which binds to proteins and peptides, with linear results over a wide range of concentrations. The excitation and emission wavelengths for Fluoraldehyde OPA are 340 nm and 455 nm, respectively.

Based on the amount of peptide initially weighed, a series of dilutions of known concentrations (detailed in Table 17) were performed to create a standard curve. Dilution was done using the

'pre-reaction' and buffer samples taken during the PEG-peptide synthesis. 40 µL of the standard curve samples were then plated out in triplicates on a white opaque 96 well plate followed by the unknown samples and buffer only blanks. 160 µL of the Fluoraldehyde OPA reagent was then added to each well and placed in a FLUOstar microplate reader *(BMG Labtech)* within 5 minutes to measure the fluorescence intensity.

Table 17: Standard preparation for conjugation assay. For YRGDS, Stock 1 was made by diluting the 'pre-reaction' sample by a factor of 2 using the buffer and Stock 2 made by taking 5 µL Stock 1 and adding 45 µL buffer. For DGEA, Stock 1 was prepared by diluting the 'pre-reaction' sample by a factor of 1.5 with buffer, and stock 2 made by adding 45 µL buffer to 5 µL Stock 1.

Concentration (µg/mL)	Stock 1 needed (µL)	Stock 2 needed (µL)	Buffer needed (µL)
0.00	-	0.00	130.00
6.15	-	4.00	126.00
15.39	-	10.00	120.00
29.23	-	19.00	111.00
61.50	4.00	-	126.00
153.90	10.00	-	120.00
246.20	16.00	-	114.00
492.30	32.00	-	98.00
1000.00	65.00	-	65.00

The results from the conjugation assay shows the quantity of free peptide still remaining in the 'post-reaction' sample, which in turn indicates the amount of peptide not conjugated to acrylate-PEG-NHS.

Matrix-Fibre Integration

Matrix-fibre integration for effective composite manufacture was investigated by adapting the method described previously. PEG-RGD fibres of either 20% or 40% PEG were fluorescently labelled via fluorescein methacrylate and embedded in 20% PEG matrix which was labelled fluorescently with Rhodamine methacrylate. PEG-DGEA fibres were not used for this

experiment as the only difference between the PEG-RGD and PEG-DGEA fibres is the substitution of YRGDS with DGEA in the latter.

The pre-polymer solutions were polymerised into fibres using the Teflon moulds containing holes of 0.3 mm diameter and 4 mm in length as described previously. These were placed into trimmed 1 mL syringe and surrounded with 100 µL 20% PEG matrix solution as before (Figure 23). The designated soak time was waited and then composites polymerised under UV light (~4mW/cm^2) for 10 minutes. Soak times were 0, 30, 60, 90 and 120 minutes. Three gels were made for each time point, with 2 fibres encapsulated per gel (total fibre n=6 per time point). The polymerised composites were then washed in PBS over 2 hours, with the PBS changed every 30 minutes, to remove excess dye.

The composites were imaged using confocal microscopy, and the distance the matrix had penetrated past the fibre edge calculated as previously described (section 2.3.1).

Cell Viability and Attachment

Additional cylindrical composites were made using the method described above, however without fluorescent dyes, to assess cell viability and cell attachment on PEG-RGD and PEG-DGEA fibres.

Both PEG-RGD and PEG-DGEA fibres were made and seeded with cells using the 24 hour static culture method (2.3.2.2).

Table 18: Serum free culture medium used for initial seeding step with bovine tenocytes.

Components for serum free media	Quantity
Dulbecco's Modified Eagle Medium (DMEM), low glucose	500 mL
HEPES (1M)	10 mL
L-Glutamine (200mM)	5 mL
Penicillin/Streptomycin (10000U/10mg per mL)	5 mL
Non-essential amino acids	5 mL

For viability analysis within the composites, the next day a 20% PEGDM solution for the composite matrix was made by mixing 20% w/v PEGDM, 0.05% w/v Irgacure 2959 and 10% FBS media in a 5 mL vial. This solution was then sterile filtered using 0.22 µM syringe filters.

In a sterile hood, 2 cell seeded fibres were placed into a sterile cylindrical mould (a trimmed 1 mL syringe shown previously in Figure 22) and filled with 100 µL sterile 20% PEG solution. The designated soak time was waited and then composites polymerised under UV light (~4mW/cm^2) for 10 minutes. Soak times used were 0, 30, 60, 90 and 120 minutes. The polymerised composites were immediately placed in 6 well plates with 10% FBS media and live/dead cell staining performed. Three gels were made for each time point, with 2 fibres encapsulated per gel (total fibre n=6 per time point).

Live/dead staining was done by placing a composite in 1 mL media and adding 4 µM Calcein AM and 4 µM ethidium homodimer. Composites were kept in an incubator for 30 minutes at 37°C, 5 % CO_2 after which the gels were imaged using an epi-fluorescent microscope to count live and dead cells.

Cell attachment was also investigated on PEG-RGD fibres at 3 hours and 24 hours post-seeding to confirm cell attachment and spreading. PEG-RGD fibres (n=3) at 3 hours and 24 hours post seeding were fixed in 4% paraformaldehyde for 30 minutes and then cells permeabilised with 0.1% triton X-100 for 4 minutes. The fibres were then stained with Phalloidin (Alexa Fluor 488) diluted 1:40 in PBS with 1% bovine serum albumin (BSA) for 30 minutes at room temperature. Fibres were then rinsed twice with PBS and counterstained with DAPI diluted 1:1000 in PBS for 1 min. Fibres were rinsed once again in PBS and then imaged using a confocal microscope (Model SP2, *Leica*).

Micromechanics

Composites were made using different stiffness PEG-RGD fibres and different soak times to see if the micromechanics of the resulting composite when subjected to tensile strain could be manipulated, to create different shear/tension ratios locally in the material.

Table 19: List of fibre types and soak times use to make composites.

Fibre Type	Soak Time	Abbrev.
20% PEG-RGD	0 minutes	20-0
20% PEG-RGD	60 minutes	20-60
40% PEG-RGD	0 minutes	40-0
40% PEG-RGD	60 minutes	40-60
60% PEG-RGD	0 minutes	60-0
60% PEG-RGD	60 minutes	60-60

Fibres of 20%, 40% and 60% PEG-RGD were made as previously described, but without the inclusion of fluorescein.

Fibres were sterilised with short wavelength UV light for 30 minutes in a sterile hood. Using sterile forceps the fibres were transferred into a 24 well plate containing serum free media (Table 18). Separate wells were used for each fibre type and the plate kept in an incubator to keep warm while the cells were prepared. Bovine tenocytes, P6, were harvested from flasks via trypsinisation and re-suspended at 3.5 million cells/mL in serum free media. Media was removed from the 24 well plate containing fibres, and 1 mL cell suspension (i.e. 3.5 million cells) was added to each well and topped up with a further 0.5 mL serum free media. The plate was then left in the incubator at 37°C, 5% CO_2 for 1.5 hours. 0.5 mL media was then removed from both wells and replaced with 0.5 mL 10% FBS media (Table 16). The well plate was then left for a further 1.5 hours in the incubator. After a total of 3 hours sterile forceps were used to transfer all the fibres into new wells containing 10% FBS media and the plate left in the incubator overnight.

24 hours after seeding, the fibres were ready to make into composites. First a 20% PEGDM solution for the composite matrix was made as previously described. This solution was then sterile filtered using a 0.22 µM syringe filter. Rectangular Teflon moulds were used to make composites. Each mould made 3 composites as each contained 3 rectangular grooves of dimensions 25 mm x 2.5 mm x 1 mm (Figure 37). 7 fibres were placed within each groove and made into composites using a modified 'dipping' method (Figure 37). The 'dipping' method differs to that previously used to make composites in so far as cell seeded fibres are briefly immersed in a drop of 20% PEGDM matrix solution prior to positioning into the composite mould. This displaces media surrounding the fibre and cell surface, replacing it with PEGDM, thus giving a better matrix-fibre interface.

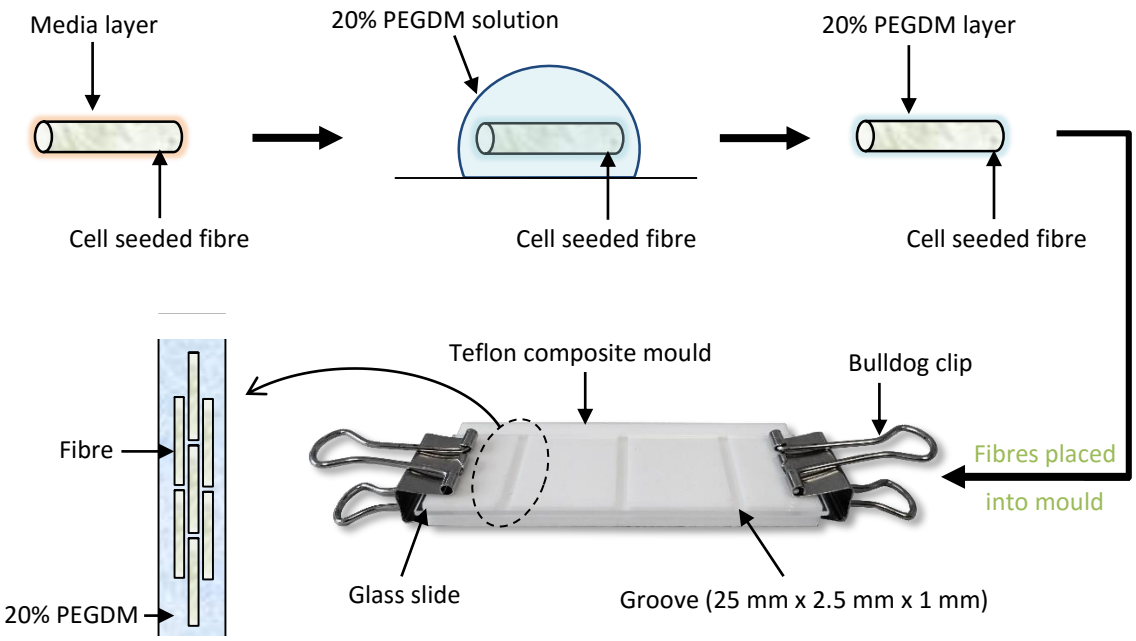

Figure 37: Schematic showing the 'dipping' method used for making composites. Cell seeded fibres were picked up with sterile forceps individually and dipped into a drop of sterile 20% PEGDM solution. This replaced any media retained on the surface of the fibres with 20% PEGDM to create a better matrix-fibre interface. Fibres were then placed into the groove in the Teflon composite mould to make composites of 25 mm x 2.5 mm x 1 mm. Three composites could be made at once.

A glass slide was placed on top of the mould and secured tightly using bulldog clips. The mould was slowly filled with the 20% PEGDM solution using a 5 mL syringe and 25 gauge needle. The

composite mould was then left for the designated soak times of either 0 or 60 minutes. After soaking, the composites were polymerised under UV light (365 nm, ~4 mW/cm^2) for 10 minutes whilst still in the sterile hood. Polymerised composites were stored in a 6 well plate containing 10% FBS media, and 16 composites of each type made.

A customised uniaxial strain rig (Figure 38a) was used in conjunction with brightfield microscopy to image composites whilst applying strain, and characterise their micromechanics. The sample chamber of the uniaxial strain rig was filled with 10% FBS media and the composites were carefully attached to the rig grips (as shown in Figure 38a). The rig grips were configured to create an initial test length of 10 mm by using a metal spacer. The rig grips, with composite attached, were lowered into the strain rig chamber and the grips secured to the rig motor arms. The spacer was then removed and the slack in the composite adjusted by operating the motor in small 0.05 mm increments whilst monitoring the edge of the composite under the microscope. Once the entire composite edge was at the same focus depth the composite was assumed to be slack free and straight. The test length was measured as the distance between the rig grips at this stage. Up to 10% strain was then applied to the composites at a rate of 15% strain/min. Images were taken at 0%, 2%, 4%, 5%, 8% and 10% applied strain. All 16 composites were tested, but do to some breaking during handling, n = 12-15 for each composite type.

In order to characterise local fibre strains, the change in fibre length (fibre strain) relative to gross applied strain was calculated at each applied strain by analysing images in ImageJ and monitoring fibre length changes (Figure 38b). The fibre strain was then calculated by dividing the fibre length change by the original length.

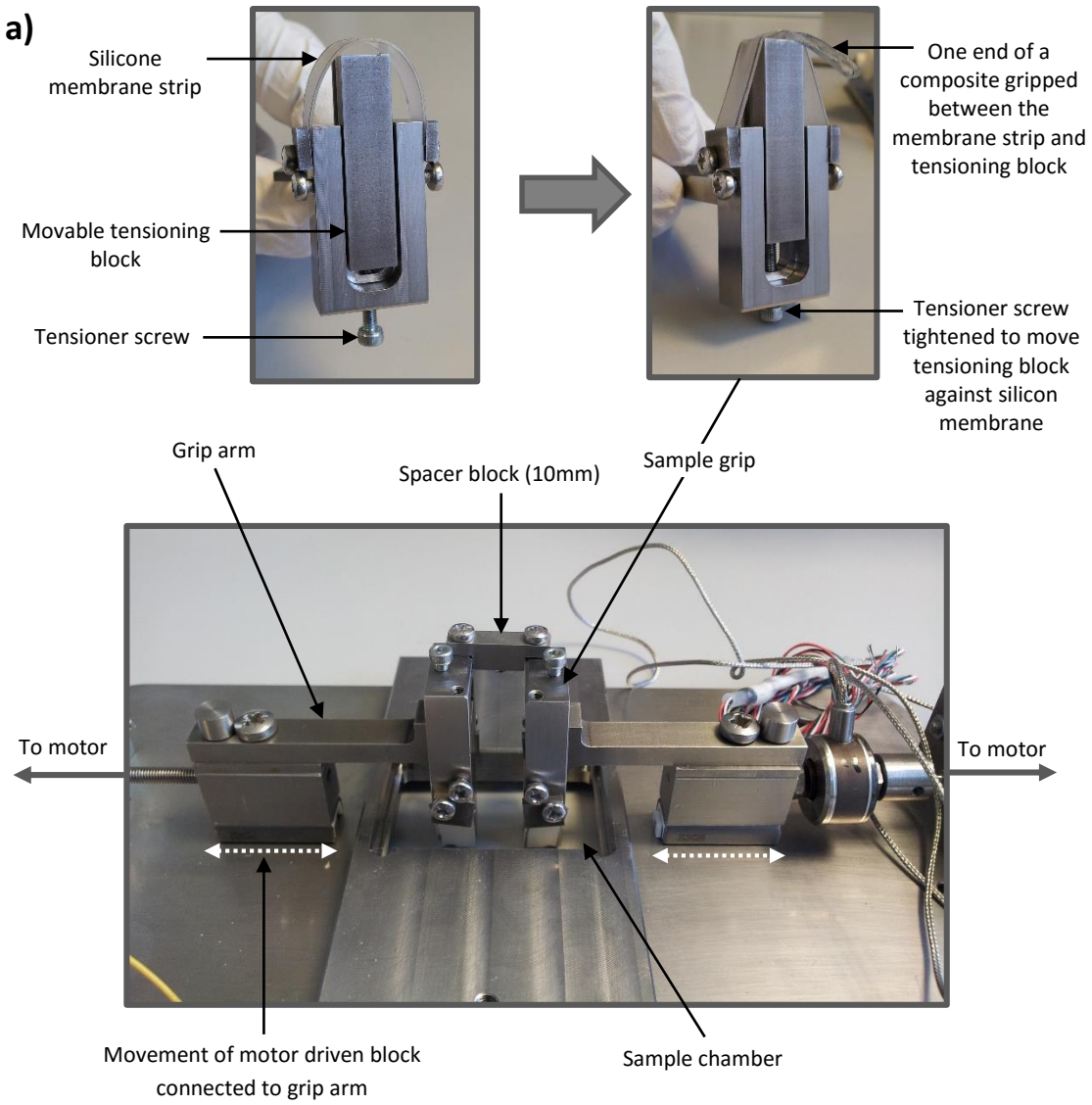

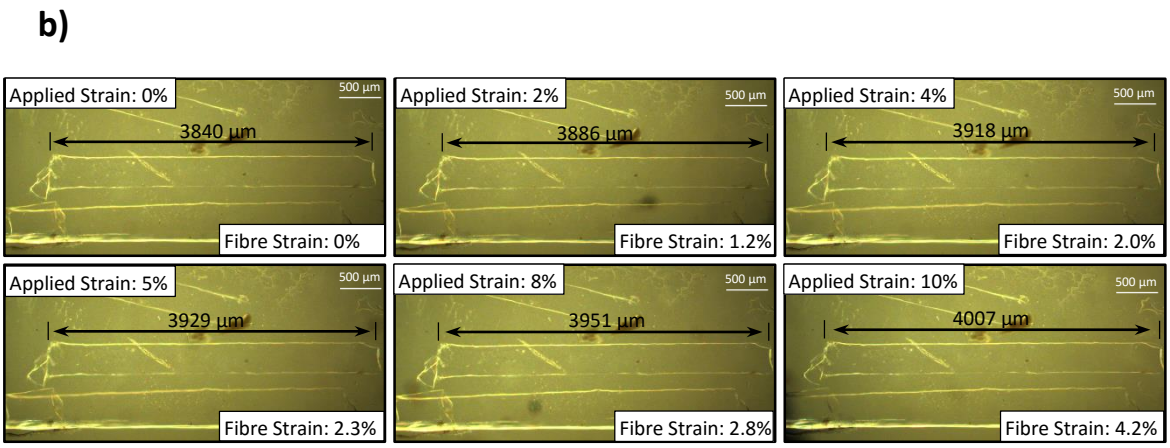

Figure 38: a) Uniaxial strain rig and grip setup. Grips use a flexible silicon membrane to hold sample firmly in place without exerting too much pressure which could crush the composite. The entire assembled rig is placed on top of a microscope stage and images taken through the transparent sample chamber. b) Example images of fibre extension calculations; the change in fibre length was measured and divided by the original length to obtain fibre strain. This was done at each applied strain increment.

Gross Mechanics

Bulk mechanical properties of fibre composites were determined using a Hounsfield tensile test machine and 5N load cell. Composites were made using the same method as that for the micromechanics with 20%, 40% and 60% PEG-RGD fibres seeded with tenocytes (3.5 million cells per well, each containing 100 fibres) and encapsulated in 20% PEG matrix. Plain PEG gels of 20%, 40% and 60% PEG were also characterised to assess the mechanical properties of the separate materials.

For testing, each end of the composite was placed inside a folded piece of card using glue (Loctite Power Flex Control Gel) with the test length defined as the distance between the edges of each card (Figure 39). The specimens were then setup up into the tensile test machine and grips placed on the card to prevent specimen slippage and damage. Composites were then strained at a rate of 15% / min, with force and extension recorded (n = 9-13).

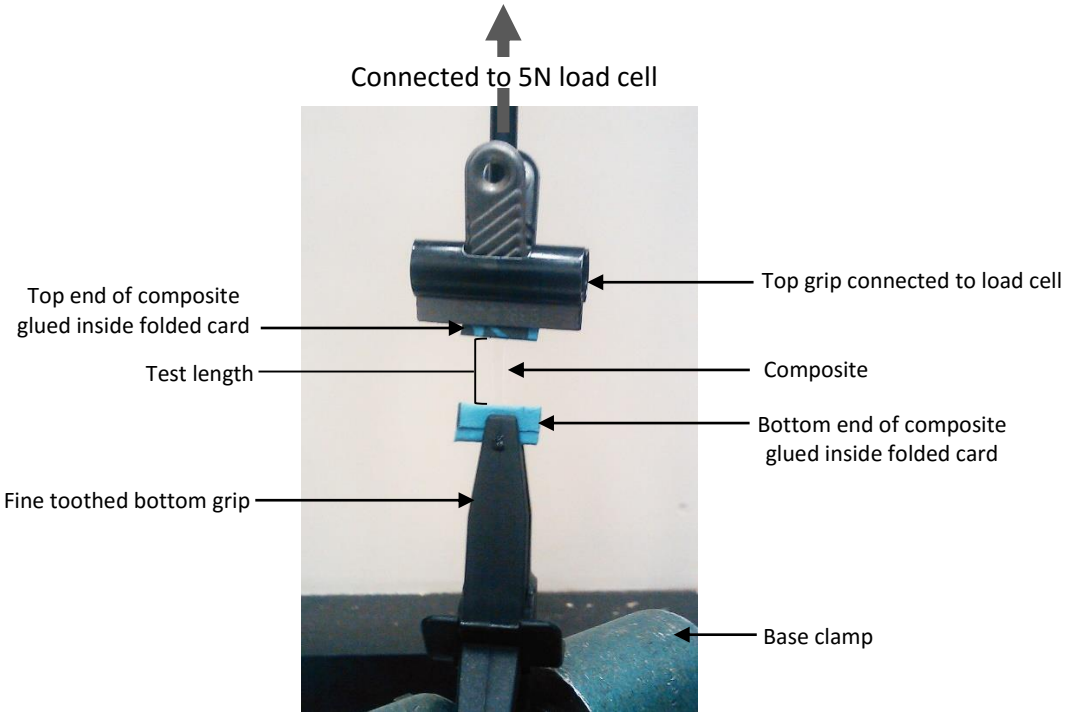

Figure 39: Configuration for the bulk mechanical testing of composites using the Hounsfield Test Machine. Composite ends were glued in-between sturdy folded card pieces. These could then be gripped firmly and the composites tested to failure without sample slippage. The sample test length was defined as the distance between the top card edge and the bottom card edge, and load measured using a 5N load cell.

Results

Peptide Conjugation

The assay showed successful conjugation of YRGDS and DGEA to acrylate-PEG-NHS, with conjugation values of 96% and 80% respectively (Figure 40).

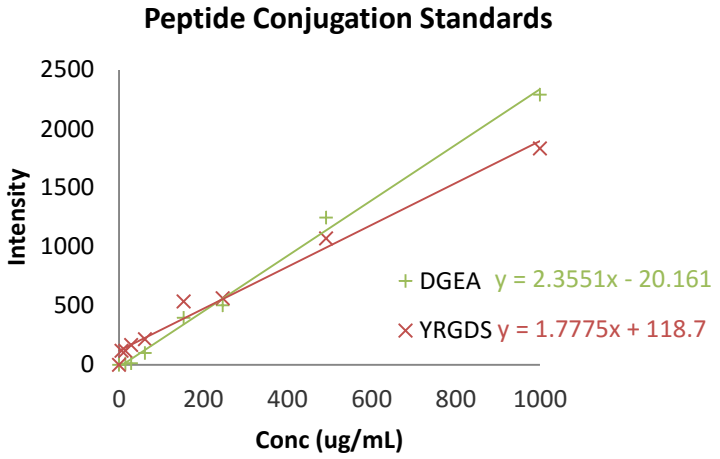

Peptide	Intensity	Peptide not conjugated (µg/mL)	% Conjugation
DGEA	1384	596.3	80
YRGDS	413	165.3	96

Figure 40: Graph and table summarising standards and peptide conjugation percentage for YRGDS and DGEA.

Fibre integration

The average integration distance was calculated by plotting the intensity profile of the fibre (green) and the matrix (red) across a line (Figure 41a). An intensity cut-off threshold was created for the red (matrix) channel by averaging the intensity of red at the central 25 µm of the fibre, essentially correcting for background fluorescence. The integration distance was then taken as the amount of red matrix inside the green fibre up to the threshold line. The average integration distance at increasing soak times was found to show a non-significant weak positive trend; at 0 and 120 minutes the average integration distances were 43 µm and 68 µm for 40% PEG-RGD and 66 µm and 75 µm for 20% PEG-RGD fibres, respectively (Figure 41b).

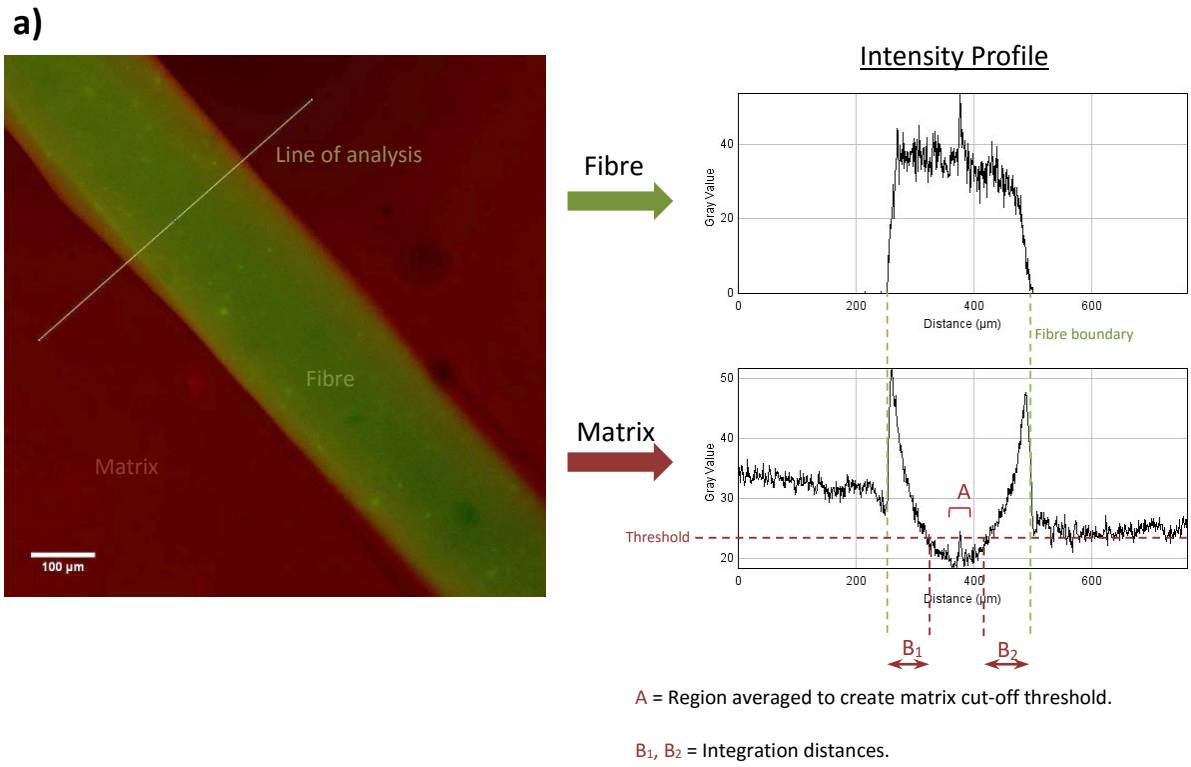

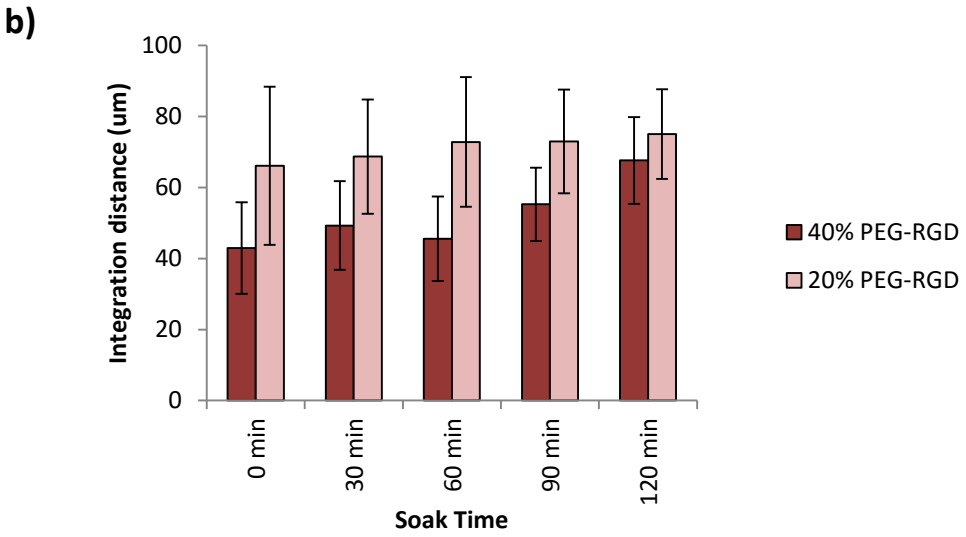

Figure 41: a) Example of matrix-fibre integration calculation on a 20% PEG-RGD fibre with 0 min soak. Intensity profiles were plot along 3 lines running across the fibre (only one line shown) for the red (matrix) and green (fibre) channels separately. The green channel was used to define the boundaries of the fibre. The distance of red fluorescence past these boundaries was then measured up to the matrix 'cut-off threshold' and taken as the integration distance. The cut-off threshold was determined by averaging the intensity of red at the central 20 µm portion of the fibre, thus correcting for background fluorescence. b) Integration data from composites made from 20% and 40% PEG-RGD fibres at varying soak times. (n=3, with 3 composites containing 2 fibres each and 6 measurements on each fibre). Integration of the matrix into the fibre can be seen to be successful, with a weak-positive trend as soak time is increased.

Cell attachment

Figure 42 shows cells attached to the surface of fibres 3 hours after seeding possess a closely packed and circular morphology. However, at 24 hours, the cells were seen to spread and cover the surface of the fibre.

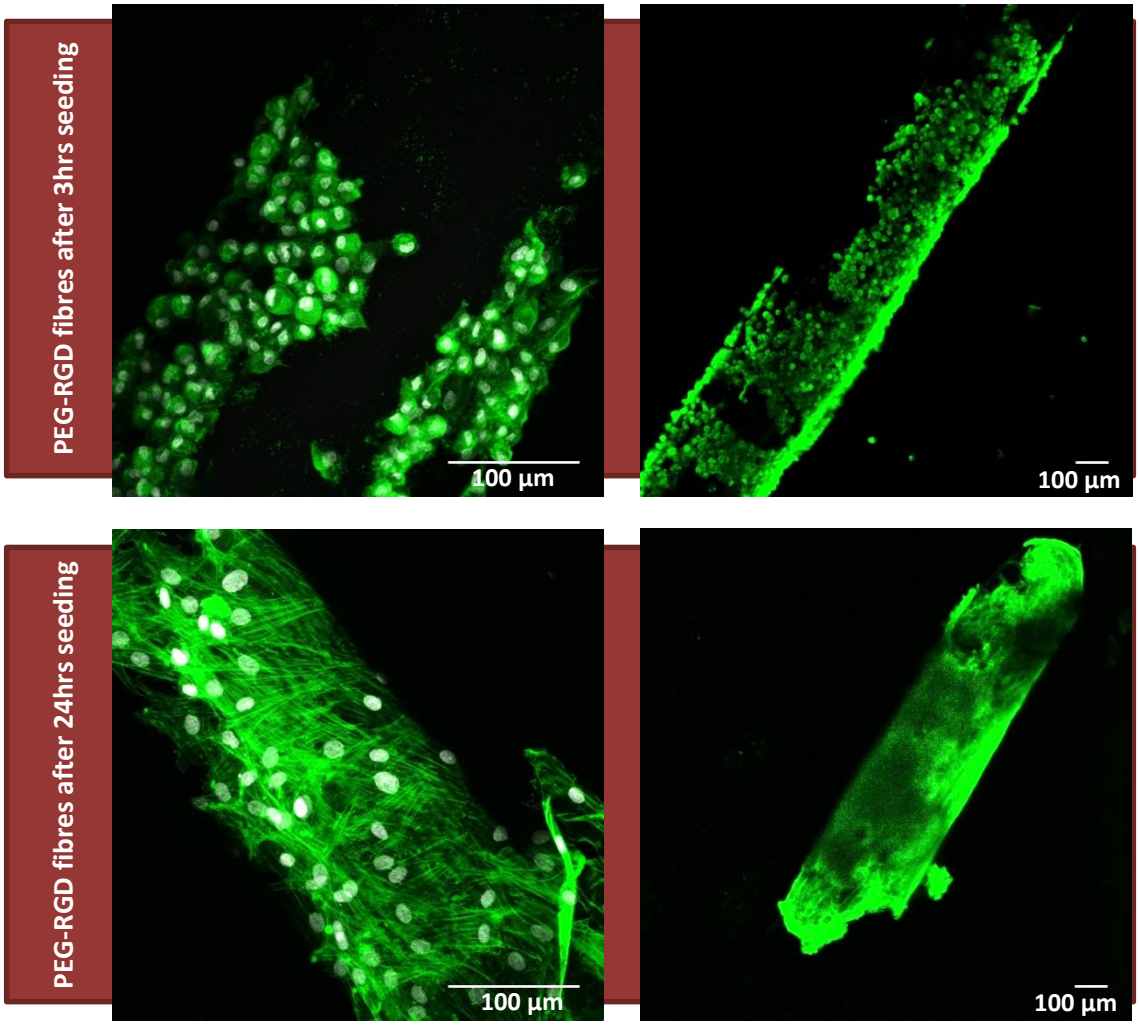

Figure 42: Phalloidin (Alexa Fluor 488) and DAPI staining of PEG-RGD fibres at 3hrs and 24 hrs post seeding using confocal imaging at x10 and x40 magnification. Cells were seen to attach to fibres 3 hours post seeding, however they exhibited a spherical morphology suggesting they were not well attached. After 24 hours the cells spread across the surface of fibres and no longer showed the compact spherical appearance.

The cells were seen to remain viable at all soak times used, with the final time point of 120 minutes possibly showing slightly more dead cells (visually) (Figure 43). Dead cells were also visible around areas devoid of cells, however this was due the handling of fibres; areas where the fibres have been picked up with forceps will consequently result in crushed cells, with such areas identified by having viable cells on either side of the small empty region (indicated on Figure 43).

The cylindrical structure of fibres resulted in cells being present at varying depths relative to the microscope lens and therefore at varying levels of focus. Consequently, images of fibres within composites had both a focused region and an out of focus region where the fibre curved. Nonetheless, it was still possible to get an overview of cell viability qualitatively from these images. It should be noted that the images in Figure 42 look clearer than those in Figure 43 since a confocal microscope was used; as fibres for Figure 42 were not encapsulated in gels, it was possible to get the fibres close to the high magnification lens such that they were within the lens working distance, enabling the use of confocal microscopy.

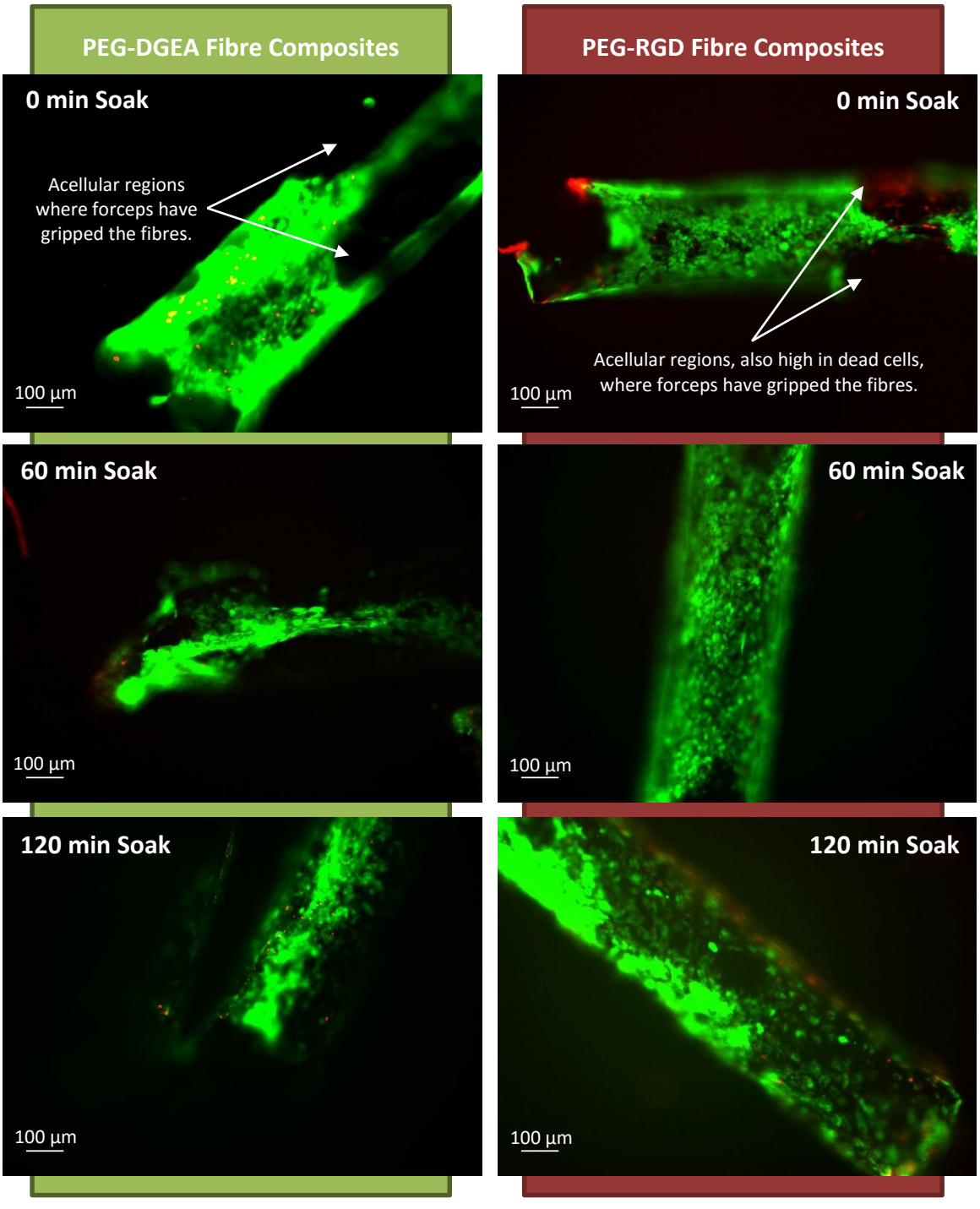

Figure 43: PEG-RGD and PEG-DGEA fibres within 20% PEG matrix with a 0, 60 and 120 minutes soak before polymerisation. Cells stained with Calcein AM and Ethidium Homodimer and imaged using an epi-fluorescent microscope at X10 magnification. Cells remain viable after soaking in 20% PEG for 0, 60 and 120 minutes, with only a slight increase in dead cells seen visually at the 120 minutes time point. This is true for both PEG-RGD and PEG-DGEA fibres. Acellular regions are seen as a result of forceps crushing cells when the fibres are picked up.

Gross Mechanics

The mechanical properties of plain PEG was seen to differ with PEG concentration, confirming that increasing PEG concentration increased the stiffness of PEG (Figure 44). On the other hand, bulk mechanical properties of the composites (Figure 45) were seen to be similar for all composites with no significance between the groups. When looking at the data paired by fibre stiffness, i.e. bars of the same colour in Figure 45, it can be seen there was a trend for a small increase in the ultimate tensile strength (UTS) when the soak time increased; when 60 minutes soak was used instead of 0 minutes, the mean UTS increased by approximately 4, 13 and 7 kPa for 20%, 40% and 60% PEG-RGD fibres respectively. Similarly, this pattern was also seen with the failure strain differences of the composites and, to a lesser extent, with the modulus differences. Additionally, the modulus of the composites generally showed a small increase when the PEG percentage, i.e. the fibre stiffness, was increased (Figure 45c).

Micromechanics

Figure 46 shows the micromechanics of the composites made from 20%, 40% and 60% PEG-RGD fibres with either a 0 or 60 minutes soak. The fibre strain was seen to change depending on the type of composite even though bulk mechanical properties remained the same, with softer 20% PEG-RGD fibres stretching more than stiffer 60% PEG-RGD fibres. Figure 47 further investigates this relationship, 20% PEG-RGD fibre composites with 60 minute soak creating the least shear while 60% PEG-RGD composites with 0 minutes soak produced the highest amount of shear.

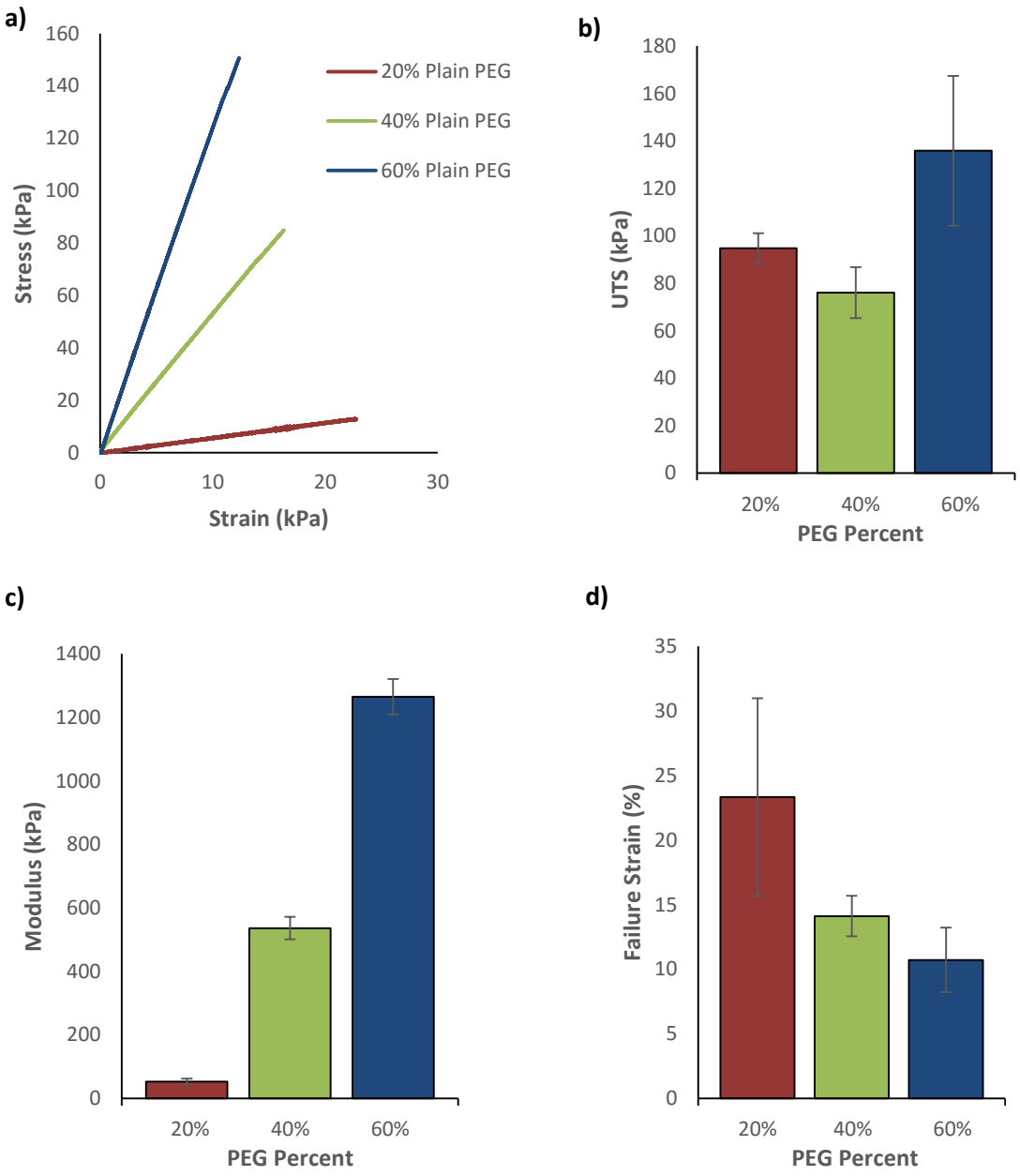

Figure 44: Average mechanical properties of plain PEG gels made from 20%, 40% or 60% PEG. a) Shows stress-strain curves of representative samples, b) shows the average failure strain (%), c) shows the average UTS (kPa) and d) shows the average modulus (kPa) of the composites (n = 10-11). The gross mechanical properties are seen to increase slightly with increasing soak times, but no significant differences are evident. Significance difference can be observed in the modulus of PEG, with higher PEG concentration resulting in a stiffer material. The failure strain also decreases with increasing PEG concentration.

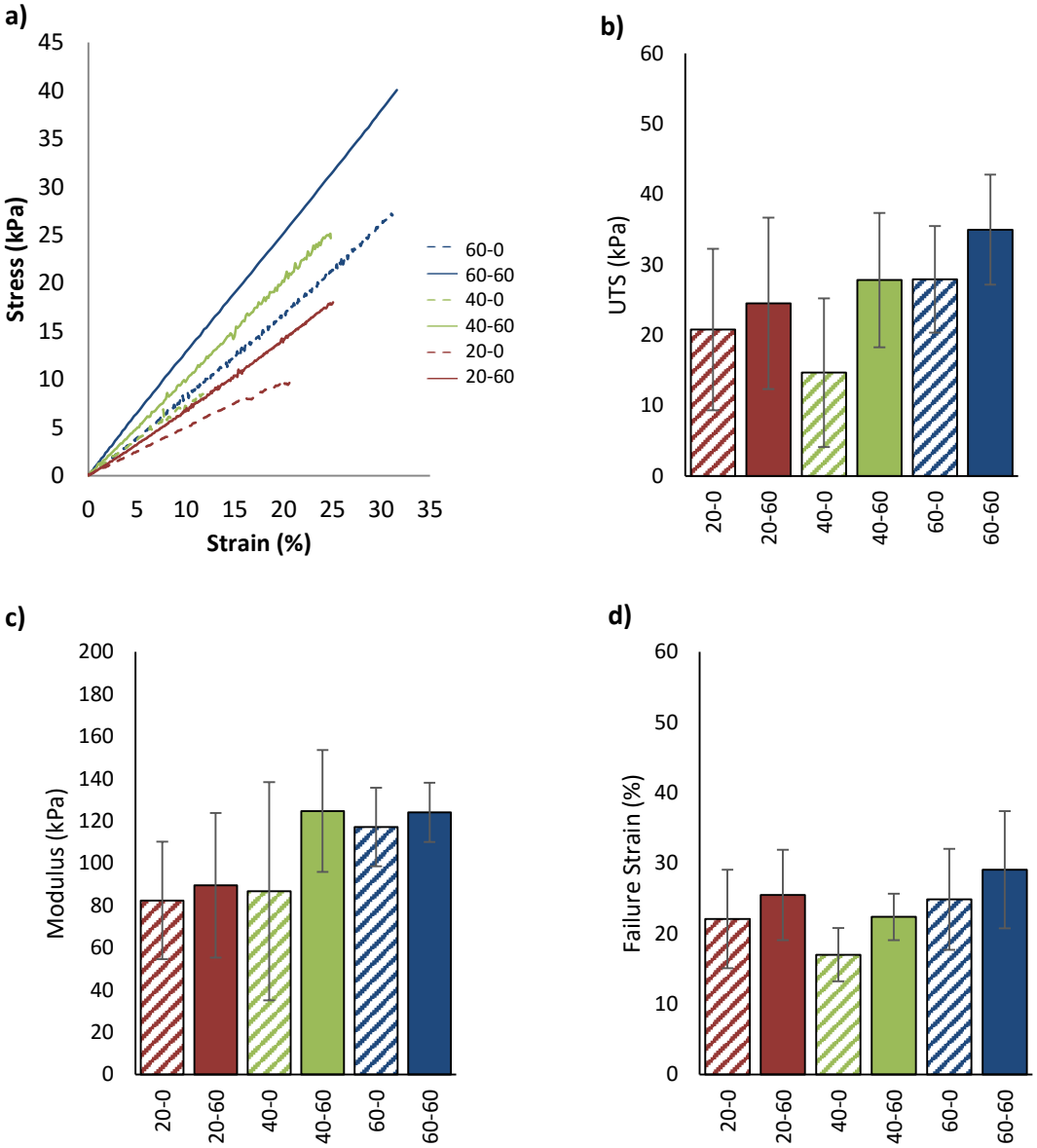

Figure 45: Average gross mechanical properties of composites made with 20%, 40% and 60% PEG-RGD fibres seeded with cells and soaked for either 0 or 60 minutes. Samples are labelled as 'XX-YY', with 'XX' indicating the PEG fibre type and 'YY' indicating the soak time. Similarly, bars of the same colour indicate the same fibre type, while striped and solid colours indicate 0 and 60 minutes soak respectively. a) Shows stress-strain curves of representative samples, b) shows the average failure strain (%), c) shows the average UTS and d) shows the average modulus of the composites (n = 9-13). The gross mechanical properties are seen to increase slightly with increasing soak times, but no significant differences are evident.

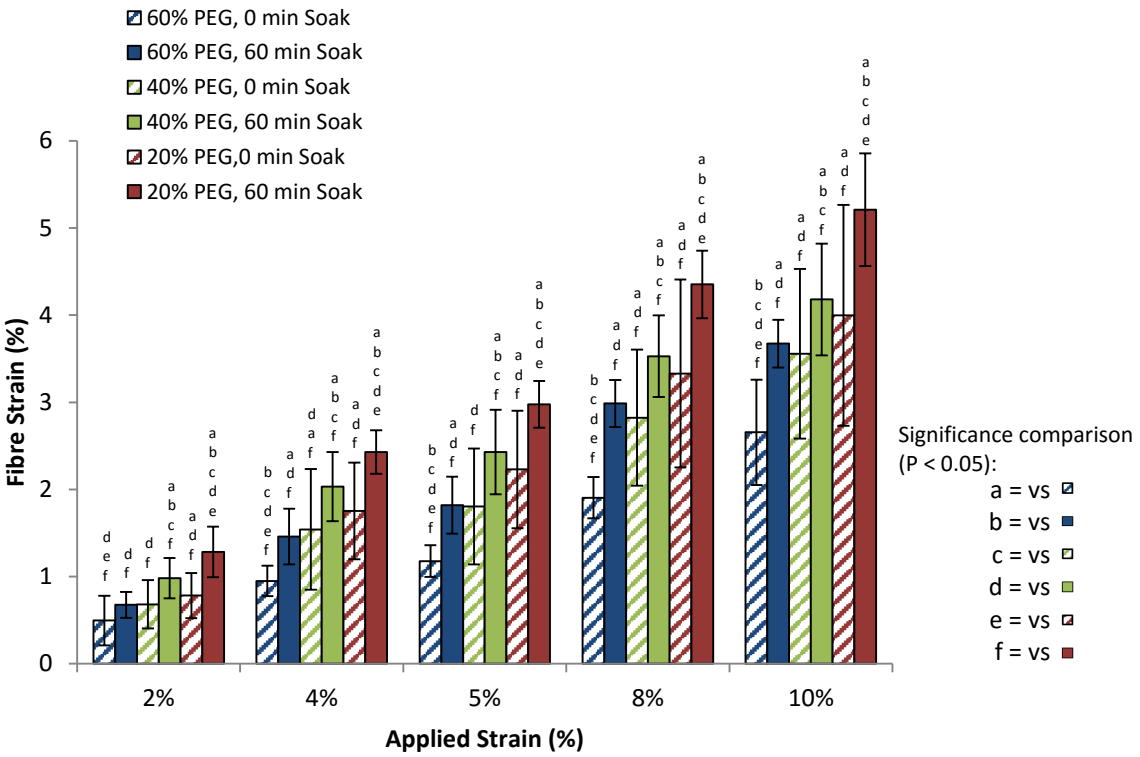

Figure 46: Summary of micromechanics data obtained after image analysis of cell seeded composites (n=12-15). It can be seen that at any given gross applied strain, the resulting fibre extension can be changed by using a combination of fibre stiffness and soak time; using stiffer fibres (higher percentage PEG fibres) the magnitude of fibre strain is reduced, while increasing the soak time increases the magnitude of fibre strain. For example, at 5% applied strain, composites can be made where the fibres stretch by approximately 1.2% or up to 3%, which translates to a range of 24%-60% of the applied strain.

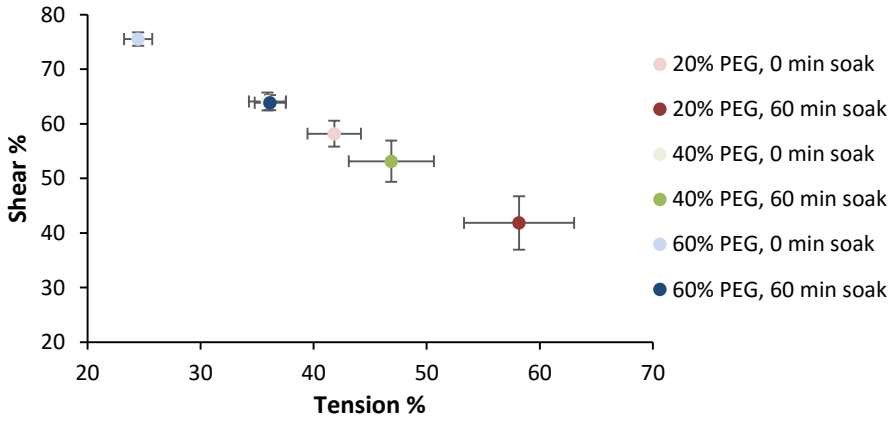

Figure 47: Shear-tension ratio averaged across 2%, 4%, 5%, 8% and 10% applied strain for each composite type (n=12-15). As 100% tension would theoretically result in 0% shear, shear % was calculated as 100%-tension %. It can be seen that the different combinations of fibre stiffness and soak time create a range of shear-tension ratios, ranging from high shear and low tension (fibres with 60% PEG and 0 minutes soak) to low shear and high tension (fibres with 20% PEG and 60 minutes soak).

Discussion

The new system replaces PHEMA fibres used in previous iterations of the composite with PEG-peptide fibres. This eliminates the self-crosslinking problem seen with coupling agents used on PHEMA fibres that prevented matrix-fibre integration and hence reduced control over micromechanics. Although the matrix-fibre interface study summarised in Figure 41 confirmed the presence of matrix interpenetration and showed a weak positive trend with increasing soak times, the data obtained did not show significant differences between the different composite types. Moreover, it is unknown how slight changes in integration may affect mechanical properties of the composites at the fibre level, so having successfully achieved integration, micromechanical analysis of the composites was pursued to investigate the capacity to generate varies shear-tension ratios.

As can be seen from Figure 46, the data obtained from micromechanics analysis reveals the properties of the composites more clearly, with a distinct pattern through the different groups. Following fibre composite theory, stiffer fibres in composites result in less fibre extension at any given applied strain, while increasing the soak time to increase fibre-matrix integration, increases the extent of fibre extension. As these micromechanical data are collected with fibres seeded with cells, the data obtained shows the expected properties of the composite during future mechanotransduction studies. Figure 46 also shows an ideal range of properties can be created from the composites. For example, at 5% applied strain, we can have composites where fibres stretch approximately 1% through to composites where the fibres stretch approximately 3% (illustrated in Figure 48). Studies have found that the fibres within physiological tendons stretch by about 40% of the applied strain (or 2% for an applied strain of 5%) (Shepherd et al., 2014). Composites made from 20% PEG-RGD fibres with 0 minutes soak, 40% PEG-RGD fibres with 0 minutes soak, 40% PEG-RGD fibres with 60 minutes soak and 60% PEG-RGD fibres with 0 minutes soak all recreate shear/tension ratios similar to these physiological conditions for cells. Additionally, the low fibre extension composite (60% PEG-RGD with 0 minute soak) and

the high fibre extension composite (20% PEG-RGD with 60 minute soak) can create pathological conditions of high and low shear, respectively.

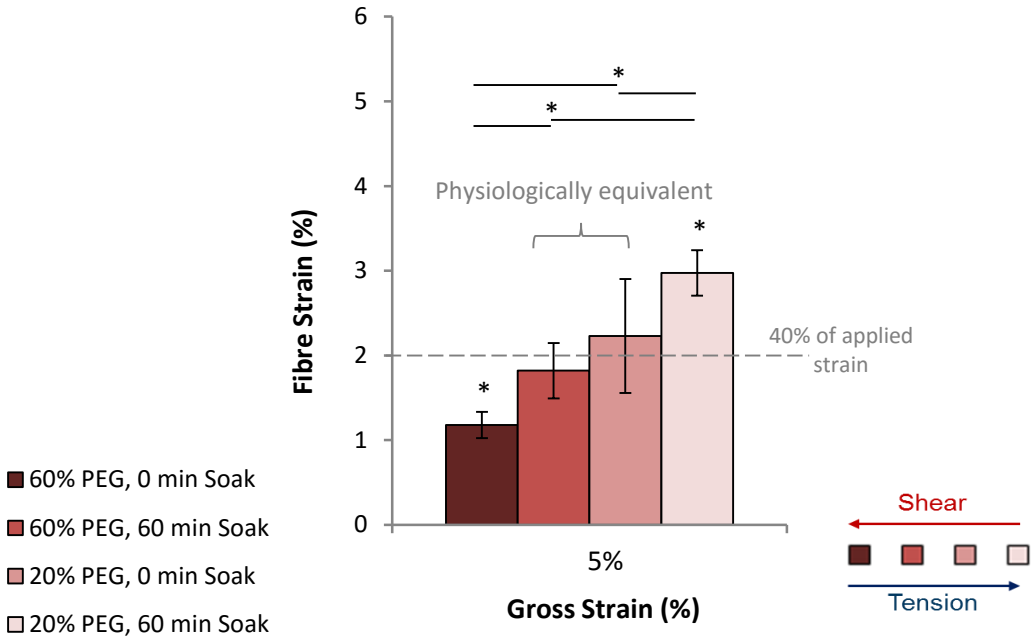

Figure 48: Graph of average fibre strain (%) at 5% gross applied strain for all composite types (n=12-15). Fibre strain ~40% of the applied strain is seen in physiological tendons (Shepherd et al., 2014). The graph indicates two composites capable of creating physiologically equivalent conditions (60% PEG fibres with 60 minute soak and 20% fibres PEG with 0 minute soak). A high shear - low tension condition can also be created (60% PEG fibres with 0 minute soak) in addition to a low shear – high tension condition (60% PEG fibres with 60 minute soak). * = P<0.05.

The gross mechanics was essentially similar for all types of composites, with only slight non-significant differences evident in the modulus when stiffer fibres were used (Figure 45). This is to be expected as PEG itself is not a very stiff material when hydrated, and since a large molecular weight was used (PEG MW ~ 3000), the increase of PEG concentration in fibres, combined with the relatively low numbers of rods is likely insufficient to dramatically affect the bulk mechanical properties. Additionally, since cells were present, the matrix-fibre interface would be intermittent, consequently reducing the effect of fibre stiffness on the extension of the bulk material. Nonetheless, although the bulk properties remain the same, the critical variation in the micromechanics of the composites differ when using the different fibre types.

The cylindrical nature of fibres present a problematic scenario for imaging as higher magnification lens have a limited depth of field and the changing fibre depth blurs cells in the background. This is further accentuated when the fibres are encapsulated into composites as the matrix thickness increases the distance the fibres are from the microscope lens. Therefore it is difficult to image cells clearly with high clarity and magnification. However, by using x10 magnification, it is still possible to get an overview of the viability of cells qualitatively as seen from Figure 43. Cell attachment was confirmed on both PEG-RGD and PEG-DGEA composites, with the majority of cells remaining viable after soaking fibres for up to 120 minute before polymerisation. This, along with the conjugation assay, demonstrates the ability to conjugate the desired peptide sequence group to PEG while also retaining the intended biofunctionality of the peptide.

Further imaging of cell-seeded PEG-RGD fibres with Phalloidin (Alexa Fluor 488) and DAPI dyes showed cells attached 3 hours post seeding (Figure 42). After 24 hours the cells spread to cover the surface of the fibres, indeed showing results similar to that seen in the previous system (2.3.2.2). Therefore, the previously established cell seeding protocol was kept the same for this system.

In conclusion, the new system eliminates the integration problems seen with previous attempts, successfully allows cell attachment through protein mimetic peptides, and creates controllable high and low shear cellular environments. As such, it is presented as a viable system to allow the exploration of shear-tension ratio effects on cells.

Chapter 3: Protocols and Protocol Optimisation

With the final fibre composite system validated, this chapter covers the necessary protocols for composite manufacture with different resident cells and also outlines the optimisation of gene analysis protocols.

Note 1: Further details of all chemicals used, including supplier details, are present in Table 35 and Table 36, in Appendix B: Chemicals and Materials List.

.

3.1 Cell Resuscitation, Culture and Passaging

10% FBS (section 2.3.2.2) was warmed to 37°C in a water bath. A sterile hood was prepared along with 50 mL conical tubes, 10 mL stripettes, sterile pipette tips and a T150 flask. The cell vial to be resuscitated was removed from the cryobank and briefly opened under the hood to release pressure. The vial cap was then closed firmly and the vial thawed quickly by dipping in a 37°C water bath for 2-3 minutes. Once completely thawed the cell suspension in the vial (usually 1 mL) was transferred into 10 mL of media. This was then centrifuged as 2000rpm for 5 minutes, after which the media was aspirated and the cell pellet re-suspended in 5 mL media. The T150 flask was filled with 20 mL media and the 5 mL cell suspension added. This was then incubated at 37°C and 5% CO_2.

During culture, the culture media was changed every 2-3 days until cells were more than 75% confluent. The cells were then passaged by detaching the cells through the use of Trypsin-EDTA as described previously in section 2.3.2.2, and cell culture continued until the required cell number was reached.

3.2 Fibre Composite Production

The final version of the composite system consisted of a 20% PEG matrix, encapsulating cell seeded PEG-RGD fibres made of either 20% or 60% PEG. The stages of manufacture included the synthesis of the PEG hydrogel in a photopolymerisable format, followed by fibre production, cell seeding of fibres and finally encapsulation of fibres into the surrounding PEG to create composites ready for use as depicted in Figure 49.

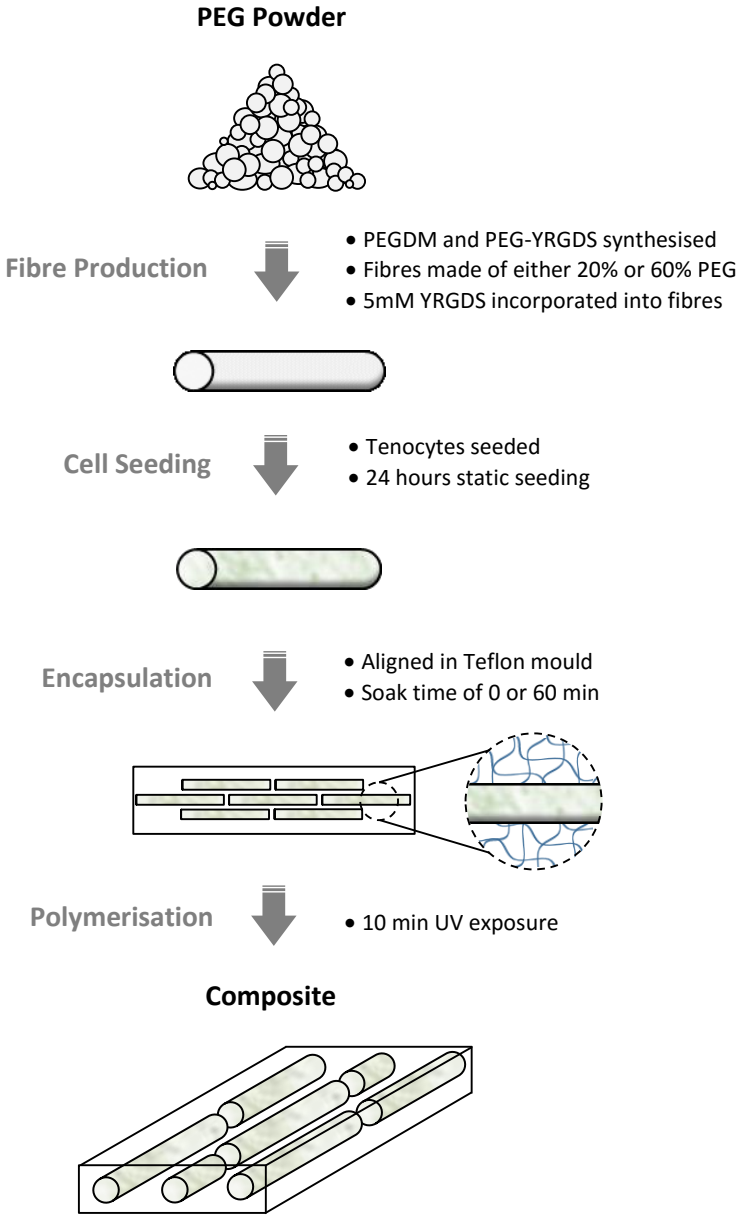

Figure 49: Schematic briefly summarising the procedure to produce composites from PEG. Stages include PEGDM synthesis, peptide conjugation, fibre production, cell seeding, encapsulation and polymerisation.

3.2.1 Material Synthesis

PEGDM was used for making both the matrix and the fibres of the composite system. It was synthesised in the laboratory using a two-step, methacrylation and purification process, as described in section 2.3.1.

Peptides were conjugated to PEG via a commercially available intermediate material, Acrylate-PEG-NHS using the procedure described in section 2.3.3.

3.2.2 PEG-RGD fibres

PEG-RGD fibres were created in two different stiffness by changing the percentage of PEG; 60% PEG and 20% PEG were used to create stiff and 'less stiff' fibres, respectively.

The solutions for both PEG % were made using a combination of PEGDM, PBS and photoinitiator (PI) made of Irgacure 2959 at 0.006 g/mL in PBS:

20% PEG:

- 0.2 g PEGDM
- 83.8 µL PI
- 716.7 µL PBS

60% PEG:

- 0.6 g PEGDM
- 83.8 µL PI
- 316.7 µL PBS

The solutions of PEG were made by mixing the 3 components described in a 5 mL vial and vortexing to dissolve the PEGDM, particularly the viscous 60% PEG solution. 5mM of acrylate-PEG-YRGDS was then added to the solution to incorporate the peptide, usually taking 1 mL PEG solution and adding 21 mg acrylate-PEG-YRGDS.

Fibres were created by pipetting the solution into Teflon moulds (arrangement depicted in Figure 50). The moulds contained holes of 0.33 mm diameter and 4 mm in length as needed for each fibre. A glass slide (75 mm x 25 mm x 1 mm) with a thin silicon gasket (0.4 mm thick) was

first placed under the mould, then the top covered with a second glass slide once the solution was pipetted into the mould. The edges of the Teflon moulds were covered with silicon grease in addition to using the gasket to create a capillary chamber to help fill the holes, efficiently producing fibres without wasting peptide (depicted in Figure 50). Magnets were used on the top and bottom of the compiled mould to keep the glass slides secures.

The fibres were polymerised by placing the filled mould under UV light (365nm wavelength, ~4mW/cm2) for 10 minutes, turning the mould over after the first 5 minutes. The fibres were then extracted as described previously, collected in a small petri dish containing 70% ethanol and stored at 4°C until needed. The mould was cleaned with 70% ethanol, the holes cleared using a thin wire and re-used to create more fibres.

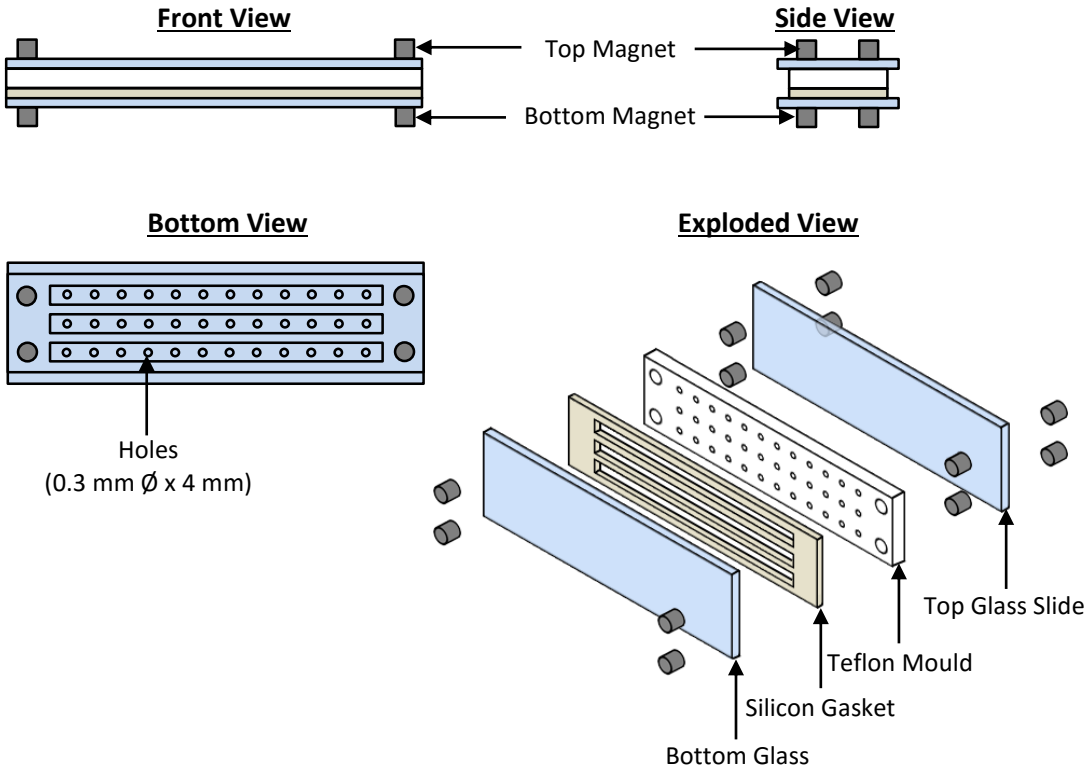

Figure 50: Front, side, bottom and exploded view of Teflon mould setup to efficiently create fibres. Mould contained 36 holes of 0.3 mm in diameter (Ø) and 4 mm in length. The edges of the glass slides are lightly covered in silicon grease to provide a liquid tight seal. All parts excluding the top glass slide and top magnets are greased and assembled first, then the hydrogel solution pipetted into each hole, after which the top glass slide can be placed on top and secured with magnets (and bulldog clips if needed) and placed under the UV lamp. Not to scale.

3.2.3 Cell seeding

Once enough fibres were made for an experiment they were seeded with cells using the static culture method and serum free media.

Serum Free media (i.e. without FBS):

- DMEM, low glucose (500 mL)
- HEPES (1M) (10 mL)
- L-glutamine (200mM) (5 mL)
- Penicillin/Streptomycin (10000U/10mg per mL) (5 mL)
- Non-essential amino acids (5 mL)

The fibres were sterilised before seeding. This was partly done by storing the fibres in 70% ethanol (minimum 2 hours in ethanol before use) when made, but was further ensured by briefly exposing fibres to short wavelength UV light for 1 hour in a sterile hood and using aseptic techniques when working with them. Once sterile, the fibres were transferred into a 24 well plate using sterile forceps, with a single well containing between 150-200 fibres and serum free media. Each fibre type was kept in separate wells to enable easy identification and temporarily placed in the incubator to warm up and displace the ethanol while the cells were prepared.

Cells were harvested from flasks using Trypsin-EDTA as described in section 2.3.2.2. After re-suspending the cells in a known volume of 10% FBS media, the cells were counted using a haemocytometer and trypan blue and re-suspended in serum-free media such that the resultant solution was 3.5 million cells/mL. The well plate containing fibres was retrieved from the incubator and the serum free media aspirated. The fibres were then slowly covered with 1 mL of the cell solution (i.e. 3.5 million cells) and topped up with an additional 0.5 mL serum free media. The plates were then incubated for the cells to attach. After 1.5 hours, 0.5 mL media was removed from each well and replaced with fresh 10% FBS media to introduce some serum. After a further 1.5 hours (i.e. total 3 hours after seeding) sterile forceps were used to transfer

the fibres into new wells containing 10% FBS media. Fibres were then incubated overnight to let the cells fully attach.

A full 24 hours after seeding, the fibres were ready to be encapsulated.

3.2.4 Fibre encapsulation

Encapsulation was performed as described previously in section 2.3.3 in a sterile hood and required aseptic techniques similar to those for cell seeding fibres to maintain sterility. The quantity of 20% PEGDM solution needed to create the required number of composites was calculated and prepared by following the formulation described in 3.2.2. PBS was substituted with 10% FBS media to keep media present around cells once fibres were encapsulated, and 1 composite required approximately 0.1 mL PEGDM solution. The solution was sterile filtered using 0.22 µm filters and warmed in a water bath to 37°C.

The 24 well plate containing seeded fibres was retrieved from the incubator. A small quantity of PEGDM solution was drawn into a 5 mL syringe with a 25 gauge needle while the rest was placed back into the water bath. The composite moulds were rectangular (2.5 mm x 25 mm x 1 mm) as shown in Figure 51, where a Teflon strip contained 3 moulds. The outer areas of the Teflon strips were lightly greased with silicon, taking care to avoid the area where the hydrogel solution would be in contact and thus reduce the possibility of contamination. A sterile glass slide was placed to one side and a small drop of PEGDM placed on this as a dipping agent for fibres, to displace any media and coat with PEGDM prior to positioning in moulds. A small drop of PEGDM was also placed in the centre of each individual composite mould to help fibres stay in place once positioned. A total of 10 fibres were placed in each composite mould and arranged axially. The Teflon strip allowed up to three composites to be made at once.

Once fibres were placed in the moulds, a glass slide was placed on top of the Teflon strip, overhanging one edge (as depicted in Figure 51), and secured with bulldog clips. Each composite

mould was then filled with PEGDM solution. The solution was injected slowly to prevent fibres from being pushed towards the end of the mould and only filled ¾ full. At this point the mould was filled from the other end to push the fibres back towards the middle of the groove and further align them axially. The mould was then left for either 0 minutes or 60 minutes to soak depending on the type of composite being made and then placed under the UV (365 nm, ~4mW/cm^2) lamp for 10 minutes to polymerise. The composites produced were removed from the mould and stored in a petri dish containing 10% FBS media, and housed in the incubator.

The procedure was repeated, dipping fibres in PEGDM, aligning in the mould, injecting PEGDM solution and polymerising until all the composites were made.

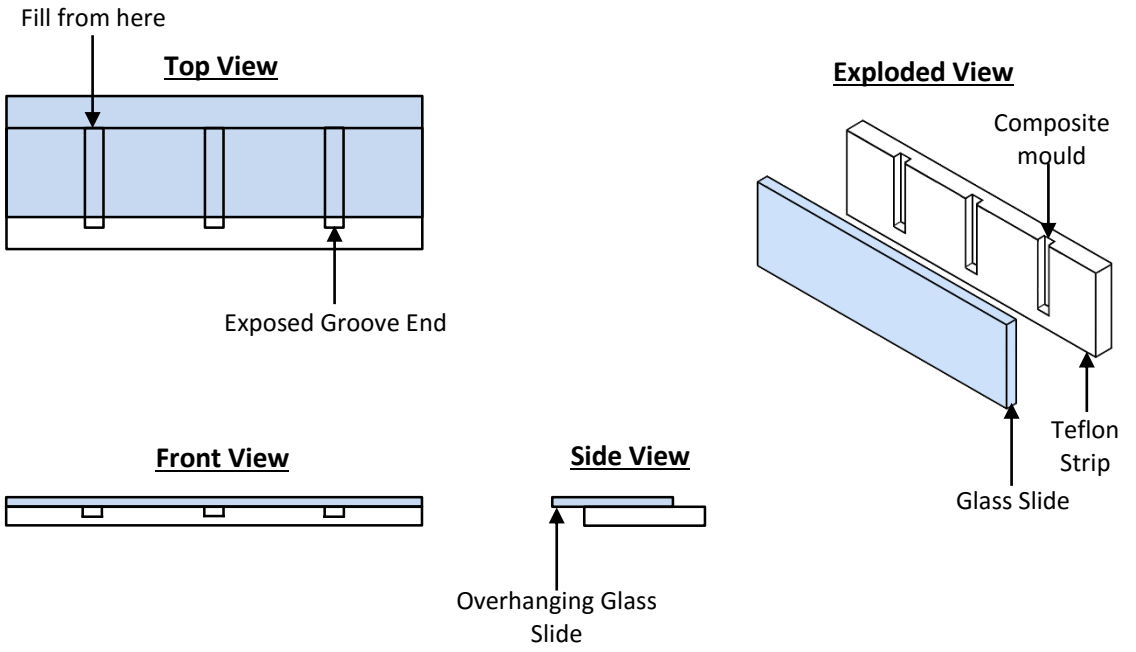

Figure 51: Teflon Mould and glass slide configuration. The glass slide was left overhanging to expose one end of the groove allowing air to escape while filling and to enable filling from both ends. Teflon mould surface in contact with glass slide was lightly greased, with care taken not to clog the grooves, and the glass slides held firmly on top through the use of multiple bulldog clips.

3.3 RNA Extraction

In order to investigate cell response to strain within composites, gene expression approaches were adopted. This requires the extraction of RNA from the composites, reverse transcription into cDNA and then cDNA amplification via polymerase chain reaction (PCR). There are a number of methods for sample homogenisation to extract RNA such as digestion, shearing or grinding, with the method selected being dependent on the sample type. The composites present a unique challenge with a complex structure and relatively low cell numbers per construct compared to other tissues. It was necessary to first optimise the RNA extraction procedure to produce sufficient yields of useable RNA.

3.3.1 RNA extraction Optimisation

Experimental Overview and Methods

The optimisation of RNA extraction with composites followed a trial and error route starting from an established protocol (Ireland et al., 2001) with changes made sequentially based on the results. The range of protocols tested is summarised in Figure 52.

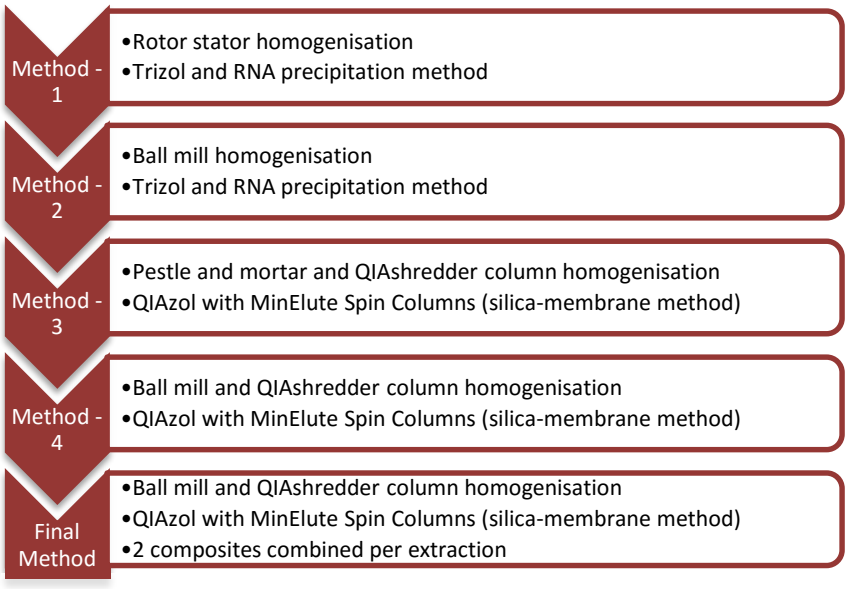

Figure 52: Summary of optimisation route

Method – 1

The first method of RNA extraction involved using Trizol, a rotor stator homogeniser for sample disruption and phenol-chloroform based phase separation as described by Ireland et al. (2001).

Both 20% and 60% cell seeded PEG-RGD composites with both 0 and 60 minutes soak (total 58 composites) were made for analysis. The composites were placed into 2 mL cryovials (each vial containing 1 composite) and snap frozen in liquid nitrogen either at 0 hours, 24 hours or 48 hours after production. The samples were then stored in a -80°C freezer until ready for processing. To begin the extraction process the vials were retrieved from the freezer and placed on dry ice in a fume hood. The rotor stator homogeniser tip was first rinsed in 70% ethanol, followed by RNase free water, operating the device while submerged in the respective solutions. 1 mL ice cold Trizol was added to a vial and 3 x 30 second bursts performed using the homogeniser. After the third burst, the state of the sample was checked and additional bursts performed if the composite was not fully homogenised. The sample vial was then placed on ice and the homogeniser tip cleaned with 70% ethanol and RNase free water. This was repeated until all samples were homogenised. The vials were then placed at RT, and 125 µg glycogen added as an RNA carrier. This was then incubated at RT for 5 minutes, after which 300 mL chloroform (~1/5 ratio) was added to each vial and shaken vigorously for 15 seconds to thoroughly mix the solution. The vials were incubated at room temperature (RT) for 3 minutes and then centrifuged for 15 minutes at 12,000g and 4°C to allow phase separation. The upper clear aqueous phase was transferred into a new micro-centrifuge tube with care taken not to transfer or touch the interphase. This was done for all the vials separately. An equal volume of isopropanol was added to each tube and incubated at RT for at least 10 minutes. The tubes were then centrifuged at 12,000g for 10 minutes at 4°C to pellet the RNA/glycogen. The supernatant was then discarded, with care taken not to discard the pellet, and washed by adding 70% ethanol and gently mixing with a pipette. The tubes were then centrifuged at 7,500g

for 5 minutes at 4°C and the wash step repeated with 70% ethanol and centrifuged again. After discarding the supernatant after the second rinse, the pellet was left to air dry for ~15-20 minutes (i.e. until the pellet appeared transparent). Once dry, 50 µL RNase free water was added to each vial and incubated for ~10 minutes. The tubes were mixed gentle agitation whilst housed in a tube rack and then stored at -80°C until ready to measure the quantity.

The RNA quantity is easily found by measuring the absorbance of the solution, with RNA absorbing strongly at a specific wavelength of 260nm. A NanoDrop spectrophotometer is an instrument capable of measuring the absorbance of UV wavelengths through samples as small as 1 µL. Hence the RNA quantity was determined using a NanoDrop 1000 spectrophotometer (*Thermo Scientific*). Samples were retrieved from the -80°C freezer and transferred onto ice. The NanoDrop sample pedestal was cleaned and RNase free water used as a blank. Samples were thawed, briefly centrifuged to collect the solution at the bottom of the tube, and 1 µL taken to place on the NanoDrop pedestal to measure RNA quantity. All the samples were measured, with the pedestal being cleaned after every sample.

The total RNA quantity was calculated from the implied concentration per µL given by the NanoDrop results and the 260/280 ratio compared.

Denaturing formaldehyde gel electrophoresis was performed on 8 samples to check sample integrity. One each from a range of composite conditions were tested: 20-60-0h, 20-60-24h, 20-60-48h, 60-60-0h, 60-60-24h and 60-60-48h (sample labels are described in the legend of Table 20). The Sample with the lowest RNA concentration (20-10-48h) and the sample with the highest RNA concentration (20-60-48h) were also tested. A rectangular gel with 8 sample wells was first made of agarose. This was done by heating a 1% agarose in RNase free water (DEPC treated) in a microwave for 30-40 seconds. The solution was then cooled in a rectangular mould and a ‘comb’ inserted to create wells. The gel was placed into the electrophoresis tank and filled with 1 X 3-morpholinopropanesulfonic acid (MOPS) buffer. 5 µL of each sample was mixed with

2.5 µL formaldehyde loading dye in a 0.5 mL micro-centrifuge tube and heat denatured at 65°C for 10 minutes. These were then chilled immediately after heating and loaded into the gel ports and the gel electrophoresis run for approximately 1 hour at 50-60V. The gel was then removed and imaged on top of a UV plate.

Results – 1

Table 20: Summary of NanoDrop results of all samples, showing mean (n=3 for 0 hour samples and n=6 for 24 and 48 hour samples) and standard deviation (SD) for the concentration, 260/230 and 260/230 ratio. Sample IDs indicate the composite type in the format 'XX-YY-ZZh' with 'X' indicating the type of fibre, 'Y' indicating the soak time and 'Z' indicating the time at which the composites were frozen after making. Total sample quantity was 50 µL.

No.	Sample type	Nucleic Acid Conc. ng/µl		260/280		260/230		Total RNA (ng)	
		Average	SD	Average	SD	Average	SD	Average	SD
1	20-60-0h	15.3	2.7	1.61	0.08	0.12	0.07	765	135
2	20-60-24h	22.2	6.2	1.63	0.07	0.09	0.06	1110	310
3	20-60-48h	41.7	58.8	1.63	0.09	0.15	0.06	2085	2940
4	60-60-0h	21.8	5.6	1.70	0.04	0.26	0.04	1090	280
5	60-60-24h	18.6	4.1	1.66	0.11	0.13	0.06	930	205
6	60-60-48h	18.3	7.5	1.63	0.06	0.15	0.04	915	375
7	60-0-0h	16.4	2.1	1.72	0.05	0.23	0.09	820	105
8	60-0-24h	25.5	7.7	1.61	0.04	0.18	0.07	1275	385
9	60-0-48h	19.8	9.2	1.67	0.15	0.14	0.07	990	460
10	20-0-0h	18.3	3.2	1.66	0.11	0.17	0.10	915	160
11	20-0-24h	18.2	4.7	1.64	0.09	0.12	0.07	910	235
12	20-0-48h	18.8	9.8	1.61	0.06	0.12	0.06	940	490

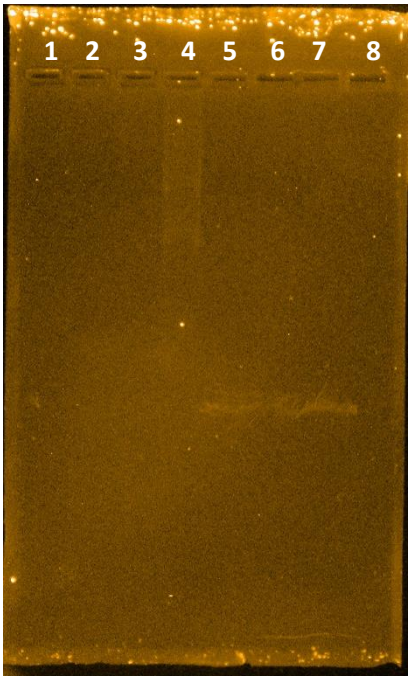

Figure 53: Gel electrophoresis image for 8 selected samples; 1) 20-60-0h, 2) 20-60-24h, 3) 20-60-48h, 4) 60-60-0h, 5) 60-60-24h, 6) 60-60-48h, 7) the individual sample with the lowest concentration (20-0-48h) and 8) the individual sample with the highest concentration (20-60-48h). Results show poor sample quality with only one sample (well 4) being at all visible.

Discussion and Conclusion – 1

The NanoDrop results show that the RNA concentrations extracted, although low, are above the detection limit of 2ng/µL imposed by the instrument. The yield itself is also sufficient for performing PCR as 100ng is usually required. However, the purity of the sample inferred by the 260/280 and 260/230 ratios suggests the samples are not reliable and the sample integrity is compromised. This is implied by the different absorbing UV wavelengths; RNA absorbs at 260 nm whilst contaminants such as phenol absorbs strongly at 230 nm and proteins absorb at 280 nm (NanoDrop Technologies, 2007). Hence 260/280 and 260/230 ratios are used to gauge the amount of possible contamination, although the effect is exaggerated at lower RNA concentrations and hidden at higher RNA concentrations. The 260/280 ratio is used most often for this purpose and RNA is said to be 'pure' if the 260/280 ratio is 2.0. However, since factors such as the composition of nucleic acids, pH of the RNA solution itself and the concentration of RNA are all known to affect the ratio magnitude, the ratio is used as a guideline and generally

accepted to be sufficient if between 2 ± 0.3 (Thermo Fisher Scientific, 2010). Since the results in Table 20 show the 260/280 ratio falls outside this range consistently, the possibility of contamination or sample degradation arose.

The results from the gel electrophoresis confirmed the above as the expected distinct 18S and 28S bands were not visualised, and only 1 sample (well 4) showed any signal at all. This suggested there was severe degradation of the samples and the procedure used for RNA extraction was not suitable.

One of the main stages where degradation could occur was during the homogenisation step as the samples need to be processed quickly to avoid RNases destroying the sample. Additionally, since the composites are tough to fully homogenise, the time required to sufficiently homogenise with the rotor stator may have generated too much heat and therefore degraded the sample.

Thus it was decided to try another means of homogenising the sample while also taking into consideration steps to keep possible RNase activity minimised.

Method – 2

Method – 1 was adapted by substituting the rotor stator homogeniser with a ball mill based machine (Mikro-Dismembrator U, *Sartorius*) which can keep the sample cooled for longer whilst homogenising.

Cell seeded composites were made with 40% PEG-RGD fibres and a 60 minutes soak, and snap frozen in 2 mL cryovials either as pairs (n=5) or individually (n=5) 24 hours after production and stored at -80°C until ready to use. On the day of RNA extraction, a small Dewar filled with liquid nitrogen along with a box of dry ice were prepared and a steel shaker chamber and steel grinding ball cooled inside the Dewar. The samples were retrieved from the -80°C freezer and kept on dry ice throughout the procedure except during necessary processing. Each sample was

removed from the vial and placed in the cooled shaker chamber along with the grinding ball, after which it was swiftly secured in the Mikro-Dismembrator and homogenised at 2000rpm for 1 minute. Once homogenised, the shaker chamber was quickly moved into a fume hood and the chamber opened to pipette in 1 mL Trizol. Due to the chamber being made of metal and cooled in liquid nitrogen, the chamber remains cold when Trizol is added and therefore freezes on contact. As soon as the Trizol started to thaw, the mixture was thoroughly mixed by pipetting and transferred into a 1.5 mL micro-centrifuge tube and kept on ice. The shaker chamber and grinding ball were cleaned with 70% ethanol and RNase free water before being used again to process the rest of the samples. Once all samples were homogenised and in Trizol, the remaining steps described in Method – 1 were followed; glycogen was added to each tube, then chloroform added to perform phase separation, the supernatant collected into separate tubes and centrifuged to create a pellet which was then washed with 70% ethanol twice and re-suspended in RNase free water. To create a more concentrated sample, 40 µL of RNase free water was used instead of 50 µL to re-suspend the RNA and then samples stored at -80°C.

NanoDrop was used to measure the RNA quantity of the samples and denaturing gel electrophoresis performed to check the integrity as described in Method – 1.

Results – 2

Table 21: NanoDrop results for RNA extracted from composites using the modified method. Doubling composites during extraction does not seem to always increase the quantity of RNA and thus seems variable (samples 6-10).

Sample No	No. of Composites	Concentration (ng/µL)	260/280	260/230	Total RNA (ng)
1	1	6.86	1.63	0.13	274.4
2	1	4.66	1.57	0.23	186.4
3	1	14.93	1.84	0.05	597.2
4	1	19.62	1.72	0.08	784.8
5	1	18.21	1.77	0.51	728.4
6	2	53.82	1.61	0.22	2152.8
7	2	49.14	1.57	0.11	1965.6
8	2	14.70	1.65	0.49	588.0
9	2	12.14	2.07	0.03	485.6
10	2	17.43	1.76	0.53	697.2

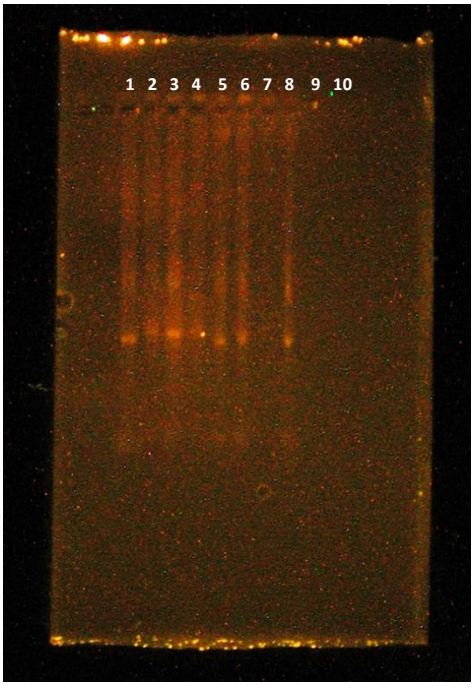

Figure 54: Image of RNA samples after gel electrophoresis. Wells 1-5 are of samples extracted from 1 composite, while 6-10 are for samples from 2 composites.

Discussion and Conclusion – 2

The NanoDrop results from the new homogenisation method showed improved 260/280 ratios, although data remained highly variable. The gel electrophoresis image also confirmed this as the samples were visible, however they were still considerably degraded with only one band visible. The samples with low RNA concentration in Table 21 (samples 1 and 2) did not show up in the gel, confirming the low RNA concentration and its highly degraded nature. Surprisingly, combining 2 composites during extraction did not always produce higher RNA yields. This could be due to loss during the pellet washing stages.

The results from this modified homogenisation improved upon the previous method as the RNA was less degraded. However, quality remained insufficient for use. As the yield was extremely variable and the method not producing sufficient quality RNA, the method was concluded as insufficient.

Method – 3

An alternative method for RNA extraction is the use of silica-membrane columns to selectively bind RNA. The QIAgen MiRneasy micro kit (Cat no. 217084, QIAgen) is based on this technique and was selected for trial as, unlike other membrane based columns, it retains smaller RNA molecules (>18 nucleotides compared to >200 of other available columns) and thus provides a similar total RNA spectrum to the Trizol methods. It is designed for use with small cell numbers and hence ideal for the composites. Furthermore, QIAshredder columns were also used as an additional step for the homogenisation process. The new procedure was based off the standard protocol provided in the kit (miRNeasy Micro Handbook by QIAgen, 2012) and used phenol-chloroform phase separation similar to the previous methods.

Cell seeded composites were made with 40% PEG-RGD fibres and a 60 minute soak (n=6), and snap frozen in 2 mL cryovials 24 hours post production. Buffers in the kit were reconstituted as instructed in the manual. The first specimen was then transferred into a 1.5 mL micro-centrifuge tube and held in a shallow well of liquid nitrogen in a small mortar. The sample was ground down as much as possible by hand using a disposable pestle, taking care not to let the sample thaw by keeping the bottom of the tube in the cooled mortar. 1 mL QIAzol (supplied with kit) was added to the tube whilst in a fume hood and pipetted vigorously. The next sample was then processed in the same manner using a new disposable pestle for each one.

Once all samples were homogenised by hand and in QIAzol, 700 µL of each sample was transferred into individual QIAshredder columns and centrifuged at full speed for 2 minutes to completely lyse the cells. The flow through was collected and the remaining 300µL of each sample was added to the respective columns and centrifuged in the same manner. Once all the samples were full processed, the collected homogenate was incubated at RT for 5 minutes and QIAshredder columns disposed of. 200 µL chloroform (~1/5 ratio) was then added to each tube, shaken vigorously for 15 seconds and then incubated at RT for 3 minutes.

Following incubation, all the tubes were centrifuged at 12,000g for 15 minutes at 4°C. The upper aqueous phase was then transferred to new tubes and 1.5 x the volume 100 % ethanol added. After mixing this solution gently by pipetting, 700 µL of each sample was transferred into RNeasy MinElute Spin Columns (supplied with kit) with a re-useable collection tube (to collect flow through) and centrifuged at 8,000g for 30 seconds at RT. After this step the RNA was bound to the silica membrane and therefore the flow through discarded.

The emptied collection tube was reused, and the remaining solution added to the respective columns, centrifuge repeated and the flow through discarded again. The membrane bound RNA was then washed with the two proprietary buffers supplied in the QIAgen kit. The collection tubes were reused and 700 µL of the first wash buffer added to each spin column. This was

centrifuged at 8,000g for 30 seconds at RT and the flow through discarded. Re-using the collection tubes, 500 µL of the second wash buffer was pipetted onto all the spin columns and all tubes centrifuged at 8,000 g for 30 seconds at RT. The flow through was discarded once again and the collection tubes reused once more. 80% ethanol was pipetted into each spin column, 500 µL each, then centrifuged at RT for 2 minutes at 8,000g.

Having completed all wash-through steps, both the flow through and collection tubes were then discarded. The spin columns were placed in new 2 mL collection tubes and centrifuged with lids open at full speed for 5 minutes at RT to dry the membrane. The new collection tubes were discarded again after this centrifuge and spin columns placed in a smaller 1.5 mL micro-centrifuge tube for the final collection of RNA. 14 µL RNase free water was pipetted directly onto the centre of the membrane and left to incubate at RT for 5 minutes. These were then centrifuged at full speed for 1 minute at RT and the spin columns discarded. During this final elution step, 2 µL water is lost in the column and therefore the final flow through containing RNA was 12 µL. The tubes containing RNA were stored at -80°C until ready to measure.

NanoDrop and gel electrophoresis were performed as described previously to check the quality of the RNA collected.

Results – 3

Table 22: NanoDrop results for third method. Sample 1 showed significantly low 260/230 ratio and was therefore "re-dropped" and scanned to confirm it was not an anomaly. Total of 12 µL of RNA solution was extracted from each sample.

Sample ID	RNA Concentration (ng/µl)	260/280	260/230	Total RNA (ng)
1	45.43	1.86	0.21	545.16
1 (Re-drop & scan)	45.49	1.87	0.21	545.88
2	51.44	2.01	1.67	617.28
3	40.05	1.91	1.77	480.60
4	48.14	2.02	1.49	577.68
5	44.70	1.78	1.25	536.40
6	31.86	2.00	1.23	382.32

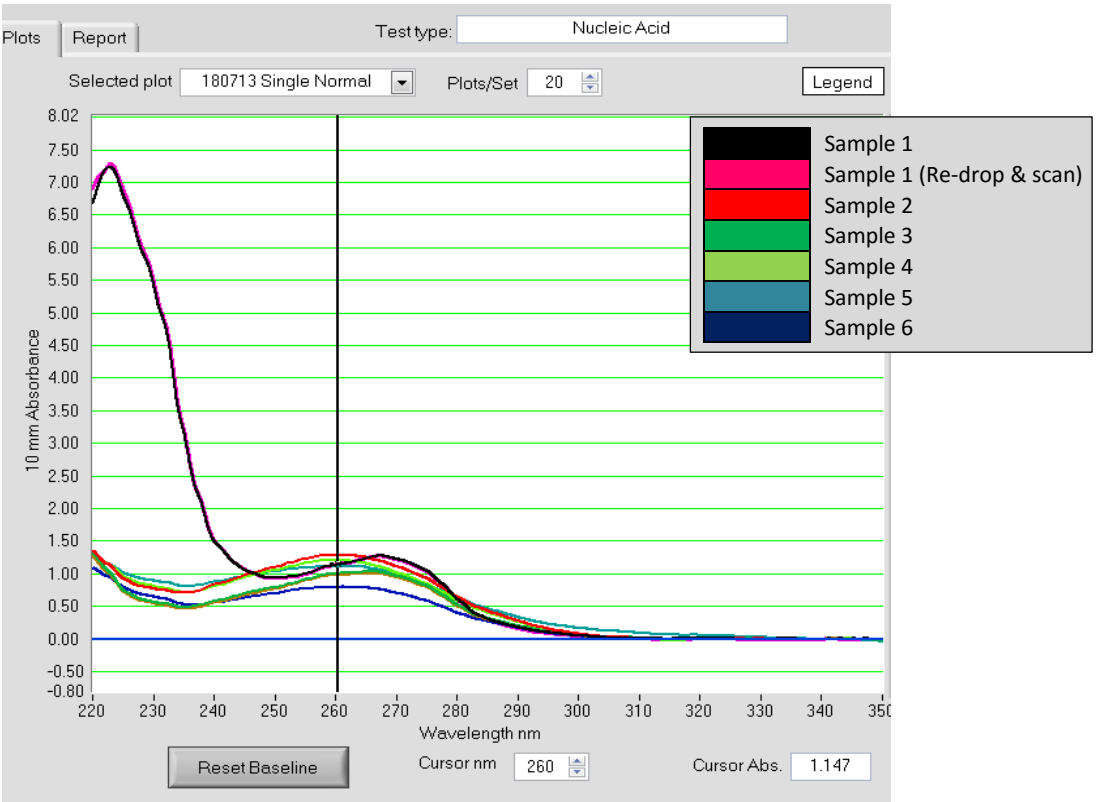

Figure 55: Screenshot of absorbance spectrum created by the NanoDrop spectrophotometer. The high absorbance between 220 and 230 nm is not an anomalous result and a re-drop and scan creates the same profile and thus contamination is present in the sample.

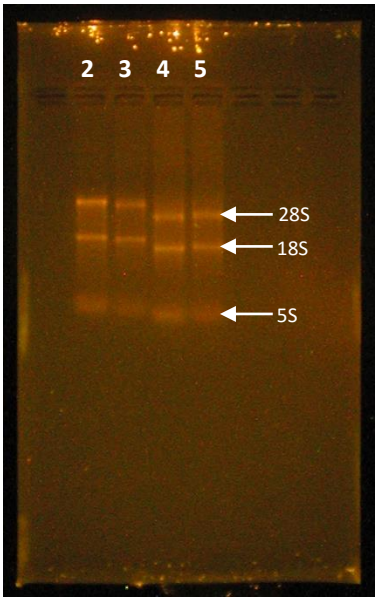

Figure 56: Denaturing gel electrophoresis results for RNA samples extracted using membrane column based method. Sample 1 and 6 were lost whilst trying to pipette into the gel wells, hence only samples 2-5 indicated. Bands 28S, 18S and 5S indicated with white arrows.

Discussion and Conclusion – 3

The new method using QIAshredder columns and silica based membranes for RNA collection provided improved RNA purity, with 260/280 being within the acceptable range of 2±0.3. The 260/230 was also improved and generally over 1.2, whereas previous attempts saw a 260/230 of less than 1. Sample 1 was seen to have a low 260/230 ratio and contamination was clearly observed in the absorbance spectrum (Figure 55). The gel electrophoresis results also provided confidence in the new technique as clear bands of 28S, 18S and 5S were seen with minimal smearing, thus indicating intact RNA.

Although the concentration of RNA was higher, the procedure itself proved too time consuming for large sample numbers, due to the first manual homogenisation step. Large chunks of composite also remained stuck in the QIAshredder column meshes, suggesting the inefficiency of homogenisation.

Method – 4

Successful aspects of Method – 2 were taken forward, namely the improved homogenising capability of the Mikro-Dismembrator U and the multi sample holder.

Cell seeded composites made with both 20% and 40% PEG-RGD fibres and a 60 minute soak were snap frozen in 1.2 mL cryovials 24 hours post production and kept in a Dewar containing liquid nitrogen for the first homogenisation step. A steel grinding ball (9 mm chromium steel) was added to each tube. The new holder for the Mikro-Dismembrator U can hold 4 vials at a time, hence the sample vials were processed in batches of 4. The sample holder was briefly cooled, 4 vials placed inside, and the holder secured tightly in the homogeniser and run at 2000 rpm for 1 minute. The tubes were then kept in another small Dewar containing liquid nitrogen while the rest of the vials were processed in the same way. QIAzol (700 µL) was added to each vial individually. The QIAzol freezes once added to the tubes due to the low temperature and therefore care was taken to mix the homogenate as soon as it starts to thaw, to ensure it did not fully thaw without being in contact with QIAzol. At this stage the samples were processed in the same way as described in 'Method – 3'; the QIAzol/RNA solution was pipetted into QIAshredder columns to ensure the cells were completely lysed; chloroform added (~ 1:5 ratio) to perform phase separation; solutions diluted by adding 100% ethanol in a 1:1.5 ratio; RNA collected on RNeasy MinElute Spin Columns; spin columns washed sequentially with the two supplied buffers and then 80% ethanol; spin columns dried by centrifuging with lids open for 5 minutes; and then the final elution performed using 14 µL RNase free water.

Additionally, an extra elution was performed on 3 spin columns (using 14 µL RNase free water) to confirm how much RNA was left behind and thus whether it was necessary to perform a second elution.

NanoDrop was performed on these samples using the NanoDrop 1000 spectrophotometer as previously described.

Results – 4

Table 23: NanoDrop results for samples tried with new method using Mikro-Dismembrator U, QIAshredder columns and QIAgen MiRNeasy Micro Kit. Spin columns used for samples 7, 8 and 9 were eluted with RNase free water a second time in separate tubes and indicated as 'second elute' in the table.

Sample ID	Composite Type	ng/µl	260/280	260/230	Total RNA (ng)
1	40% PEG-RGD	11.17	1.77	1.77	134.04
2	40% PEG-RGD	12.69	2.03	2.03	152.28
3	40% PEG-RGD	24.16	1.71	1.71	289.92
4	20% PEG-RGD	22.15	1.7	1.11	265.8
5	20% PEG-RGD	13.28	1.76	1.03	159.36
6	20% PEG-RGD	14.8	1.66	0.6	177.6
7	20% PEG-RGD	34.16	1.8	1.4	409.92
8	20% PEG-RGD	20.04	1.8	1.2	240.48
9	20% PEG-RGD	22.65	1.75	0.19	271.8
7 - second elute	20% PEG-RGD	5.66	1.57	1.01	67.92
8 - second elute	20% PEG-RGD	6.73	1.48	0.84	80.76
9 - second elute	20% PEG-RGD	6.84	1.37	0.69	82.08

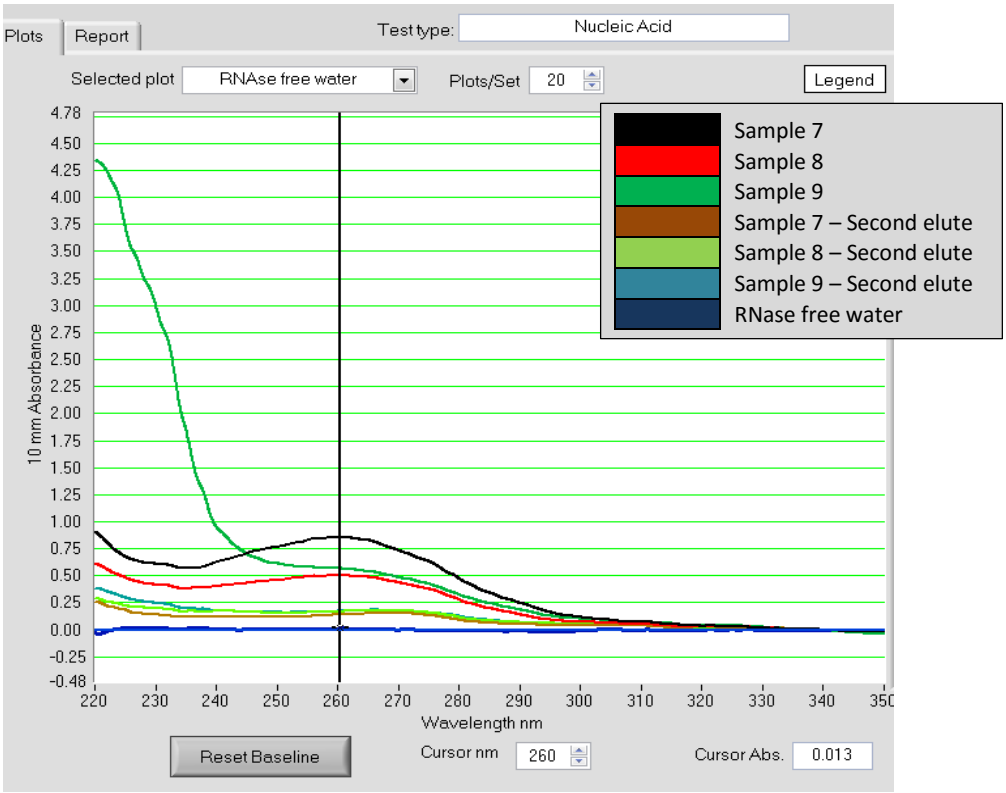

Figure 57: Screen shot of NanoDrop results from samples 7, 8 and 9 after the first and second elution. Sample 9 shows high absorbance at 220 nm suggesting some contamination.

Discussion and Conclusion – 4

The method combining the Mikro-Dismembrator U, QIAshredder columns and MiRNeasy Micro Kit (Method – 4) consistently allowed extraction of RNA with 260/280 ratios within the acceptable 2±0.3 range (Table 23). The 260/230 ratios are similar to the previous method, and much improved compared to Method – 1 and Method – 2. Sample 9 has the lowest 260/230 and is evident in Figure 57 to be due to high absorbance at 220nm, suggesting possible contamination. Interestingly, the second elute of sample 9 did not have a high absorbance at 220nm, indicating that the contaminant may have transferred from the outer edge of the spin column on the first elute or possibly have been present in the tube beforehand. Additionally, while the samples from the second elute showed low 260/280 and 260/230 ratios, there does not seem to be contaminants in the actual absorbance spectra obtained, emphasising the concentration related effect of the ratios, where at lower RNA concentrations the impurity is over exaggerated. This observation was incorporated into the protocol for future use wherein the spectral profile obtained from the NanoDrop is used more so than the 260/230 ratio alone, particularly at lower RNA concentrations. Consequently, samples with a high peak at the 220 region were rejected for use.

The yield of RNA extracted with Method – 4 still remained lower than that with Method – 1. However, as the first method produced highly degraded RNA, the results obtained could have been artefacts and therefore not reliable. A second elute was performed on the spin columns to investigate whether any RNA still remained and whether it could be retrieved. The results in Table 23 showed some RNA was indeed left behind on the membrane, with approximately 67-82 ng RNA recovered in a second elute. Incorporating a second elute into the protocol would require combining two RNA solutions, however as the concentration of the second RNA solution is low, combining both solutions would further dilute the concentration. As 9.5 µL of sample (~ 100 ng total) is necessary for performing reverse transcription, a concentrated solution is

preferable and thus a second elution step is not a suitable approach. Although the yield of RNA extracted is not significantly improved, the quantity obtained is still higher than 100ng and therefore sufficient for downstream applications. To ensure enough RNA is obtained, in future experiments, samples will be combined in pairs (i.e. two composites used to create one RNA solution) at the spin columns step, creating a higher concentration of RNA.

The use of a multi sample holder and Mikro-Dismembrator U significantly reduced the time required for homogenising samples compared to the previous method and is ideal for performing multiple extractions at once. This improved protocol, with its consistent 260/280 ratio and sufficient RNA yield, was therefore adopted as the final method for further experiments looking into gene expression.

3.3.2 Final Optimised RNA Extraction Protocol

The final optimised version of the RNA extraction protocol is based on Method-4. Composites are combined during extraction and therefore experiments require all composite conditions in multiples of two. For example, 2 composites are paired and extracted together to provide 1 RNA sample, thus 6 composites are needed if 3 individual RNA samples are required for PCR.

The rest of the procedure is the same as that described in Method-4, where composites are homogenised via the Mikro-dismembrator U and QIAshredder columns and RNA collected and purified using the QIAgen MiRNeasy micro kit.

3.4 Bose Strain System and Setup

Cyclic strain was applied to the composites using a Bose ElectroForce 5500 test system with custom made chambers to house individual samples. This system can be used within a cell culture incubator, maintaining cells in a viable environment during testing. The custom cylindrical chambers along with their setup within the Bose system is shown in Figure 58. The system was used to apply 5% cyclic strain at 1 Hz for 24 hours (86400 cycles) to composites.

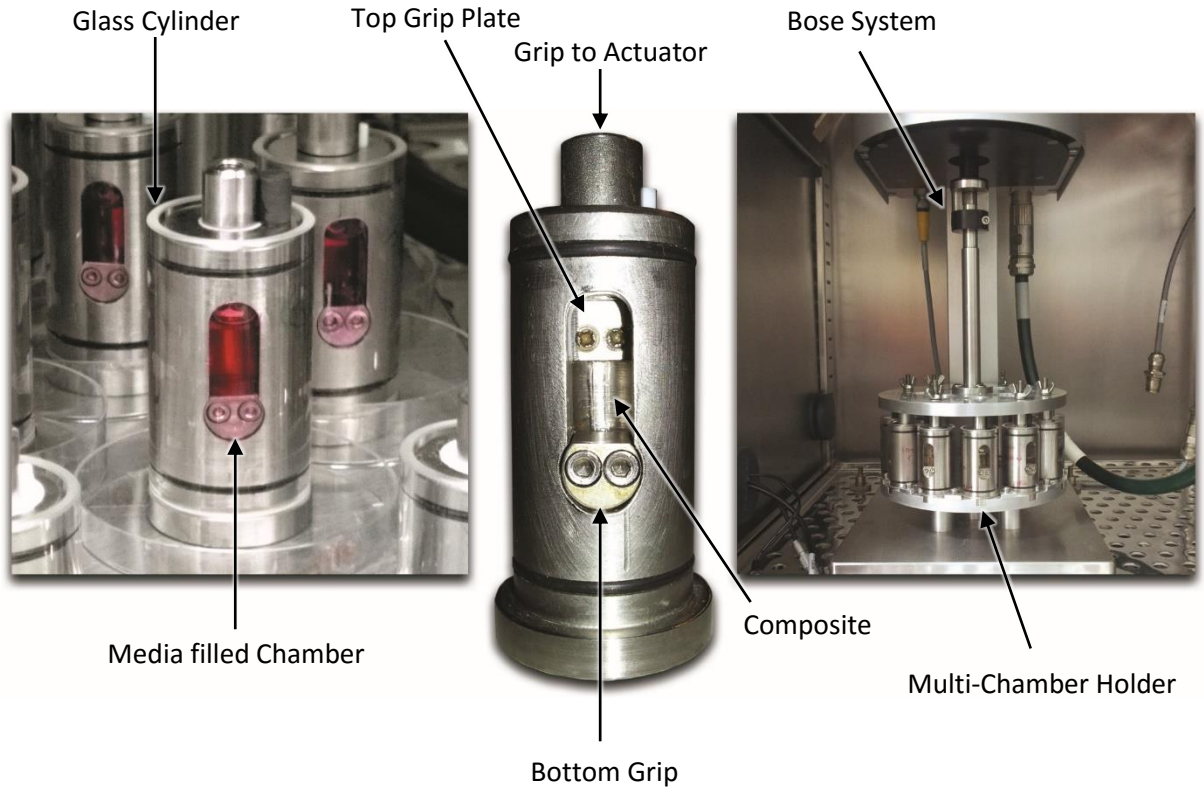

Figure 58: Images showing the Bose system and custom chamber setup. Image in the centre shows the stainless steel chambers with a composite setup inside. The image on the left shows the chamber filled with media and sealed with a glass cylinder. The image on the right shows the chambers attached to a multi chamber holding plate and connected to the Bose system inside an incubator.

3.4.1 Custom chamber setup

Before setting up the samples into the chambers, the chambers themselves along with the glass cylinders and tools used for assembly were put into autoclave bags and sterilised by autoclaving. They were then transferred into a sterile hood for assembly, securing the composites ready for loading chambers. Handling of all parts of the chambers and the composites was carried out with sterile tools which included screwdrivers, hex keys, forceps and spatulas. This was to prevent contamination of the composites and thus ensured viability over the test period.

The top grip was removed from a chamber and placed on a petri dish, acting as a sterile work surface. The composite was placed into the dish with a few drops of media to keep it hydrated. The composite was then held on the top grip and the top grip plate screwed in slowly until the composite was secure. This assembled piece was then carefully slid into the chamber from the top, being careful not to crush or damage the sample. Once in, the bottom grip was screwed into place to secure the composite. The glass cylinder was then placed over the chamber and pushed down to create a tight seal. Approximately 2 mL of media was then pipetted into the chamber from the top, by temporarily offsetting the top grip slightly from the centre to expose a small gap into which media could be injected without damaging the sample. The top gap was re-centred and the filled chamber labelled, and temporarily placed on a small petri dish in case of leaks and placed into an incubator while the next chamber was prepared.

Once all the composites were setup, the chambers were moved into the multi-chamber holder. The chambers were secured in the circular base plate first, after which the top circular plate was placed on top and the top grips of each chamber carefully connected. The entire setup was then moved into the incubator and connected to the Bose actuator securely ready for use.

3.4.2 Stable Gene Expression

Preliminary data (not shown) from RT-qPCR data using human tenocyte seeded composites showed the expression of some genes, particularly MMP-1, changed significantly after encapsulation and handling, remaining unstable for up to 24 hours. Therefore gene expression of cells within the composite was investigated over time once set up into customised Bose chambers to determine the ideal time point for starting strain application.

Experimental Overview

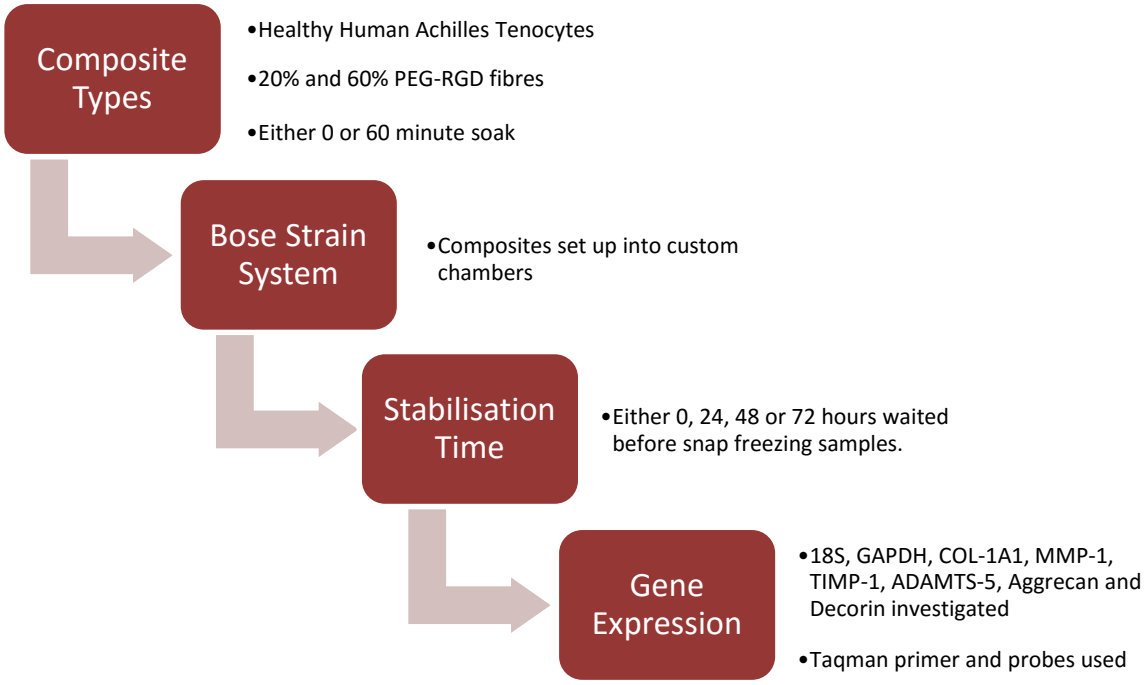

Figure 59: Overview of experimental flow and variables investigated to determine the ideal experimental start point.

Method

PEG-RGD fibres were made with 20% and 60% PEG according the previously described method. Human tenocytes from a healthy Achilles tendon (obtained from 76 year old male patient, courtesy of University of East Anglia, further cell details and ethics statement provided in Appendix A: Human cell source and ethics) were resuscitated and cultured until P10, at which

point enough cells were ready to create all the composites. 4 time points were investigated; 0, 24, 48 and 72 hours after Bose setup. Composites were made using either a 0 or 60 minutes soak, and enough composites made for all 4 time points and 3 repeats for each variable (total of 48 composites created, see Table 24). These were left overnight and set up into Bose chambers the next day.

Table 24: Summary of composite type, time points analysed and no of samples.

Composite Type	No. of composites for time points:			
	0 hours	24 hours	48 hours	72 hours
20% PEG-RGD, 0 minute soak	3	3	3	3
20% PEG-RGD, 60 minute soak	3	3	3	3
60% PEG-RGD, 0 minute soak	3	3	3	3
60% PEG-RGD, 60 minute soak	3	3	3	3

36 custom strain chambers were autoclaved in preparation for use along with an autoclavable Philips screwdriver and hex keys. The composites were set up into the chambers as previously described and left for the designated time points. At this time, the 12 composites for the 0 hour time point were simply placed in 1.2 mL cryovials and snap frozen in liquid nitrogen and stored at -80°C. At 24 hours 12 composites were removed from the chambers, snap frozen in liquid nitrogen and stored at -80°C. This was repeated at 48 and 72 hours.

Once all the samples were obtained the RNA was extracted using the Mikro-Dismembrator U, QIAshredder columns and MiRNeasy Micro Kit as described previously (section3.3, Final Optimised RNA Extraction Protocol). Due to the limited number of chambers and the number of time points investigated, the composites were not doubled during extraction and kept single.

The RNA quantity was determined using the NanoDrop 1000 spectrophotometer and samples were all diluted to 80 ng/9.5 µL (i.e. the lowest possible RNA quantity per 9.5 µL). 9.5 µL of each RNA solution was pipetted out into 0.5 mL tubes and 200ng Random Hexomers added. The tubes were briefly centrifuged (~2000g for 10 seconds) and then placed in a thermocycler set to heat the samples to 70°C for 10 minutes and then held at 4°C until opened. A stock mastermix

of the reverse transcriptase solution was prepared using a Superscript II kit such that there was enough for all 48 samples, with 9 µL required per sample. For 1 sample (i.e. 9 µL) mastermix contained 1 µL Superscript II, 4.5 µL 5x Sample Buffer, 2 µL dithiothreitol, 1 µL deoxynucleotides and 0.5 µL recombinant RNasin ribonuclease inhibitor. The tubes were retrieved from the thermocycler, 9 µL of this mastermix solution added and re-incubated in the thermocycler for 60 minutes at 42°C, then 70°C for 10 minutes and finally 4°C until the thermocycler was opened.

Table 25: List of Human TaqMan primers and probes used (Ordered from *Life Technologies)*. References listed below table.

Target Gene	Primer/Probe	Sequence	Amplicon size (bp)	Location (bp)	Ref
COL-1A1	Forward	5'- CGC ACG GCC AAG AGG AA -3'	66	185-251	1
	Reverse	5'- CAT GGT ACC TGA GGC CGT TCT -3'			
	Probe	5'- FAM - CCA AGA CGA AGA CAT CCC ACC AAT CAC C –TAMRA -3'			
18S	Forward	5'- GCC GCT AGA GGT GAA ATT CTT G -3'	45	949-994	2
	Reverse	5'- CAT TCT TGG CAA ATG CTT TCG -3'			
	Probe	5'- FAM - ACC GGC GCA AGA CGG ACC AG – TAMRA -3'			
GAPDH	Forward	5'- TTT TAA CTC TGG TAA AGT GGA TAT TGT TG -3'	97	240-337	1
	Reverse	5'- TGA CGG TGC CAT GGA ATT T -3'			
	Probe	5'- FAM- ATT GAC CTC AAC TAC ATG GTT TAC ATG TTC CAA TAT G -3'			
MMP-1	Forward	5'- AAG ATG AAA GGT GGA CCA ACA ATT -3'	59	587-646	4
	Reverse	5' –CCA AGA GAA TGG CCG AGT TC -3'			
	Probe	5'- FAM – CAG AGA GTA CAA CTT ACA TCG TGT TGC GGC TC - TAMRA -3'			
TIMP-1	Forward	5'- GAC GGC CTT CTG CAA TTC C -3'	53	288-341	3
	Reverse	5'- GTA TAA GGT GGT CTG GTT GAC TTC TG -3'			
	Probe	5'- FAM – ACC TCG TCA TCA GGG CCA AGT TCG T –TAMRA -3'			
ADAMTS-5	Forward	5'- AGG AGC ACT ACG ATG CAG CTA TC -3'	53	1796-1849	5
	Reverse	5'- CCC AGG GTG TCA CAT GAA TG -3'			
	Probe	5'- FAM - TGC CCA CAT AAA TCC TCC CGA GTA AAC A – TAMRA -3'			
Aggrecan	Forward	5'- CCG CTA CGA CGC CAT CTG -3'	50	1400-1450	2
	Reverse	5'- CCC CCA CTC CAA AGA AGT TTT -3'			
	Probe	5'- FAM - TAC ACA GGT GAA GAC TTT GTG GAC ATC CCA – TAMRA -3'			
Decorin	Forward	5'- GCT GTC AAT GCC ATC TTC GA -3'	50	264-314	2
	Reverse	5'- GGG AAG ATC CTT TGG CAC TTT -3'			
	Probe	5'- FAM - CCA GAC CCA AAT CAG AAC ACT GGA CCA - TAMRA -3'			

1) Ireland et al. (2001), 2) Corps et al. (2006), 3) Nuttall et al. (2003), 4) Jones et al. (2013), 5) Porter et al. (2004)

1 µL of each cDNA sample was collected into a single micro-centrifuge tube to act as a standard curve stock (SCS). The remaining cDNA samples were diluted by adding 90 µL RNase free water to provide a total volume of 90 µL and kept on ice. Serial dilutions were performed on SCS using RNase free water (1:1.5) with a total of 5 standards being produced and kept on ice. All 48 samples, 5 serial dilutions for standards and 3 non-template controls (RNase free water) were plated into a 96 well plate. A stock gene mix containing TaqMan primers and probes was then prepared for all the samples, with 0.5 µL forward primer (10 µM), 0.5 µL reverse primer (10 µM), 0.5 µL TaqMan probes, 8.33 µL Mastermix and 5.17 µL RNase free water needed per sample. A different stock gene mix was prepared for each gene, with the specific TaqMan primers and probes listed in Table 25. 15 µL of the stock gene mix was added to the plate and run on an Applied Biosystems 7500 Real-Time PCR system, setting the reporter and quencher to FAM and TAMARA, respectively, and the reaction volume to 25 µL.

The threshold Ct was obtained through the software supplied with the machine (7500 Software V2.06, *Applied Biosystems*) and the expression fold change calculated relative to the 0 hour samples and normalised to reference genes 18S and GAPDH using the Pfaffl efficiency corrected method (Pfaffl, 2001):

$$\text{Fold change} = \frac{E_{\text{target}}^{\Delta Ct_{\text{target}}}}{E_{\text{reference}}^{\Delta Ct_{\text{reference}}}}$$

Where:

E_{target} = Efficiency of the target gene

$E_{\text{reference}}$ = Efficiency of the reference gene

$\Delta Ct_{\text{target}}$ = Threshold Ct control target gene - sample target gene

$\Delta Ct_{\text{reference}}$ = Threshold Ct of control reference gene - sample reference gene

Results

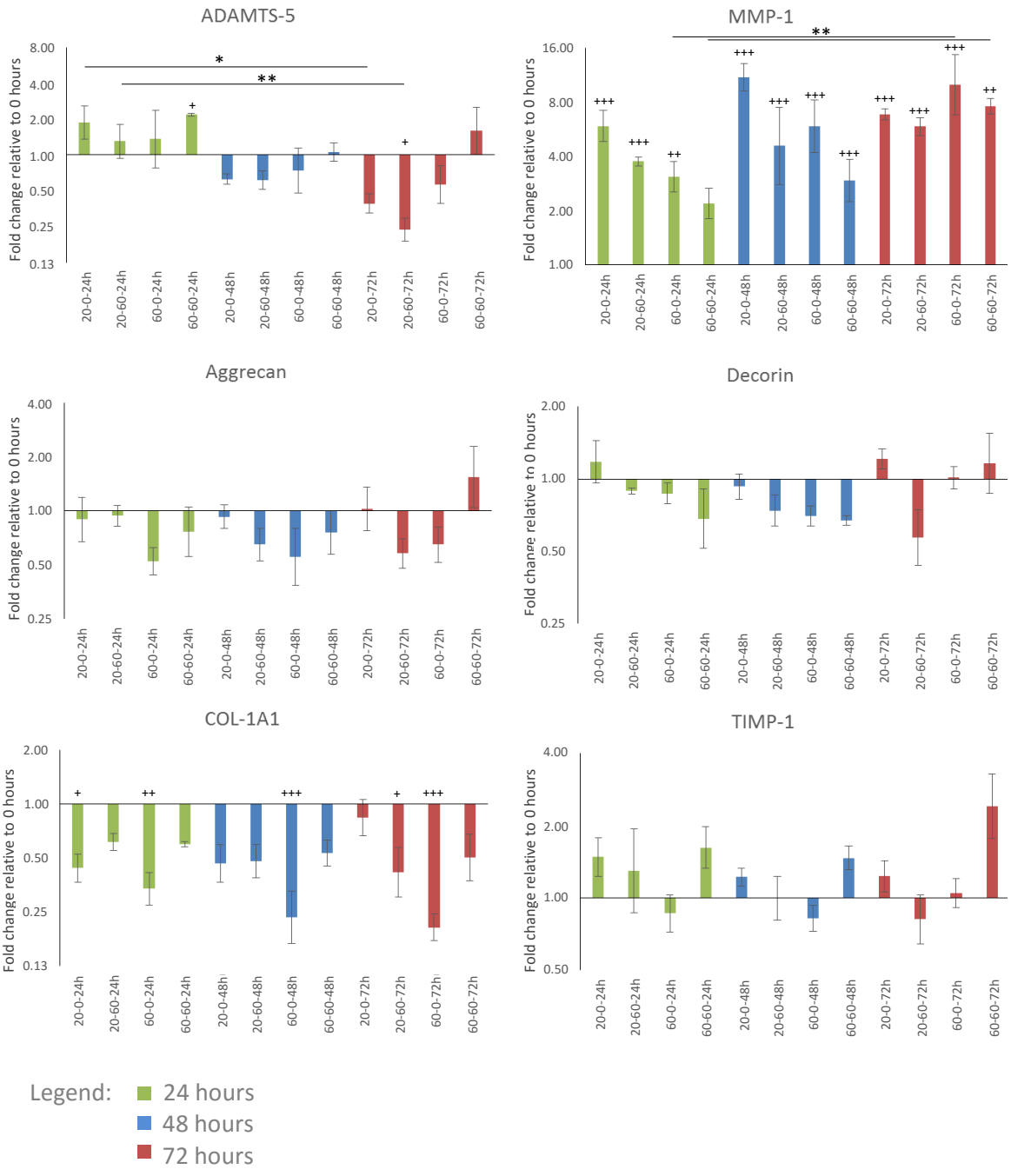

Figure 60: Gene expression graphs showing average fold change relative to the 0 hours composites and normalised to 18S and GAPDH (n=3). Bars show mean expression and error bars indicate standard deviation. Different composite types are kept separate, with colours indicating the time point. Samples are labelled as XX-YY-ZZ where 'XX' indicates fibre type, 'YY' indicates soak time and 'ZZ' indicates the analysis time point. The biggest gene expression changes occur within 24 hours setting up into chambers. The gene expression then stays relatively consistent for the next 72 hours, although with small variations. '+' indicates significant differences compared to 0 hour control composites (+ = P<0.05, ++ = P<0.01 and +++ = P<0.001), while '*' indicates significant differences between other time points (* = P<0.05, ** = P< 0.01 and *** = P<0.001).

Discussion and Conclusion

The gene expression data obtained from leaving samples static in chambers for up to 72 hours (Figure 60) showed the largest gene expression changes, for genes such as COL1A1 and MMP1 during the first 24 hours. The expression levels then stay fairly stable, either in the elevated or reduced state, over the next 48 hours. Although small variations were observed during these additional 48 hours, the changes were not as dramatic as the initial change. The initial change was also an interesting observation in itself, as the only differences between the 0 hour samples and the 24 hours samples are the handling, suggesting that this brief period of handing, approximately 3-5 minutes, was enough to evoke a response from the cells. Such a finding reflects previous studies that have shown that brief loading periods such as 100 cycles of up to 5% cellular strain at 0.1 Hz result in changes in gene expression (Huisman et al., 2014; Scott et al., 2011).

Alternatively, another difference between the two groups was the state of tension, as before being placed in chambers the composites were in a free swelling state, whereas once set up, the composites were held taut. It is possible that gripping samples and securing them in chambers, preventing free-swelling influenced gene expression, supported by the fact that initial changes observed in the current study remained for the duration of the experiment. Indeed, dissecting and incubating rat tail tendon fascicles (RTTFs) in culture media, i.e. stress deprivation, has been shown to significantly change matrix related gene expression in tenocytes for the first 24 hours (Leigh et al., 2008), and change the mechanical properties of RTTFs compared to those held taught, i.e. not stress deprived (Abreu et al., 2008).

The aim of this investigation was to find a stable point at which strain application could be engaged, allowing confidence the gene expression observations would be due to the loading regime itself rather than other factors. The biggest changes occurred within the first 24 hours after composites were set into chambers, suggesting a minimum wait time of 24 hours prior to

loading. As leaving the composites in chambers for longer increases the risk of contamination, it was decided leaving the composites for 24 hours is ideal and therefore the procedure taken forward.

Chapter 4: Healthy and Tendinopathic Human Tenocyte Metabolism

This chapter focuses on the use of the newly developed fibre composite system (summarised in Chapter 2) for investigating the metabolism of healthy and tendinopathic human tenocytes. The preliminary results obtained are discussed under 3 subheadings ('Results: Differences between pre-seeded tendinopathic and healthy tenocytes', 'Results: Substrate stiffness effects and differences between tendinopathic and healthy tenocytes in non-strained composites' and 'Results: Shear-tension ratio effect'). These look at a baseline gene expression profile differences in healthy and tendinopathic tenocytes before encapsulation into composites, differences in gene expression after encapsulation in composites and the effect of substrate stiffness, and the gene expression changes in response to different shear-tension ratios, respectively. An overall conclusion is provided at the end of the chapter.

4.1 Rationale and Hypotheses

Research from literature, summarised in Chapter 1, revealed that the aetiology of tendinopathy is complex and riddled with uncertainty. The possible effects of mechanical stimulation, collagen synthesis rates, matrix enzymes, neuropeptides, growth factors and other receptive chemicals are difficult to isolate and study using currently established *in vivo* models, while *in vitro* models have mostly been limited to either 2D or non-physiological 3D systems (Andersson et al., 2011; Arnoczky et al., 2007; Butler et al., 2009; Goodman et al., 2004; Jones et al., 2013; Zhang and Wang, 2010b). The fibre composite system was developed to solve this problem, allowing research into tenocyte behaviour using a physiologically equivalent cellular environment under tightly controlled conditions. More specifically, the composites can recapitulate the shear and tension experienced by tenocytes within tendons both physiologically and non-physiologically, thus allowing the effect of shear-tension ratios to be investigated objectively.

Tendinopathies are thought to be instigated by changes in cell-matrix interactions triggered by microdamage after tendon overuse. Matrix microdamage increases fibre shear, consequently increasing the magnitude of cellular shear. Shear is thus a potentially important mechanotransduction cue involved in ECM maintenance, but its effects on matrix anabolism and catabolism are unknown. An imbalance in ECM synthesis and degradation is also thought to contribute to the failed healing response seen in tendinopathies.

As ECM changes are prominent in tendinopathies, the fibre composite system was used to investigate the effect of varying levels of shear on ECM matrix turnover. This included the physiological tendon equivalent (40% fibre tension and 60% fibre shearing within the matrix), along with non-physiological conditions of high shear (25% tension and 75% shear) and low shear (60% tension and 50% shear). Furthermore, the response of tenocytes derived from

healthy Hamstring tendons were compared to those derived from tendinopathic Achilles tendons to investigate differences between diseased and healthy cells.

The net response of cells (i.e. anabolic or catabolic) can be established by monitoring the gene expression levels of substances involved in ECM turnover. This was used to determine the type of response evoked by different shear-tension ratios, hypothesising that the shear ratio would affect ECM turnover. It was also hypothesised that the response pattern of the two cell types (tenocytes derived from healthy and tendinopathic tissue) would not differ as both are essentially tenocytes and shear would affect both in a similar manner.

To investigate the changes in matrix turnover, a broad spectrum gene expression analysis was performed. This included gene expression levels of several MMPs, ADAMTSs, proteoglycans and collagen types, along with the gene expression of a few other specific ECM proteins, cell type markers and interleukins. An overview of the function and associations of these components with tendinopathies are provided in the Chapter 1 (section 1.4.2).

4.2 Experimental Overview

A broad spectrum gene expression analysis was performed using custom TaqMan® low density array (TLDA) cards. The benefit of TLDA cards is the ability to analyse a large variety of genes with a small volume of sample. The TLDA cards were chosen with a 48 well layout (Figure 61); each card had 8 sample reservoirs, with each port connected to 48 wells and each well containing the TaqMan® assay for a different gene. As the quantity of ECM related genes is extremely large and the chosen TLDA cards limited to 48 genes, genes associated specifically with tendons and tendinopathy were selected to perform a more targeted investigation. The genes selected for analysis (listed in Table 28) covered a variety of collagens, MMPs, ADAMTS, proteoglycans, interleukins, other ECM proteins and some cell type markers.

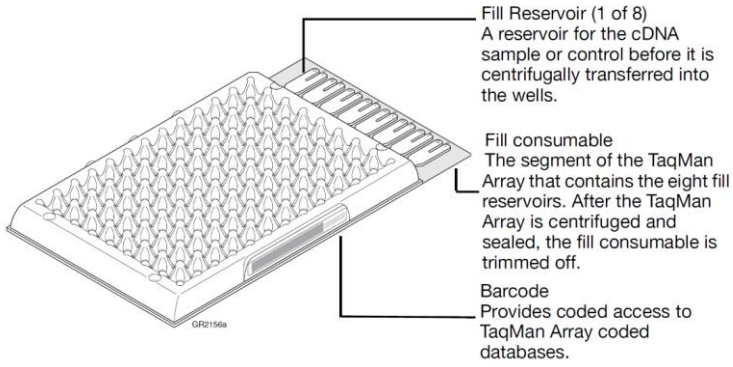

Figure 61: TLDA card graphic showing 8 port layout and connected wells. Cards are custom-ordered to specify TaqMan gene expression assays for each well. Image adapted from Applied Biosystems (2006).

Performing such a broad spectrum gene analysis is costly, therefore only one cell attachment peptide type was investigated to reduce unnecessary variables. Due to the slightly more consistent cell coverage observed with PEG-RGD than PEG-DGEA fibres and wider use of RGD with PEG in literature (DeLong et al., 2005; Dettin et al., 2009; Lynn et al., 2011; Steinmetz and Bryant, 2011; Yang et al., 2005), YRGDS peptide was used for these studies instead of DGEA.

The study used human tenocytes derived from healthy and tendinopathic tissue in PEG-RGD fibre composites containing either physiological or non-physiological shear-tension ratios

(variables summarised in Figure 62). These were loaded to 5% strain at 1Hz for 24 hours, after which the samples were snap frozen.

Experiments with all 4 shear-tension conditions were repeated 4 times with cells from 4 different cell donors (2 healthy and 2 tendinopathic). Due to the limited number of human cell donors available for each cell type at the time of experiment, the data is presented as preliminary data. As such, statistical analysis in this chapter is only used to identify possible trends and are specific for the cells used only. The statistics cannot be used as conclusive evidence for the trends of tenocytes in all humans.

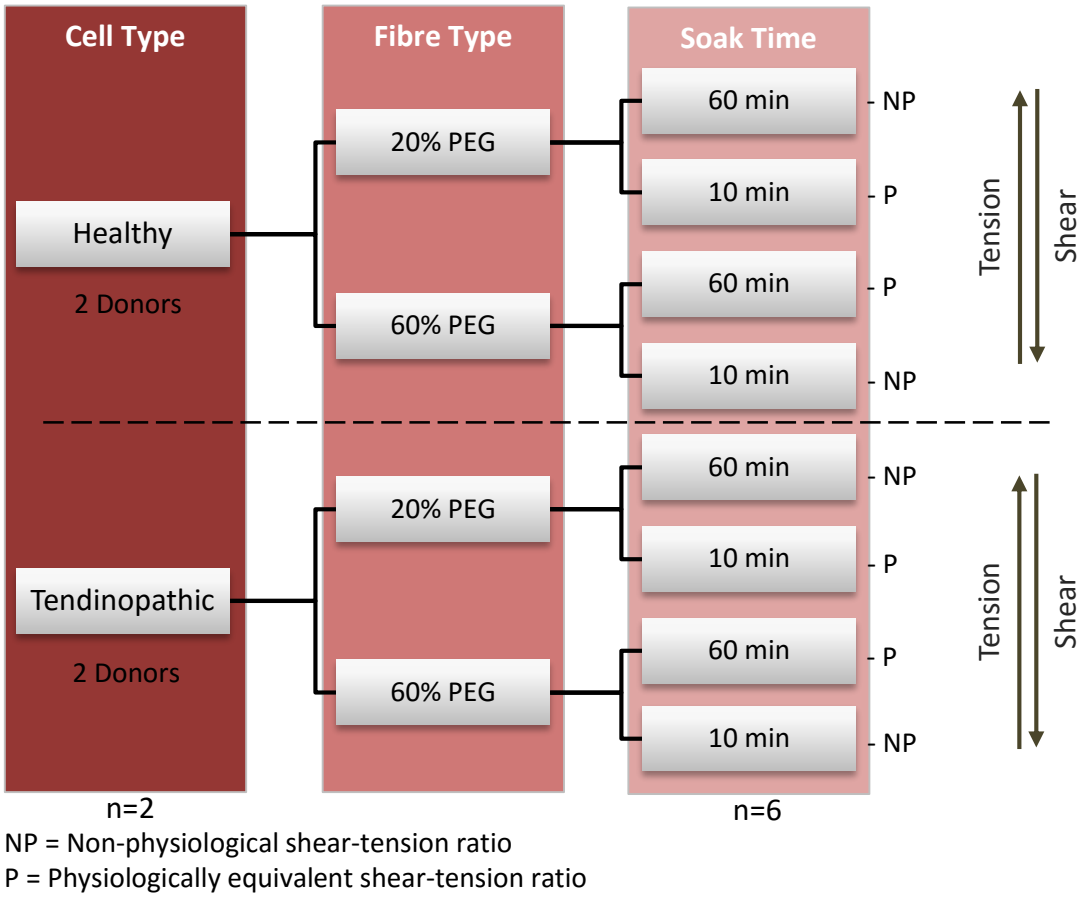

Figure 62: Overview of variables within experiment. Healthy (n=2) and tendinopathic (n=2) cells were tested within composites made using PEG-RGD fibres of 20% and 60% PEG. Fibres are also left to soak for either 0 or 60 minutes before polymerisation, thus a total of 4 composite types are created per cell type. 6 composites of each type were made (n=6), but after loading the specimens are combined in pairs for RT-qPCR, so n=3 for the final results.

4.3 Methods

Note 1: The protocols for cell culture, manufacturing composites, setting up the Bose strain system and RNA extraction are detailed comprehensively in Chapter 3 and only stated in brief under this section. Other additional procedures, such as RT-qPCR with TLDA cards which have not been previously detailed, are described fully.

Note 2: Further details of all chemicals used, including supplier details, are present in Table 35 and Table 36, in Appendix B: Chemicals and Materials List.

Cells and Cell Culture

Frozen human tenocytes derived from healthy hamstring tendons (19 year old female and 22 year old male) and tendinopathic Achilles tendons (45 year old male and 51 year old male) were received from the University of East Anglia (further details and ethics statement provided in Appendix A: Human cell source and ethics). Both healthy and tendinopathic tenocytes were resuscitated and grown in culture flasks in the same manner until the required cell number were reached (P3-4 and P5-6, respectively). Human tenocyte growth media (referred to as 10% FBS media) used during cell culture consisted of Dulbecco's Modified Eagle Medium with low glucose and GlutaMAX™ (DMEM-G), 10% FBS (Batch No. 111M339) and 1% Penicillin/Streptomycin (Pen/Strep).

PEG-RGD Fibre Production

PEG-RGD fibres were made by preparing solutions of 60% or 20% w/v PEGDM in PBS, with 0.05% w/v Irgacure 2959 and 5mM YRGDS peptide conjugated to acrylate-PEG-NHS. These were pipetted into Teflon fibre moulds and polymerised for 10 minutes under UV light (365 nm wavelength, ~4mW/cm^2). Fibres were then extracted from the moulds and stored in a petri dish

with 70% ethanol. A total of 3200 fibres were made; 1600 20% PEG-RGD fibres and 1600 60% PEG-RGD fibres.

Fibre Seeding

Fibres were prepared for seeding by moving the fibres into a sterile hood and sterilising under UV light for 1 hour. Sterile forceps were then used to transfer 400 20% PEG-RGD fibres equally into 2 wells of a non-tissue culture treated 24 well plate, i.e. 2 wells with 200 fibres each. The same was done with 60% PEG-RGD fibres. This was to ensure enough fibres were seeded to create fibre composites with soak times of 0 minutes and 60 minutes for both fibre types. The wells containing fibres were filled with 2 mL serum free culture media (media containing only DMEM-G and 1% Pen/Strep) and left in an incubator (37°C, 5% CO_2) for 30 minutes to acclimatise while cells were prepared for seeding.

One cell type was harvested from flasks via trypsinisation and re-suspended in serum free culture media at 3.5 million cells/mL. At this point a cell sample was taken to analyse the gene expression of cells in their 'pre-seeded' state. To do this, 3 micro-centrifuge tubes were prepared with 700 µL QIAzol Lysis Reagent and 40000 cells (11.4 µL of the cell suspension above) pipetted into each tube. The tubes were vortexed vigorously for a few minutes to lyse the cells and stored at -80°C until ready for RNA extraction.

The 24 well plate containing PEG-RGD fibres was then retrieved from the incubator and media aspirated from the wells. 1 mL of the cell suspension (i.e. 3.5 million cells) was added to each well containing fibres and the plate placed back into the incubator. After 1.5 hours, 0.5 mL media was removed from each well and 0.5 mL 10% FBS media added. This was left for a further 1.5 hours in the incubator after which the fibres were transferred into different wells containing fresh media with serum. The plate was then left overnight in the incubator for the cells to fully attach.

Composite Production

The next day composites were made using the cell seeded fibres. A solution of 20% PEGDM was first prepared by mixing 20% w/v PEGDM with 10% v/v FBS media and 0.05% w/v Irgacure 2959. The solution was then sterile filtered using 0.22 µm syringe filters and moved into a sterile hood along with sterilised tools, Teflon composite moulds, glass slides and a UV lamp. A drop of 20% PEGDM was placed on a glass slide and 10 20% PEG-RGD fibres were dipped into the drop before placing the fibres in a prepared Teflon composite mould. A glass slide was then placed on top of the mould and the 20% PEGDM solution injected in slowly using a 5 mL syringe and 25 gauge needle. Once filled, the mould was left for 60 minutes for the fibres to soak and then polymerised under UV light (365nm wavelength, ~4mW/cm^2) for 10 minutes. The composites were then extracted from the moulds and stored in separate petri dishes containing 10% FBS media. This was repeated until 18 20% PEG-RGD composites with 60 minutes soak were made, after which the soak time was decreased to 0 minutes and a further 18 composites made. The entire process was repeated again using 60% PEG-RGD fibres until 18 60% PEG-RGD composites with 0 and 60 minute soak were made. All composites, in their separate petri dishes, were stored in an incubator overnight. Note, only 12 of each type of composite were required for the experiment and the 6 additional composites were made in case composites were damaged or broken whilst setting up in chambers in the later stages.

Strain Application

The next day 48 loading chambers, along with tools for assembly (screwdriver, hex keys, spatula and forceps) were autoclaved and moved into a sterile hood. The composites were retrieved from the incubator and each composite secured into an individual chamber carefully using aseptic techniques and filled with approximately 2 mL 10% FBS media. 24 chambers, 6 of each composite type, were allocated as non-strained controls, whilst the remaining 24 were labelled as strained samples. The chambers allocated for loading were connected to the Bose strain

system inside an incubator while the non-strained controls were left secured in their chambers, but disconnected in the same incubator. All chambers were then left to equilibrate for 24 hours in the incubator before initiating loading.

The following day, the Bose system was set to load samples to 5% strain at 1 Hz for 24 hours (86400 cycles). At the end of the loading regime, the composites from all test groups, strained and unstrained, were removed from the chambers and paired into 1.2 mL cryovials; 2 composites of the same type were put into the same cryovial, so for each composite type there were only 3 cryovials instead of 6. The cryovials were then snap frozen in liquid nitrogen and stored at -80°C until ready for RNA extraction.

RNA Extraction

RNA was extracted, using the optimised protocol described in Chapter 3 and eluted in 15 µL RNase free water. The quantity of RNA was measured using a NanoDrop Spectrophotometer 1000 and 1 µL of sample. All the samples where then diluted to 140.7 ng/9.5 µL using RNase free water and stored at -80°C.

RT-qPCR with TLDA Cards

The tubes containing diluted RNA were thawed and 9.5 µL of each transferred into new micro-centrifuge tubes. 250 ng of Random Hexomers (1.5µL of stock solution) was added to each tube and then the tubes centrifuged at ~2000g for 10 seconds. These were then placed into a thermal cycler (model 2720, *Applied Biosystems*) set to run at 70°C for 10 minutes and then 4°C until opened.

A reverse transcriptase mastermix solution was made, enough for 62 samples (60 samples plus 2 extra in case of loss);

Table 26: Details of reverse transcription mastermix solution made.

Substance *(Supplier)*	**Quantity for 1 sample (µL)**	**Quantity for 62 samples (µL)**
Superscript II *(Life Technologies)*	1	62
5x Sample Buffer *(supplied in Superscript II kit)*	4.5	279
Dithiothreitol (DTT) *(supplied in Superscript II kit)*	2	124
Deoxynucleotide triphosphates (dNTPs) *(Promega)*	1	62
Recombinant RNasin Ribonuclease Inhibitor *(Promega)*	0.5	31

Once the thermal cycler had stopped in the final hold stage, the tubes were removed and 9 µL of the reverse transcriptase mastermix added to each tube. The tubes were then centrifuged at ~2000g for 10 seconds to collect the solution at the bottom of the tubes and placed in the thermal cycler to run for 60 minutes at 42°C, then 70°C for 10 minutes and finally 4°C until the thermal cycler was opened.

Once the reverse transcription process had finished, the tubes containing the resulting complimentary DNA (cDNA) were removed from the thermal cycler and kept on ice whilst proceeding with the next steps. The cDNA was diluted to a total volume of 55 µL by adding 35 µL RNase free water and mixed gently through pipetting.

A 96 well plate was prepared to check the 18S gene expression of all the samples before continuing with the TLDA cards. This was to ensure the samples were of good quality before using the TLDA cards. 8 µL RNase free water was pipetted into 63 wells - 60 samples plus 3 non-template controls (NTC), followed by 2 µL of each cDNA sample. A stock gene mix was made enough for 62 samples (2 extra included in case of loss) as detailed in the Table 27.

Table 27: Details of the components for the stock gene mix made for 18S. 18S design reference from Corps et al., 2006.

Substance *(Supplier)*	**Quantity for 1 sample (µL)**	**Quantity for 62 samples (µL)**
18S Forward Primer (10 µM) *(Life Technologies)* *5'-GCCGCTAGAGGTGAAATTCTTG-3'*	0.5	31
18S Reverse Primer (10 µM) *(Life Technologies)* *5'-CATTCTTGGCAAATGCTTTCG-3'*	0.5	31
18S TaqMan Probe *(Life Technologies)* *5'-ACCGGCGCAAGACGGACCAG-3'*	0.5	31
KAPA Universal qPCR Kit *(Anachem)*	8.33	516.46
RNase free water *(Sigma Aldrich)*	5.17	320.54

15 µL of this stock gene mix was then pipetted into the 96 well plate containing cDNA and a sealing tape *(Life Technologies)* applied on top of the plate to seal the wells. The plate was briefly centrifuged at ~2000g for 10 seconds to collect the solution at the bottom of the wells and then placed into the 7500 Real-Time PCR system *(Applied Biosystems)*. The two dyes, FAM and TAMRA, were set as the reporter and quencher respectively, and the thermal profile set to run at 50°C for 2 minutes, 95°C for 10 minutes and followed by 40 cycles of 97°C for 30 seconds and 60°C for 1 minute.

The resulting 18S amplification curves were analysed to check any anomalies in samples and ensure all samples were amplified before proceeding with the TLDA cards. The threshold cycle (Ct) values were extracted through the Applied Biosystems 7500 Software V2.0.6 *(Life Technologies)* by setting the threshold near the end of the linear amplification region (example shown in Figure 63). The Cts were compared to identify potentially contaminated or degraded samples by seeing if any deviated more than ± 2 cycles from the mean Ct.

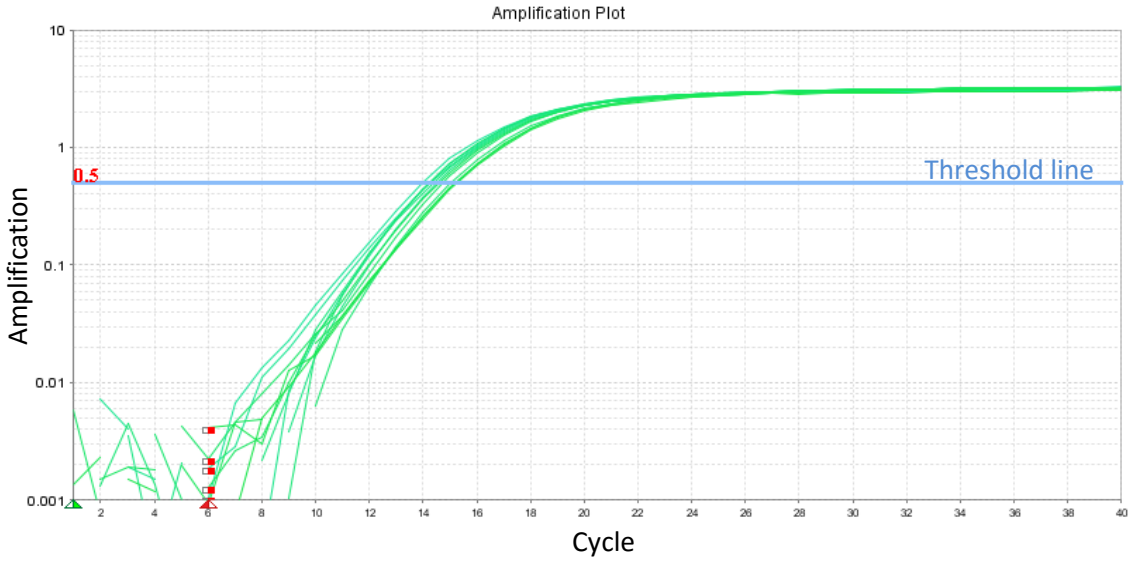

Figure 63: Example of threshold cycle calculation using the Applied Biosystems 7500 software V2.0.6 (Life Technologies) for 18S. The threshold line was set to intersect the amplification lines towards the end of the linear region, and the cycle number at intersection extracted. This value was labelled as the threshold cycle (Ct).

Once the samples were confirmed to be of good quality, the remaining cDNA was prepared for use in the TLDA cards. As the TLDA cards only have 8 sample reservoirs, only 8 samples could be tested at a time and therefore samples were prepared for qPCR in batches of 8. The TLDA card gene layout is shown in Table 28 and the TLDA card preparation procedure summarised in Figure 64. The first TLDA card was retrieved from 4°C storage and left on the bench for 15 minutes to bring to room temperature. 8 cDNA samples were diluted with 52 µL TaqMan® Universal PCR Master Mix, i.e. 1:1 ratio, and gently mixed through pipetting. The TLDA card was then carefully opened from its packaging to avoid contaminating the bottom of the plate and 100 µL of each sample pipetted into separate sample reservoirs. The plate was then centrifuged for 1 minute at 1200 rpm to fill the wells centrifugally and the wells sealed using a plate sealer. The reservoir edge of the card was then cut away and the card placed into a 7900HT Real-Time PCR System *(Applied Biosystems)*. The thermal profile was set to run at 50°C for 2 minutes, then 94.5°C for 10 minutes followed by 40 cycles of 97°C for 30 seconds and 59.7°C for 1 minute. After the machine had finished 40 cycles, the next TLDA card was prepared and the above process repeated until all samples had been processed.

The raw data obtained from the machine was analysed using RQ Manager *(Applied Biosystems)*. Similar to the analysis method described in Figure 63, the threshold was set at the end of the linear region of the amplification curve and the threshold cycles (Ct) extracted for all the samples and genes. The threshold for each gene was set at the same value for all composite and cell types, with undetected samples given an arbitrary value of 40 to represent the max cycle number. The extracted Ct values were then imported into Excel *(Microsoft)* to calculate the gene expression normalised to the reference gene TOP1 ($2^{\Delta Ct}$) and as fold changes ($2^{\Delta\Delta Ct}$) using the formulas:

$$2^{\Delta Ct} = 2^{Ct_{Target} - Ct_{Reference}}$$

Where:
Ct_{Target} = Ct of target gene
$Ct_{Reference}$ = Ct of reference gene

$$2^{\Delta\Delta Ct} = 2^{Strained\Delta Ct / Control\Delta Ct}$$

Where:
$\Delta Ct = \mathrm{Ct}_{\mathrm{Target}} - \mathrm{Ct}_{\mathrm{Reference}}$
StrainedΔCt = ΔCt of strained sample
ControlΔCt = ΔCt of reference sample

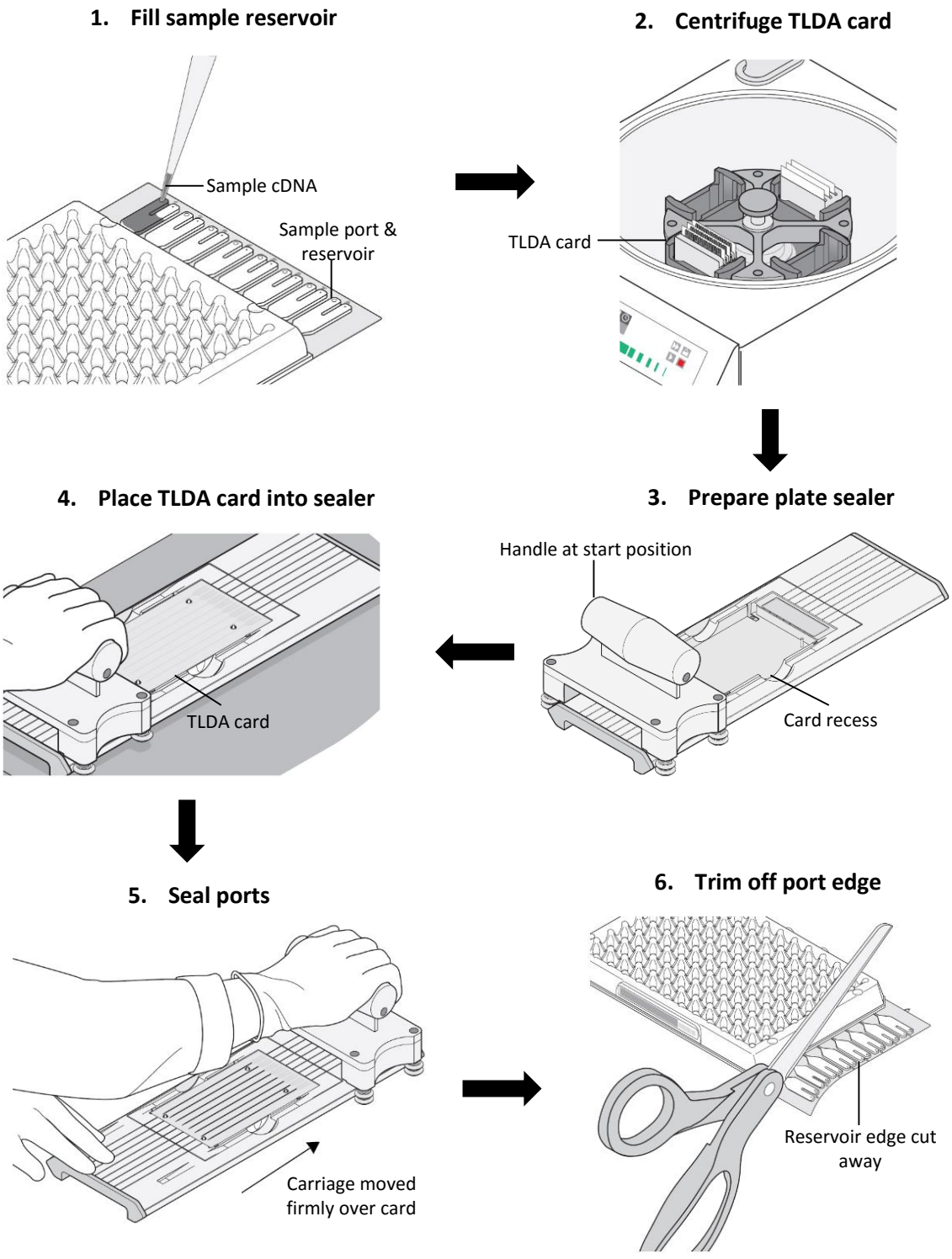

Figure 64: Flow diagram depicting the procedure for preparing TLDA cards. The Sample reservoirs are first fill with the sample cDNA which is then forced centrifugally into the connected 48 wells. The wells are then sealed in the plate sealer and the reservoir edge cut off. Images adapted from Applied Biosystems (2006).

Table 28: TLDA card layout for wells 1-35 (wells 36-48 listed in Table 29). Each well contained a different TaqMan® gene expression assay.

Well	Gene	Symbol	Assay ID
1	Tenomodulin	TNMD	Hs00223332_m1
2	Scleraxis	SCX	Hs03054634_g1
3	Tenascin-C	TNC	Hs01115665_m1
4	Cartilage Oligomeric Protein	COMP	Hs00164359_m1
5	Fibronectin	FN-1	Hs00365052_m1
6	Interleukin-1	IL-1β	Hs01555410_m1
7	Interleukin-2	IL-2	Hs00174114_m1
8	Interleukin-6	IL-6	Hs00985639_m1
9	Interleukin-8	IL-8	Hs00174103_m1
10	A Disintegrin And Metalloproteinase with Thrombospondin Motifs-1	ADAMTS-1	Hs00199608_m1
11	A Disintegrin And Metalloproteinase with Thrombospondin Motifs-2	ADAMTS-2	Hs01029111_m1
12	A Disintegrin And Metalloproteinase with Thrombospondin Motifs-3	ADAMTS-3	Hs00610744_m1
13	A Disintegrin And Metalloproteinase with Thrombospondin Motifs-4	ADAMTS-4	Hs00192708_m1
14	A Disintegrin And Metalloproteinase with Thrombospondin Motifs-5	ADAMTS-5	Hs00199841_m1
15	A Disintegrin And Metalloproteinase with Thrombospondin Motifs-6	ADAMTS-6	Hs01058097_m1
16	A Disintegrin And Metalloproteinase with Thrombospondin Motifs-12	ADAMTS-12	Hs00229594_m1
17	A Disintegrin And Metalloproteinase with Thrombospondin Motifs-14	ADAMTS-14	Hs01548449_m1
18	Matrix Metalloproteinase-1	MMP-1	Hs00899658_m1
19	Matrix Metalloproteinase-2	MMP-2	Hs01548727_m1
20	Matrix Metalloproteinase-3	MMP-3	Hs00968305_m1
21	Matrix Metalloproteinase-7	MMP-7	Hs01042796_m1
22	Matrix Metalloproteinase-8	MMP-8	Hs01029057_m1
23	Matrix Metalloproteinase-9	MMP-9	Hs00234579_m1
24	Matrix Metalloproteinase-13	MMP-13	Hs00233992_m1
25	Tissue Inhibitor of Metalloproteinase-1	TIMP-1	Hs00171558_m1
26	Tissue Inhibitor of Metalloproteinase-2	TIMP-2	Hs00234278_m1
27	Tissue Inhibitor of Metalloproteinase-3	TIMP-3	Hs00165949_m1
28	Tissue Inhibitor of Metalloproteinase-4	TIMP-4	Hs00162784_m1
29	Lubricin	PRG-4	Hs00195140_m1
30	Aggrecan	ACAN	Hs00153936_m1
31	Biglycan	BGN	Hs00156076_m1
32	Versican	VCAN	Hs00171642_m1
33	Decorin	DCN	Hs00370384_m1
34	Fibromodulin	FMOD	Hs00157619_m1
35	Laminin	LAMA-1	Hs00300550_m1

Table 29: Continuation of TLDA card layout for wells 36-48. Each well contained a different TaqMan® gene expression assay.

Well	Gene	Symbol	Assay ID
36	Collagen Type I, Alpha 1	COL-1A1	Hs00164004_m1
37	Collagen Type II, Alpha 1	COL-2A1	Hs00264051_m1
38	Collagen Type III, Alpha 1	COL-3A1	Hs00943809_m1
39	Collagen Type IV, Alpha 1	COL-4A1	Hs00266237_m1
40	Collagen Type V, Alpha 1	COL-5A1	Hs00609133_m1
41	Collagen Type VI, Alpha 1	COL-6A1	Hs01095585_m1
42	Collagen Type IX, Alpha 1	COL-9A1	Hs00932129_m1
43	Collagen Type XI, Alpha 1	COL-11A1	Hs01097664_m1
44	Collagen Type XII, Alpha 1	COL-12A1	Hs00189184_m1
45	Collagen Type XIV, Alpha 1	COL-14A1	Hs00964045_m1
46	Glyceraldehyde 3-phosphate dehydrogenase	GAPDH	Hs99999905_m1
47	18S ribosomal ribonucleic acid	18S	Hs99999901_s1
48	Topoisomerase-1	TOP-1	Hs00243257_m1

Although the n number is low, statistical analysis was used for comparisons between experimental repeats and between composite types to assess the possibility of real differences. These statistics reflect the differences and trends present in the cells used only, and are not intended as statistics for tenocyte trends in all humans. Statistical analysis was performed using Student's *t*-test for comparing basal gene expression between tendinopathic and healthy cell types, while one way analysis of variance (one way ANOVA) was used for comparison of the different shear-tension ratios, followed by Tukey's Honest Significant Difference (HSD) pot-hoc test, if differences were found through the one way ANOVA, and P values < 0.05 were considered significant.

4.4 Preliminary Data and Discussion

4.4.1 Results: Differences between pre-seeded tendinopathic and healthy tenocytes

The basal gene expression of tenocytes in the pre-seeded state, i.e. after harvesting from culture flasks, was analysed to identify differences in cell types before incorporation into composites. This included two healthy and two tendinopathic tenocyte types. Interestingly, it was found that the two cell types showed differences in their basal gene expression – particularly collagens type 12 and 14, MMP-3 and 4, ADAMTS-2, 5 and 12, lubricin, versican and IL-8. To look at these in more detail, gene expression data has been graphed in the categories: 'Collagens', 'MMPs', 'ADAMTSs', 'TIMPs', 'Proteoglycans', 'Interleukins' and 'Other Proteins'.

Collagens

The collagens investigated via RT-qPCR were collagen type I, II, III, IV, V, VI, IX, XI, XII and XIV. Figure 65 shows the basal expression of these collagens for pre-seeded tendinopathic and healthy cells. Significant differences were seen in the gene expression levels of COL-12A1 and COL-14A1, with both significantly lower in tendinopathic cells than healthy cells. Although not statistically significant, COL-6A1 also showed notably lower expression in tendinopathic tenocytes compared to healthy tenocytes (p=0.08).

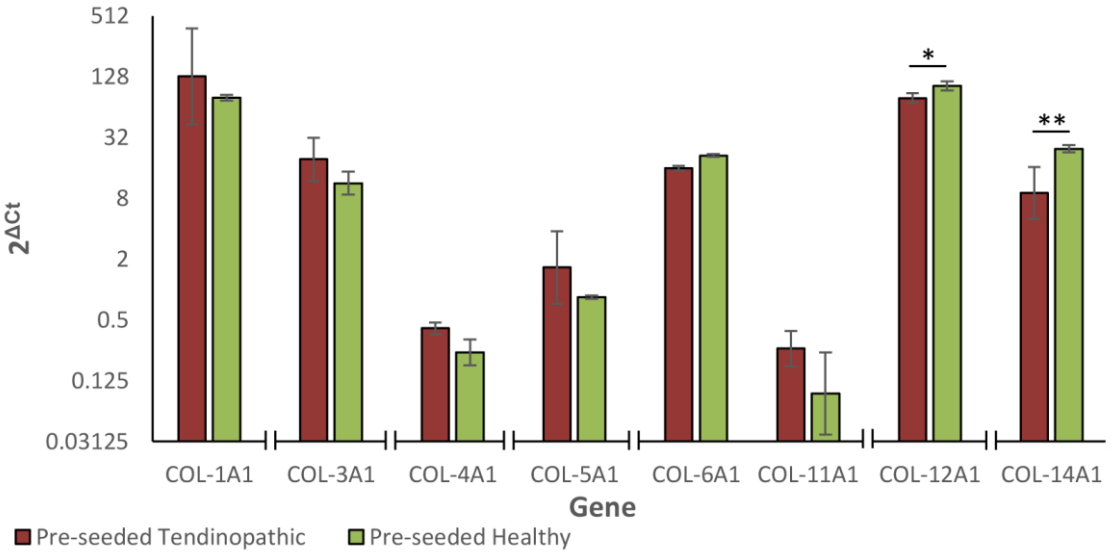

Figure 65: Average collagen basal expression for pre-seeded cells. Expression shown as $2^{\Delta Ct}$ (normalised to TOP-1) with both healthy and both tendinopathic cell types averaged. Error bars represent standard deviations. Tendinopathic tenocytes generally showed more variability in basal gene expression, as seen in COL-1A1, COL-5A1 and COL-14A1 expression, and also showed significantly less COL12A1 and COL-14A1 expression. Cell type n=2, with 3 repeats per cell type. * = P<0.05, ** = P<0.01.

The gene expression levels of collagens were generally more variable in tendinopathic tenocytes compared to healthy tenocytes (indicated by larger standard deviation bars in Figure 65), particularly in COL-1A1, COL-5A1 and COL-14A1. This was attributed to the tendinopathic tenocytes from the two donors having different basal levels; one tendinopathic tenocyte group had 9 times higher COL-1A1, 5 times higher COL-5A1 and 3 times less COL-14A1 gene expression than the other group. Other distinct differences between tendinopathic donors were also seen in other genes (discussed under further subheadings).

MMPs

The MMPs investigated were MMP-1, 2, 3, 7, 8, 9 and 13, however the gene expression levels of MMP-8 and 9 were too low for detection in all pre-seeded cell types. MMP-7 was only detected in 1 tendinopathic cell sample, in which expression levels were extremely low. MMP-1 and MMP-2 gene expression were similar for both healthy and tendinopathic tenocytes. However, MMP-3 and MMP-13 varied between cell type, and while undetected in all pre-seeded healthy tenocyte samples, low levels were detected in tendinopathic tenocytes (Figure 66). The large standard deviations in MMP-3 and MMP-13 expression were again due to differences between the two tendinopathic tenocyte donors; one tendinopathic tenocyte expressed 20 times less MMP-3 and 42 times less MMP-13 than the other.

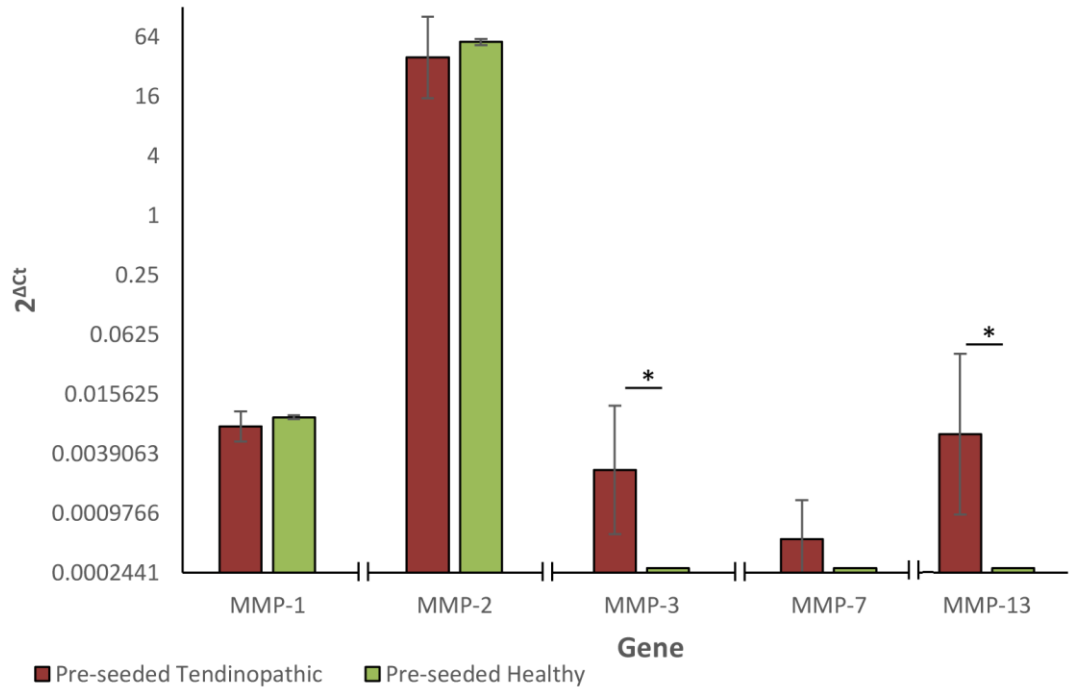

Figure 66: Average MMP basal expression for pre-seeded cells. Expression shown as $2^{\Delta Ct}$ (normalised to TOP-1) and undetected samples given a Ct value of 40 to represent the max cycle number. Both healthy and both tendinopathic cell types were averaged and error bars represent standard deviations. MMP-8 and MMP-9 were undetected for all samples, while MMP-3 and MMP-13 were only detected in tendinopathic samples. Tendinopathic tenocytes showed significantly higher basal MMP-3 and MMP-13 gene expression. Cell type n=2, with 3 repeats per cell type. * = P<0.05.

ADAMTSs

The ADAMTSs investigated were ADAMTS-1, 2, 3, 4, 5, 6, 12 and 14. Figure 67 clearly shows that many of these genes differed in basal expression levels between healthy and tendinopathic cells; the gene expression of ADAMTS-2 and ADAMTS-12 were significantly higher, and ADAMTS-5 significantly lower in tendinopathic cells compared to healthy cells. Additionally, although not statistically significant, ADAMTS-3 was notably lower (P=0.06) and ADAMTS-4 higher (P=0.06) in tendinopathic cells compared to healthy cells.

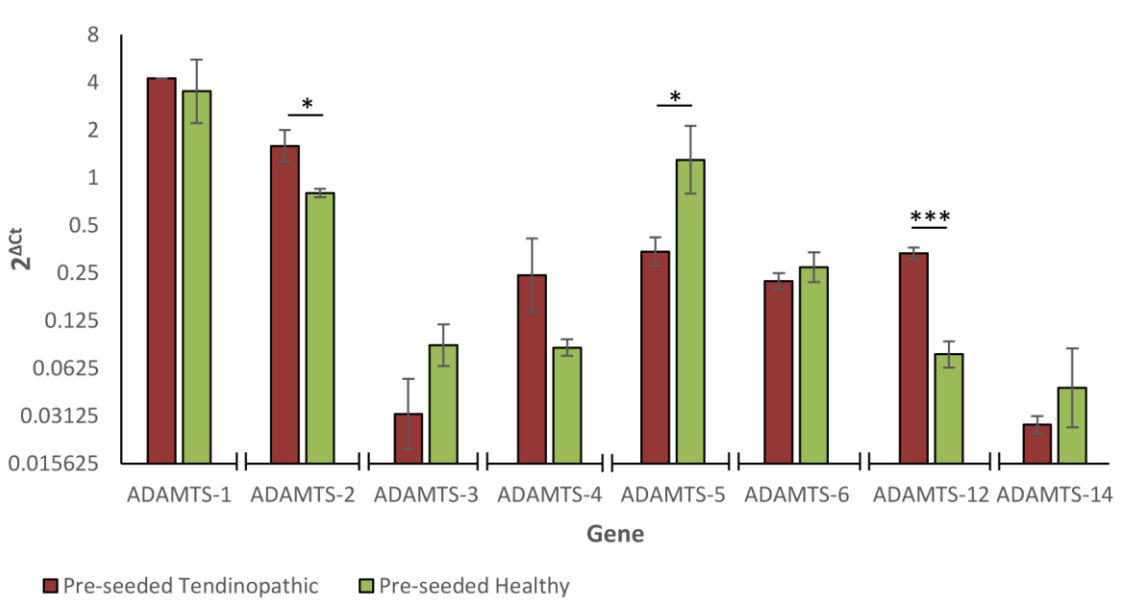

Figure 67: Average ADAMTS basal expression for pre-seeded cells. Expression shown as $2^{\Delta Ct}$ (normalised to TOP-1). Both healthy and both tendinopathic cell types were averaged and error bars represent standard deviations. ADAMTS-2 and ADAMTS-12 are seen to be expressed significantly more by tendinopathic cells while ADAMTS-5 is significantly less. Cell type n=2, with 3 repeats per cell type. * = P<0.05, ***=P<0.001.

TIMPs

TIMP-1, TIMP-2, TIMP-3 and TIMP-4 gene expression was profiled in the pre-seeded tenocytes. No significant differences were seen between healthy and tendinopathic tenocyte types. The basal expression for TIMP-4 was found to be lower than that of TIMP-1, TIMP-2 and TIMP-3, with TIMP-2 having the highest expression.

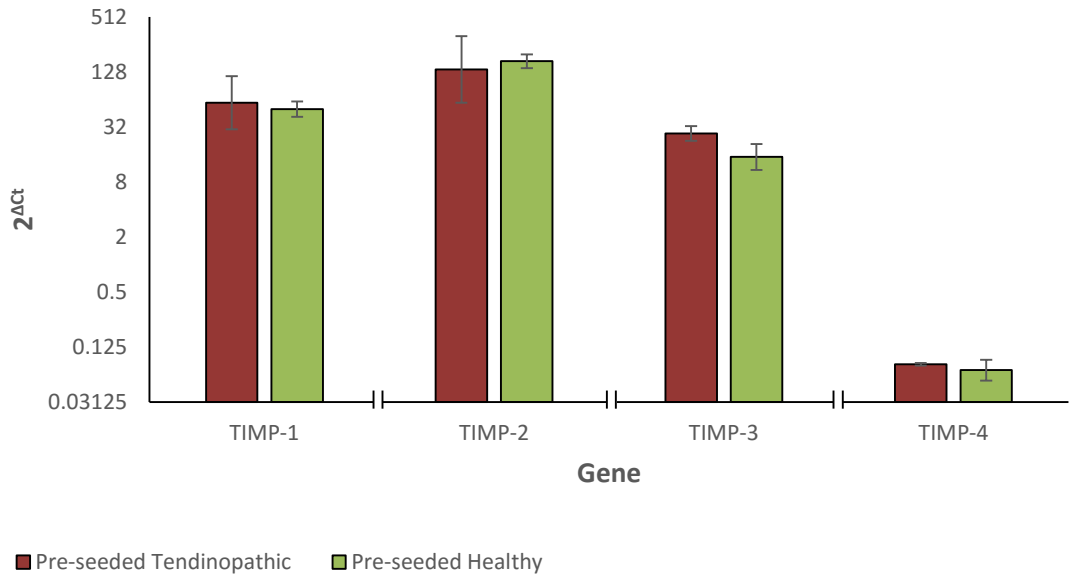

Figure 68: Average TIMP basal gene expression for pre-seeded cells. Expression shown as $2^{\Delta Ct}$ (normalised to TOP-1). Both healthy and both tendinopathic cell types were averaged and error bars represent standard deviations. TIMP-4 is seen to have the lowest gene expression whilst TIMP-2 is the highest. No significant differences were seen between healthy and tendinopathic tenocytes. Cell type n=2, with 3 repeats per cell type.

Proteoglycans

Figure 69 summarises the basal expression levels for aggrecan (ACAN), biglycan (BGN), decorin (DCN), fibromodulin (FMOD), lubricin (PRG-4) and versican (VCAN) for pre-seeded cells. FMOD, PRG-4 and VCAN were expressed significantly less by tendinopathic cells compared to healthy cells. Additionally, BGN also showed notable differences as it was expressed more by tendinopathic cells (P=0.06). Interestingly, although both tendinopathic cells expressed PRG-4 less than healthy cells, one tendinopathic cell type expressed PRG-4 ~38 times less than the other, thus contributing to the large standard deviation in tendinopathic PRG-4 gene expression seen in Figure 69. The same tendinopathic cells also showed higher ACAN expression (~11 times more) than the other tendinopathic tenocytes.

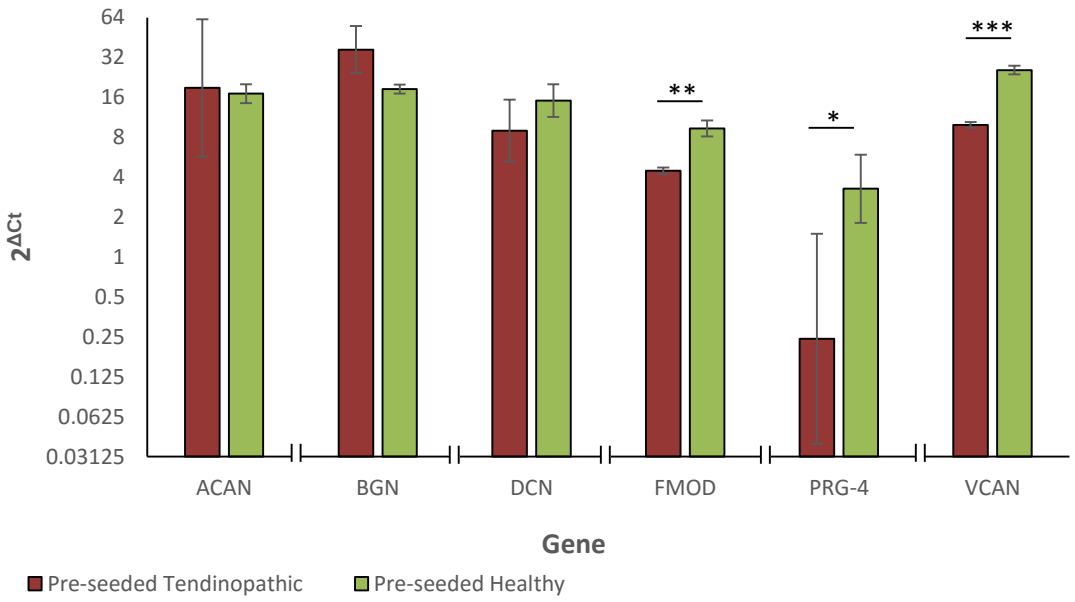

Figure 69: Average proteoglycan basal gene expression for pre-seeded cells. Expression shown as $2^{\Delta Ct}$ (normalised to TOP-1). Both healthy and both tendinopathic cell types were averaged and error bars represent standard deviations. Tendinopathic cells express significantly less FMOD, PRG-4 and VCAN, and notably more BGN (P=0.06). ACAN and PRG-4 are also seen to exhibit large standard deviations due to one tendinopathic cell type showing ~17 times more ACAN and ~21 times less VCAN expression than the other tendinopathic cell type. Cell type n=2, with 3 repeats per cell type. *=P<0.05, **=P<0.01, ***=P<0.001.

Interleukins

The interleukins profiled were IL-1β, IL-2, IL-6 and IL-8, however, IL-2 was not detected in any sample. Figure 70 shows that IL-8 was expressed significantly less by pre-seeded tendinopathic tenocytes compared to healthy tenocytes. The basal expression was highest for IL-6 compared to the other three interleukins investigated, although overall the expression of interleukins was generally lower than the other type of genes investigated. Once again, differences amongst the two tendinopathic tenocytes are also observed; gene expression for IL-1β was seen to be ~58 times more in one tendinopathic group than the other.

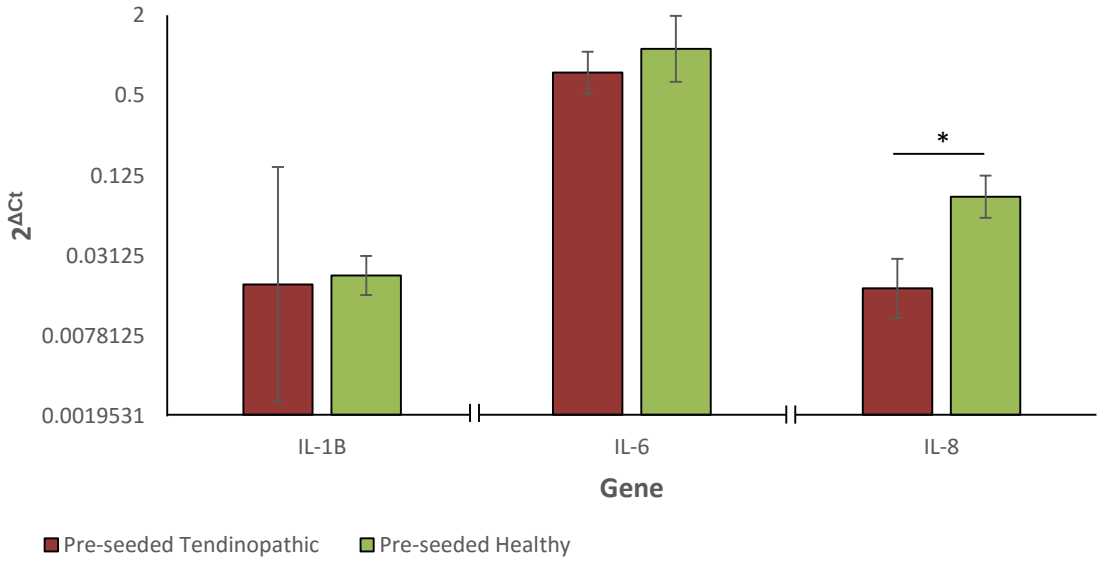

Figure 70: Average basal interleukin gene expression for pre-seeded cells. Expression shown as $2^{\Delta Ct}$ (normalised to TOP-1). Both healthy and both tendinopathic cell types were averaged and error bars represent standard deviations. Tendinopathic cells express significantly less IL-8 basally compared to healthy cells. Cell type n=2, with 3 repeats per cell type. *=P<0.05

Other Proteins

Figure 71 summarises the pre-seeded basal gene expression of proteins classed in the 'other' category. This included cartilage oligomeric protein (COMP), fibronectin (FN1), laminin (LAMA-1), scleraxis (SCX) and tenascin-C (TNC). Tendinopathic cells were seen to exhibit significantly higher TNC gene expression compared to healthy tenocytes. FN1 was also seen to be notably higher in tendinopathic cells compared to healthy cells (P=0.08). Interestingly, the large standard deviation bar present for SCX gene expression in tendinopathic cells once again highlights differences between the tendinopathic cell donors; the same cells which showed differences in PRG-4 and ACAN expression also showed ~21 times less SCX expression compared to the other tendinopathic tenocyte type.

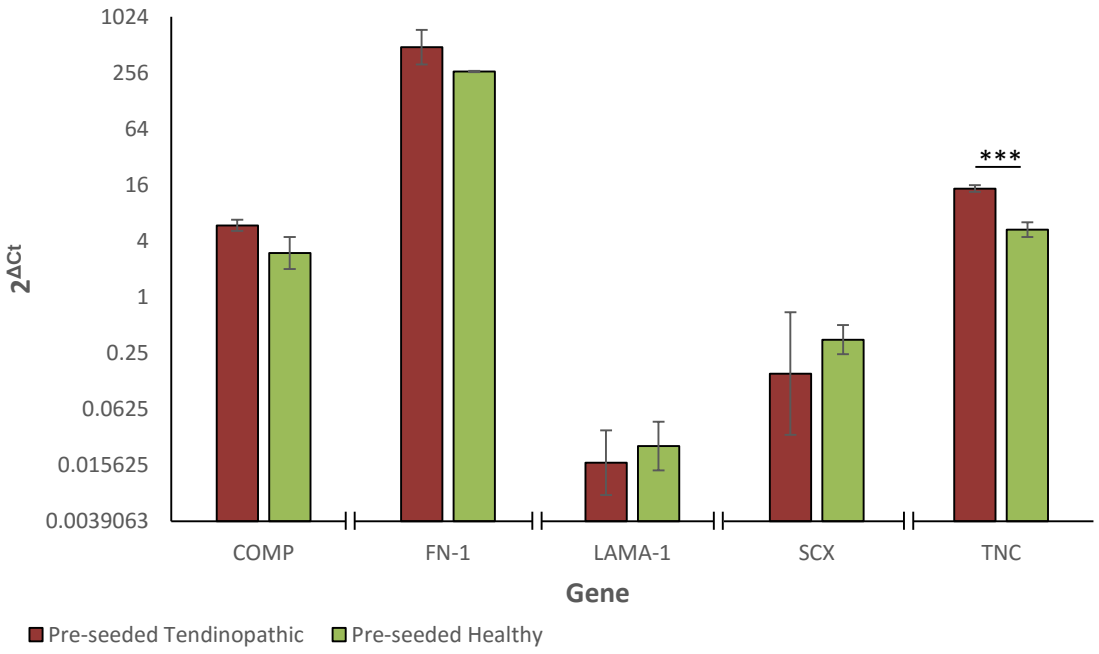

Figure 71: Average basal gene expression of a variety of other proteins in pre-seeded cells. Expression shown as $2^{\Delta Ct}$ (normalised to TOP-1). Both healthy and both tendinopathic cell types were averaged and error bars represent standard deviations. Tendinopathic cells express significantly more TNC basally compared to healthy cells. FN1 gene expression is also marginally higher in tendinopathic cells (P=0.08). Cell type n=2, with 3 repeats per cell type. ***=P<0.001.

4.4.2 Discussion: Differences between pre-seeded tendinopathic and healthy tenocytes

From all the genes analysed, COL-2A1, COL9A1, IL-2 and TNMD were undetected in all samples. As TNMD is a common gene reported in tenocytes (Andia et al., 2014; Fong et al., 2013; Mazzocca et al., 2012; Qiu et al., 2013; Ruzzini et al., 2014; Wagenhauser et al., 2012), it is likely the assay sequence chosen for the TLDA card layout might not have be suitable and TND was indeed expressed. In the case of COL-2A1 and COL-9A1, both have been previously reported as undetected in tenocyte studies (Jelinsky et al., 2011; Jones et al., 2013; Steiner et al., 2012) so no detection in this study was considered normal. IL-2 proteins have been found through microdialysis in tendons (Waugh et al., 2015), however the gene expression by tenocytes is not documented in literature, so it was not determined whether the assay sequence was unsuitable or whether IL-2 gene expression is commonly undetected in tenocytes.

The differences between tenocytes derived from healthy and tendinopathic tendons in their pre-seeded state is shown in Figures 65 to 71. From these figures it is evident a number of significant differences in the basal gene expression levels were present:

Higher expression in tendinopathic cells:

- MMP-3
- MMP-13
- ADAMTS-2
- ADAMTS-12
- TNC

Lower expression in tendinopathic cells:

- COL-12A1
- COL-14A1
- ADAMTS-5
- PRG-4
- VCAN
- FMOD
- IL-8

The basal gene expression levels of collagens were generally much higher than other gene types, including MMPs and ADAMTSs, implying a net anabolic state for both cell types. However, the higher MMP (MMP-3 and MMP-13) and ADAMTS (ADAMTS-2 and ADAMT-12) gene expression along with the lower collagen (COL-12A1 and COL-14A1) and proteoglycan

(PRG-4, VCAN and FMOD) gene expression in tendinopathic tenocytes suggested they were set towards a slightly more catabolic profile.

The difference in basal gene expression between healthy and tendinopathic cells was an interesting find, as one of the limitations for this study was the cell passage number. Cells received from collaborators at the Bio-Medical Research Centre, University of East Anglia, were in limited supply and previously passaged past P0. As a large number of cells were required to make sufficient composites (~14 million cells for each cell type), cells had to be grown and passaged further until the required quantity was reached. It is known that extensive cell culture can result in phenotypic drifts, with a study on human tenocytes noting a reduction in collagen type I and collagen type III gene expression after P3 and protein content after P4, tenascin-C gene expression after P5, and decorin protein content after P4 (Mazzocca et al., 2012). Another investigation into phenotypic drifts in human tenocyte culture saw a slight reduction in decorin protein levels at P4, with significant differences at P8 Yao et al. (2006). P10 has also been used as an arbitrary passage limit in a study using human tenocytes (Jones et al., 2013). Gene expression changes from phenotypic drift during *in vitro* culture would potentially mask differences between tendinopathic and healthy cells. However, despite this, the results obtained clearly showed differences which persisted after culture. Additionally, the changes observed by Mazzocca et al. (2012) were not seen in the results presented here, particularly with respect to tenascin-C; the tendinopathic tenocytes were cultured for 1-2 passages more than the healthy cells, yet an increase in tenascin-C gene expression was observed instead of the decrease which has been previously been associated with excessive culture. Overall, current data suggests the effects of phenotypic drift were limited, probably due to the tenocytes being cultured for much less than P10, ranging between P3 and P6.

The fact that differences between tendinopathic and healthy tenocytes were persistent during culture could suggest cellular changes after tendinopathy are slow to revert back to normal or

that individuals may possess tenocytes which are predisposed to a tendinopathic state. Indeed, genetic factors have been implicated in the development of tendinopathies (Magra and Maffulli, 2008). This includes polymorphisms of COL-5A1 gene which have been associated with Achilles tendinopathy (Abrahams et al., 2013) as well as polymorphisms of TIMP-2, and ADAMTS-14 (El Khoury et al., 2013), and tenascin-C (Mokone et al., 2005). Cells which behave differently to tenocytes in healthy individuals could lead to a different gene expression balance during healing which in turn would contribute to the susceptibility of developing tendinopathies.

It is also possible the differences observed could be due to the source of the tissue; healthy tenocytes originated from hamstring tendons while tendinopathic tenocytes were from Achilles tendons. However, some of the differences observed were more comparable to changes seen in tendinopathies, such as increased MMP-13, ACAN, and TNC gene expression and decreased ADAMTS-5 and VCAN gene expression (Corps et al., 2012; Corps et al., 2006; Corps et al., 2004; Ireland et al., 2001), providing confidence the differences observed were tendinopathy associated. In addition, the age of tendon donors could have played a role in the observed differences. Ideally the same age range should have been compared, however the available cell types and ages were limited thus the closest matching ages were chosen. The healthy tenocytes were obtained from an age range of 20.5 ± 1.5 years and tendinopathic from 48 ± 3 years, a relatively young and middle aged group respectively. Typical changes observed with ageing include decreased levels of GAGs (Riley et al., 1994a) and SLRPs (Peffers et al., 2014) in the tendon matrix. However, apart from a decrease in fibromodulin, other age related differences were not observed in the results. The data remains more consistent with gene expression changes seen in tendinopathic tissue. It is possible that age related effects were not evident here because studies usually go beyond 50 years, typically between ~70-100 years, when studying ageing affects in human tendons (Maganaris et al., 2004; Riley et al., 1994a; Yamada

et al., 2003). The ages of the donors used here could both be classified as 'mature' rather than 'old, therefore they might not significantly show changes associated with older age.

Another interesting observation was the differences amongst the two tendinopathic tenocyte samples from different donors. Both were obtained from donors with chronic tendinopathy (noted as a duration of more than 18 months), and both had the same general gene expression profile and trends when compared to healthy tenocytes. However, a few genes were expressed at distinctly different levels between the two tendinopathic donors (summarised in Figure 72). For example, one tendinopathic tenocyte sample was found to have ~38 times less PRG-4, 21 times less SCX, 42 times less MMP-13 and 20 times less MMP-3 than the other. These were extremely large differences, which were further emphasised by a range of other genes, such as ADAMTS-1, COL-6A1, VCAN and TNC, which showed no difference at all. These results could suggest the donors had a different state of tendinopathy or even type of tendinopathy.

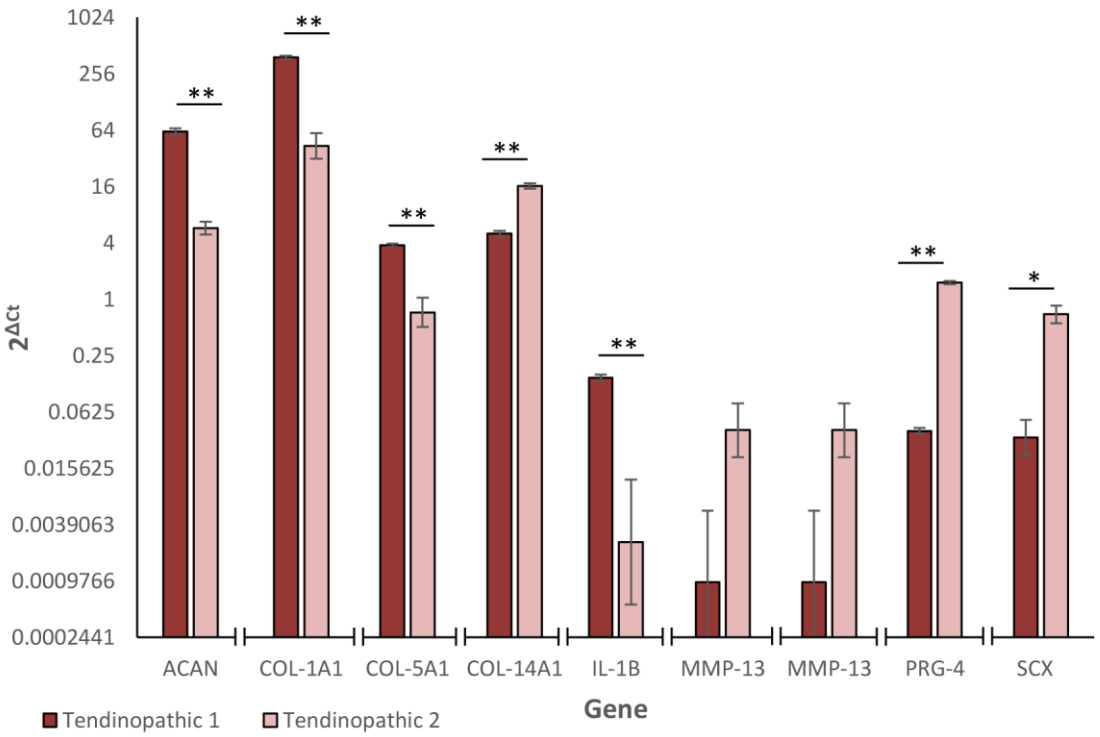

Figure 72: Average expression of genes which are distinctly different among the two pre-seeded tendinopathic tenocyte populations (normalised TOP-1). Error bars indicate standard deviation. These graphs suggest the two tendinopathic tenocytes are of different tendinopathy states or types. Cell type n=2, with 3 repeats per cell type. Post-hoc students T Test performed to calculate significance, *=P<0.05, **=P<0.01.

It should be noted that the basal gene expression levels of the pre-seeded cells would differ to an extent to those during actual culture and therefore are not presented as standalone tendinopathic or healthy tenocyte gene expression profiles. This is due to the cells being harvested via trypsin-EDTA, an enzyme used to detach cells from culture surfaces, which would consequently instigate changes in gene expression. However, as the period of trypsin exposure was not excessive (~5 min exposure only) and the same procedure used for both healthy and tendinopathic tenocytes, the gene expression profiles obtained can be used comparatively with confidence to distinguish differences between the two tenocyte types. Nonetheless, to obtain basal expression without the effects of trypsin, further comparisons of tendinopathic and healthy tenocytes were made using non-strained composites, with the results discussed in the next section.

4.4.3 Results: Substrate stiffness effects and differences between tendinopathic and healthy tenocytes in non-strained composites

The gene expression of tenocytes within composites were compared to further assess differences between the basal gene expression of tendinopathic and healthy tenocytes and to assess the influence of culture within a 3D system. The basal levels were expected to differ slightly to those seen with the pre-seeded cells, as the tenocytes were now in an environment dissimilar to that found in culture flasks. Firstly, gene expression levels were averaged for all non-strained composites, to simply compare tendinopathic tenocytes and healthy tenocytes, with Student's *t*-tests performed between the two to assess significance. Gene expression results of cells analysed in this manner are referred to as non-strained gene expression.

Additionally, as composites were made of either 60% or 20% PEG fibres, i.e. stiff and less stiff fibres respectively, the effect of substrate stiffness on gene expression was also explored. For both cell types Student's *t*-tests were performed between composites with stiff fibres and composites with less stiff fibres.

As reported for pre-seeded cells, gene expression data is grouped into 'Collagens', 'MMPs', 'ADAMTSs', 'TIMPs', 'Proteoglycans', 'Interleukins' and 'Other Proteins'. The observations are then summarised and discussed in section 4.4.4.

Collagens

All the collagens detected, apart from COL-11A1, showed statistically significant differences between composites containing tendinopathic tenocytes and composites containing healthy tenocytes (Figure 73); COL1A1, COL3A1, COL4A1, COL5A1, COL6A1 and COL-12A1 expression were all higher in composites containing tendinopathic tenocytes while COL-14A1 expression was lower. The gene expression of COL-2A1 and COL-9A1 were once again undetected in all samples. From the collagens investigated, the levels of COL-1A1, COL-3A1 and COL-5A1 in tendinopathic samples were observed to exhibit high standard deviations. This was once again due to the two tendinopathic tenocyte donors having differences in select genes as discussed in 4.4.2.

Substrate stiffness was seen to affect COL-6A1 and COL-12A1 gene expression in composites containing tendinopathic tenocytes. No other genes were affected by substrate stiffness.

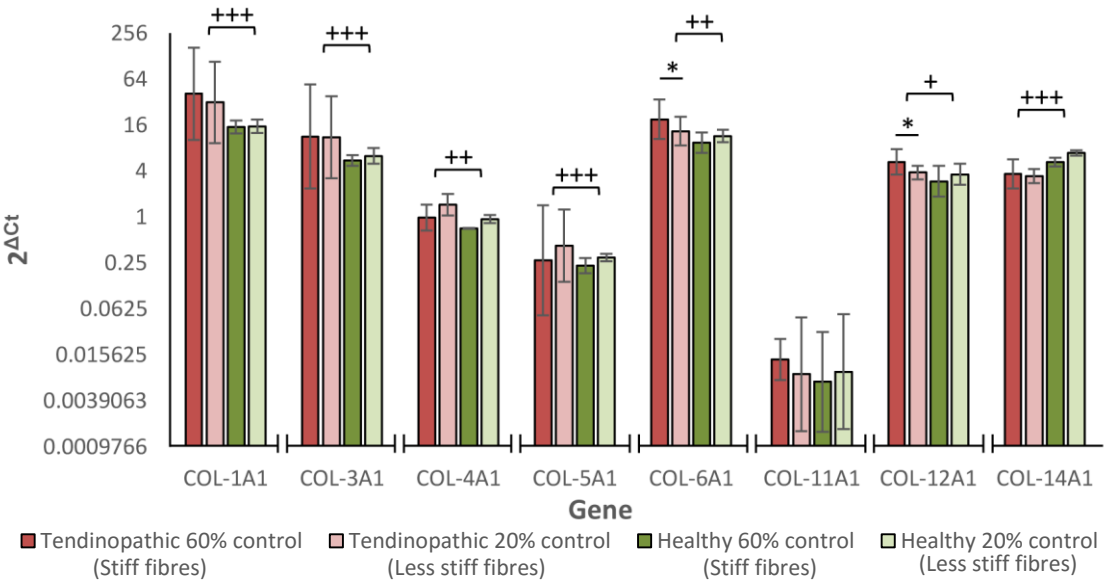

Figure 73: Average gene expression of collagens in non-strained composites containing either tendinopathic or healthy tenocytes (red and green bars respectively), and expression shown as $2^{\Delta Ct}$ (normalised to TOP-1). Composites made with 60% PEG-RGD fibres (i.e. stiff fibres) compared with composites made with 20% PEG-RGD fibres (i.e. less stiff fibres) to assess fibre stiffness effect. COL-6A1 and COL-12A1 were the only genes affected significantly by substrate stiffness. All genes, except COL11A1, showed significant differences between tendinopathic and healthy tenocytes. Error bars represent standard deviations. * indicates significance due to substrate stiffness, while + indicates significance between composites containing healthy and tendinopathic tenocytes. Cell type n=2, with 6 composites per cell type. *=P<0.05, +=P<0.05, ++=P<0.01, +++=P<0.001.

MMPs

MMPs 7, 8 and 9 expression levels were extremely low and in some samples undetected. However, overall their expression levels were still higher than those seen in pre-seeded cells where MMP-8 and MMP-9 were undetected in all samples. MMP-2 was the most highly expressed MMP gene and was seen to be extremely consistent across all composite types. No substrate stiffness related effects were observed with MMPs. Composites containing tendinopathic tenocytes showed significantly higher MMP-13 gene expression and lower MMP-3 gene expression, contrasting to the observations in pre-seeded cells.

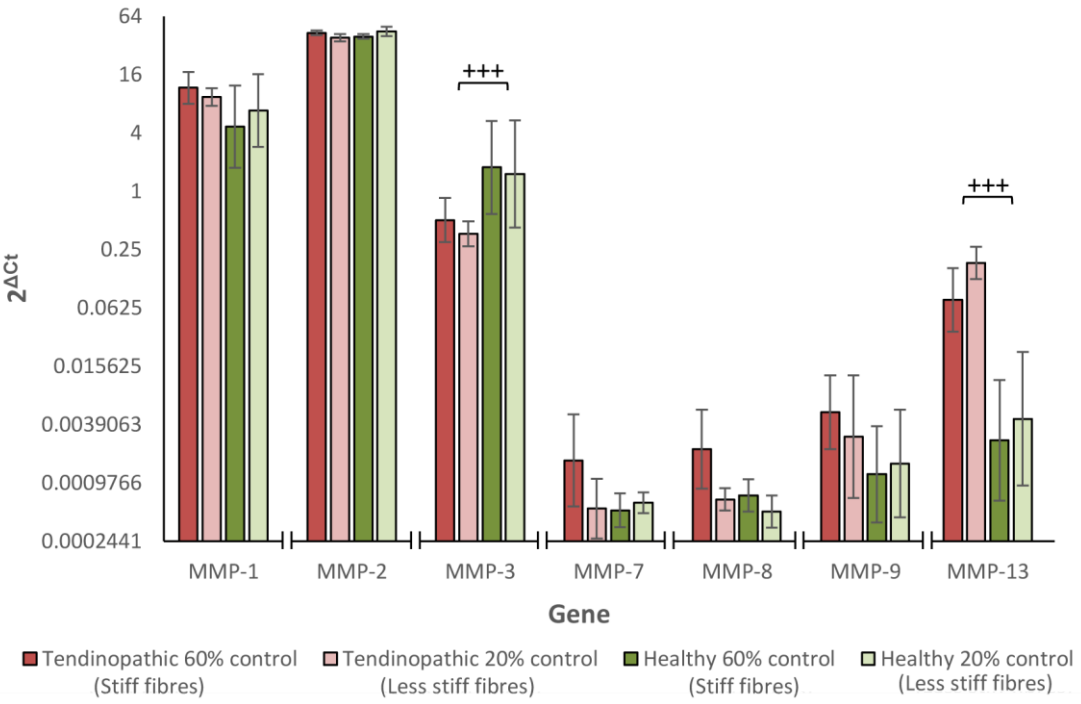

Figure 74: Average gene expression of MMPs in non-strained composites containing either tendinopathic or healthy tenocytes (red and green bars respectively), and expression shown as $2^{\Delta Ct}$ (normalised to TOP-1). Composites made with 60% PEG-RGD fibres (i.e. stiff fibres) were compared with composites made with 20% PEG-RGD fibres (i.e. less stiff fibres) to assess the effect of fibre stiffness on gene expression. No substrate dependent differences were observed, however differences in MMP-13 and MMP-3 were seen when comparing composites containing and healthy cells. Cell type n=2, with 6 composites per cell type. (Error bars represent standard deviations, +++=P<0.001).

ADAMTSs

Many significant differences in ADAMTS gene expression were seen when comparing composites containing tendinopathic and healthy tenocytes. ADAMTS-2, ADAMTS-4, ADAMTS-12 and ADAMTS-14 were all expressed more in composites containing tendinopathic tenocytes, while ADAMTS-1 and ADAMTS-6 were expressed less. Tendinopathic tenocytes also showed substrate dependent differences in ADAMTS-14, which was expressed more on stiffer substrates. No other substrate stiffness effects were observed.

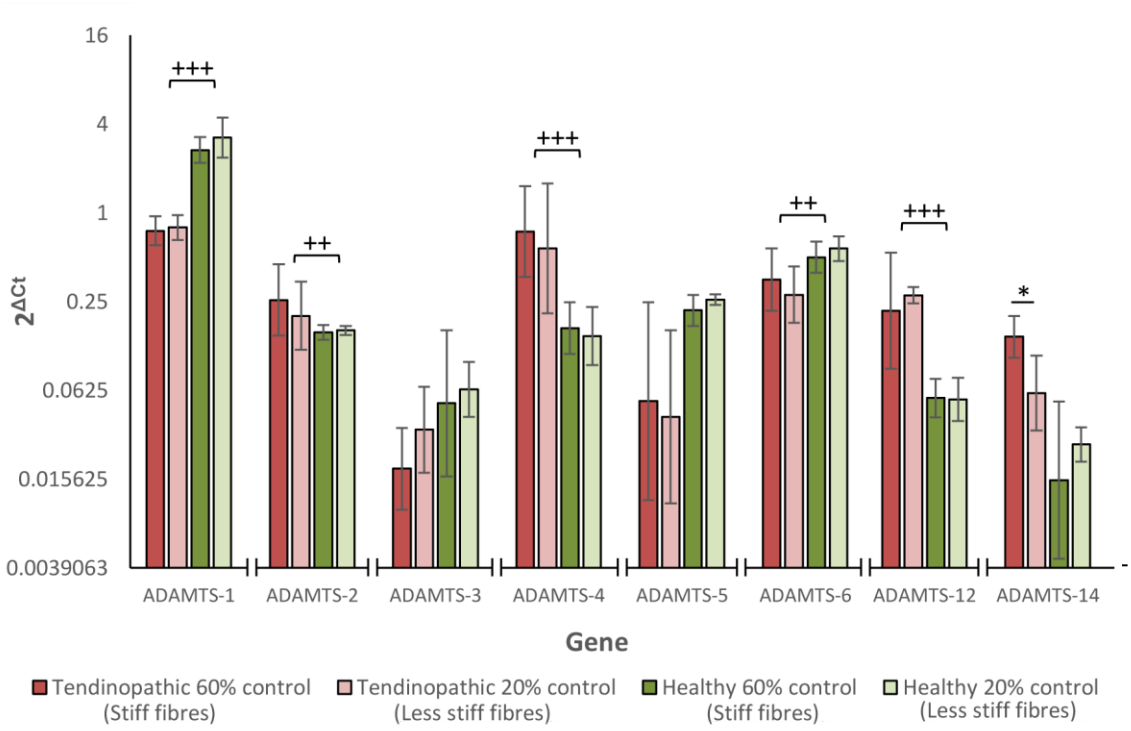

Figure 75: Average gene expression of ADAMTS in non-strained composites containing either tendinopathic or healthy tenocytes (red and green bars respectively), and expression shown as $2^{\Delta Ct}$ (normalised to TOP-1). Composites made with 60% PEG-RGD fibres (i.e. stiff fibres) were compared with composites made with 20% PEG-RGD fibres (i.e. less stiff fibres) to assess the effect of fibre stiffness on gene expression. ADAMTS-14 is seen to increase with higher stiffness substrates in tendinopathic cells only. ADAMTS-1, 2, 4, 6, and 12 are all seen to differ significantly between tendinopathic and healthy cells. * indicates significance due to substrate stiffness, while + indicates significance between composites containing healthy and tendinopathic tenocytes. Cell type n=2, with 6 composites per cell type. *=P<0.05, +=P<0.05, ++=P<0.01, +++=P<0.001.

TIMPs

TIMP-1 and TIMP-2 were the most highly expressed TIMPs while TIMP-4 was the lowest. Similar to the pre-seeded cells, there were no differences in the TIMP expression between tendinopathic and healthy tenocytes. However, substrate dependent differences were seen in composites containing tendinopathic tenocytes, with TIMP-1 and TIMP-3 expressed more when tenocytes were on stiffer substrates.

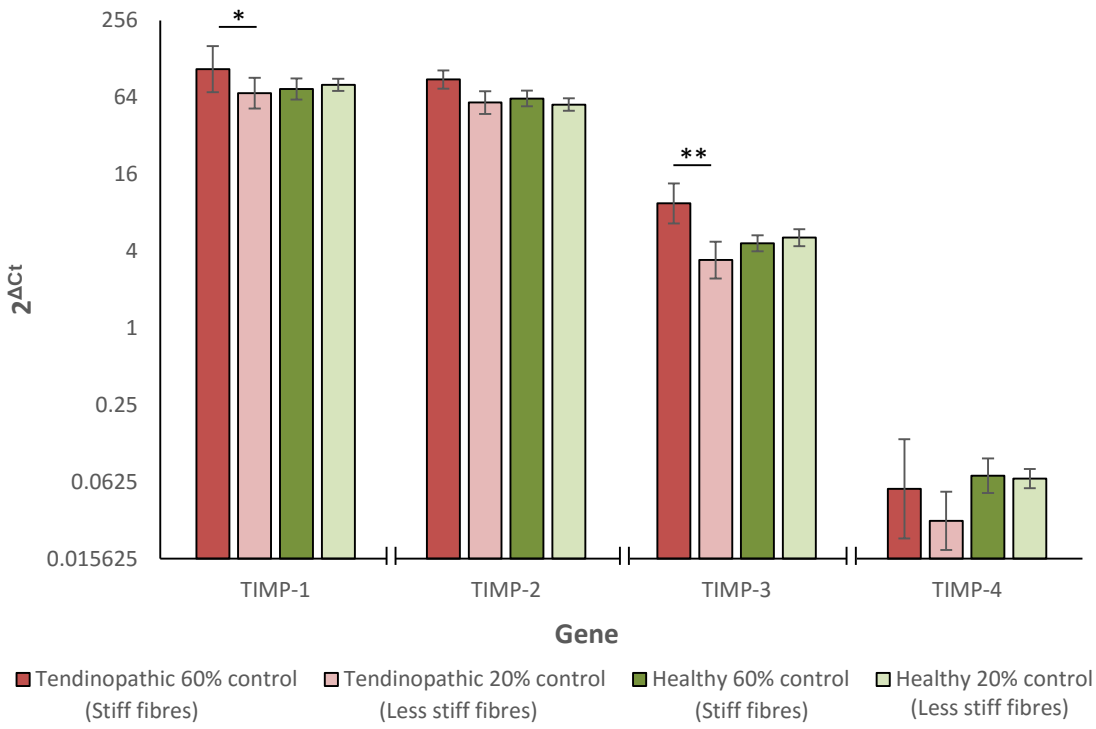

Figure 76: Average gene expression of TIMPs in non-strained composites containing either tendinopathic or healthy tenocytes (red and green bars respectively), and expression shown as $2^{\Delta Ct}$ (normalised to TOP-1). Composites made with 60% PEG-RGD fibres (i.e. stiff fibres) were compared with composites made with 20% PEG-RGD fibres (i.e. less stiff fibres) to assess the effect of fibre stiffness on gene expression. Tendinopathic tenocytes increase TIMP-1 and TIMP-3 gene expression significantly when seeded on stiffer substrates. Cell type n=2, with 6 composites per cell type. *=P<0.05, *=P<0.01.

Proteoglycans

Interestingly, the gene expression levels of all the proteoglycans was seen to be significantly different when comparing composites containing tendinopathic tenocytes to those containing healthy tenocytes. ACAN, DCN, FMOD, PRG-4 and VCAN were expressed less by tendinopathic cells while BGN was expressed more. Tendinopathic cells also showed dependence on substrate stiffness for ACAN and PRG-4, with both genes expressed more when tenocytes were on stiffer substrates.

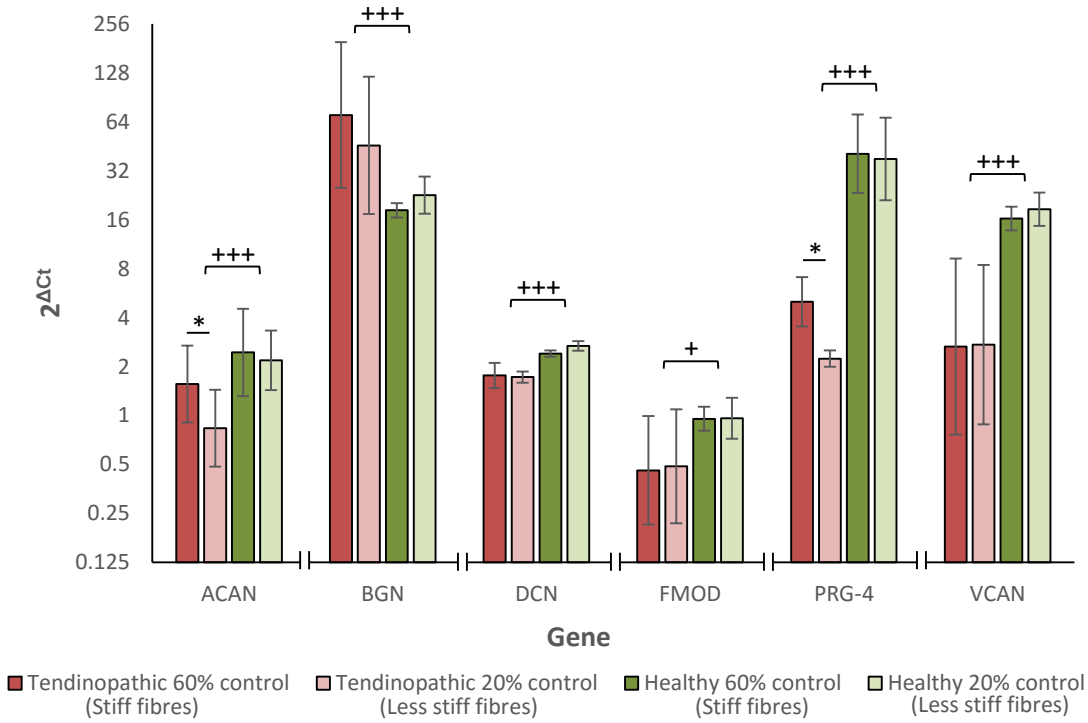

Figure 77: Average gene expression of proteoglycans in non-strained composites containing either tendinopathic or healthy tenocytes (red and green bars respectively), and expression shown as $2^{\Delta Ct}$ (normalised to TOP-1). Composites made with 60% PEG-RGD fibres (i.e. stiff fibres) were compared with composites made with 20% PEG-RGD fibres (i.e. less stiff fibres) to assess the effect of fibre stiffness on gene expression. Tendinopathic tenocytes increase ACAN and PRG-4 gene expression significantly when seeded on stiffer substrates. Tendinopathic tenocytes also exhibit significantly different expression levels of all proteoglycan genes investigated when compared to healthy tenocytes. * indicates significance due to substrate stiffness, while + indicates significance between composites containing healthy and tendinopathic tenocytes. Cell type n=2, with 6 composites per cell type. *=P<0.05, +=P<0.05, ++=P<0.01, +++=P<0.001.

Interleukins

IL-2 was undetected in all samples, similar to that seen with pre-seeded cells. IL-8 was found to be the most highly expressed interleukin investigated. No substrate dependent differences were found for interleukins, however, composites containing tendinopathic tenocytes did show significantly less IL-6 and IL-8 gene expression than the healthy cells.

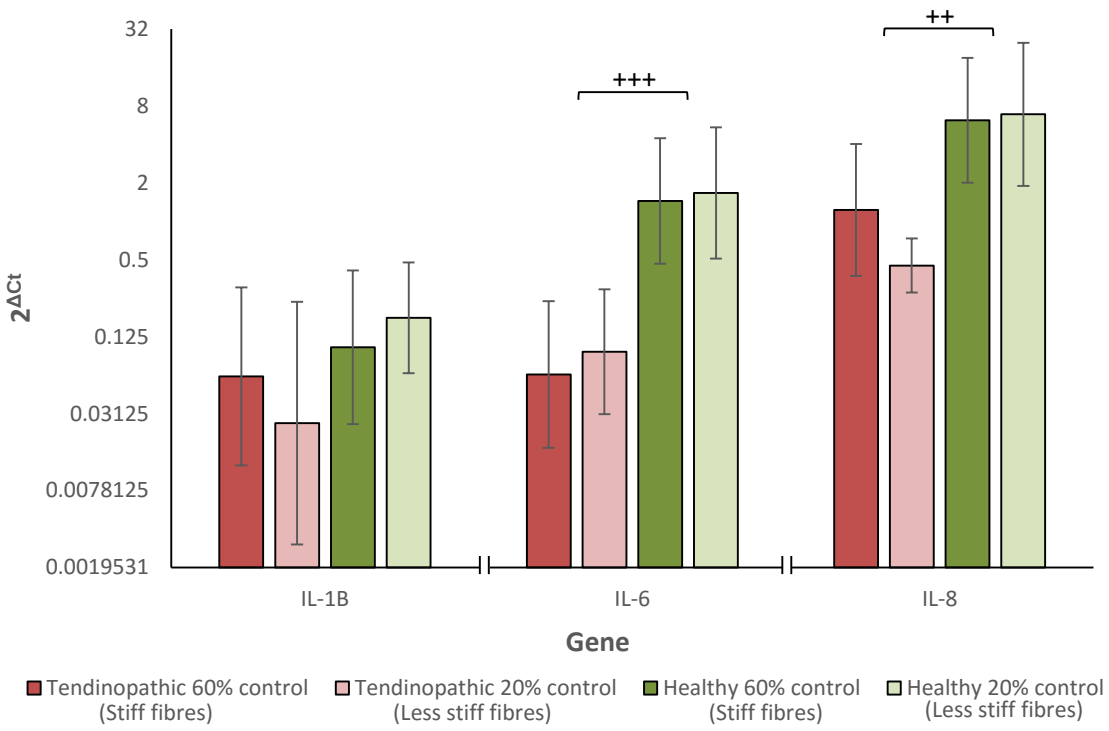

Figure 78: Average gene expression of interleukins in non-strained composites containing either tendinopathic or healthy tenocytes (red and green bars respectively), and expression shown as $2^{\Delta Ct}$ (normalised to TOP-1). Composites made with 60% PEG-RGD fibres (i.e. stiff fibres) were compared with composites made with 20% PEG-RGD fibres (i.e. less stiff fibres) to assess the effect of fibre stiffness on gene expression. Tendinopathic tenocytes exhibit significantly less expression levels of IL-6 and IL-8 when compared to healthy tenocytes. Cell type n=2, with 6 composites per cell type. ++=P<0.01, +++=P<0.001.

Other Proteins

Substrate stiffness was seen to affect the gene expression levels of most of the other proteins to an extent. FN-1 gene expression was seen to increase when tendinopathic tenocytes were on stiffer substrates, while healthy tenocytes decreased COMP, LAMA-1 and TNC when seeded on stiffer substrates. The gene expression levels of FN-1 and TNC were also seen to be significantly more in tendinopathic tenocytes than healthy tenocytes.

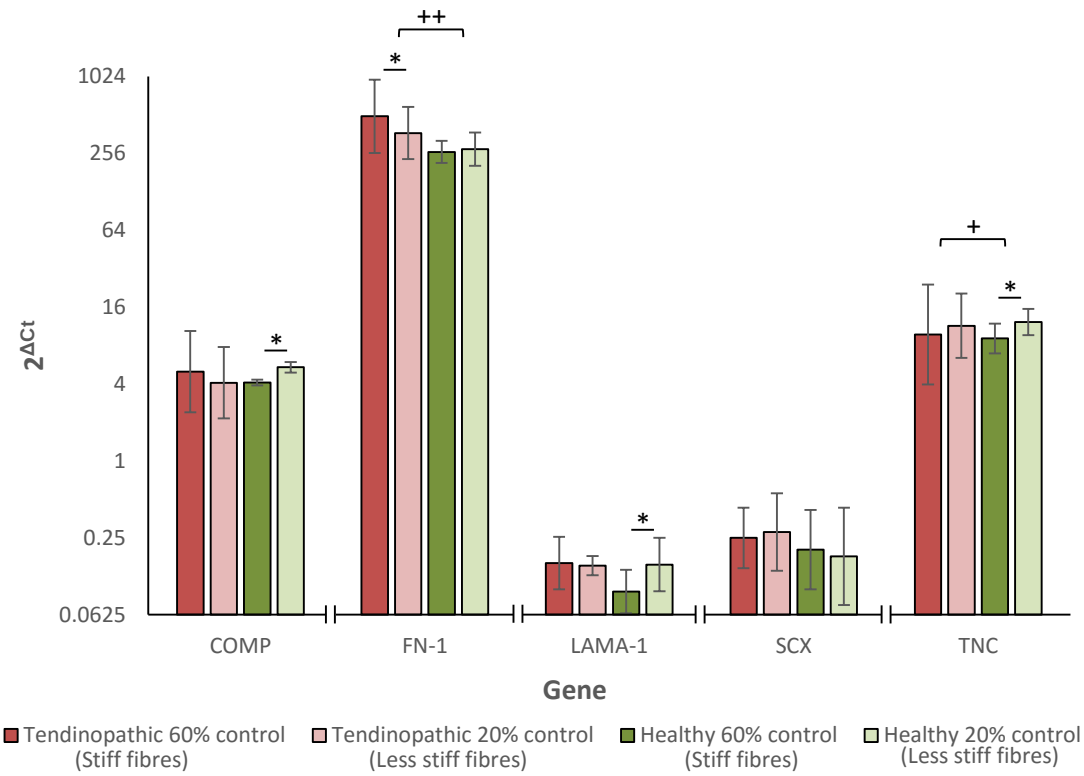

Figure 79: Average gene expression of a range of other proteins in non-strained composites containing either tendinopathic or healthy tenocytes (red and green bars respectively), and expression shown as $2^{\Delta Ct}$ (normalised to TOP-1). Composites made with 60% PEG-RGD fibres (i.e. stiff fibres) were compared with composites made with 20% PEG-RGD fibres (i.e. less stiff fibres) to assess the effect of fibre stiffness on gene expression. Higher substrate stiffness increases FN-1 gene expression in tendinopathic tenocytes, while higher stiffness decreases COMP, LAMA-1 and TNC gene expression in healthy tenocytes. Tendinopathic tenocytes also exhibit significantly more FN-1 and TNC gene expression when compared to healthy tenocytes. * indicates significance due to substrate stiffness, while + indicates significance between composites containing healthy and tendinopathic tenocytes. Cell type n=2, with 6 composites per cell type. *=P<0.05, +=P<0.05, ++=P<0.01.

4.4.4 Discussion: Substrate stiffness effects and differences between tendinopathic and healthy tenocytes in non-strained composites

Non-strained composites made with tendinopathic and healthy tenocytes were compared to further assess differences between basal gene expression levels of healthy and tendinopathic tenocytes within a 3D culture environment, and also to review the effects of substrate stiffness on these cells. All gene expression data is summarised in the heatmap in Figure 80. Statistically significant differences were evident in a number of genes including ADAMTS-2, ADAMTS-4, ADAMTS-12, BGN, COL-12A1, COL-1A1, COL-3A1, COL-4A1, COL-5A1, COL-6A1, FN-1, and MMP-13 (all higher in composites containing tendinopathic tenocytes) and TNC, ACAN, ADAMTS-1, ADAMTS-6, COL-14A1, DCN, FMOD, IL-6, IL-8, MMP-3, PRG-4 and VCAN (all lower in composites containing tendinopathic tenocytes).

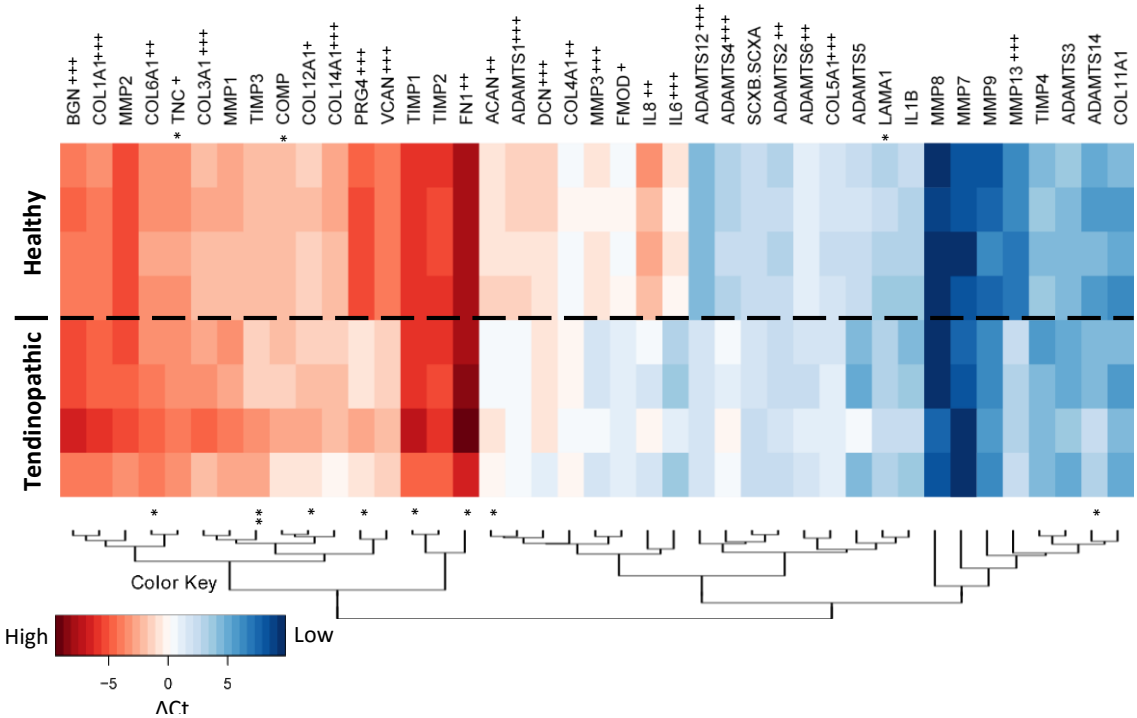

Figure 80: Heatmap summarising average gene expression (ΔCt, normalised to TOP-1) of non-strained composites containing tendinopathic tenocytes (bottom half) and healthy tenocytes (top half). Each row represents a composites type with all technical and biological repeats averaged. The non-strained gene expression of a number of genes are seen differ between tendinopathic and healthy tenocytes ('+' indicates significant differences between composites containing tendinopathic and healthy tenocytes, + = P<0.05, ++ = P<0.01, +++ = P<0.001). Substrate stiffness was seen to effect more genes in composites containing tendinopathic tenocytes ('*' above and below the heatmap indicate genes significantly affected by substrate stiffness in composites containing healthy cells and tendinopathic cells, respectively (* = P<0.05, ** = P<0.01). Cell type n=2, with 6 composites per cell type.

Although many of the cell type differences observed in the pre-seeded cell comparison were present when the cells were seeded in composites, there were also a couple of changes. For example, MMP-3 and TNC gene expression was seen to be higher in the pre-seeded tendinopathic tenocytes than the healthy tenocytes, whereas in the non-strained composites the opposite was true. This is likely due to the pre-seeded cells being exposed to trypsin right before processing for RNA analysis, as described earlier in section 4.4.2. Specifically, trypsin exposure would likely decrease matrix degradation related gene expression, as cells would respond to the catabolic nature of the enzyme. Indeed it has been found that trypsin can change the expression of a number of genes, including a reduction in MMP-3 gene expression by cells (Chaudhry, 2008).

The gene expression profile of tendinopathic tenocytes in constructs was even more fitting to that seen in typical tendinopathic tissue; more BGN, COL-1A1, COL-3A1, and MMP-13 expression and lower MMP-3 and VCAN observed in composites containing tendinopathic cells, as seen in tendinopathy (Corps et al., 2012; Corps et al., 2006; Corps et al., 2004; Ireland et al., 2001; Legerlotz et al., 2012; Riley et al., 1994b). As discussed with the pre-seeded cells, this supported the idea that the differences seen between the tenocyte types in this study are more likely due to tendinopathy and less likely due to phenotypic drift, tendon age or tendon type, although each of the latter will probably have a small effect. Moreover, the results showed that tenocytes could retain a tendinopathic profile during culture and after incorporation into composites, suggesting that tendinopathy development is not simply a case of microdamage, but that there are long lasting phenotypic changes in cells, which may mean they are unable to respond like normal tenocytes to the microdamage.

IL-6 and IL-8 were less expressed in tendinopathic tenocyte than healthy tenocytes. This observation was counterintuitive to the findings in tendinopathic tissues, where IL-6 is increased (Legerlotz et al., 2012). However, inflammation, and consequently interleukins, are

associated with the early stages of tendinopathy (Dakin et al., 2014; Millar et al., 2010; Rees et al., 2013), and in chronic tendinopathies, inflammation and inflammatory chemicals are not evident (Alfredson and Lorentzon, 2002; Dakin et al., 2014). The tenocytes used in this study were obtained from donors exhibiting chronic tendinopathy, thus it is possible the lower IL-6 and IL-8 was a reflection of this advanced state of tendinopathy.

It should be noted that some differences observed between the non-strained gene expression levels of tendinopathic and healthy tenocytes, although statistically significant, were quite small. This is also evident from the heatmap where the colour differences between the two cell types cannot be distinguished visually in some cases. However, the gene expression differences emphasised in this summary as those associated with tendinopathy were clear as larger, discernible differences, providing confidence in the results.

Substrate stiffness has been seen to affect the behaviour of cells. In Human fibroblasts, MMP-2, TIMP-2 and COL-3 gene expression increase with substrate stiffness (Karamichos et al., 2007) while cardiac fibroblasts have been reported to decrease MMP-2 and MMP-9 gene expression on decreasing substrate stiffness (Xie et al., 2014). Substrate stiffness has also been shown to affect the differentiation of human mesenchymal stem cells (Guvendiren and Burdick, 2012). In the current study, substrate dependent changes were seen in a number of genes. Healthy tenocytes showed significant changes in 3 genes whereas 8 genes were significantly affected by substrate stiffness in tendinopathic tenocytes:

<u>Tendinopathic tenocytes on stiffer substrates:</u>

- COl-12A1 ↑
- COL-6A1 ↑
- ADAMTS-14 ↑
- TIMP-1 ↑
- TIMP-3 ↑
- ACAN ↑
- PRG-4 ↑
- FN-1 ↑

<u>Healthy tenocytes on stiffer substrates:</u>

- COMP ↓
- LAMA-1 ↓
- TNC ↓

↑ = Increase
↓ = Decrease

It is interesting the tendinopathic cells showed more sensitivity to the substrate stiffness than the healthy tenocytes, particularly in genes which can be related to an anabolic response such as COL-12A1 and COL-6A1 which are collagens associated with type I collagen fibrils, TIMP-1 and TIMP-3 which are involved in the inhibition of various matrix degrading MMPs and ADAMTSs, and ADAMTS-14 which is a procollagen I and II N-propeptidase (i.e. involved in collagen type I and II synthesis). It was not possible to conclude why the tendinopathic tenocytes are more sensitive to the substrate within this study, but the results do suggest they were more active in sensing and responding to their surrounding environment than healthy tenocytes.

4.4.5 Results: Shear-tension ratio effect and tenocyte differences

Gene expression data for tenocytes exposed to different shear-tension ratios are compared in this section for both tendinopathic and healthy tenocytes. Composites creating the high shear condition were made with stiff 60% PEG-RGD fibres while composites creating a low shear condition were made of less stiff 20% PEG-RGD fibres. To reduce the effects of substrate stiffness, composites of physiologically equivalent shear were made of each fibre type, to find relative expression, leading to four test groups; a low shear-high tension ratio (20% PEG fibres with 60 min soak), 2 physiologically equivalent shear-tension ratios (20% PEG fibres with 0 min soak, and 60% PEG fibres with 60 min soak) and a high shear-low tension ratio (60% PEG fibres with 0 min soak). Conditions were analysed as high shear relative to physiological and low shear relative to physiological.

As some variability with the basal gene expression was observed with cell type and substrate stiffness (discussed in previous sections of this chapter), a fold change of 2 was used as a threshold for identifying changes, to provide confidence the observations were large enough to be a result of shear-tension ratio changes and not due to other effects. Volcano plots were used to visualise results with this 2 fold change boundary and separated into two figures; 'high shear' relative to 'physiological shear', and 'low shear' relative to 'physiological shear'. Volcano plots were created using DataAssist™ (*Applied Biosystems*), plotting "-log10(p-value)" against "log2(fold change)" for each gene. Additionally, tendinopathic and healthy tenocytes are shown in separate volcano plots.

Bar graphs showing $2^{\Delta Ct}$ results for each shear-tension ratio and cell type are provided as supplementary figures in Appendix C: Additional shear-tension ratio graphs (2ΔCt).

The volcano plots in Figure 81 show that the healthy and tendinopathic tenocytes respond differently to shear. In healthy tenocytes, low shear was seen to significantly increase IL-8 and MMP-3 gene expression, and significantly decrease FN-1 gene expression. High shear significantly increased COL1-A1 gene expression and significantly decreased ADAMTS-4 and IL-6 gene expression. In tendinopathic tenocytes, low shear did not cause any statistically significant changes, but extremely large negative fold changes were seen in IL-8, IL-6, MMP-3 and IL-1β. High shear caused a significant increase in VCAN gene expression and a significant decrease in MMP-1 and MMP-13 gene expression. Although not statistically significant, ADAMTS-3 and ADAMTS-14 showed large negative fold changes with high shear in tendinopathic tenocytes.

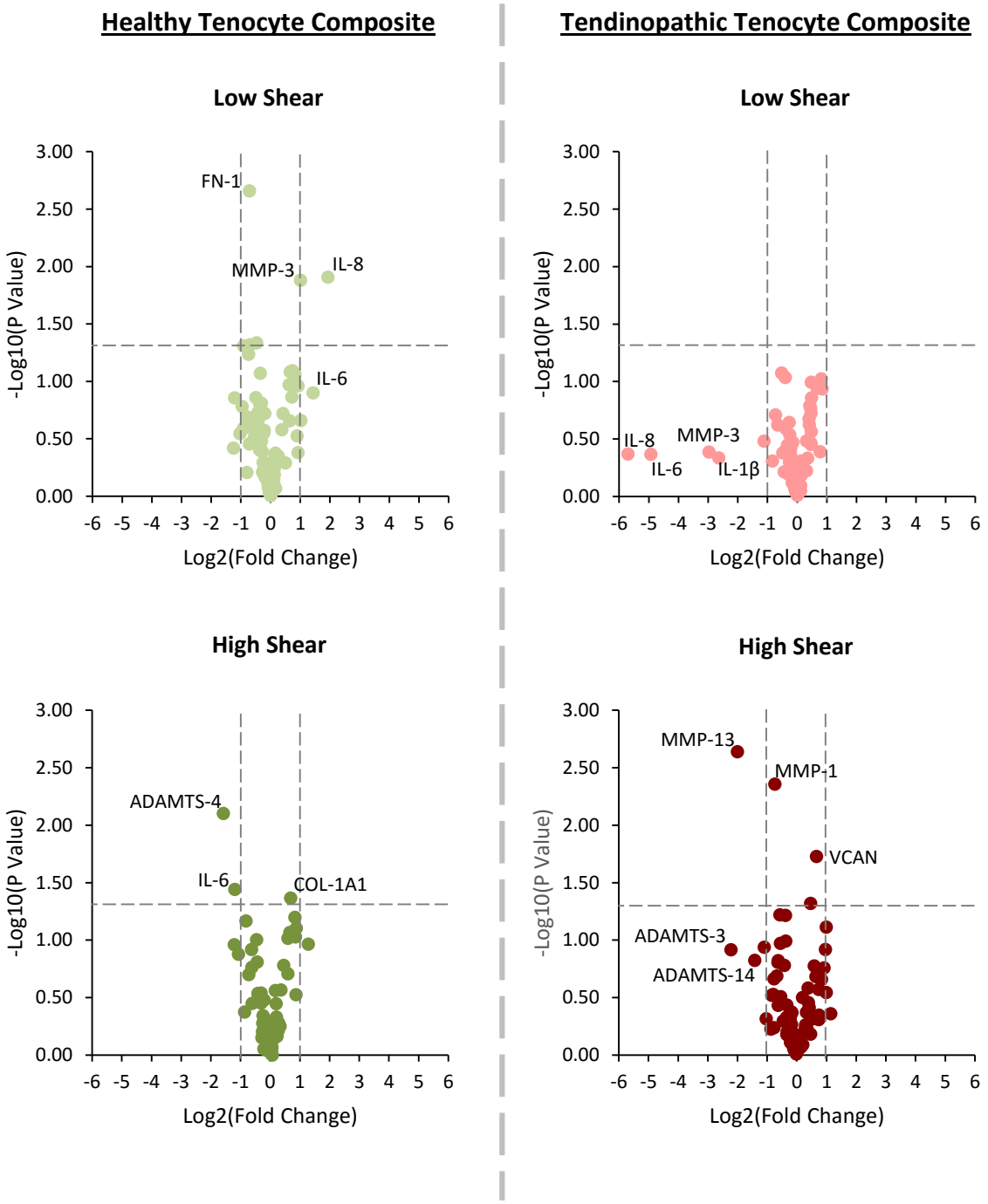

Figure 81: Volcano plots for healthy and tendinopathic tenocytes showing gene fold change vs significance, expressed as Log2(fold change) vs –log10(p-value), under low and high shear conditions. The horizontal dotted line indicates the 5% significance level (P<0.05) and the vertical dotted lines indicate values for ±2 fold change. Graphs show that tendinopathic tenocytes have more expression variability and larger fold changes compared to healthy tenocytes, particularly under low shear conditions. Genes regulated by shear also differ between the two tenocyte types. Cell type n=2, with 6 composites per cell type.

4.4.6 Discussion: Shear-tension ratio effect and tenocyte differences

The shear-tension ratio effect was compared between tendinopathic and healthy tenocytes after cyclically loading fibre composites of each type to 5% strain for 24 hours at 1Hz. As composites used 60% PEG-RGD fibres and 20% PEG-RGD fibres to create high and low shear conditions, respectively, physiologically equivalent shear conditions were created for each fibre type as controls to eliminate substrate stiffness effects. The results of these comparisons show some genes responded in low shear conditions while others responded to high shear conditions.

It was not surprising that the genes regulated by shear differed for both tenocyte types, as it has already been established in sections 4.4.2 and 4.4.4 that the tendinopathic and healthy tenocytes used in this study exhibit different basal expression levels and respond to substrate stiffness differently. It was interesting to note that high shear caused more downregulation of genes in both tenocyte types than upregulation, suggesting that shear strains above and below the physiological equivalent initiate different responses from tenocytes and there is not a simple linear relationship between applied shear and cell response. Healthy tenocytes showed a significant increase in IL-8 gene expression with low shear and a significant decrease in IL-6 gene expression with high shear. In addition to inflammatory roles, IL-6 has been shown to stimulate collagen type I synthesis (Andersson et al., 2011), increase with loading (Langberg et al., 2002; Legerlotz et al., 2013), and also regulate TGFβ (Zhang et al., 2005) which is also capable of inducing collagen type I and III synthesis (Heinemeier and Kjaer, 2011). This could suggest the high shear-low tension condition was reducing matrix synthesis in healthy tenocytes as both IL-6 and COL-1A1 are downregulated. Little has been studied with IL-8 in tendons, a marker often only associated with inflammatory responses by tendons and tenocytes (Ackermann et al., 2013; Andia et al., 2014). IL-8 has also been found to increase immediately after extracorporeal shock wave therapy, a tendinopathy treatment, in human Achilles tendons (Waugh et al., 2015) so it is potentially involved in promoting changes in tendon matrix during healing. The

upregulation of IL-8 and MMP-3 in the low shear-high tension condition could therefore signify that healthy tenocytes were instigating remodelling of the matrix in response to low shear.

In contrast to the healthy tenocytes, tendinopathic tenocytes did not show any significant changes in gene expression in the low shear condition, but the high shear-low tension condition significantly downregulated MMP-3 and MMP-13 gene expression in tendinopathic tenocytes. Both MMP-3 and MMP-13 act on a number of common substrates which include, but are not limited to, collagen type III, IV, IX and X, aggrecan, decorin and tenascin. However unlike MMP-3, MMP-13 can also degrade collagen type I fibrils. Moreover, MMP-3 is also involved in the activation of MMP-13 (Klein and Bischoff, 2011; McCawley and Matrisian, 2001; Nagase et al., 2006). Therefore the downregulation of both MMP-3 and MMP-13 by tendinopathic tenocytes subjected to low shear potentially signifies an attempt to reduce matrix degradation.

Although tendinopathic tenocytes did not show statistically significant changes in the low shear condition, they did show much more variability. As such some extremely high fold changes in some genes were noted, but with low significance values. This included a ~52 fold decrease in IL-8, ~30 fold decrease in IL-6 , ~8 fold decrease in MMP-3 and ~6 fold decrease in IL-1β. Moreover, comparing healthy tenocyte and tendinopathic tenocyte volcano plots for both high and low shear, the data points for the tendinopathic tenocytes were seen to be generally wider spread with larger fold changes, whereas the healthy tenocytes data points were more closely packed. This suggested the tendinopathic tenocytes were less stable than the healthy tenocytes and produced larger expression changes, possibly due to more mechano-sensitivity. This was further emphasised by the tendinopathic tenocytes showing substrate stiffness dependent changes in the previous section. Although not statistically significant, the fact that IL-8 and MMP-3 were regulated in the opposite direction to healthy tenocytes in the low shear condition further highlights the extent of differences between the two tenocyte types. It should be noted that the variability in gene expression changes of tendinopathic tenocytes also results in low

significance, but if more samples were repeated, it is possible the changes observed would be more pronounced.

Shear has been observed to alter matrix turnover related gene expression in tenocytes, including an increase in MMP-2, 3, 7, 9, 10, 12, 13, 23 and 24 gene expression and a decrease in TIMP-2 and TIMP-3 gene expression (Fong et al., 2005). However such studies are not completely comparable to the study performed in this chapter as the former neglected the inclusion of tension and was restricted to fluid shear. Nonetheless, as some MMPs did show changes with shear (healthy tenocytes in the low shear condition and tendinopathic tenocytes in the high shear condition), the involvement of shear in regulating matrix turnover can be agreed upon.

4.5 Conclusion

The study described in this chapter employed the fibre composite system to explore differences in gene expression of tenocytes derived from healthy and tendinopathic tissue, both basally and in response to altered shear-tension ratios. The results clearly indicated significant differences between the two cell types, with tendinopathic tenocytes showing higher ADAMTS-2, ADAMTS-4, ADAMTS-12, BGN, COL-12A1, COL-1A1, COL-3A1, COL-4A1, COL-5A1, COL-6A1, FN-1, and MMP-13 gene expression, and lower TNC, ACAN, ADAMTS-1, ADAMTS-6, COL-14A1, DCN, FMOD, IL-6, IL-8, MMP-3, PRG-4 and VCAN gene expression. Furthermore, it was established that phenotypic changes between tenocyte types remained throughout culture and after encapsulation into composites. The persistent nature of these differences was theorised to either be due to persistent cell changes during long term tendinopathy or possibly inherent genetics, consequently leading to individuals being more susceptible to tendinopathies than others. Differences between the two tendinopathic tenocyte donors were also found, with ACAN, COL-1A1, COL-5A1, COL-1A1, IL-1β, MMP-3, PRG-4 and SCX all being significantly different, possibly due to a different stage or even type of tendinopathy.

Using the composites, it was found the tendinopathic tenocytes were more mechano-sensitive than healthy tenocytes, responding more significantly to substrate stiffness and exhibiting more variability after loading. Shear was also found to be an important cue in altering the behaviour of both type of tenocytes. Shear higher and lower than the physiological equivalent was found to evoke responses different from one another; healthy tenocytes downregulated matrix synthesis with high shear and upregulated matrix degradation with low shear, while tendinopathic tenocytes downregulated matrix degradation with high shear. Although it appears the cells responded to the different shear-tension ratios, a simple linear relationship between gene expression and shear was not exhibited in the genes analysed. Differences in the response to shear by the healthy and tendinopathic tenocytes, along with the different basal

gene expression levels and mechano-sensitivity, suggested the behaviour of tendinopathic tenocytes was fundamentally different to healthy tenocytes and could be a response of cells perceiving the same stimuli differently.

Limitations within the study included the tendon type, tendon donor age and potential for phenotypic drift during culture. However, as discussed earlier in this chapter, the possible effects of these factors on gene expression seen in literature, along with the magnitude of differences observed, could not wholly account for the differences between the tenocyte types. Additionally, as the changes were more in line with those seen in tendinopathy, it was concluded the differences between cell types were indeed related to tendinopathy. The low n number for the experiments is another limitation to the study, and a result of the difficulty in obtaining human tenocytes. However the data can be considered as preliminary data in its current form, and used as an indicator for possible trends exhibited by human tenocytes.

Chapter 5: Cell Attachment Peptides - A critical factor for shear-tension sensitivity

5.1 Introduction and Hypotheses

The hierarchical tendon structure results in a complex mechanical strain environment, with tenocytes experiencing both tension and shear during tendon loading. The previous chapter has shown that tenocytes alter their gene expression in response to different levels of shear-tension as well as substrates of different degrees of stiffness. There has been increasing investigation into the mechanisms involved in sensing these environmental cues, with integrins implicated as key components (Arnaout et al., 2007; Chiquet, 1999; Legate et al., 2009; Pavalko et al., 1998; Roca-Cusachs et al., 2013; Schwartz, 2010).

Integrins are transmembrane structures used by cells to adhere to extracellular proteins (summary provided in Chapter 1). Different combinations of integrin subunits recognise different ligands, providing cells the utility to distinguish between different proteins (Plow et al., 2000). Additionally, the intracellular portion of integrins can connect to the cytoskeleton resulting in direct force transmission (Giannone et al., 2003; Roca-Cusachs et al., 2013). The mechanical environment is therefore thought to regulate integrins in tenocytes and subsequently direct ECM organisation (Bayer et al., 2014). As different integrins are used to attach to different proteins, it is possible the response to a mechanical stimulus could differ depending on the integrin employed. For example, the integrins used to attach to collagen include α1β1, α2β1, α3β1, α10β1, α11β1 and αIIbβ3 (Hynes, 1992; Jokinen et al., 2004; Plow et al., 2000; Yamamoto et al., 1995), while those for fibronectin have been reported to include α2β1, α3β1, α4β1, α4β7, α5β1, α8β1, αvβ1, αvβ3, αvβ5, αvβ6, αvβ8 and αIIbβ3 although with

different affinities (Askari et al., 2009; Campbell and Humphries, 2011; Hynes, 1992; Plow et al., 2000). Moreover, it has been seen that integrin α2β1 is more important than α1β1 for cell attachment and spreading on fibrillar type I collagen (Abair et al., 2008; Jokinen et al., 2004), while α1β1 is suggested to function more for collagen type IV recognition (Grzesiak and Bouvet, 2007). Integrin α1β1 has also been suggested to function to induce cell proliferation and reduce collagen synthesis while integrin α2β1 increases matrix remodelling (Heino, 2000), emphasising the unique functions of each integrin combination.

Peptides DGEA and GFOGER are sequences found in fibrillar collagen, which can bind to integrin α2β1, leading to their description as collagen mimetic peptides (Knight et al., 2000; Luzak et al., 2003; Mizuno et al., 2000). RGD is a sequence commonly associated with fibronectin, although it is also a functional attachment site in other proteins such as vitronectin, and can bind to a number of integrins, mainly α5β1, αVβ3, and αIIbβ3 (Danen et al., 2002; Hynes, 1992; Ruoslahti, 1996; Sechler et al., 1996), which are all different to those used by cells on native type I collagen.

The fibre composite system developed in Chapter 2 incorporates changeable cell attachment peptides. It was hypothesised that the cell attachment peptide, and consequently the integrins engaged in cell attachment, alter the gene expression of tenocytes and their response to shear-tension ratios. The fibre composite system was used to compare a collagen mimetic peptide, DGEA, with a non-collagen-like peptide, YRGDS. This allowed investigation of integrins that would be involved in tenocyte attachment to collagen in native tendon.

5.2 Experimental Overview

The experiment was conducted using primary bovine tenocytes digested from bovine extensor tendons. 8 types of composites were made; 4 with RGD and 4 with DGEA as the cell attachment peptide. Two degrees of rod stiffness (20% and 60% PEG) and two soak times (0 and 60 min) created a range of shear-tension ratios for each peptide. Composites were cyclically strained to 5% for 24 hours at 1 Hz, after which RT-qPCR analysis was used to investigate the expression of a number of genes. Other analysed samples included pre-seeded cells and composites in a non-strained free-swelling state. 3 experimental repeats were performed, using different bovine tenocyte donors each time (i.e. 3 biological repeats).

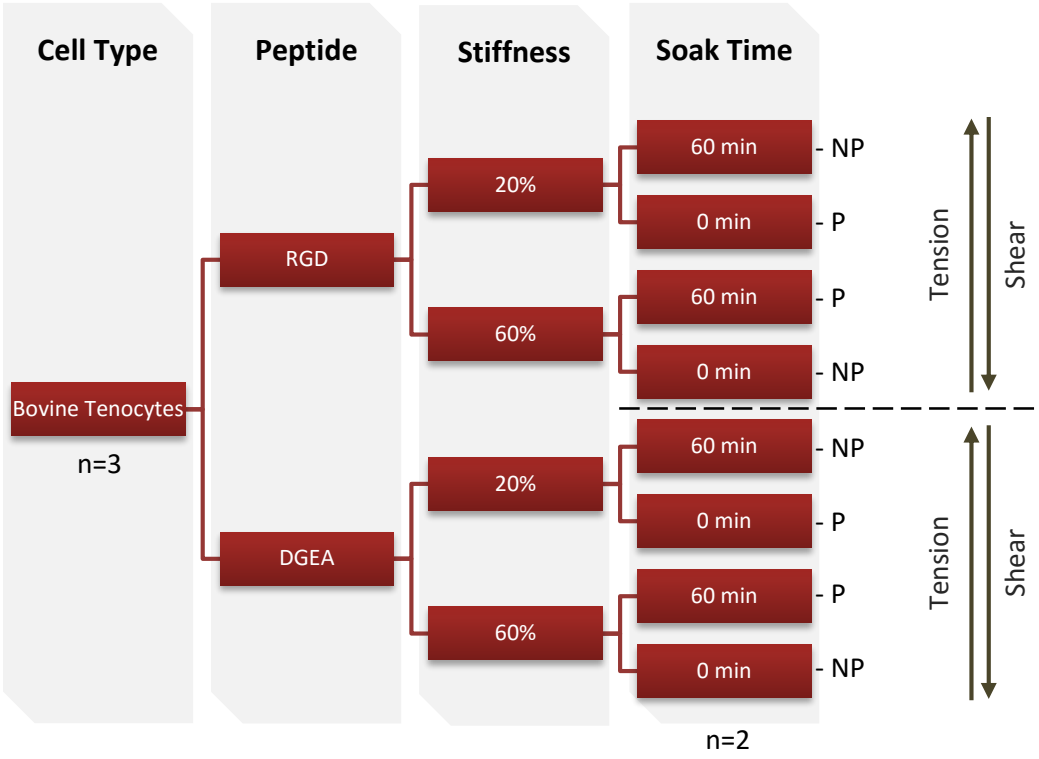

NP = Non-physiological shear-tension ratio
P = physiologically equivalent shear-tension ratio

Figure 82: Overview of composite types used in study. The resulting type of shear-tension ratio is indicated by the arrows on the right hand side, with both RGD and DGEA composites having the same conditions (emphasised by the dotted line). 3 bovine feet were used to provide 3 biological repeats, with 2 composites for each condition in each biological repeat.

5.3 Methods

Note 1: The protocols for manufacturing composites and RNA extraction are detailed comprehensively in Chapter 3 and only stated in brief under this section. Other additional procedures, such as cell isolation via tendon digestion, which have not been previously detailed are described fully.

Note 2: Further details of all chemicals used, including supplier details, are present in Table 35 and Table 36, in Appendix B: Chemicals and Materials List.

Cell Isolation through Tissue Digestion

Fresh surplus bovine feet joints obtained from a local abattoir *(Arapahoe Meat Co, USA)* were cleaned in water and soaked in 70% ethanol. The extensor tendon was then dissected from the joint in a sterile hood, and the tendon diced into ~ 3mm^3 pieces using a scalpel. Diced tendon was rinsed twice in a PBS solution containing 1% Pen/Strep and placed into a 50mL falcon tube. A digestion media was then made by adding 2mg/mL Collagenase Type 2 to a Dispase solution (1 U/mL), which was then sterile filtered using 0.22µm syringe filters and warmed to 37°C in a water bath. The diced tendon pieces in the 50mL tubes were covered with digestion media in a 1:2 volume ratio, i.e. ~10mL tendon pieces covered in 20mL digestion media. The tubes were then tightly closed, wrapped in parafilm and placed onto a rocker inside an incubator (37°C, 5% CO_2). This was left for 48 hours for the tissue to completely digest. After complete digestion, the digested tendon solution was diluted 10 times with PBS containing 1% Pen/Strep. This solution was subsequently filtered using a 100 µm cell strainer, taking care to slowly pipette the tendon solution through the strainer into another 50 mL falcon tube and changing the strainer whenever necessary. The resulting cell suspension was then centrifuged for 10 minutes at 1500 rpm. The supernatant was discarded and the cell pellet washed by re-suspending in PBS

containing 1% Pen/Strep. The cell solution was then centrifuged again at 1500 rpm for 10 minutes and re-suspended in PBS containing 1% Pen/Strep to further wash the cells. After the second wash, the solution was centrifuged for 10 minutes at 1500 rpm and the pellet re-suspended in 10% FBS media (DMEM, 1% Pen/Strep and 10% FBS). The cells were then counted using trypan blue and a haemocytometer, and re-suspended at 1.75 million cells/mL.

Fibre Production and Seeding

PEG-RGD fibres were made by preparing solutions of 60% or 20% w/v PEGDM in PBS, with 0.05% w/v Irgacure 2959 and 5mM YRGDS peptide conjugated to acrylate-PEG-NHS. PEG-DGEA fibres were made by preparing solutions of 60% or 20% w/v PEGDM in PBS, with 0.05% w/v Irgacure 2959 and 5mM DGEA peptide conjugated to acrylate-PEG-NHS. To make fibres, the solutions were pipetted into Teflon fibre moulds and polymerised for 10 minutes under UV light (365 nm wavelength, ~4mW/cm^2) as described previously. Fibres were then extracted from the moulds and stored in a petri dish with 70% ethanol. A total of 1600 fibres were made; 400 20% PEG-RGD fibres, 400 60% PEG-RGD fibres, 400 20% PEG-DGEA fibres, and 400 60% PEG-DGEA fibres.

Sterile forceps were used to transfer 100 of each fibre type (20% PEG-RGD, 60% PEG-RGD, 20% PEG-DGEA and 60% PEG-DGEA) into separate wells of a non-tissue culture treated 48 well plate. The fibres were then seeded with 1.75 million cells per well using the optimised seeding protocol described previously.

A cell sample was taken to analyse the gene expression of cells in their ‘pre-seeded’ state. To do this, 3 micro-centrifuge tubes were prepared with 700 µL QIAzol Lysis Reagent and 100000 cells (~57.2 µL of the cell suspension above used to seed fibres) pipetted into each tube. The tubes were vortexed vigorously for a few minutes to lyse the cells and stored at -80°C until ready for RNA extraction. An extra tube of 100000 cells was lysed with QIAzol to use for primer validation and efficiency calculations.

Composite Production

The next day composites were made using the cell seeded fibres using the method described in section 3.2. The procedure was repeated to make 20% PEG-RGD, 60% PEG-RGD, 20% PEG-DGEA and 60% PEG-DGEA fibres with either 0 minutes or 60 minutes soak time. All composites were stored in separate wells of a 6 well plate containing 10% FBS media, and left in an incubator overnight. 3 biological repeats were performed using the same procedure (n=3).

Strain Application

Composites were retrieved from the incubator and 2 of each composite type (strained group) were set up into the strain rig, with each composite submerged in 2 mL 10% FBS media. An additional 2 composites of each type (non-strained group) were placed into separate wells in a 6 well plate and filled with 2 mL 10% FBS media. Both the rig (strained samples) and well plates (non-strained samples) were placed into an incubator overnight before initiating loading.

Once the composites had stabilised for 24 hours, the strain system was set to apply 5% sinusoidal cyclic strain at 1 Hz for 24 hours (86400 cycles). At the end of the loading regime, the composites were removed from the rig or well plates and paired into 1.2 mL cryovials, i.e. 2 composites of the same type were put into the same cryovial. The cryovials were then snap frozen in liquid nitrogen and stored at -80°C until ready for RNA extraction.

RNA Extraction

RNA was extracted, using the optimised protocol described in Chapter 3. First cryovials containing frozen composites were retrieved from the -80°C storage and chromium steel grinding balls (9mm diameter) added to each tube. The tubes were then further cooled in liquid nitrogen before homogenising the composites with a Tissue Lyser II system (*QIAgen*). This ball mill homogeniser was set to 30 Hz and run for two 30 second bursts. Homogenised tubes were placed back in liquid nitrogen and taken into a fume hood, where 700 µL QIAzol was added to

each tube. The QIAzol/homogenate solution was mixed thoroughly and transferred into individual QIAshredder columns which were then centrifuged for 2 minutes at full speed to fully lyse the cells. The MiRNeasy micro kit was then used to collect and wash the extracted RNA. The clean RNA was released from the spin column membrane in 15 µL RNase free water (supplied in MiRNeasy kit).

The quantity of RNA was measured using a NanoDrop Spectrophotometer 1000 and 1 µL of sample. All samples where then diluted to 18 ng/µL using RNase free water and stored at -80°C.

RT-qPCR

The tubes containing diluted RNA were thawed and 10 µL of each RNA sample transferred into new micro-centrifuge tubes. A reverse transcription mastermix was made, enough for 85 samples (including extra in case of loss), according to the formula in Table 30.

Table 30: Reverse transcription mastermix was made by combining components of the High-Capacity cDNA Reverse Transcription Kit *(Life Technologies)* as detailed in the table.

Substance	Quantity for 1 sample (µL)	Quantity for 85 samples (µL)
MultiScribe Reverse Transcriptase	1	85
10x Sample Buffer	2	180
Deoxynucleotide triphosphates	0.8	68
25x RT Random Primers	2	170
RNase free Water	4.2	357

10 µL of the reverse transcription mastermix was then added to each RNA tube and centrifuged at ~2000g for 10 seconds. Tubes were then placed into a thermocycler (model 2720*, Applied Biosystems*) set to run at 25°C for 10 minutes, 37°C for 120 minutes, 85°C for 5 minutes and then 4°C until opened.

Once the reverse transcription process had finished, the tubes containing the resulting complimentary DNA (cDNA) were removed from the thermal cycler and kept on ice whilst

proceeding with the next steps. The cDNA was diluted to a total volume of 200 µL by adding 180 µL RNase free water and mixed gently through pipetting.

A stock gene mix was made for all genes and enough for all samples (plus extra in case of loss) as detailed in the Table 31. A list of primer sequences for the genes investigated is provided in Table 32.

Table 31: Details of the components for the stock gene mix made for each gene type. Sequences for forward and reverse primers for each gene are provided in Table 32.

Substance *(Supplier)*	**Quantity for per sample (µL)**
Forward Primer (10 µM) *(Custom primers from Life Technologies)*	0.5
Reverse Primer (10 µM) *(Custom primers from Life Technologies)*	0.5
FastStart Universal SYBR Green Master *(Roche Life Science)*	5

The primer efficiencies were first calculated using the cDNA samples allocated for primer validation before running the experimental samples. This cDNA was diluted 1:1, 1:10 and 1:100 in RNase-free water. A 96 well plate was then prepared by pipetting 4 µL of each cDNA sample in triplicate, along with 3 wells of 4 µL RNase free water to act as non-template controls (NTC). Each well was then filled with 6 µL of the relevant stock gene mix.

The plates were sealed and briefly centrifuged at ~2000g for 10 seconds to collect the solution at the bottom of the wells. Plates were then placed into the 7500 Fast Real-Time PCR system *(Applied Biosystems)*. SYBR was set as the reporter, and the thermal profile set to run at 95°C for 10 minutes, followed by 40 cycles of 95°C for 10 seconds and 60°C for 30 seconds. This was repeated until all genes had been run.

The threshold cycles (Ct) were extracted through the Applied Biosystems 7500 Software V2.0.6 *(Life Technologies)* by setting the threshold near the end of the linear amplification region (as previously described in Chapter 4. The extracted Ct values were then imported into Excel *(Microsoft)* and plot against log10 of the initial cDNA dilution. The gradient of the correlation was then used to calculate the efficiency of the primer as:

$$E = 10^{1/Slope}$$

Where:
E = Primer Efficiency
Slope = Gradient of line when Ct plotted against Log10(dilution)

Once the efficiency of primers had been calculated, PCR was run on the experimental samples. Similar to the method for primer validation, a 96 well plate was prepared by pipetting 4 µL of each cDNA sample in duplicate, along with 3 wells of 4 µL RNase free water (NTC) and each well then filled with 6 µL of the relevant stock gene mix. The plates were then sealed, briefly centrifuged at ~2000g for 10 seconds and then placed into the 7500 Fast Real-Time PCR system *(Applied Biosystems)*. SYBR was set as the reporter, and the thermal profile set to run at 95°C for 10 minutes, followed by 40 cycles of 95°C for 10 seconds and 60°C for 30 seconds. For any sample where duplicates (i.e. technical repeats) showed differences of more than 1 Ct, RT-qPCR was repeated to verify the true value by eliminating pipetting or contamination error.

Ct values were extracted as described previously and used to calculate the gene expression normalised to the reference gene L30 and efficiency corrected ($E^{\Delta Ct}$). The expression of strained composites were also calculated as efficiency corrected fold changes normalised to L30 ($E^{\Delta\Delta Ct}$) using the Pfaffl analysis Method (Pfaffl, 2001):

$$E^{\Delta Ct} = E^{Ct_{Target} - Ct_{Reference}}$$

Where:
Ct_{Target} = Ct of target gene
$Ct_{Reference}$ = Ct of reference gene
E = Primer efficiency of target gene

$$E^{\Delta\Delta Ct} = \frac{E_{Target}{}^{\Delta Ct_{Target}}}{E_{Reference}{}^{\Delta Ct_{Reference}}}$$

Where:
ΔCt_{Target} = $\mathrm{Ct_{Control}} - \mathrm{Ct_{Sample}}$ of target gene
$\Delta Ct_{Reference}$ = $\mathrm{Ct_{Control}} - \mathrm{Ct_{Sample}}$ of reference gene
E_{Target} = Primer efficiency of target gene
$E_{Reference}$ = Primer efficiency of reference gene

Statistical analysis was performed using student *T*-Tests for comparing basal gene expression, while one way analysis of variance (one way ANOVA) was used for comparison of the different shear-tension ratios and followed by Tukey's Honest Significant Difference (HSD) pot-hoc test if differences were found through the one way ANOVA, with p values < 0.05 considered significant.

Table 32: List of all custom primers used for gene expression analysis. Primers ordered from Life Technologies.

Gene	Primer Sequence		Amplicon Size (bp)	Location (bp)
ADAMTS-5	**Forward**	5'-AGCTGTGCGGTGATTGAAGA-3'	54	1189-1243
	Reverse	5'-GCCAAGCAGATGTCCAATTTC-3'		
COL1	**Forward**	5'-GCCTGGTCAGAGAGGAGAAAGA-3'	50	3004-3054
	Reverse	5'-CCTTGTTTGCCGGGTTCAC-3'		
COL-11A1	**Forward**	5'-GTCTACCAGGTGACAAGGGTC-3'	170	2166-2336
	Reverse	5'-CGGCTATACCAGGCTGTCC-3'		
COL-3	**Forward**	5'-CTGACATTTAGACATGATGAG-3'	105	63-168
	Reverse	5'-ACTGACCGAGATGGGAGCAT -3'		
IL6	**Forward**	5'-CCAGACAAAACCGAAGCTCTCA-3'	56	190-246
	Reverse	5'-CTCATCATTCTTCTCACATATCTCCTTT-3'		
ITGA-2	**Forward**	5'-TGTGGTGCAGAAGACACCTC-3'	130	1215-1345
	Reverse	5'-GGAGCACCAGCAACAAAGTG-3'		
ITGA-3	**Forward**	5'-CGGTTTTCCGTGGACATTGA-3'	153	3246-3399
	Reverse	5'-CTTCATACAGGGCGCGAGT-3'		
L30	**Forward**	5'-GGCAGGCGGATTCTTTACC-3'	62	113-175
	Reverse	5'-TAGAGGCTTTCTCTCGGACAGATG-3'		
MMP-1	**Forward**	5'-GCTTTCTCAGGACGACATTGATG-3'	51	752-803
	Reverse	5'-CGACTGGCTGAGTGGGATTT-3'		
MMP-13	**Forward**	5'-TCCTGGCTGGCTTCCTCTT-3'	88	14-102
	Reverse	5'-GTAGCTCTCTGCAAACTGGAAGTCT-3'		
MMP-2	**Forward**	5'-TACGACCGCGACAAGAAGTAT-3'	89	1151-1240
	Reverse	5'-TTGTTGCCCAGGAAAGTGAAG-3'		
MMP-3	**Forward**	5'-TCCGCCTTTCTCAGGATGAT-3'	62	801-863
	Reverse	5'-GGCACCACAGGGTCATTAGG-3'		
SCX	**Forward**	5'-GAGAAAGTTGGTGAGTGTTGC-3'	82	1839436-1839518
	Reverse	5'-GGGTGGTTTGGAGGTGG-3'		
TIMP-3	**Forward**	5'-AGTCTCTGTGGCCTTAAGCTTGA-3'	88	549-637
	Reverse	5'-TGGTCCCACCTCTCTACAAAGTTAC-3'		
TNMD	**Forward**	5'-TCTGGCGTGACGGGTCTT-3'	54	637-691
	Reverse	5'-AAAAAAGGCATTGAACAAAACGA-3'		

5.4 Results and Discussion

5.4.1 Basal Gene Expression of RGD and DGEA Composites

The basal gene expression of pre-seeded primary bovine tenocytes (i.e. tenocytes after isolation from tendon tissue) was first compared with the gene expression levels of tenocytes in non-strained composites made of PEG-RGD and PEG-DGEA fibres. Composites with RGD and DGEA peptides were additionally separated by substrate stiffness (i.e. those with 20% or 60% PEG fibres) to assess the effect of substrate stiffness on expression level.

The pre-seeded tenocytes were found to have similar basal gene expression levels amongst the biological repeats. Comparing non-strained composites showed that substrate stiffness did not any effect any of the genes investigated, except COL-3 in composites with PEG-DGEA fibres. Accordingly, fibre stiffness was removed from the comparisons, and all non-strained composites with PEG-DGEA fibres and all with PEG-RGD fibres were averaged to focus specifically on the differences caused by peptide type. Indeed, the results from this comparison showed that the type of cell attachment peptide affected tenocyte gene expression differently, with DGEA resulting in increased mechano-sensitivity.

The results are presented in groups of genes, relating to: 1. Collagen synthesis, 2. Matrix proteinases and inhibitors, and finally 3. Other characteristic genes. This is then followed by a discussion of the results.

Collagens

From the 3 collagen genes analysed (Figure 83), COL-1 was found to be the most highly expressed. After encapsulation, the expression of COL-1 by cells decreased significantly in PEG-DGEA composites, while tenocytes in PEG-RGD composites showed a smaller drop (P=0.12). COL-11A1 gene expression was seen to be the same for pre-seeded cells and PEG-RGD composite cells, however the expression level was seen to increase significantly in PEG-DGEA composite cells. Although not statistically significant, COL-3 gene expression by tenocytes was seen to increase notably after encapsulation for both PEG-RGD and PEG-DGEA composites (P=0.07 and P=0.11, respectively). When composites were separated by substrate stiffness, the only gene seen to be substrate stiffness dependent was COL-3: PEG-DGEA composite cells showed a significant decrease (6 fold) in COL-3 gene expression when cells were seeded on stiff (60% PEG) fibres compared to less stiff (20% PEG) fibres (P<0.05).

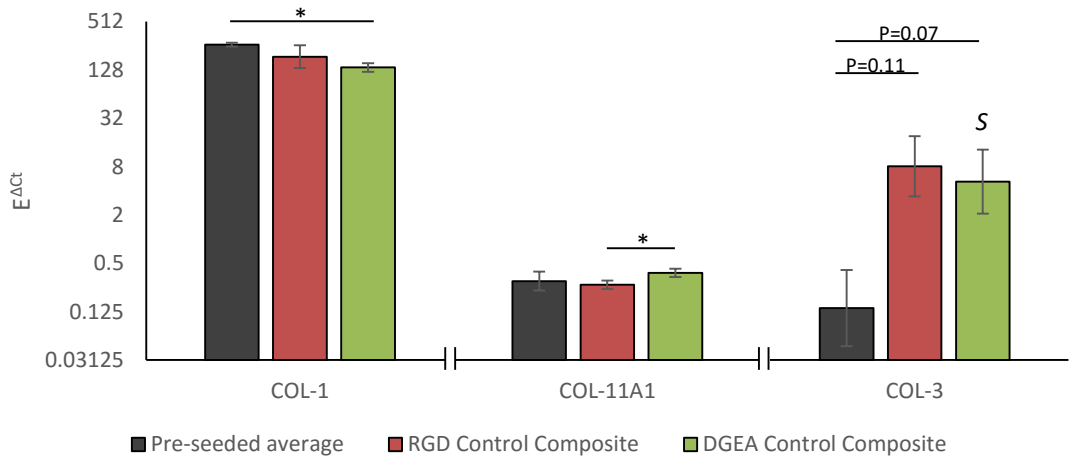

Figure 83: Average collagen gene expression levels of pre-seeded primary bovine tenocytes, cells in non-strained PEG-RGD composites (both stiffness types) and cells in PEG-DGEA composites (both stiffness types) (n=3). Each gene was normalised to the reference gene L30 and corrected for primer efficiency ($E^{\Delta Ct}$). Error bars indicate standard deviation between biological repeats. PEG-DGEA composite cells were found to have significantly less COL-1 gene expression compared to pre-seeded tenocytes and significantly more COL-11A1 gene expression than cells in PEG-RGD composites. PEG-DGEA composite cells also exhibited downregulation of COL-3 gene expression on stiffer substrates, contributing to the large standard deviation. * = P<0.05, *S* = P<0.05 for substrate stiffness comparison.

Matrix Proteinases and Inhibitors

A selection of proteinases, ADAMTS-5, MMP-1, MMP-2, MMP-3 and MMP-13, were analysed at the gene expression level along with the inhibitor TIMP-3 (Figure 84). The response of these genes after encapsulation and to different cell attachment peptides is notably more pronounced than those seen with collagens. Pre-seeded tenocytes exhibited significantly more ADAMTS-5 and MMP-3 than tenocytes in both PEG-RGD and PEG-DGEA composites, and were also found to have significantly lower MMP-1, MMP-13, MMP-2 and TIMP-3 gene expression levels compared to tenocytes in PEG-RGD composites. PEG-DGEA composite cells showed significantly less MMP-1, MMP-2 and TIMP-3 gene expression than cells in PEG-RGD composites, in each instance, data showing a similar response in pre-seeded tenocytes and DGEA composite cells, with expression levels only increasing when cells attached to RGD. No substrate dependent changes were observed in any of these genes.

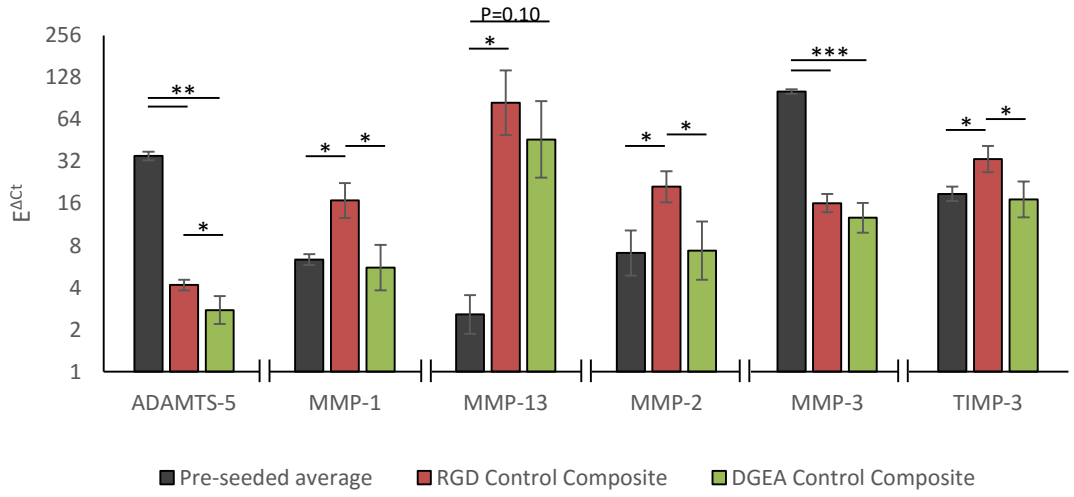

Figure 84: Average gene expression levels of matrix proteinases and their inhibitor comparing pre-seeded primary bovine tenocytes, cells in non-strained PEG-RGD (both stiffness types) and cells in PEG-DGEA composites (both stiffness types) (n=3). Each gene was normalised to the reference gene L30 and corrected for primer efficiency ($E^{\Delta Ct}$). Error bars indicate standard deviation between biological repeats. PEG-RGD composites exhibited more differences from pre-seeded tenocytes than PEG-DGEA composites. This was particularly evident with MMP-1, MMP-2 and TIMP-3 where the gene expression is similar for both pre-seeded tenocytes and PEG-DGEA composites, but significantly higher in PEG-RGD composites. * = P<0.01, ** = P<0.01, *** = P<0.001.

Other Characteristic Genes

Other characteristic genes analysed include the inflammatory cytokine inteleukin-6 (IL-6), tenocyte associated phenotypic markers scleraxis (SCX) and tenomodulin (TNMD), and cell attachment associated genes integrin-α2 (ITGA-2) and integrin-α3 (ITGA-3) (Figure 85). Pre-seeded tenocytes showed significantly higher IL-6 gene expression compared to cells in both PEG-RGD and PEG-DGEA composites, while PEG-RGD composite cells showed significantly higher IL-6 gene expression than PEG-DGEA composite cells. ITGA-2 was seen to increase significantly in PEG-DGEA composite cells compared to pre-seeded cells, while PEG-RGD composite cells showed an even larger increase. ITGA-3 was seen to increase for cells in both PEG-DGEA and PEG-RGD composites, but was significant only in the latter (P=0.12 for PEG-DGEA composites). SCX was seen to significantly decrease in PEG-RGD composite cells compared to pre-seeded cells whilst TNMD significantly decreased in both PEG-RGD and PEG-DGEA composite cells. Once again, no substrate stiffness dependent gene expression changes were observed in any of these genes.

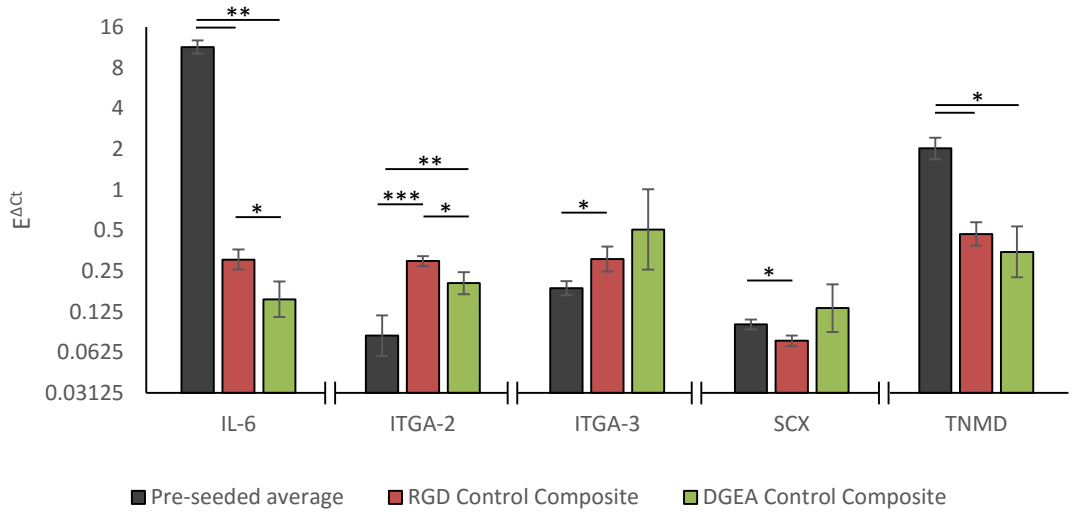

Figure 85: Average gene expression levels of other characteristic genes in pre-seeded primary bovine tenocytes, cells in non-strained PEG-RGD (both stiffness types) and cells in PEG-DGEA composites (both stiffness types) (n=3). Each gene was normalised to the reference gene L30 and corrected for primer efficiency ($E^{\Delta Ct}$). Error bars indicate standard deviation between biological repeats. IL-6 gene expression was significantly less in PEG-DGEA composite, while ITGA-2 differed for both composite types. PEG-RGD composite cells were also found to have lower SCX gene expression. * = P<0.01, ** = P<0.01, *** = P<0.001.

Table 33: a) Summary of gene expression fold changes observed in RGD and DGEA composite cells compared to pre-seeded tenocytes (n=3). b) Summary of gene expression fold changes of cells in RGD composites compared to cells in DGEA composites (n=3). RGD composite cells showed higher gene expression of many genes, while DGEA composites tended to show expression closer to that in pre-seeded tenocytes. * = P<0.05, ** = P<0.01 and *** = P<0.001.

a) Compared to pre-seeded tenocytes:

Gene	RGD Composites	DGEA Composites
COL-1		*
COL-11A1		
COL-3		
ADAMTS-5	**	**
MMP-1	*	
MMP-13	*	
MMP-2	*	
MMP-3	***	***
TIMP-3	*	
IL-6	**	*
ITGA-2	***	**
ITGA-3	*	
SCLERAXIS	*	
TNMD	*	*

b) RGD compared to DGEA Composites:

Gene	RGD Composites
COL-1	
COL-11A1	*
COL-3	
ADAMTS-5	*
MMP-1	*
MMP-13	
MMP-2	*
MMP-3	
TIMP-3	*
IL-6	*
ITGA-2	*
ITGA-3	
SCLERAXIS	
TNMD	

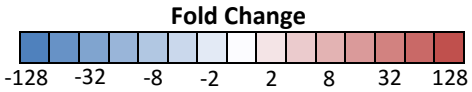

5.4.2 Discussion – Cell attachment peptide effect on basal gene expression

The comparison of basal gene expression levels in pre-seeded primary bovine tenocytes with tenocytes in non-strained composites made of PEG-RGD and PEG-DGEA fibres revealed the importance of attachment peptide on cellular behaviour, with a number of differences in cell response once encapsulated into composites with either PEG-RGD or PEG-DGEA fibres. The significant differences between the two types of composites are summarised in Table 33.

Pre-seeded tenocytes showed more changes once encapsulated in RGD composites than in DGEA composites with MMP-1, MMP-2, MMP-13, TIMP-3 and ITGA-3 gene expression all

increased, and SCX gene expression decreased specifically, while tenocytes in DGEA composites showed a basal expression profile closer to that of the pre-seeded primary bovine tenocytes.

It should be noted that the gene expression profile of pre-seeded primary bovine tenocytes would show some differences compared to tenocytes in tendon tissue due to the method used to collect the cells and therefore it is not presented here as a standalone profile. Tenocytes were isolated by digesting the tendons with a dispase/collagenase solution. These enzymes, similar to trypsin described in Chapter 4, would instigate changes in gene expression during tissue digestion. However, the gene expression profile of these cells are still suitable for use as a reference point for comparison of changes once tenocytes were encapsulated into composites. The gene expression change due to dispase/collagenase exposure could explain why some genes in pre-seeded tenocytes showed significant differences in DGEA composites (i.e. collagen like composites), while other genes such as MMP-1, MMP-2 and SCX remained similar. Additionally, pre-seeded tenocytes showed little variability between biological repeats (indicated by small standard deviation bars), indicating little difference between the cell sources used and consistent expression levels between biological repeats.

A direct comparison of cell response in non-strained RGD and non-strained DGEA composites provided further evidence for attachment peptides altering basal gene expression profiles. Tenocytes in RGD composites showed significantly higher ADAMTS-5, MMP-1, MMP-2, TIMP-3, IL-6 and ITGA-2 gene expression and significantly lower COL-11A1 gene expression than tenocytes in DGEA composites. These differences are interesting, as ADAMTS-5, MMP-1 and MMP-2 are all functionally related to matrix degradation, while IL-6 is associated with inflammation. This indicates that PEG-RGD fibres potentially evoked an inflammatory and catabolic response in tenocytes. Furthermore, IL-6 has also been associated with increased collagen synthesis in human tendons (Andersen et al., 2011). So, although an increase in collagen synthesis is not observed, the cells could be in the process of initiating collagen

synthesis, suggesting tenocytes could be targeting remodelling of the matrix rather than just matrix degradation. The integrin predominantly used to bind to RGD is α5β1 (Hynes, 1992; Ruoslahti, 1996) while α2β1 is primarily adapted for DGEA binding (Knight et al., 2000; Luzak et al., 2003; Mizuno et al., 2000). As RGD does not require an α2 integrin subunit for recognition, it is possible the higher expression of ITGA-2 in RGD composites was a response by tenocytes to increase the availability of integrin α2β1, a collagen type I receptor (Heino, 2000; Jokinen et al., 2004), which in turn would aid in sensing collagen type I. Increased cell surface integrin α2β1 has also been previously found to correlate with MMP-1 expression (Langholz et al., 1995; Riikonen et al., 1995), suggesting that integrin α2β1 functions as a feedback mechanism for collagen type I turnover. Collectively, these attributes suggest that tenocytes perceived the local environment differently when attached to RGD due to the different integrins involved, resulting in a gene expression profile biased towards matrix remodelling through an upregulation of matrix degradation, collagen synthesis promotion and increased sensitivity to collagen type I.

Comparison of cell response in RGD and DGEA composites grouped by fibre stiffness showed that the only gene to exhibit stiffness dependent changes was COL-3, and that the stiffness response was only evident for DGEA composite cells. This is interesting as, although RGD composite cells saw more differences compared to pre-seeded tenocytes, the replacement of RGD with DGEA may have increased the sensitivity of tenocytes to the substrate stiffness. The idea of increased mechano-sensitivity in cells attached to different peptides is further explored in the next section, where the results showing the effect of shear-tension ratio on gene expression using both RGD and DGEA composites is discussed.

5.4.3 Shear Tension Ratio Effect on Tenocyte Gene Expression

Composites made from PEG-RGD and PEG-DGEA fibres and seeded with primary bovine tenocytes were strained at 5% strained for 24 hours (86400 cycles) at 1Hz to investigate the effect of shear-tension ratio on gene expression. The previous section showed the substrate stiffness did not affect bovine tenocyte gene expression except for COL-3 in the DGEA composites. This led to the possibility of comparing the effect of shear-tension ratios on other genes without interrelated effects of substrate stiffness, while bias from stiffness effects was taken into consideration specifically for COL-3 gene expression. Results were consequently analysed as strained composites relative to non-strained control composites, using the efficiency corrected Pfaffl analysis method (described at the end of section 5.3). The results are presented in subheadings as before, followed by a discussion of the results.

Collagens

All composites made from PEG-RGD fibres showed downregulation of COL-1 with loading (~2 fold on average), while highly variable changes were observed with COL-11A1 and COL-3 gene expression (Figure 86a). No genes were found to be regulated by shear-tension ratios in RGD composites. Conversely, in composites made from PEG-DGEA fibres, significant differences were seen in COL-3 gene expression between the composite conditions (Figure 86b).

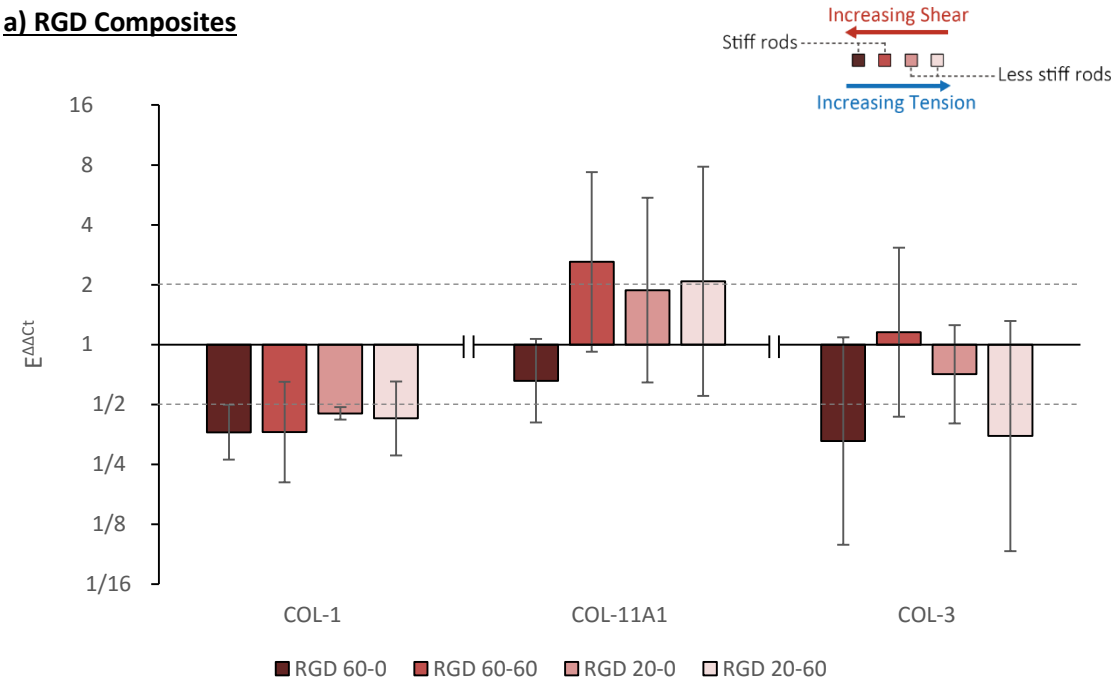

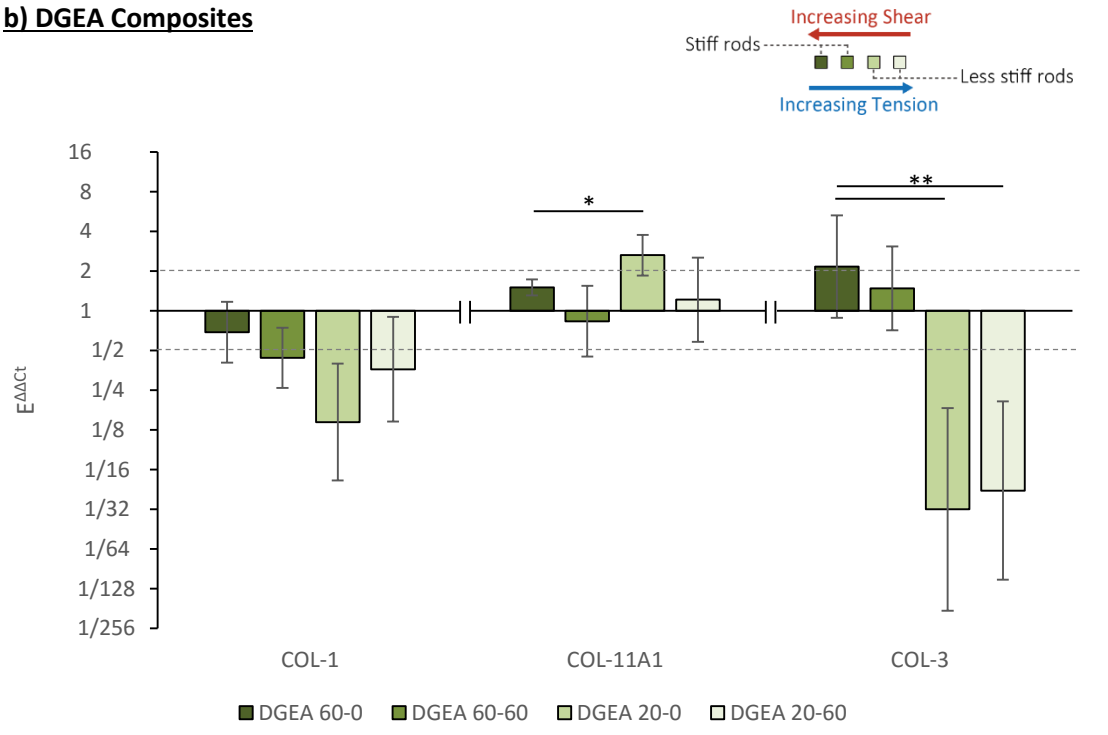

Figure 86: Average COL-1, COL-11A1 and COL-3 gene expression in strained RGD composites (a) and DGEA composites (b), expressed as fold changes relative to the non-strained controls and normalised to reference gene L30 using the Pfaffl analysis method ($E^{\Delta\Delta Ct}$) (n=3). Composite types labelled as "peptide-XX-YY", where "peptide" is either DGEA or RGD, "XX" indicates the fibre type and "YY" indicates the soak time. Error bars indicate standard deviation between biological repeats. DGEA composites exhibited changes between composites types in COL-3 gene expression, while RGD composites showed no such changes. * = P<0.01, ** = P<0.01, *** = P<0.001.

Matrix Proteinases and Inhibitors

Gene expression changes in RGD composite cells after loading resulted in high variability in ADAMTS-5, MMP-1 and MMP-13 as evident from the large error bars (Figure 87a). MMP-3 gene expression was found to generally increase with loading (~4 fold increase on average) in RGD composite cells, while TIMP-3 was generally downregulated. Only one gene showed a response to shear-tension ratio, with high shear downregulating TIMP-3 gene expression by up to ~4 fold.

There was notably less variability in gene expression overall in PEG-DGEA composite cells (Figure 87b). PEG-DGEA composite cells exhibited downregulation of MMP-13 by 4-16 fold after loading and showed significant shear mediated changes in MMP-3 gene expression, which was upregulated by ~4 fold in the high shear condition. Although not significant, notable shear mediated changes were also observed in MMP-2 gene expression, with low shear downregulating gene expression (P=0.07).

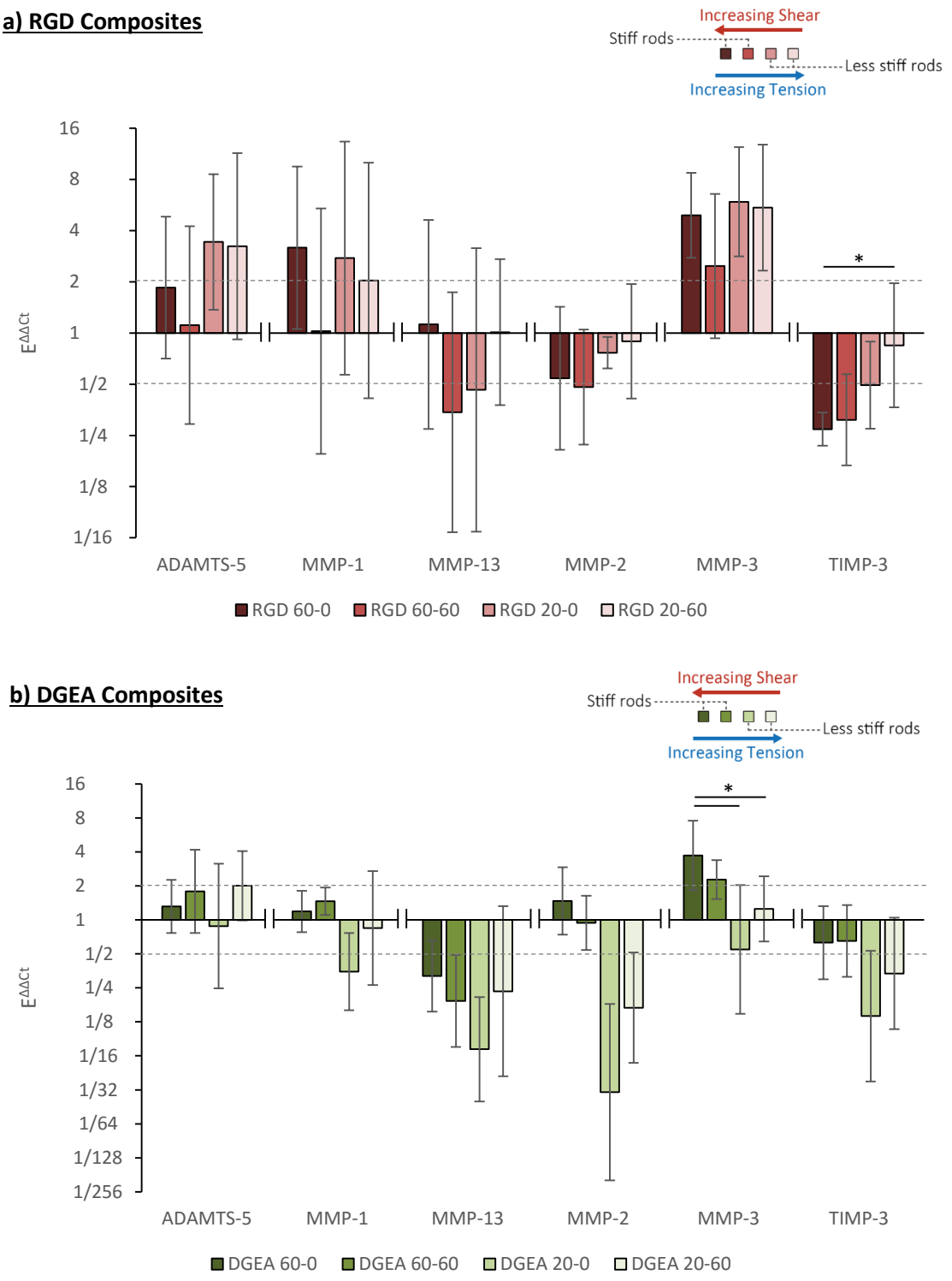

Figure 87: Average gene expression of matrix proteinases and their inhibitor in strained RGD composites (a) and DGEA composites (b), expressed as fold changes relative to the non-strained controls and normalised to reference gene L30 using the Pfaffl analysis method ($E^{\Delta\Delta Ct}$) (n=3). Composite types labelled as "peptide-XX-YY", where "peptide" is either DGEA or RGD, "XX" indicates the fibre type and "YY" indicates the soak time. Error bars indicate standard deviation between biological repeats. TIMP-3 was found to be regulated by shear in RGD composites while MMP-3 was regulated by shear in DGEA composites. Higher gene expression variability was also observed in RGD composites compared to DGEA composites. * = P<0.01, ** = P<0.01, *** = P<0.001.

Characteristic Genes

Loading upregulated IL-6 gene expression in all RGD composite types by up to 16 fold (Figure 88a). No significant shear-tension regulated changes were observed in RGD composite cells, however, a trend for upregulation of ITGA-3 with decreasing shear (P=0.24 between the high and low shear conditions) was noted, such that there was a ~9 fold increase at the lowest shear condition relative to the highest.

All DGEA composite types showed an upregulation of IL-6 gene expression after loading. Additionally, IL-6 was found to be significantly upregulated with shear in PEG-DGEA composite cells, with the high shear condition resulting in a ~16 fold upregulation relative to the non-strained controls (Figure 88b). SCX gene expression was also found to be downregulated by shear, increasing by ~3 fold in the low shear condition and decreasing by ~5 fold in the high shear condition.

a) RGD Composites

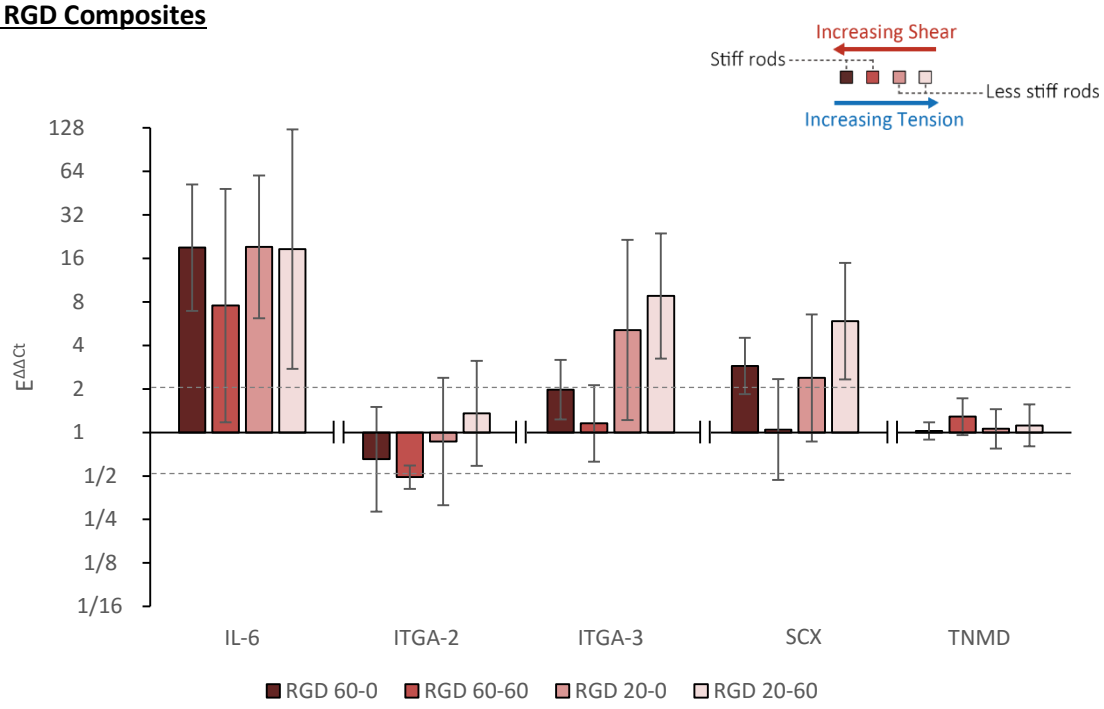

b) DGEA Composites

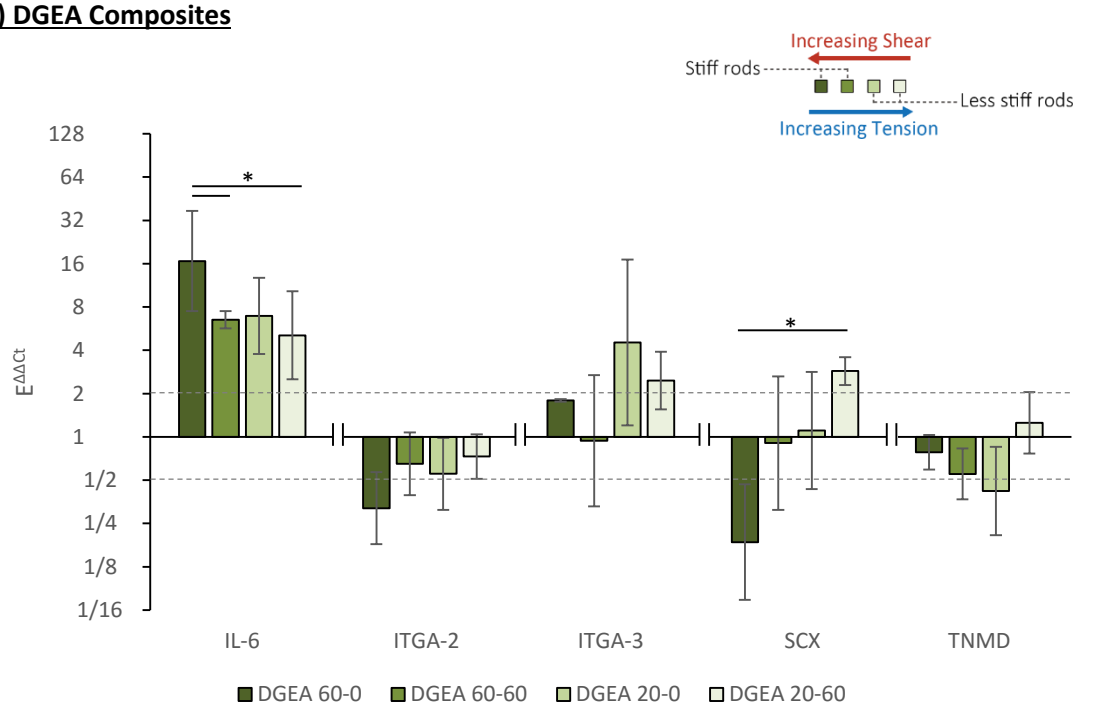

Figure 88: Average gene expression of other characteristic genes in strained RGD composites (a) and DGEA composites (b), expressed as fold changes relative to the non-strained controls and normalised to reference gene L30 using the Pfaffl analysis method ($E^{\Delta\Delta Ct}$) (n=3). Composite types labelled as "peptide-XX-YY", where "peptide" is either DGEA or RGD, "XX" indicates the fibre type and "YY" indicates the soak time. Error bars indicate standard deviation between biological repeats. Shear regulated changes were observed in DGEA composites (IL-6 and SCX) while none were observed in RGD composites. * = P<0.01, ** = P<0.01, *** = P<0.001.

5.4.4 Discussion – RGD and DGEA effect on shear-tension ratio sensitivity

Shear-tension ratio mediated gene expression changes were investigated in primary bovine tenocytes seeded on PEG-RGD and PEG-DGEA fibres. Tenocytes in composites made from PEG-RGD fibres exhibited shear regulated changes in TIMP-3, while tenocytes in composites made from PEG-DGEA fibres showed regulation of COL-3, MMP-3, IL-6 and SCX with shear:

Shear regulated genes in DGEA Composites

- COL-3 ↑
- MMP-3 ↑
- IL-6 ↑
- SCX ↓

Shear regulated genes in RGD composites

- TIMP-3 ↓

↑ = Upregulated with shear
↓ = Downregulated with shear

The increased number of shear regulated genes by cells in DGEA composites compared to cells in RGD composites suggests that DGEA bound tenocytes possessed increased sensitivity to the shear environment. Moreover, as different genes were regulated by shear in RGD and DGEA composites, it is apparent that tenocytes can react to the same stimuli differently depending on their attachment peptide. Collagen type III is a fibrillar collagen which can form heterotypic fibrils with collagen type I (Ricard-Blum, 2011), while MMP-3, although not involved in collagen type I degradation, is able to process collagen type III (Visse and Nagase, 2003). In addition to pro- and anti- inflammatory pathways, IL-6 has been seen to increase collagen type I synthesis (Andersen et al., 2011). Taken together the simultaneous upregulation of COL-3, MMP-3 and IL-6 with shear by tenocytes in DGEA composites, could indicate a response potentially targeted towards remodelling collagen type III within the matrix. Conversely, tenocytes in RGD composites only responded to increasing shear with the downregulation of TIMP-3, a wide acting proteinase inhibitor. This possibly suggests that tenocytes under these conditions were promoting a larger and wider range of catabolic activity through less enzyme inhibition when exposed to increasing magnitudes of shear in RGD composite cells.

Integrins have been seen to exhibit unique functions. For example, previous studies have found integrin α2β1 to induce MMP-1 gene expression once cells are seeded onto collagen type I matrices, and also show some involvement in the regulation of collagen type I gene expression (Grzesiak and Bouvet, 2007; Langholz et al., 1995; Riikonen et al., 1995). By contrast integrin α5β1, recognising RGD, has been associated with initiating fibronectin fibril assembly (Danen et al., 2002; Sechler et al., 1997; Sechler et al., 1996; Takahashi et al., 2007). Cryptic RGD motifs are present in collagen type I, i.e. sequences not accessible by cells in the native triple helical structure, which can be exposed through denaturing or enzyme digestion (Gullberg et al., 1992; Ricard-Blum, 2011). Indeed, studies exploring this trait have found that cells alter their behaviour when attached to partially-denatured collagen type I compared to native collagen type I (Taubenberger et al., 2010). Therefore, as the functions of integrins differ, it is not completely surprising the translation of shear-tension by integrins into cellular cues also differs

The differences in the mechanisms by which RGD and DGEA (and the integrins involved in their binding) translate mechanical cues was not investigated and is out of the scope of this study, particularly due to the variety of possible pathways which range from integrin-actin cytoskeleton links to integrin regulation of ion channels (Arcangeli and Becchetti, 2006). However, it is interesting to note that the force required to unbind fibronectin (i.e. the fibronectin and integrin α5β1 interaction) has been reported to range from 69-93 pN, while that of collagen type I (i.e. the collagen type I and integrin α2β1 interaction) is 160 pN (Roca-Cusachs et al., 2012), suggesting that collagen integrins are more specialised for force transmission as they can withstand higher loads.

Characterisation of tendinopathic tissue has shown increased collagen type III (Bank et al., 1999; Corps et al., 2012; Riley et al., 1994b). As previously described in Chapter 1 and Chapter 4, tendinopathies are thought to be instigated by changes in cell-matrix interactions triggered by microdamage after tendon overuse. Matrix microdamage would result in increased fibre shear,

consequently increasing the magnitude of cellular shear. The results obtained with DGEA composites is consistent with this concept as COL-3 gene expression was seen to be downregulated with less shear, lending weight to the hypothesis that shear is an important aspect in tendinopathy development.

It should be noted that when looking at non-strained controls, COL-3 gene expression was found to be significantly downregulated by cells on stiffer PEG-DGEA fibres (Figure 83). However, in strained PEG-DGEA composites, COL-3 was seen to be downregulated by cells on less stiff PEG-DGEA fibres, a trend opposite to the non-strained controls (Figure 86b). Consequently, this stiffness dependent trend also contributes to the appearance of shear highly upregulating COL-3 gene expression in strained PEG-DGEA composites. Although non-strained composites of the same fibre type, stiffness and soak time were used as controls for each strained composite type, allowing the effect of substrate stiffness to be eliminated to an extent, it is difficult to separate the effects of the shear-tension ratio on COL-3 gene expression to those from fibre stiffness. Therefore the results for COL-3 gene expression in Figure 86b represents a combination of both fibre stiffness and shear-tension ratio effects.

A limitation of this study was the use of free swelling non-strained controls rather than composites held taut in the rig under a small static strain, essentially creating a stress deprived condition. Stress deprivation has been seen to alter matrix related gene expression in tenocytes (Leigh et al., 2008), hence it is possible the control condition used in the current study may contain such changes. Additionally, it was observed that composites would warp and curl slightly once made and stored in media. Tenocytes are known to exert contractive forces onto their substrates (Tilley et al., 2012; Torres et al., 2000), thus it is possible such forces contributed towards composite warping, altering the stress experienced by cells in the process and potentially changing the basal gene expression of control composites. However, care was taken

to position composites flat onto the base of the 6 well plates, helping to keep composites flat during the experiment and limiting problems arising from using a non-confined condition.

5.5 Conclusion

This study successfully used two different attachment peptides, RGD and DGEA, to compare shear-tension mediated changes in primary bovine tenocytes. The main integrin involved in DGEA binding is α2β1 while the integrins associated with RGD attachment include α5β1, αVβ3 and αIIbβ3, thus the fundamental difference between the use of RGD and DGEA was the integrins involved in ligand binding. Consequently, the findings of this study emphasises the importance of integrins in the role of mechanotransduction as both peptides resulted in different responses to shear-tension. Specifically, the results suggest integrins involved in collagen type I binding induce functionally different responses in tenocytes to those not involved in collagen type I binding when sensing mechanical stimuli comprised of shear and tension. This information is critical in future studies investigating tenocyte behaviour and tissue engineering approaches, as physiological integrin binding may be key in maintaining normal tenocyte pathways.

Chapter 6: Overall Conclusion and Future Work

Research into the effects of shear on cellular metabolism and its involvement in mechanotransduction pathways have been limited, due to the lack of appropriate systems which create controllable, physiologically representative *in vitro* strain environments. The fibre composite system detailed in Chapter 2 was developed to meet this need, creating a platform to provide physiologically representative cellular shear and tension ratios, in addition to the ability to control the amount of tension and shear. The precise and reproducible nature of the manufactured composites allows the investigation of shear and tension ratio effects in a reproducible manner. The fibre composite system also possesses a number of beneficial aspects, including optical transparency to allow imaging and monitoring of cells encapsulated within, and customisable attachment peptides to alter the method of attachment by cells. Furthermore, the system is based on PEG chemistry, which has been used extensively in research and allows modifications such as enzyme degradable or photodegradable cross-links (Kloxin et al., 2010; Liu et al., 2010; Zhu, 2010), providing extra versatility to the system for future applications.

Using the fibre composite system with PEG-RGD fibres, it was shown that healthy and tendinopathic human tenocytes respond to shear differently, with tendinopathic cells exhibiting more mechano-sensitivity. The relationship between applied shear and cell response was also found to be complex and not a simple linear relationship, with high and low shear-tension ratios altering gene expression levels differently. The shear-tension ratios tested ranged from approximately 40% shear and 60% tension to 75% shear and 25% tension. This range of shear-tension ratios is small, with 5% applied strain at a whole composite level translating to

1.5% - 3% local strain, specifically along each fibre. However, even with these comparatively small changes in local mechanisms, gene expression regulation is still observed, suggesting tenocytes are extremely sensitive to this mechanical cue.

Differences between healthy and tendinopathic human tenocytes was also found in the basal gene expression level: ADAMTS-2, ADAMTS-4, ADAMTS-12, BGN, COL-12A1, COL-1A1, COL-3A1, COL-4A1, COL-5A1, COL-6A1, FN-1, and MMP-13 gene expression were all higher, and TNC, ACAN, ADAMTS-1, ADAMTS-6, COL-14A1, DCN, FMOD, IL-6, IL-8, MMP-3, PRG-4 and VCAN gene expression lower in tendinopathic tenocytes. This data supports the observations from the shear-tension ratio comparison, emphasising that differences were present between healthy and tendinopathic tenocytes. The fact that differences between tendinopathic and healthy tenocytes remained after *in vitro* culture and encapsulation into composites suggests that either cell behaviour is fundamentally changed during tendinopathy and tenocytes are slow to revert to normal, or that some individuals are genetically prone to tendinopathies with cells always showing a different profile. Basal gene expression differences were also found between the two tendinopathic tenocyte donors, with one showing significantly higher ACAN, COL1-A1, COL5-A1 and IL-1B gene expression and lower COL-14A1, MMP-13, MMP-3, PRG-4 and SCX gene expression than the other. This finding suggests the two donors may have had different states of tendinopathy, or even a different type of tendinopathy altogether.

Further experiments using bovine tenocytes in composites with PEG-DGEA and PEG-RGD fibres found the peptides used by tenocytes to attach to fibres dramatically affected cell behaviour. The peptide DGEA, a collagen mimetic peptide associated with integrin α2β1 binding, was found to increase mechano-sensitivity of bovine tenocytes and result in many genes being regulated by shear, compared to the RGD based fibronectin associated peptide which binds to integrin α5β1. RGD composite cells down regulated TIMP-3 gene expression in response to shear, while cells in DGEA composites upregulated COL-3, MMP-3 and IL-6 and downregulated SCX gene

expression in response to shear. These findings reveal that shear and tension are interpreted differently by tenocytes depending on the integrins employed in perceiving strains, emphasising the importance of integrins in mechanotransduction pathways and future applications where cell behaviour manipulation is required. This finding could also explain why many genes were not seen to be regulated by shear in the human tenocyte study (Chapter 4), as composites used in that study were made with RGD peptides.

Additionally, another factor which could contribute to differences between the human tenocyte and bovine tenocyte experiments (i.e. Chapter 4 and Chapter 5) is the method by which cells were isolated: human tenocytes were obtained via an explant outgrowth method whereas bovine tenocytes were obtained through enzymatic digestion. Enzymatic digestion extracts cells from the whole tendon tissue, whereas explant outgrowth is inherently more selective, favouring tenocytes closer to the perimeter of the explant, i.e. those more likely to migrate onto the tissue culture plastic. As tenocytes *in vivo* reside on collagen fibres and between fascicles in the IFM (Clegg et al., 2007; Richardson et al., 2007; Spiesz et al., 2015; Thorpe et al., 2015a), and populations of tendon progenitor stem cells (TSCs) reported to exist (Bi et al., 2007; de Mos et al., 2007; Zhang and Wang, 2010a; Zhang and Wang, 2013), possibly localised in the IFM, the two isolation methods would result in cell populations with different characteristics. This population difference could potentially result in different shear responses, as cell function and local micro-environment *in vivo* would differ. Indeed, cell populations extracted through the two different methods have shown differences in studies with periodontal ligament cells (Tanaka et al., 2011), keratinocytes (Orazizadeh et al., 2015), osteoblastic cells (Declercq et al., 2004) and dental pulp cells (Souza et al., 2010). Furthermore, MSCs derived from equine SDFT tendons have been shown to express higher COL-1A2 and SCX gene expression when isolated through tissue digestion rather than explant outgrowth (Gittel et al., 2013). Studies comparing cells from the two cell isolation methods have found that cells digested from tissue generally exhibit higher proliferation rates (Declercq et al., 2004; Souza et al., 2010; Tanaka et al., 2011).

This is in contrast to the logic that explant outgrowth would favour isolation of more active, migratory and proliferative cells. One possible reason for more proliferative activity in digested cells could be the exposure to catabolic enzymes and dramatic matrix changes, which are stressful events, potentially stimulating cells into an active state. Explant outgrown cells could also be influenced by the increased time spent on tissue culture plastic, potentially allowing more time for tenocytes to de-differentiate.

Overall, the results obtained from this work broadens the knowledge on tendinopathy, confirming tenocytes do indeed behave differently compared to normal healthy tenocytes. It also shows that tenocytes behave differently under non-physiological shear-tension ratios. As microdamage from tendon overuse alters this property, increasing the amount of shear experienced by tenocytes, the results strengthen the idea that microdamage is involved in tendinopathy development. Cell attachment peptides, and thus integrins, are implicated as important structures used by tenocytes to sense this environment and therefore needs to be investigated further to assess the extent of their involvement in tendinopathy development.

6.1 Future work

6.1.1 Response to shear over time and under different loading regimes

The studies conducted in this thesis involved applying 5% cyclic strain at 1Hz for 24 hours, after which gene expression was analysed. Different genes have been shown to peak at different time points in tenocytes, such as MMP-1 gene expression downregulation peaking at 48 hours and collagen type I upregulation peaking at 24 hours (Jones et al., 2013), and IL-6 content peaking immediately after exercise (Andersen et al., 2011; Langberg et al., 2002). Thus, although 24 hours was selected as a compromise to obtain a general overview of changes, many shear mediated changes may have been lost if they occurred before or after the 24 hours loading period.

The duration of loading could be another parameter to alter. The number of cycles used in this study was 86400 (total duration of 24 hours), and is more representative of extensive use rather than normal physiological use. Short loading periods of 100 cycles and intermittent loading have been shown to invoke gene expression changes (Huisman et al., 2014; Scott et al., 2011) and would be interesting to explore. Loading mimicking tendon overuse has also shown an increase in IL-6 levels (Spiesz et al., 2015). Therefore shorter loading periods to represent normal exercise could be used in addition to strains representing tendon overuse to investigate tenocyte behaviour under normal and overuse exercise.

The aspects analysed could also be expanded to include protein quantity and protein level expression changes. As described in section 1.4.2, MMPs and ADAMTS have many levels of regulation. Therefore, although gene expression may appear to stay constant, the activated protein levels of these components could be regulated. Similarly, genes which appear to be regulated by loading may show different trends in the protein levels due to post translation interactions. Investigating the protein levels via zymography would therefore provide a more holistic view of tenocyte response to loading.

Proposed Future Study:

- Use fibre composites made from PEG-DGEA fibres
- Loading composites for 15 and 30 minutes at 1Hz (i.e. 900 and 1800 cycles) to create shorter loading periods
- Using both 5% and 10% cyclic strain to simulate normal and excessive strains
- Analyse gene expression immediately (0 hours), 6 hours, 24 hour and 48 hours after loading.
- Analyse protein levels immediately (0 hours), 6 hours, 24 hours and 48 hours after loading.

6.1.2 Tendinopathic tenocyte gene expression changes

Results in Chapter 4 showed that tendinopathic tenocytes reported gene expression changes similar to those seen in tendinopathic tissue even after *in vitro* culture and encapsulation into composites, suggesting that the changes which occur during tendinopathy development are slow to revert. It would be interesting to monitor the gene expression of tendinopathic and healthy tenocytes during *in vitro* culture to characterise the difference between the two cells types and to monitor the time required for tendinopathic tenocytes to lose their tendinopathic profile.

Proposed Future Study:

- Obtain samples from one individual - one healthy and one tendinopathic tendon.
- Culture tenocytes obtained from healthy and tendinopathic tissue.
- Analyse tenocyte gene expression directly from the tissue, followed by analysis at every passage number throughout culture.

6.1.3 Characterising tenocyte deformation under load

The studies conducted were focused on the effects of shear and tension on tenocyte gene expression. Investigation of the mechanisms by which tenocytes sense these mechanical cues was limited to integrins.

The fibre composite system is optically transparent allowing cells within to be imaged, as shown in section 2.3 where cell attachment was characterised. Tenocytes could therefore be monitored during loading to characterise the extent of cellular deformation, providing information on how cells deform under the different shear-tension ratios. Characterisation can be achieved through staining the cytoskeleton and nucleus of tenocytes in composites and applying load whilst imaging the cells in real-time.

Proposed Future Study:

- Stain the cytoskeleton and nucleus of tenocytes within composites.
- Load composites up to 10% strain.
- Image cells via confocal microscopy at increments of 2% to characterise cellular deformation.

6.1.4 Integrin involvement in tendinopathy

Tendons are predominantly comprised of collagen type I and provide the matrix for cellular attachment. Tenocytes would consequently use integrin α2β1 to bind to this matrix. Cell attachment peptides RGD and DGEA, and the integrins involved in their binding, were shown to affect the gene expression of tenocytes, with tenocytes behaving differently when exposed to the same mechanical stimuli. Thus, integrins are key components in translating the shear-tension environment into cellular cues and important for tendon homeostasis.

Tendinopathy is seen to be accompanied by severe matrix degeneration. Cryptic RGD motifs are known to be present in collagen type I, which can be exposed to cells after its degradation or denaturation (Gullberg et al., 1992; Ricard-Blum, 2011). Therefore it is possible that tenocyte integrin binding is altered in tendinopathy due to the release of these cryptic motifs, contributing further to the severe degenerative process by altering mechano-sensitivity. Consequently, it would be interesting to analyse the integrins expressed by tenocytes in healthy and tendinopathic tendon samples, which can be achieved through confocal imaging after anti-body staining.

Proposed Future Study:

- Obtain and section healthy and tendinopathic tendon samples.
- Stain sections with anti-bodies for integrin α2β1 (collagen type I specific integrin), along with other collagen associated integrins (α1β1, α3β1, α10β1, α11β1 and αIIIβ3) and

integrins associated with RGD motifs (α2β1, α3β1, α4β1, α4β7, α5β1, α8β1, αvβ1, αvβ3, αvβ5, αvβ6, αvβ8 and αIIbβ3).

- Image sections via confocal microscopy to characterise differences in integrin deployment.
- Analyse gene expression levels post treatment to assess the effects of substances.

6.1.5 Further Improvements to the Fibre Composite System

One of the limitations of the fibre composite system was the diameter of the fibres. Fibres were made from moulds containing holes of 0.3 mm in diameter. Considering the diameter of collagen fibres is considerably less, found to be up to 30 µm in human tendons (Jarvinen et al., 2004), tenocytes in the composites are likely perceive the fibres as flat surfaces. This may affect the response of tenocytes as wrapping around fibres potentially changes cellular structures and stresses distributed to integrins.

To address this limitation, the method of creating fibres could be adapted to allow production of thinner fibres, more representative of collagen fibres. As the fibres within the composites are made using a PEG solution containing peptides, methods such as electrospinning could be used to achieve thin fibres. This would also require re-characterisation of the fibre composite as the micromechanics would inevitably change.

Proposed Future Study:

- Create pre-polymer PEG-Peptide solutions compatible with electrospinning.
- Determine electrospinning parameters to create fibres of desired diameters.
- Seed electrospun fibres with cells and encapsulate into composites.
- Characterise cell morphology, viability, gross mechanics and micro-micromechanics of composites.

Bibliography

Abair, T. D., Sundaramoorthy, M., Chen, D., Heino, J., Ivaska, J., Hudson, B. G., Sanders, C. R., Pozzi, A. & Zent, R. 2008. Cross-talk between integrins alpha1beta1 and alpha2beta1 in renal epithelial cells. *Exp Cell Res,* 314**,** 3593-604.

Abrahams, Y., Laguette, M. J., Prince, S. & Collins, M. 2013. Polymorphisms within the COL5A1 3'-UTR that alters mRNA structure and the MIR608 gene are associated with Achilles tendinopathy. *Ann Hum Genet,* 77**,** 204-14.

Abramoff, M. D. M., Paulo J.; Ram, Sunanda J. 2004. Image Processing with ImageJ. *Biophotonics International,* 11**,** 36-42.

Abreu, E. L., Leigh, D. & Derwin, K. A. 2008. Effect of altered mechanical load conditions on the structure and function of cultured tendon fascicles. *J Orthop Res,* 26**,** 364-73.

Abubacker, S., Ham, H. O., Messersmith, P. B. & Schmidt, T. A. 2013. Cartilage boundary lubricating ability of aldehyde modified proteoglycan 4 (PRG4-CHO). *Osteoarthritis Cartilage,* 21**,** 186-9.

Ackermann, P. W., Domeij-Arverud, E., Leclerc, P., Amoudrouz, P. & Nader, G. A. 2013. Anti-inflammatory cytokine profile in early human tendon repair. *Knee Surg Sports Traumatol Arthrosc,* 21**,** 1801-6.

Ahmadzadeh, H., Connizzo, B. K., Freedman, B. R., Soslowsky, L. J. & Shenoy, V. B. 2013. Determining the contribution of glycosaminoglycans to tendon mechanical properties with a modified shear-lag model. *J Biomech,* 46**,** 2497-503.

Aimes, R. T. & Quigley, J. P. 1995. Matrix metalloproteinase-2 is an interstitial collagenase. Inhibitor-free enzyme catalyzes the cleavage of collagen fibrils and soluble native type I collagen generating the specific 3/4- and 1/4-length fragments. *J Biol Chem,* 270**,** 5872-6.

Alfredson, H. & Lorentzon, R. 2002. Chronic tendon pain: no signs of chemical inflammation but high concentrations of the neurotransmitter glutamate. Implications for treatment? *Curr Drug Targets,* 3**,** 43-54.

Andarawis-Puri, N. & Flatow, E. L. 2011. Tendon fatigue in response to mechanical loading. *J Musculoskelet Neuronal Interact,* 11**,** 106-14.

Andersen, M. B., Pingel, J., Kjaer, M. & Langberg, H. 2011. Interleukin-6: a growth factor stimulating collagen synthesis in human tendon. *J Appl Physiol (1985),* 110**,** 1549-54.

Andersson, G., Forsgren, S., Scott, A., Gaida, J. E., Stjernfeldt, J. E., Lorentzon, R., Alfredson, H., Backman, C. & Danielson, P. 2011. Tenocyte hypercellularity and vascular proliferation in a rabbit model of tendinopathy: contralateral effects suggest the involvement of central neuronal mechanisms. *Br J Sports Med,* 45**,** 399-406.

Andia, I., Rubio-Azpeitia, E. & Maffulli, N. 2014. Hyperuricemic PRP in tendon cells. *Biomed Res Int,* 2014**,** 926481.

Applied Biosystems 2006. *User Bulletin: Applied Biosystems TaqMan® Low Density Array*.

Arcangeli, A. & Becchetti, A. 2006. Complex functional interaction between integrin receptors and ion channels. *Trends Cell Biol,* 16**,** 631-9.

Arnaout, M. A., Goodman, S. L. & Xiong, J. P. 2007. Structure and mechanics of integrin-based cell adhesion. *Curr Opin Cell Biol,* 19**,** 495-507.

Arnoczky, S. P., Lavagnino, M. & Egerbacher, M. 2007. The mechanobiological aetiopathogenesis of tendinopathy: is it the over-stimulation or the under-stimulation of tendon cells? *Int J Exp Pathol,* 88**,** 217-26.

Arnoczky, S. P., Lavagnino, M., Whallon, J. H. & Hoonjan, A. 2002a. In situ cell nucleus deformation in tendons under tensile load; a morphological analysis using confocal laser microscopy. *J Orthop Res,* 20**,** 29-35.

Arnoczky, S. P., Tian, T., Lavagnino, M., Gardner, K., Schuler, P. & Morse, P. 2002b. Activation of stress-activated protein kinases (SAPK) in tendon cells following cyclic strain: the effects of strain frequency, strain magnitude, and cytosolic calcium. *J Orthop Res,* 20**,** 947-52.

Askari, J. A., Buckley, P. A., Mould, A. P. & Humphries, M. J. 2009. Linking integrin conformation to function. *J Cell Sci,* 122**,** 165-70.

Atala, A., Lanza, R., Thomson, J. A. & Nerem, R. M. 2008. *Principles of regenerative medicine,* Amsterdam; Boston, Elsevier/Academic Press.

Backman, L. J., Fong, G., Andersson, G., Scott, A. & Danielson, P. 2011. Substance P is a mechanoresponsive, autocrine regulator of human tenocyte proliferation. *PLoS One,* 6**,** e27209.

Badylak, S. F., Vorp, D. A., Spievack, A. R., Simmons-Byrd, A., Hanke, J., Freytes, D. O., Thapa, A., Gilbert, T. W. & Nieponice, A. 2005. Esophageal reconstruction with ECM and muscle tissue in a dog model. *J Surg Res,* 128**,** 87-97.

Banes, A. J., Qi, J., Anderson, D. S., Maloney, M. & Sumanasinghe, R. (eds.) 2009. *Tech Report 100 - Tissue Train® Culture System: A Method for Culture and Mechanical Loading of Cells in a 3D Matrix*: Flexcell International Corporation.

Bank, R. A., TeKoppele, J. M., Oostingh, G., Hazleman, B. L. & Riley, G. P. 1999. Lysylhydroxylation and non-reducible crosslinking of human supraspinatus tendon collagen: changes with age and in chronic rotator cuff tendinitis. *Ann Rheum Dis,* 58**,** 35-41.

Baselt, D. R., Revel, J. P. & Baldeschwieler, J. D. 1993. Subfibrillar structure of type I collagen observed by atomic force microscopy. *Biophys J,* 65**,** 2644-55.

Bayer, M. L., Schjerling, P., Herchenhan, A., Zeltz, C., Heinemeier, K. M., Christensen, L., Krogsgaard, M., Gullberg, D. & Kjaer, M. 2014. Release of tensile strain on engineered human tendon tissue disturbs cell adhesions, changes matrix architecture, and induces an inflammatory phenotype. *PLoS One,* 9**,** e86078.

Benjamin, M., Kaiser, E. & Milz, S. 2008. Structure-function relationships in tendons: a review. *J Anat,* 212**,** 211-28.

Bernard-Beaubois, K., Hecquet, C., Houcine, O., Hayem, G. & Adolphe, M. 1997. Culture and characterization of juvenile rabbit tenocytes. *Cell Biol Toxicol,* 13**,** 103-13.

Bi, Y., Ehirchiou, D., Kilts, T. M., Inkson, C. A., Embree, M. C., Sonoyama, W., Li, L., Leet, A. I., Seo, B. M., Zhang, L., Shi, S. & Young, M. F. 2007. Identification of tendon stem/progenitor cells and the role of the extracellular matrix in their niche. *Nat Med,* 13**,** 1219-27.

Birch, H. L. 2007. Tendon matrix composition and turnover in relation to functional requirements. *Int J Exp Pathol,* 88**,** 241-8.

Birk, D. E., Nurminskaya, M. V. & Zycband, E. I. 1995. Collagen fibrillogenesis in situ: fibril segments undergo post-depositional modifications resulting in linear and lateral growth during matrix development. *Dev Dyn,* 202**,** 229-43.

Blewitt, M. J. & Willits, R. K. 2007. The effect of soluble peptide sequences on neurite extension on 2D collagen substrates and within 3D collagen gels. *Ann Biomed Eng,* 35**,** 2159-67.

Bulmus, V., Chan, Y., Nguyen, Q. & Tran, H. L. 2007. Synthesis and characterization of degradable p(HEMA) microgels: use of acid-labile crosslinkers. *Macromol Biosci,* 7**,** 446-55.

Busch, C., Girke, G., Kohl, B., Stoll, C., Lemke, M., Krasnici, S., Ertel, W., Silawal, S., John, T. & Schulze-Tanzil, G. 2013. Complement gene expression is regulated by pro-inflammatory cytokines and the anaphylatoxin C3a in human tenocytes. *Mol Immunol,* 53**,** 363-73.

Butler, D. L., Hunter, S. A., Chokalingam, K., Cordray, M. J., Shearn, J., Juncosa-Melvin, N., Nirmalanandhan, S. & Jain, A. 2009. Using functional tissue engineering and bioreactors to mechanically stimulate tissue-engineered constructs. *Tissue Eng Part A,* 15**,** 741-9.

Butler, G. S. & Overall, C. M. 2009. Updated biological roles for matrix metalloproteinases and new "intracellular" substrates revealed by degradomics. *Biochemistry,* 48**,** 10830-45.

Butler, G. S. O., C. M. 2000. Matrix metalloproteinase processing of signaling molecules to regulate inflammation. *Periodontology 2000,* 63.

Campbell, I. D. & Humphries, M. J. 2011. Integrin structure, activation, and interactions. *Cold Spring Harb Perspect Biol,* 3.

Canty, E. G. & Kadler, K. E. 2002. Collagen fibril biosynthesis in tendon: a review and recent insights. *Comp Biochem Physiol A Mol Integr Physiol,* 133**,** 979-85.

Canty, E. G. & Kadler, K. E. 2005. Procollagen trafficking, processing and fibrillogenesis. *J Cell Sci,* 118**,** 1341-53.

Carcamo, J. J., Aliaga, A. E., Clavijo, E., Branes, M. & Campos-Vallette, M. M. 2012. Raman and surface-enhanced Raman scattering in the study of human rotator cuff tissues after shock wave treatment. *Journal of Raman Spectroscopy,* 43**,** 248-254.

Chaudhry, M. A. 2008. Induction of Gene Expression Alterations by Culture Medium from Trypsinized Cells. *Journal of Biological Sciences,* 8**,** 81-87.

Cheng, V. W. T. & Screen, H. R. C. 2007. The micro-structural strain response of tendon. *Journal of Materials Science,* 42**,** 8957-8965.

Chiquet, M. 1999. Regulation of extracellular matrix gene expression by mechanical stress. *Matrix Biol,* 18**,** 417-26.

Christiansen, V. J., Jackson, K. W., Lee, K. N. & McKee, P. A. 2007. Effect of fibroblast activation protein and alpha2-antiplasmin cleaving enzyme on collagen types I, III, and IV. *Arch Biochem Biophys,* 457**,** 177-86.

Chung, L., Dinakarpandian, D., Yoshida, N., Lauer-Fields, J. L., Fields, G. B., Visse, R. & Nagase, H. 2004. Collagenase unwinds triple-helical collagen prior to peptide bond hydrolysis. *EMBO J,* 23**,** 3020-30.

Clegg, P. D., Strassburg, S. & Smith, R. K. 2007. Cell phenotypic variation in normal and damaged tendons. *Int J Exp Pathol,* 88**,** 227-35.

Connelly, J. T., Petrie, T. A., Garcia, A. J. & Levenston, M. E. 2011. Fibronectin- and collagen-mimetic ligands regulate bone marrow stromal cell chondrogenesis in three-dimensional hydrogels. *Eur Cell Mater,* 22**,** 168-76; discussion 176-7.

Cook, J. L., Feller, J. A., Bonar, S. F. & Khan, K. M. 2004. Abnormal tenocyte morphology is more prevalent than collagen disruption in asymptomatic athletes' patellar tendons. *J Orthop Res,* 22**,** 334-8.

Cook, J. L., Khan, K. M., Kiss, Z. S. & Griffiths, L. 2000. Patellar tendinopathy in junior basketball players: a controlled clinical and ultrasonographic study of 268 patellar tendons in players aged 14-18 years. *Scand J Med Sci Sports,* 10**,** 216-20.

Corps, A. N., Jones, G. C., Harrall, R. L., Curry, V. A., Hazleman, B. L. & Riley, G. P. 2008. The regulation of aggrecanase ADAMTS-4 expression in human Achilles tendon and tendon-derived cells. *Matrix Biol,* 27**,** 393-401.

Corps, A. N., Robinson, A. H., Harrall, R. L., Avery, N. C., Curry, V. A., Hazleman, B. L. & Riley, G. P. 2012. Changes in matrix protein biochemistry and the expression of mRNA encoding matrix proteins and metalloproteinases in posterior tibialis tendinopathy. *Ann Rheum Dis,* 71**,** 746-52.

Corps, A. N., Robinson, A. H., Movin, T., Costa, M. L., Hazleman, B. L. & Riley, G. P. 2006. Increased expression of aggrecan and biglycan mRNA in Achilles tendinopathy. *Rheumatology (Oxford),* 45**,** 291-4.

Corps, A. N., Robinson, A. H., Movin, T., Costa, M. L., Ireland, D. C., Hazleman, B. L. & Riley, G. P. 2004. Versican splice variant messenger RNA expression in normal human Achilles tendon and tendinopathies. *Rheumatology (Oxford),* 43**,** 969-72.

Cribb, A. M. & Scott, J. E. 1995. Tendon response to tensile stress: an ultrastructural investigation of collagen:proteoglycan interactions in stressed tendon. *J Anat,* 187 (Pt 2)**,** 423-8.

Cucurulo, T., Louis, M. L., Thaunat, M. & Franceschi, J. P. 2009. Surgical treatment of patellar tendinopathy in athletes. A retrospective multicentric study. *Orthop Traumatol Surg Res,* 95**,** S78-84.

Culpepper, B. K., Phipps, M. C., Bonvallet, P. P. & Bellis, S. L. 2010. Enhancement of peptide coupling to hydroxyapatite and implant osseointegration through collagen mimetic peptide modified with a polyglutamate domain. *Biomaterials,* 31**,** 9586-94.

Dahl, K. N., Ribeiro, A. J. & Lammerding, J. 2008. Nuclear shape, mechanics, and mechanotransduction. *Circ Res,* 102**,** 1307-18.

Dakin, S. G., Dudhia, J. & Smith, R. K. 2014. Resolving an inflammatory concept: the importance of inflammation and resolution in tendinopathy. *Vet Immunol Immunopathol,* 158**,** 121-7.

Danen, E. H., Sonneveld, P., Brakebusch, C., Fassler, R. & Sonnenberg, A. 2002. The fibronectin-binding integrins alpha5beta1 and alphavbeta3 differentially modulate RhoA-GTP loading, organization of cell matrix adhesions, and fibronectin fibrillogenesis. *J Cell Biol,* 159**,** 1071-86.

De Boer, J., Van Blitterswijk, C., Thomsen, P., Hubbell, J., Cancedda, R., de Bruijn, J. D., Lindahl, A., Sohier, J. & Williams, D. F. 2008. *Tissue Engineering*, Elsevier Science.

de Jonge, S., van den Berg, C., de Vos, R. J., van der Heide, H. J., Weir, A., Verhaar, J. A., Bierma-Zeinstra, S. M. & Tol, J. L. 2011. Incidence of midportion Achilles tendinopathy in the general population. *Br J Sports Med,* 45**,** 1026-8.

de Mos, M., Koevoet, W. J., Jahr, H., Verstegen, M. M., Heijboer, M. P., Kops, N., van Leeuwen, J. P., Weinans, H., Verhaar, J. A. & van Osch, G. J. 2007. Intrinsic differentiation potential of adolescent human tendon tissue: an in-vitro cell differentiation study. *BMC Musculoskelet Disord,* 8**,** 16.

de Vos, R. J., Weir, A., Visser, R. J., de Winter, T. & Tol, J. L. 2007. The additional value of a night splint to eccentric exercises in chronic midportion Achilles tendinopathy: a randomised controlled trial. *Br J Sports Med,* 41**,** e5.

Deckert, A. A., Anderson, K. A., Mullaugh, K. M. & Delaney, C. 2004. Comprehensive Study of the Formation and Reaction of a Tethered N-Hydroxysulfosuccinimidyl Ester Used to Covalently Tether Proteins to Surfaces. *The Journal of Physical Chemistry B,* 108**,** 15808-15814.

Declercq, H., Van den Vreken, N., De Maeyer, E., Verbeeck, R., Schacht, E., De Ridder, L. & Cornelissen, M. 2004. Isolation, proliferation and differentiation of osteoblastic cells to study cell/biomaterial interactions: comparison of different isolation techniques and source. *Biomaterials,* 25**,** 757-68.

DeLong, S. A., Moon, J. J. & West, J. L. 2005. Covalently immobilized gradients of bFGF on hydrogel scaffolds for directed cell migration. *Biomaterials,* 26**,** 3227-34.

Dettin, M., Herath, T., Gambaretto, R., Iucci, G., Battocchio, C., Bagno, A., Ghezzo, F., Di Bello, C., Polzonetti, G. & Di Silvio, L. 2009. Assessment of novel chemical strategies for covalent attachment of adhesive peptides to rough titanium surfaces: XPS analysis and biological evaluation. *J Biomed Mater Res A,* 91**,** 463-79.

Dowling, B. A., Dart, A. J., Hodgson, D. R. & Smith, R. K. 2000. Superficial digital flexor tendonitis in the horse. *Equine Vet J,* 32**,** 369-78.

Dumitriu, S. 2001. *Polymeric Biomaterials, Revised and Expanded*, CRC Press.

Dunkman, A. A., Buckley, M. R., Mienaltowski, M. J., Adams, S. M., Thomas, S. J., Satchell, L., Kumar, A., Pathmanathan, L., Beason, D. P., Iozzo, R. V., Birk, D. E. & Soslowsky, L. J. 2013. Decorin expression is important for age-related changes in tendon structure and mechanical properties. *Matrix Biol,* 32**,** 3-13.

El Khoury, L., Posthumus, M., Collins, M., Handley, C. J., Cook, J. & Raleigh, S. M. 2013. Polymorphic variation within the ADAMTS2, ADAMTS14, ADAMTS5, ADAM12 and TIMP2 genes and the risk of Achilles tendon pathology: a genetic association study. *J Sci Med Sport,* 16**,** 493-8.

Elliott, D. H. 1965. Structure and Function of Mammalian Tendon. *Biol Rev Camb Philos Soc,* 40**,** 392-421.

Everaerts, F., Torrianni, M., Hendriks, M. & Feijen, J. 2007. Quantification of carboxyl groups in carbodiimide cross-linked collagen sponges. *J Biomed Mater Res A,* 83**,** 1176-83.

Filmon, R., Grizon, F., Basle, M. F. & Chappaard, D. 2002. Effects of negatively charged groups (carboxymethyl) on the calcification of poly(2-hydroxyethyl methacrylate). *Biomaterials,* 23**,** 3053-9.

Fitzgerald, J., Rich, C., Zhou, F. H. & Hansen, U. 2008. Three novel collagen VI chains, alpha4(VI), alpha5(VI), and alpha6(VI). *J Biol Chem,* 283**,** 20170-80.

Fong, G., Backman, L. J., Andersson, G., Scott, A. & Danielson, P. 2013. Human tenocytes are stimulated to proliferate by acetylcholine through an EGFR signalling pathway. *Cell Tissue Res,* 351**,** 465-75.

Fong, K. D., Trindade, M. C., Wang, Z., Nacamuli, R. P., Pham, H., Fang, T. D., Song, H. M., Smith, R. L., Longaker, M. T. & Chang, J. 2005. Microarray Analysis of Mechanical Shear Effects on Flexor Tendon Cells. *Plastic and Reconstructive Surgery,* 116**,** 1393-1404.

Franchi, M., Fini, M., Quaranta, M., De Pasquale, V., Raspanti, M., Giavaresi, G., Ottani, V. & Ruggeri, A. 2007a. Crimp morphology in relaxed and stretched rat Achilles tendon. *J Anat,* 210**,** 1-7.

Franchi, M., Ottani, V., Stagni, R. & Ruggeri, A. 2010. Tendon and ligament fibrillar crimps give rise to left-handed helices of collagen fibrils in both planar and helical crimps. *J Anat,* 216**,** 301-9.

Franchi, M., Trire, A., Quaranta, M., Orsini, E. & Ottani, V. 2007b. Collagen structure of tendon relates to function. *ScientificWorldJournal,* 7**,** 404-20.

Fratzl, P., Misof, K., Zizak, I., Rapp, G., Amenitsch, H. & Bernstorff, S. 1997. Fibrillar structure and mechancial properties of collagen. *Journal fo Structural Biology,* 122**,** 119-122.

Frazer, C., Wall, M. E., Sumanasinghe, R. & Banes, A. J. 2009. *Tech Report 101: Loading Stations Quantification of Strain on the Membrane Surface*, Flexcell International Corporation.

Fredberg, U. & Stengaard-Pedersen, K. 2008. Chronic tendinopathy tissue pathology, pain mechanisms, and etiology with a special focus on inflammation. *Scand J Med Sci Sports,* 18**,** 3-15.

Freed, A. D. & Doehring, T. C. 2005. Elastic Model for Crimped Collagen Fibrils. *Journal of Biomechanical Engineering,* 127**,** 587.

Fu, S. C., Chan, B. P., Wang, W., Pau, H. M., Chan, K. M. & Rolf, C. G. 2002. Increased expression of matrix metalloproteinase 1 (MMP1) in 11 patients with patellar tendinosis. *Acta Orthop Scand,* 73**,** 658-62.

Fung, D. T., Wang, V. M., Andarawis-Puri, N., Basta-Pljakic, J., Li, Y., Laudier, D. M., Sun, H. B., Jepsen, K. J., Schaffler, M. B. & Flatow, E. L. 2010. Early response to tendon fatigue damage accumulation in a novel in vivo model. *J Biomech,* 43**,** 274-9.

Garvin, J., Qi, J., Maloney, M. & Banes, A. J. 2003. Novel system for engineering bioartificial tendons and application of mechanical load. *Tissue Eng,* 9**,** 967-79.

Gattazzo, F., Urciuolo, A. & Bonaldo, P. 2014. Extracellular matrix: a dynamic microenvironment for stem cell niche. *Biochim Biophys Acta,* 1840**,** 2506-19.

Gelse, K. 2003. Collagens—structure, function, and biosynthesis. *Advanced Drug Delivery Reviews,* 55**,** 1531-1546.

Giannone, G., Jiang, G., Sutton, D. H., Critchley, D. R. & Sheetz, M. P. 2003. Talin1 is critical for force-dependent reinforcement of initial integrin-cytoskeleton bonds but not tyrosine kinase activation. *J Cell Biol,* 163**,** 409-19.

Gittel, C., Brehm, W., Burk, J., Juelke, H., Staszyk, C. & Ribitsch, I. 2013. Isolation of equine multipotent mesenchymal stromal cells by enzymatic tissue digestion or explant technique: comparison of cellular properties. *BMC Vet Res,* 9**,** 221.

Goodman, S. A., May, S. A., Heinegard, D. & Smith, R. K. 2004. Tenocyte response to cyclical strain and transforming growth factor beta is dependent upon age and site of origin. *Biorheology,* 41**,** 613-28.

Grzesiak, J. J. & Bouvet, M. 2007. Determination of the ligand-binding specificities of the alpha2beta1 and alpha1beta1 integrins in a novel 3-dimensional in vitro model of pancreatic cancer. *Pancreas,* 34**,** 220-8.

Gullberg, D., Gehlsen, K. R., Turner, D. C., Ahlen, K., Zijenah, L. S., Barnes, M. J. & Rubin, K. 1992. Analysis of alpha 1 beta 1, alpha 2 beta 1 and alpha 3 beta 1 integrins in cell--collagen interactions: identification of conformation dependent alpha 1 beta 1 binding sites in collagen type I. *EMBO J,* 11**,** 3865-73.

Gungormus, C. & Kolankaya, D. 2008. Characterization of type I, III and V collagens in high-density cultured tenocytes by triple-immunofluorescence technique. *Cytotechnology,* 58**,** 145-52.

Guvendiren, M. & Burdick, J. A. 2012. Stiffening hydrogels to probe short- and long-term cellular responses to dynamic mechanics. *Nat Commun,* 3**,** 792.

Han, S., Makareeva, E., Kuznetsova, N. V., DeRidder, A. M., Sutter, M. B., Losert, W., Phillips, C. L., Visse, R., Nagase, H. & Leikin, S. 2010. Molecular mechanism of type I collagen homotrimer resistance to mammalian collagenases. *J Biol Chem,* 285**,** 22276-81.

Hancox, N. L. 1981. *Fibre composite hybrid materials*, Applied Science.

Harris, J. M. 1992. *Poly(Ethylene Glycol) Chemistry*, Springer US.

Heinemeier, K. M. & Kjaer, M. 2011. In vivo investigation of tendon responses to mechanical loading. *J Musculoskelet Neuronal Interact,* 11**,** 115-23.

Heino, J. 2000. The collagen receptor integrins have distinct ligand recognition and signaling functions. *Matrix Biol,* 19**,** 319-23.

Hennessy, K. M., Pollot, B. E., Clem, W. C., Phipps, M. C., Sawyer, A. A., Culpepper, B. K. & Bellis, S. L. 2009. The effect of collagen I mimetic peptides on mesenchymal stem cell adhesion and differentiation, and on bone formation at hydroxyapatite surfaces. *Biomaterials,* 30**,** 1898-909.

Hermanson, G. T. 2008. *Bioconjugate techniques,* London, Academic.

Hirano, Y., Okuno, M., Hayashi, T., Goto, K. & Nakajima, A. 1993. Cell-attachment activities of surface immobilized oligopeptides RGD, RGDS, RGDV, RGDT, and YIGSR toward five cell lines. *J Biomater Sci Polym Ed,* 4**,** 235-43.

Hoksrud, A. F. & Bahr, R. 2011. Injectable agents derived from or targeting vascularity: has clinical acceptance in managing tendon disorders superseded scientific evidence? *J Musculoskelet Neuronal Interact,* 11**,** 174-84.

Howes, J. M., Bihan, D., Slatter, D. A., Hamaia, S. W., Packman, L. C., Knauper, V., Visse, R. & Farndale, R. W. 2014. The recognition of collagen and triple-helical toolkit peptides by MMP-13: sequence specificity for binding and cleavage. *J Biol Chem,* 289**,** 24091-101.

Huang, K., Lee, B. P., Ingram, D. R. & Messersmith, P. B. 2002. Synthesis and characterization of self-assembling block copolymers containing bioadhesive end groups. *Biomacromolecules,* 3**,** 397-406.

Huang, K., Lee, B. P. & Messersmith, P. B. 2001. Synthesis and characterization of self-assembling block copolymers containing adhesive moieties. *Abstracts of Papers of the American Chemical Society,* 222**,** U319-U319.

Huisman, E., Lu, A., McCormack, R. G. & Scott, A. 2014. Enhanced collagen type I synthesis by human tenocytes subjected to periodic in vitro mechanical stimulation. *BMC Musculoskelet Disord,* 15**,** 386.

Hynes, R. O. 1992. Integrins: versatility, modulation, and signaling in cell adhesion. *Cell,* 69**,** 11-25.

Ifkovits, J. L. & Burdick, J. A. 2007. Review: photopolymerizable and degradable biomaterials for tissue engineering applications. *Tissue Eng,* 13**,** 2369-85.

Iozzo, R. V. & Murdoch, A. D. 1996. Proteoglycans of the extracellular environment: clues from the gene and protein side offer novel perspectives in molecular diversity and function. *FASEB J,* 10**,** 598-614.

Ireland, D., Harrall, R., Curry, V., Holloway, G., Hackney, R., Hazleman, B. & Riley, G. 2001. Multiple changes in gene expression in chronic human Achilles tendinopathy. *Matrix Biol,* 20**,** 159-69.

Ishikawa, Y. & Bachinger, H. P. 2013. A molecular ensemble in the rER for procollagen maturation. *Biochim Biophys Acta,* 1833**,** 2479-91.

James, R., Kesturu, G., Balian, G. & Chhabra, A. B. 2008. Tendon: biology, biomechanics, repair, growth factors, and evolving treatment options. *J Hand Surg Am,* 33**,** 102-12.

Jarvinen, T. A., Jarvinen, T. L., Kannus, P., Jozsa, L. & Jarvinen, M. 2004. Collagen fibres of the spontaneously ruptured human tendons display decreased thickness and crimp angle. *J Orthop Res,* 22**,** 1303-9.

Jelinsky, S. A., Rodeo, S. A., Li, J., Gulotta, L. V., Archambault, J. M. & Seeherman, H. J. 2011. Regulation of gene expression in human tendinopathy. *BMC Musculoskelet Disord,* 12**,** 86.

Jepsen, K. J., Wu, F., Peragallo, J. H., Paul, J., Roberts, L., Ezura, Y., Oldberg, A., Birk, D. E. & Chakravarti, S. 2002. A syndrome of joint laxity and impaired tendon integrity in lumican- and fibromodulin-deficient mice. *J Biol Chem,* 277**,** 35532-40.

Jokinen, J., Dadu, E., Nykvist, P., Kapyla, J., White, D. J., Ivaska, J., Vehvilainen, P., Reunanen, H., Larjava, H., Hakkinen, L. & Heino, J. 2004. Integrin-mediated cell adhesion to type I collagen fibrils. *J Biol Chem,* 279**,** 31956-63.

Jones, E. R., Jones, G. C., Legerlotz, K. & Riley, G. P. 2013. Cyclical strain modulates metalloprotease and matrix gene expression in human tenocytes via activation of TGFbeta. *Biochim Biophys Acta,* 1833**,** 2596-607.

Jones, G. C., Corps, A. N., Pennington, C. J., Clark, I. M., Edwards, D. R., Bradley, M. M., Hazleman, B. L. & Riley, G. P. 2006. Expression profiling of metalloproteinases and tissue inhibitors of metalloproteinases in normal and degenerate human achilles tendon. *Arthritis Rheum,* 54**,** 832-42.

Jozsa, L. G. & Kannus, P. 1997. *Human tendons : anatomy, physiology, and pathology,* Champaign, Ill. ; Leeds, Human Kinetics.

Juneja, S. C. & Veillette, C. 2013. Defects in tendon, ligament, and enthesis in response to genetic alterations in key proteoglycans and glycoproteins: a review. *Arthritis,* 2013**,** 154812.

Kadler, K. E., Holmes, D. F., Trotter, J. A. & Chapman, J. A. 1996. Collagen fibril formation. *Biochem J,* 316 (Pt 1)**,** 1-11.

Kamkin, A. G. & Kiseleva, I. 2008. *Mechanosensitive ion channels,* [Berlin]; [New York], Springer Verlag.

Kannus, P. 2000. Structure of the tendon connective tissue. *Scand J Med Sci Sports,* 10**,** 312-20.

Karamichos, D., Brown, R. A. & Mudera, V. 2007. Collagen stiffness regulates cellular contraction and matrix remodeling gene expression. *J Biomed Mater Res A,* 83**,** 887-94.

Khan, K. M., Cook, J. L., Bonar, F., Harcourt, P. & Astrom, M. 1999. Histopathology of common tendinopathies. Update and implications for clinical management. *Sports Med,* 27**,** 393-408.

Kjaer, M. 2004. Role of extracellular matrix in adaptation of tendon and skeletal muscle to mechanical loading. *Physiol Rev,* 84**,** 649-98.

Klein, T. & Bischoff, R. 2011. Physiology and pathophysiology of matrix metalloproteases. *Amino Acids,* 41**,** 271-90.

Kloxin, A. M., Tibbitt, M. W. & Anseth, K. S. 2010. Synthesis of photodegradable hydrogels as dynamically tunable cell culture platforms. *Nat Protoc,* 5**,** 1867-87.

Knight, C. G., Morton, L. F., Peachey, A. R., Tuckwell, D. S., Farndale, R. W. & Barnes, M. J. 2000. The collagen-binding A-domains of integrins alpha(1)beta(1) and alpha(2)beta(1) recognize the same specific amino acid sequence, GFOGER, in native (triple-helical) collagens. *J Biol Chem,* 275**,** 35-40.

Krishnakumar, V. & Balachandran, V. 2004. FTIR, FT-Raman spectral analysis and normal coordinate calculations of 2-hydroxy-3-methoxybenzaldehyde thiosemicarbozone *Indian Journal of Pure & Applied Physics,* 42**,** 313-318.

Kubo, K., Kawakami, Y., Kanehisa, H. & Fukunaga, T. 2002. Measurement of viscoelastic properties of tendon structures in vivo. *Scand J Med Sci Sports,* 12**,** 3-8.

Lahiri, J., Isaacs, L., Tien, J. & Whitesides, G. M. 1999. A strategy for the generation of surfaces presenting ligands for studies of binding based on an active ester as a common reactive intermediate: A surface plasmon resonance study. *Analytical Chemistry,* 71**,** 777-790.

Lane, S. M., Kuang, Z., Yom, J., Arifuzzaman, S., Genzer, J., Farmer, B., Naik, R. & Vaia, R. A. 2011. Poly(2-hydroxyethyl methacrylate) for enzyme immobilization: impact on activity and stability of horseradish peroxidase. *Biomacromolecules,* 12**,** 1822-30.

Langberg, H., Olesen, J. L., Gemmer, C. & Kjaer, M. 2002. Substantial elevation of interleukin-6 concentration in peritendinous tissue, in contrast to muscle, following prolonged exercise in humans. *The Journal of Physiology,* 542**,** 985-990.

Langberg, H., Skovgaard, D., Petersen, L. J., Bulow, J. & Kjaer, M. 1999. Type I collagen synthesis and degradation in peritendinous tissue after exercise determined by microdialysis in humans. *J Physiol,* 521 Pt 1**,** 299-306.

Langholz, O., Rockel, D., Mauch, C., Kozlowska, E., Bank, I., Krieg, T. & Eckes, B. 1995. Collagen and collagenase gene expression in three-dimensional collagen lattices are differentially regulated by alpha 1 beta 1 and alpha 2 beta 1 integrins. *J Cell Biol,* 131**,** 1903-15.

Lanza, R., Langer, R. & Vacanti, J. P. 2000. *Principles of Tissue Engineering*, Elsevier Science.

Laurencin, C. T. & Nair, L. S. 2008. *Nanotechnology and Tissue Engineering: The Scaffold*, CRC Press.

Lee, D. G. & Suh, N. P. 2006. *Axiomatic Design and Fabrication of Composite Structures*, Oxford University Press, USA.

Legate, K. R., Wickstrom, S. A. & Fassler, R. 2009. Genetic and cell biological analysis of integrin outside-in signaling. *Genes Dev,* 23**,** 397-418.

Legerlotz, K., Jones, E. R., Screen, H. R. & Riley, G. P. 2012. Increased expression of IL-6 family members in tendon pathology. *Rheumatology (Oxford),* 51**,** 1161-5.

Legerlotz, K., Jones, G. C., Screen, H. R. & Riley, G. P. 2013. Cyclic loading of tendon fascicles using a novel fatigue loading system increases interleukin-6 expression by tenocytes. *Scand J Med Sci Sports,* 23**,** 31-7.

Leigh, D. R., Abreu, E. L. & Derwin, K. A. 2008. Changes in gene expression of individual matrix metalloproteinases differ in response to mechanical unloading of tendon fascicles in explant culture. *J Orthop Res,* 26**,** 1306-12.

Lejard, V., Brideau, G., Blais, F., Salingcarnboriboon, R., Wagner, G., Roehrl, M. H., Noda, M., Duprez, D., Houillier, P. & Rossert, J. 2007. Scleraxis and NFATc regulate the expression of the pro-alpha1(I) collagen gene in tendon fibroblasts. *J Biol Chem,* 282**,** 17665-75.

Leslie-Barbick, J. E., Moon, J. J. & West, J. L. 2009. Covalently-immobilized vascular endothelial growth factor promotes endothelial cell tubulogenesis in poly(ethylene glycol) diacrylate hydrogels. *J Biomater Sci Polym Ed,* 20**,** 1763-79.

Lewandrowski, K. U., Wise, D. L., Yaszemski, M. J., Gresser, J. D., Trantolo, D. J. & Altobelli, D. E. 2002. *Tissue Engineering And Biodegradable Equivalents, Scientific And Clinical Applications*, Taylor & Francis.

Lichtwark, G. A. & Wilson, A. M. 2005. In vivo mechanical properties of the human Achilles tendon during one-legged hopping. *J Exp Biol,* 208**,** 4715-25.

Lichtwark, G. A. & Wilson, A. M. 2006. Interactions between the human gastrocnemius muscle and the Achilles tendon during incline, level and decline locomotion. *J Exp Biol,* 209**,** 4379-88.

Lin, E. A. & Liu, C. 2009. The emerging roles of ADAMTS-7 and ADAMTS-12 matrix metalloproteinases. *Open Access Rheumatol Res Rev*.

Liu, S., Calderwood, D. A. & Ginsberg, M. H. 2000. Integrin cytoplasmic domain-binding proteins. *J Cell Sci,* 113 (Pt 20)**,** 3563-71.

Liu, S. Q., Tian, Q., Wang, L., Hedrick, J. L., Hui, J. H., Yang, Y. Y. & Ee, P. L. 2010. Injectable Biodegradable Poly(ethylene glycol)/RGD Peptide Hybrid Hydrogels for in vitro Chondrogenesis of Human Mesenchymal Stem Cells. *Macromol Rapid Commun,* 31**,** 1148-54.

Liu, Y., Ramanath, H. S. & Wang, D. A. 2008. Tendon tissue engineering using scaffold enhancing strategies. *Trends Biotechnol,* 26**,** 201-9.

Loffek, S., Schilling, O. & Franzke, C. W. 2011. Series "matrix metalloproteinases in lung health and disease": Biological role of matrix metalloproteinases: a critical balance. *Eur Respir J,* 38**,** 191-208.

Luo, J. & Tong, Y. W. 2011. Self-assembly of collagen-mimetic peptide amphiphiles into biofunctional nanofiber. *ACS Nano,* 5**,** 7739-47.

Luzak, B., Golanski, J., Rozalski, M., Boncler, M. A. & Watala, C. 2003. Inhibition of collagen-induced platelet reactivity by DGEA peptide. *Acta Biochim Pol,* 50**,** 1119-28.

Lynn, A. D., Blakney, A. K., Kyriakides, T. R. & Bryant, S. J. 2011. Temporal progression of the host response to implanted poly(ethylene glycol)-based hydrogels. *J Biomed Mater Res A,* 96**,** 621-31.

Ma, P. X. & Elisseeff, J. 2005. *Scaffolding In Tissue Engineering*, Taylor & Francis.

Mabilleau, G., Cincu, C., Baslé, M. F. & Chappard, D. 2008. Polymerization of 2-(hydroxyethyl)methacrylate by two different initiator/accelerator systems: a Raman spectroscopic monitoring. *Journal of Raman Spectroscopy,* 39**,** 767-771.

Mabilleau, G., Stancu, I. C., Honore, T., Legeay, G., Cincu, C., Basle, M. F. & Chappard, D. 2006. Effects of the length of crosslink chain on poly(2-hydroxyethyl methacrylate) (pHEMA) swelling and biomechanical properties. *J Biomed Mater Res A,* 77**,** 35-42.

Maeda, E., Hagiwara, Y., Wang, J. H. & Ohashi, T. 2013a. A new experimental system for simultaneous application of cyclic tensile strain and fluid shear stress to tenocytes in vitro. *Biomed Microdevices,* 15**,** 1067-75.

Maeda, E., Shelton, J. C., Bader, D. L. & Lee, D. A. 2007. Time dependence of cyclic tensile strain on collagen production in tendon fascicles. *Biochem Biophys Res Commun,* 362**,** 399-404.

Maeda, E., Shelton, J. C., Bader, D. L. & Lee, D. A. 2009. Differential regulation of gene expression in isolated tendon fascicles exposed to cyclic tensile strain in vitro. *J Appl Physiol (1985),* 106**,** 506-12.

Maeda, E., Sugimoto, M. & Ohashi, T. 2013b. Cytoskeletal tension modulates MMP-1 gene expression from tenocytes on micropillar substrates. *J Biomech,* 46**,** 991-7.

Maganaris, C. N., Narici, M. V. & Reeves, N. D. 2004. In vivo human tendon mechanical properties: effect of resistance training in old age. *J Musculoskelet Neuronal Interact,* 4**,** 204-8.

Maganaris, C. N. & Paul, J. P. 2002. Tensile properties of the in vivo human gastrocnemius tendon. *J Biomech,* 35**,** 1639-46.

Magnan, B., Bondi, M., Pierantoni, S. & Samaila, E. 2014. The pathogenesis of Achilles tendinopathy: A systematic review. *Foot and Ankle Surgery*.

Magnusson, S. P., Langberg, H. & Kjaer, M. 2010. The pathogenesis of tendinopathy: balancing the response to loading. *Nat Rev Rheumatol,* 6**,** 262-8.

Magnusson, S. P., Qvortrup, K., Larsen, J. O., Rosager, S., Hanson, P., Aagaard, P., Krogsgaard, M. & Kjaer, M. 2002. Collagen fibril size and crimp morphology in ruptured and intact Achilles tendons. *Matrix Biol,* 21**,** 369-77.

Magra, M. & Maffulli, N. 2008. Genetic aspects of tendinopathy. *J Sci Med Sport,* 11**,** 243-7.

Manka, S. W., Carafoli, F., Visse, R., Bihan, D., Raynal, N., Farndale, R. W., Murphy, G., Enghild, J. J., Hohenester, E. & Nagase, H. 2012. Structural insights into triple-helical collagen cleavage by matrix metalloproteinase 1. *Proc Natl Acad Sci U S A,* 109**,** 12461-6.

Mazzocca, A. D., Chowaniec, D., McCarthy, M. B., Beitzel, K., Cote, M. P., McKinnon, W. & Arciero, R. 2012. In vitro changes in human tenocyte cultures obtained from proximal biceps tendon: multiple passages result in changes in routine cell markers. *Knee Surg Sports Traumatol Arthrosc,* 20**,** 1666-72.

McCawley, L. J. & Matrisian, L. M. 2001. Matrix metalloproteinases: they're not just for matrix anymore! *Curr Opin Cell Biol,* 13**,** 534-40.

Metzl, J. A., Ahmad, C. S. & Levine, W. N. 2008. The ruptured Achilles tendon: operative and non-operative treatment options. *Curr Rev Musculoskelet Med,* 1**,** 161-4.

Millar, N. L., Hueber, A. J., Reilly, J. H., Xu, Y., Fazzi, U. G., Murrell, G. A. & McInnes, I. B. 2010. Inflammation is present in early human tendinopathy. *Am J Sports Med,* 38**,** 2085-91.

Miller, B. F., Olesen, J. L., Hansen, M., Dossing, S., Crameri, R. M., Welling, R. J., Langberg, H., Flyvbjerg, A., Kjaer, M., Babraj, J. A., Smith, K. & Rennie, M. J. 2005. Coordinated collagen and muscle protein synthesis in human patella tendon and quadriceps muscle after exercise. *J Physiol,* 567**,** 1021-33.

Miron, T. & Wilchek, M. 1993. A Simplified Method for the Preparation of Succinimidyl Carbonate Polyethylene-Glycol for Coupling to Proteins. *Bioconjugate Chemistry,* 4**,** 568-569.

Mitchell, P. G., Magna, H. A., Reeves, L. M., Lopresti-Morrow, L. L., Yocum, S. A., Rosner, P. J., Geoghegan, K. F. & Hambor, J. E. 1996. Cloning, expression, and type II collagenolytic activity of matrix metalloproteinase-13 from human osteoarthritic cartilage. *J Clin Invest,* 97**,** 761-8.

Mizuno, M., Fujisawa, R. & Kuboki, Y. 2000. Type I collagen-induced osteoblastic differentiation of bone-marrow cells mediated by collagen-?2?1 integrin interaction. *Journal of Cellular Physiology,* 184**,** 207-213.

Mokone, G. G., Gajjar, M., September, A. V., Schwellnus, M. P., Greenberg, J., Noakes, T. D. & Collins, M. 2005. The guanine-thymine dinucleotide repeat polymorphism within the tenascin-C gene is associated with achilles tendon injuries. *Am J Sports Med,* 33**,** 1016-21.

Morita, Y., Watanabe, S., Ju, Y. & Xu, B. 2013. Determination of optimal cyclic uniaxial stretches for stem cell-to-tenocyte differentiation under a wide range of mechanical stretch conditions by evaluating gene expression and protein synthesis levels. *Acta Bioeng Biomech,* 15**,** 71-9.

Morrey, M. E., Dean, B. J. F., Carr, A. J. & Morrey, B. F. 2013. Tendinopathy: Same Disease Different Results—Why? *Operative Techniques in Orthopaedics,* 23**,** 39-49.

Movasaghi, Z., Rehman, S. & Rehman, I. U. 2007. Raman Spectroscopy of Biological Tissues. *Applied Spectroscopy Reviews,* 42**,** 493-541.

Nagase, H., Visse, R. & Murphy, G. 2006. Structure and function of matrix metalloproteinases and TIMPs. *Cardiovasc Res,* 69**,** 562-73.

NanoDrop Technologies 2007. Technical Support Bulletin T009 : 260/280 and 260/230 Ratios. Washington, Delaware, USA.

Nixon, A. J., Watts, A. E. & Schnabel, L. V. 2012. Cell- and gene-based approaches to tendon regeneration. *J Shoulder Elbow Surg,* 21**,** 278-94.

Nuttall, R. K., Pennington, C. J., Taplin, J., Wheal, A., Yong, V. W., Forsyth, P. A. & Edwards, D. R. 2003. Elevated membrane-type matrix metalloproteinases in gliomas revealed by profiling proteases and inhibitors in human cancer cells. *Mol Cancer Res,* 1**,** 333-45.

O'Brien, F. J. 2011. Biomaterials & scaffolds for tissue engineering. *Materials Today,* 14**,** 88-95.

O'Brien, M. 1997. Structure and metabolism of tendons. *Scand J Med Sci Sports,* 7**,** 55-61.

Ohuchi, E., Imai, K., Fujii, Y., Sato, H., Seiki, M. & Okada, Y. 1997. Membrane type 1 matrix metalloproteinase digests interstitial collagens and other extracellular matrix macromolecules. *J Biol Chem,* 272**,** 2446-51.

Orazizadeh, M., Hashemitabar, M., Bahramzadeh, S., Dehbashi, F. N. & Saremy, S. 2015. Comparison of the enzymatic and explant methods for the culture of keratinocytes isolated from human foreskin. *Biomed Rep,* 3**,** 304-308.

Ostroha, J. L. 2006. *PEG-Based degradable networks for drug delivery applications.* Drexel University.

Parkinson, J., Samiric, T., Ilic, M. Z., Cook, J. & Handley, C. J. 2011. Involvement of proteoglycans in tendinopathy. *J Musculoskelet Neuronal Interact,* 11**,** 86-93.

Patterson, M. L., Atkinson, S. J., Knauper, V. & Murphy, G. 2001. Specific collagenolysis by gelatinase A, MMP-2, is determined by the hemopexin domain and not the fibronectin-like domain. *FEBS Lett,* 503**,** 158-62.

Pavalko, F. M., Chen, N. X., Turner, C. H., Burr, D. B., Atkinson, S., Hsieh, Y. F., Qiu, J. & Duncan, R. L. 1998. Fluid shear-induced mechanical signaling in MC3T3-E1 osteoblasts requires cytoskeleton-integrin interactions. *Am J Physiol,* 275**,** C1591-601.

Peffers, M. J., Thorpe, C. T., Collins, J. A., Eong, R., Wei, T. K., Screen, H. R. & Clegg, P. D. 2014. Proteomic analysis reveals age-related changes in tendon matrix composition, with age- and injury-specific matrix fragmentation. *J Biol Chem,* 289**,** 25867-78.

Pfaffl, M. W. 2001. A new mathematical model for relative quantification in real-time RT-PCR. *Nucleic Acids Res,* 29**,** e45.

Piggott, M. R. 2002. *Load Bearing Fibre Composites*, Kluwer Academic Publishers.

Pingel, J., Lu, Y., Starborg, T., Fredberg, U., Langberg, H., Nedergaard, A., Weis, M., Eyre, D., Kjaer, M. & Kadler, K. E. 2014. 3-D ultrastructure and collagen composition of healthy and overloaded human tendon: evidence of tenocyte and matrix buckling. *J Anat,* 224**,** 548-55.

Plant, A. L., Bhadriraju, K., Spurlin, T. A. & Elliott, J. T. 2009. Cell response to matrix mechanics: focus on collagen. *Biochim Biophys Acta,* 1793**,** 893-902.

Plow, E. F., Haas, T. A., Zhang, L., Loftus, J. & Smith, J. W. 2000. Ligand binding to integrins. *J Biol Chem,* 275**,** 21785-8.

Porter, S., Clark, I. M., Kevorkian, L. & Edwards, D. R. 2005. The ADAMTS metalloproteinases. *Biochem J,* 386**,** 15-27.

Porter, S., Scott, S. D., Sassoon, E. M., Williams, M. R., Jones, J. L., Girling, A. C., Ball, R. Y. & Edwards, D. R. 2004. Dysregulated expression of adamalysin-thrombospondin genes in human breast carcinoma. *Clin Cancer Res,* 10**,** 2429-40.

Qin, C., Xu, J. & Zhang, Y. 2006. Spectroscopic investigation of the function of aqueous 2-hydroxyethylmethacrylate/glutaraldehyde solution as a dentin desensitizer. *Eur J Oral Sci,* 114**,** 354-9.

Qin, J., Vinogradova, O. & Plow, E. F. 2004. Integrin bidirectional signaling: a molecular view. *PLoS Biol,* 2**,** e169.

Qiu, Y., Wang, X., Zhang, Y., Carr, A. J., Zhu, L., Xia, Z. & Sabokbar, A. 2013. Development of a refined tenocyte differentiation culture technique for tendon tissue engineering. *Cells Tissues Organs,* 197**,** 27-36.

Ratner, B. D. & Bryant, S. J. 2004. Biomaterials: where we have been and where we are going. *Annu Rev Biomed Eng,* 6**,** 41-75.

Redaelli, A., Vesentini, S., Soncini, M., Vena, P., Mantero, S. & Montevecchi, F. M. 2003. Possible role of decorin glycosaminoglycans in fibril to fibril force transfer in relative mature tendons—a computational study from molecular to microstructural level. *Journal of Biomechanics,* 36**,** 1555-1569.

Rees, J. D., Stride, M. & Scott, A. 2013. Tendons - time to revisit inflammation. *Br J Sports Med*.

Rees, J. D., Wilson, A. M. & Wolman, R. L. 2006. Current concepts in the management of tendon disorders. *Rheumatology (Oxford),* 45**,** 508-21.

Reese, S. P., Underwood, C. J. & Weiss, J. A. 2013. Effects of decorin proteoglycan on fibrillogenesis, ultrastructure, and mechanics of type I collagen gels. *Matrix Biol,* 32**,** 414-23.

Reinking, M. 2012. Tendinopathy in athletes. *Phys Ther Sport,* 13**,** 3-10.

Ricard-Blum, S. 2011. The collagen family. *Cold Spring Harb Perspect Biol,* 3**,** a004978.

Richardson, S. H., Starborg, T., Lu, Y., Humphries, S. M., Meadows, R. S. & Kadler, K. E. 2007. Tendon development requires regulation of cell condensation and cell shape via cadherin-11-mediated cell-cell junctions. *Mol Cell Biol,* 27**,** 6218-28.

Rigozzi, S., Muller, R., Stemmer, A. & Snedeker, J. G. 2013. Tendon glycosaminoglycan proteoglycan sidechains promote collagen fibril sliding-AFM observations at the nanoscale. *J Biomech,* 46**,** 813-8.

Riikonen, T., Westermarck, J., Koivisto, L., Broberg, A., Kähäri, V.-M. & Heino, J. 1995. Integrin α2β1 Is a Positive Regulator of Collagenase (MMP-1) and Collagen α1(I) Gene Expression. *Journal of Biological Chemistry,* 270**,** 13548-13552.

Riley, G. 2004. The pathogenesis of tendinopathy. A molecular perspective. *Rheumatology (Oxford),* 43**,** 131-42.

Riley, G. 2008. Tendinopathy--from basic science to treatment. *Nat Clin Pract Rheumatol,* 4**,** 82-9.

Riley, G. P., Curry, V., DeGroot, J., van El, B., Verzijl, N., Hazleman, B. L. & Bank, R. A. 2002. Matrix metalloproteinase activities and their relationship with collagen remodelling in tendon pathology. *Matrix Biol,* 21**,** 185-95.

Riley, G. P., Harrall, R. L., Constant, C. R., Chard, M. D., Cawston, T. E. & Hazleman, B. L. 1994a. Glycosaminoglycans of human rotator cuff tendons: changes with age and in chronic rotator cuff tendinitis. *Ann Rheum Dis,* 53**,** 367-76.

Riley, G. P., Harrall, R. L., Constant, C. R., Chard, M. D., Cawston, T. E. & Hazleman, B. L. 1994b. Tendon degeneration and chronic shoulder pain: changes in the collagen composition of the human rotator cuff tendons in rotator cuff tendinitis. *Ann Rheum Dis,* 53**,** 359-66.

Roberts, M. J., Bentley, M. D. & Harris, J. M. 2002. Chemistry for peptide and protein PEGylation. *Adv Drug Deliv Rev,* 54**,** 459-76.

Roca-Cusachs, P., del Rio, A., Puklin-Faucher, E., Gauthier, N. C., Biais, N. & Sheetz, M. P. 2013. Integrin-dependent force transmission to the extracellular matrix by alpha-actinin triggers adhesion maturation. *Proc Natl Acad Sci U S A,* 110**,** E1361-70.

Roca-Cusachs, P., Iskratsch, T. & Sheetz, M. P. 2012. Finding the weakest link: exploring integrin-mediated mechanical molecular pathways. *J Cell Sci,* 125**,** 3025-38.

Roche, A. J. & Calder, J. D. 2013. Achilles tendinopathy: A review of the current concepts of treatment. *Bone Joint J,* 95-B**,** 1299-307.

Ruoslahti, E. 1996. RGD and other recognition sequences for integrins. *Annu Rev Cell Dev Biol,* 12**,** 697-715.

Ruzzini, L., Abbruzzese, F., Rainer, A., Longo, U. G., Trombetta, M., Maffulli, N. & Denaro, V. 2014. Characterization of age-related changes of tendon stem cells from adult human tendons. *Knee Surg Sports Traumatol Arthrosc,* 22**,** 2856-66.

Salamone, J. C. 1996. *Polymeric Materials Encyclopedia, Twelve Volume Set*, Taylor & Francis.

Sarkar, S. K., Marmer, B., Goldberg, G. & Neuman, K. C. 2012. Single-molecule tracking of collagenase on native type I collagen fibrils reveals degradation mechanism. *Curr Biol,* 22**,** 1047-56.

Sasaki, N. & Odajima, S. 1996a. Elongation mechanism of collagen fibrils and force-strain relations of tendon at each level of structural hierarchy. *J Biomech,* 29**,** 1131-6.

Sasaki, N. & Odajima, S. 1996b. Stress-strain curve and Young's modulus of a collagen molecule as determined by the X-ray diffraction technique. *J Biomech,* 29**,** 655-8.

Scheller, J., Chalaris, A., Schmidt-Arras, D. & Rose-John, S. 2011. The pro- and anti-inflammatory properties of the cytokine interleukin-6. *Biochim Biophys Acta,* 1813**,** 878-88.

Schiraldi, C., D'Agostino, A., Oliva, A., Flamma, F., De Rosa, A., Apicella, A., Aversa, R. & De Rosa, M. 2004. Development of hybrid materials based on hydroxyethylmethacrylate as supports for improving cell adhesion and proliferation. *Biomaterials,* 25**,** 3645-53.

Schonherr 1995. Interaction of biglycan with type I collagen.

Schulze-Tanzil, G., Mobasheri, A., Clegg, P. D., Sendzik, J., John, T. & Shakibaei, M. 2004. Cultivation of human tenocytes in high-density culture. *Histochem Cell Biol,* 122**,** 219-28.

Schumacher, B. L., Block, J. A., Schmid, T. M., Aydelotte, M. B. & Kuettner, K. E. 1994. A novel proteoglycan synthesized and secreted by chondrocytes of the superficial zone of articular cartilage. *Arch Biochem Biophys,* 311**,** 144-52.

Schwartz, M. A. 2010. Integrins and extracellular matrix in mechanotransduction. *Cold Spring Harb Perspect Biol,* 2**,** a005066.

Schweitzer, R., Chyung, J. H., Murtaugh, L. C., Brent, A. E., Rosen, V., Olson, E. N., Lassar, A. & Tabin, C. J. 2001. Analysis of the tendon cell fate using Scleraxis, a specific marker for tendons and ligaments. *Development,* 128**,** 3855-66.

Scott, A. & Bahr, R. 2009. Neuropeptides in tendinopathy. *Front Biosci (Landmark Ed),* 14**,** 2203-11.

Scott, A., Danielson, P., Abraham, T., Fong, G., Sampaio, A. V. & Underhill, T. M. 2011. Mechanical force modulates scleraxis expression in bioartificial tendons. *J Musculoskelet Neuronal Interact,* 11**,** 124-32.

Screen, H. R. C., Byers, S. R., Lynn, A. D., Nguyen, V., Patel, D. & Bryant, S. J. 2010. Characterization of a Novel Fiber Composite Material for Mechanotransduction Research of Fibrous Connective Tissues. *Advanced Functional Materials,* 20**,** 738-747.

Screen, H. R. C., Lee, D. A., Bader, D. L. & Shelton, J. C. 2003. Development of a technique to determine strains in tendons using the cell nuclei. *Biorheology,* 40**,** 361-368.

Sechler, J. L., Corbett, S. A. & Schwarzbauer, J. E. 1997. Modulatory roles for integrin activation and the synergy site of fibronectin during matrix assembly. *Mol Biol Cell,* 8**,** 2563-73.

Sechler, J. L., Takada, Y. & Schwarzbauer, J. E. 1996. Altered rate of fibronectin matrix assembly by deletion of the first type III repeats. *J Cell Biol,* 134**,** 573-83.

Sein, M. L., Walton, J., Linklater, J., Appleyard, R., Kirkbride, B., Kuah, D. & Murrell, G. A. 2010. Shoulder pain in elite swimmers: primarily due to swim-volume-induced supraspinatus tendinopathy. *Br J Sports Med,* 44**,** 105-13.

Seitz, A. L., McClure, P. W., Finucane, S., Boardman, N. D., 3rd & Michener, L. A. 2011. Mechanisms of rotator cuff tendinopathy: intrinsic, extrinsic, or both? *Clin Biomech (Bristol, Avon),* 26**,** 1-12.

Sela-Passwell, N., Rosenblum, G., Shoham, T. & Sagi, I. 2010. Structural and functional bases for allosteric control of MMP activities: can it pave the path for selective inhibition? *Biochim Biophys Acta,* 1803**,** 29-38.

Seltzer, J. L. & Eisen, A. Z. 1999. Native Type I Collagen is Not a Substrate for MMP2 (Gelatinase A). 112**,** 993-993.

Sharabi, O., Shirian, J., Grossman, M., Lebendiker, M., Sagi, I. & Shifman, J. 2014. Affinity- and specificity-enhancing mutations are frequent in multispecific interactions between TIMP2 and MMPs. *PLoS One,* 9**,** e93712.

Sharma, P. & Maffulli, N. 2005. Tendon injury and tendinopathy: healing and repair. *J Bone Joint Surg Am,* 87**,** 187-202.

Shearn, J. T., Kinneberg, K. R., Dyment, N. A., Galloway, M. T., Kenter, K., Wylie, C. & Butler, D. L. 2011. Tendon tissue engineering: progress, challenges, and translation to the clinic. *J Musculoskelet Neuronal Interact,* 11**,** 163-73.

Shepherd, J. H., Riley, G. P. & Screen, H. R. 2014. Early stage fatigue damage occurs in bovine tendon fascicles in the absence of changes in mechanics at either the gross or micro-structural level. *J Mech Behav Biomed Mater,* 38**,** 163-72.

Shoulders, M. D. & Raines, R. T. 2009. Collagen structure and stability. *Annu Rev Biochem,* 78**,** 929-58.

Silver, F. H., Freeman, J. W. & Seehra, G. P. 2003. Collagen self-assembly and the development of tendon mechanical properties. *Journal of Biomechanics,* 36**,** 1529-1553.

Soboyejo, W. 2002. *Mechanical Properties of Engineered Materials*, CRC Press.

Sorensen, A. K., Bak, K., Krarup, A. L., Thune, C. H., Nygaard, M., Jorgensen, U., Sloth, C. & Torp-Pedersen, S. 2007. Acute rotator cuff tear: do we miss the early diagnosis? A prospective study showing a high incidence of rotator cuff tears after shoulder trauma. *J Shoulder Elbow Surg,* 16**,** 174-80.

Souza, L. M. d., Bittar, J. D., Silva, I. C. R. d., Toledo, O. A. d., Bírígido, M. d. M. & Poças-Fonseca, M. J. 2010. Comparative isolation protocols and characterization of stem cells from human primary and permanent teeth pulp. *Brazilian Journal of Oral Sciences,* 9**,** 427-433.

Speed, C. A. 2001. Fortnightly review: Corticosteroid injections in tendon lesions. *BMJ,* 323**,** 382-6.

Spiesz, E. M., Thorpe, C. T., Chaudhry, S., Riley, G. P., Birch, H. L., Clegg, P. D. & Screen, H. R. 2015. Tendon extracellular matrix damage, degradation and inflammation in response to in vitro overload exercise. *J Orthop Res,* 33**,** 889-97.

Steele, B. L., Alvarez-Veronesi, M. C. & Schmidt, T. A. 2013. Molecular weight characterization of PRG4 proteins using multi-angle laser light scattering (MALLS). *Osteoarthritis Cartilage,* 21**,** 498-504.

Steiner, T. H., Burki, A., Ferguson, S. J. & Gantenbein-Ritter, B. 2012. Stochastic amplitude-modulated stretching of rabbit flexor digitorum profundus tendons reduces stiffness compared to cyclic loading but does not affect tenocyte metabolism. *BMC Musculoskelet Disord,* 13**,** 222.

Steinmetz, N. J. & Bryant, S. J. 2011. The effects of intermittent dynamic loading on chondrogenic and osteogenic differentiation of human marrow stromal cells encapsulated in RGD-modified poly(ethylene glycol) hydrogels. *Acta Biomater,* 7**,** 3829-40.

Sun, H. B., Andarawis-Puri, N., Li, Y., Fung, D. T., Lee, J. Y., Wang, V. M., Basta-Pljakic, J., Leong, D. J., Sereysky, J. B., Ros, S. J., Klug, R. A., Braman, J., Schaffler, M. B., Jepsen, K. J. &

Flatow, E. L. 2010. Cycle-dependent matrix remodeling gene expression response in fatigue-loaded rat patellar tendons. *J Orthop Res,* 28**,** 1380-6.

Sun, Y., Berger, E. J., Zhao, C., Jay, G. D., An, K. N. & Amadio, P. C. 2006. Expression and mapping of lubricin in canine flexor tendon. *J Orthop Res,* 24**,** 1861-8.

Sun, Y. J., Wei, G., Song, Y. H., Wang, L., Sun, L. L., Guo, C. L., Yang, T. & Li, Z. 2008. Type I collagen-templated assembly of silver nanoparticles and their application in surface-enhanced Raman scattering. *Nanotechnology,* 19.

Svensson, R. B., Hansen, P., Hassenkam, T., Haraldsson, B. T., Aagaard, P., Kovanen, V., Krogsgaard, M., Kjaer, M. & Magnusson, S. P. 2012. Mechanical properties of human patellar tendon at the hierarchical levels of tendon and fibril. *J Appl Physiol (1985),* 112**,** 419-26.

Szomor, Z. L., Appleyard, R. C. & Murrell, G. A. 2006. Overexpression of nitric oxide synthases in tendon overuse. *J Orthop Res,* 24**,** 80-6.

Taddei, P., Balducci, F., Simoni, R. & Monti, P. 2005. Raman, IR and thermal study of a new highly biocompatible phosphorylcholine-based contact lens. *Journal of Molecular Structure,* 744-747**,** 507-514.

Takahashi, S., Leiss, M., Moser, M., Ohashi, T., Kitao, T., Heckmann, D., Pfeifer, A., Kessler, H., Takagi, J., Erickson, H. P. & Fassler, R. 2007. The RGD motif in fibronectin is essential for development but dispensable for fibril assembly. *J Cell Biol,* 178**,** 167-78.

Tallon, C., Coleman, B. D., Khan, K. M. & Maffulli, N. 2001a. Outcome of surgery for chronic Achilles tendinopathy. A critical review. *Am J Sports Med,* 29**,** 315-20.

Tallon, C., Maffulli, N. & Ewen, S. W. 2001b. Ruptured Achilles tendons are significantly more degenerated than tendinopathic tendons. *Med Sci Sports Exerc,* 33**,** 1983-90.

Tam, E. M., Moore, T. R., Butler, G. S. & Overall, C. M. 2004. Characterization of the distinct collagen binding, helicase and cleavage mechanisms of matrix metalloproteinase 2 and 14 (gelatinase A and MT1-MMP): the differential roles of the MMP hemopexin c domains and the MMP-2 fibronectin type II modules in collagen triple helicase activities. *J Biol Chem,* 279**,** 43336-44.

Tanaka, K., Iwasaki, K., Feghali, K. E., Komaki, M., Ishikawa, I. & Izumi, Y. 2011. Comparison of characteristics of periodontal ligament cells obtained from outgrowth and enzyme-digested culture methods. *Arch Oral Biol,* 56**,** 380-8.

Taubenberger, A. V., Woodruff, M. A., Bai, H., Muller, D. J. & Hutmacher, D. W. 2010. The effect of unlocking RGD-motifs in collagen I on pre-osteoblast adhesion and differentiation. *Biomaterials,* 31**,** 2827-35.

Thermo Fisher Scientific 2010. *Nucleic Acid*.

Thorpe, C. T., Birch, H. L., Clegg, P. D. & Screen, H. R. 2013a. The role of the non-collagenous matrix in tendon function. *Int J Exp Pathol,* 94**,** 248-59.

Thorpe, C. T., Chaudhry, S., Lei, II, Varone, A., Riley, G. P., Birch, H. L., Clegg, P. D. & Screen, H. R. 2015a. Tendon overload results in alterations in cell shape and increased markers of inflammation and matrix degradation. *Scand J Med Sci Sports,* 25**,** e381-91.

Thorpe, C. T., Godinho, M. S., Riley, G. P., Birch, H. L., Clegg, P. D. & Screen, H. R. 2015b. The interfascicular matrix enables fascicle sliding and recovery in tendon, and behaves more elastically in energy storing tendons. *J Mech Behav Biomed Mater*.

Thorpe, C. T., Klemt, C., Riley, G. P., Birch, H. L., Clegg, P. D. & Screen, H. R. 2013b. Helical sub-structures in energy-storing tendons provide a possible mechanism for efficient energy storage and return. *Acta Biomater,* 9**,** 7948-56.

Thorpe, C. T., Riley, G. P., Birch, H. L., Clegg, P. D. & Screen, H. R. 2014. Effect of fatigue loading on structure and functional behaviour of fascicles from energy-storing tendons. *Acta Biomater,* 10**,** 3217-24.

Thorpe, C. T., Spiesz, E. M., Chaudhry, S., Screen, H. R. & Clegg, P. D. 2015c. Science in brief: recent advances into understanding tendon function and injury risk. *Equine Vet J,* 47**,** 137-40.

Thorpe, C. T., Udeze, C. P., Birch, H. L., Clegg, P. D. & Screen, H. R. 2012. Specialization of tendon mechanical properties results from interfascicular differences. *J R Soc Interface,* 9**,** 3108-17.

Thorpe, C. T., Udeze, C. P., Birch, H. L., Clegg, P. D. & Screen, H. R. 2013c. Capacity for sliding between tendon fascicles decreases with ageing in injury prone equine tendons: a possible mechanism for age-related tendinopathy? *Eur Cell Mater,* 25**,** 48-60.

Tilley, J. M., Chaudhury, S., Hakimi, O., Carr, A. J. & Czernuszka, J. T. 2012. Tenocyte proliferation on collagen scaffolds protects against degradation and improves scaffold properties. *J Mater Sci Mater Med,* 23**,** 823-33.

Torres, D. S., Freyman, T. M., Yannas, I. V. & Spector, M. 2000. Tendon cell contraction of collagen-GAG matrices in vitro: effect of cross-linking. *Biomaterials,* 21**,** 1607-19.

Tsubone, T., Moran, S. L., Subramaniam, M., Amadio, P. C., Spelsberg, T. C. & An, K. N. 2006. Effect of TGF-beta inducible early gene deficiency on flexor tendon healing. *J Orthop Res,* 24**,** 569-75.

Uria, J. A. & Lopez-Otin, C. 2000. Matrilysin-2, a new matrix metalloproteinase expressed in human tumors and showing the minimal domain organization required for secretion, latency, and activity. *Cancer Res,* 60**,** 4745-51.

Vader, D., Kabla, A., Weitz, D. & Mahadevan, L. 2009. Strain-induced alignment in collagen gels. *PLoS One,* 4**,** e5902.

van der Plas, A., de Jonge, S., de Vos, R. J., van der Heide, H. J., Verhaar, J. A., Weir, A. & Tol, J. L. 2012. A 5-year follow-up study of Alfredson's heel-drop exercise programme in chronic midportion Achilles tendinopathy. *Br J Sports Med,* 46**,** 214-8.

Vesentini, S., Redaelli, A. & Montevecchi, F. M. 2005. Estimation of the binding force of the collagen molecule-decorin core protein complex in collagen fibril. *J Biomech,* 38**,** 433-43.

Visse, R. & Nagase, H. 2003. Matrix metalloproteinases and tissue inhibitors of metalloproteinases: structure, function, and biochemistry. *Circ Res,* 92**,** 827-39.

Vozzi, G., Flaim, C. J., Bianchi, F., Ahluwalia, A. & Bhatia, S. 2002. Microfabricated PLGA scaffolds: a comparative study for application to tissue engineering. *Materials Science and Engineering: C,* 20**,** 43-47.

Wagenhauser, M. U., Pietschmann, M. F., Sievers, B., Docheva, D., Schieker, M., Jansson, V. & Muller, P. E. 2012. Collagen type I and decorin expression in tenocytes depend on the cell isolation method. *BMC Musculoskelet Disord,* 13**,** 140.

Wall, M. E. & Banes, A. J. 2005. Early responses to mechanical load in tendon: role for calcium signaling, gap junctions and intercellular communication. *J Musculoskelet Neuronal Interact,* 5**,** 70-84.

Wang, J. H. 2006. Mechanobiology of tendon. *J Biomech,* 39**,** 1563-82.

Waugh, C. M., Morrissey, D., Jones, E., Riley, G. P., Langberg, H. & Screen, H. R. 2015. In vivo biological response to extracorporeal shockwave therapy in human tendinopathy. *Eur Cell Mater,* 29**,** 268-80; discussion 280.

Weber, L. M., Hayda, K. N., Haskins, K. & Anseth, K. S. 2007. The effects of cell-matrix interactions on encapsulated beta-cell function within hydrogels functionalized with matrix-derived adhesive peptides. *Biomaterials,* 28**,** 3004-11.

Wnek, G. E. & Bowlin, G. L. 2004. *Encyclopaedia of Biomaterials and Biomedical Engineering; Tissue Engineering of Tendons. Tenth Edition*.

Wojtowicz, A. M., Shekaran, A., Oest, M. E., Dupont, K. M., Templeman, K. L., Hutmacher, D. W., Guldberg, R. E. & Garcia, A. J. 2010. Coating of biomaterial scaffolds with the collagen-mimetic peptide GFOGER for bone defect repair. *Biomaterials,* 31**,** 2574-82.

Woo, S. L. Y., Renström, P. & Arnoczky, S. P. 2007. *Tendinopathy in athletes,* Oxford, Blackwell.

Wu, J. J. & Eyre, D. R. 1995. Structural analysis of cross-linking domains in cartilage type XI collagen. Insights on polymeric assembly. *J Biol Chem,* 270**,** 18865-70.

Xia, W., Szomor, Z., Wang, Y. & Murrell, G. A. 2006. Nitric oxide enhances collagen synthesis in cultured human tendon cells. *J Orthop Res,* 24**,** 159-72.

Xie, J., Zhang, Q., Zhu, T., Zhang, Y., Liu, B., Xu, J. & Zhao, H. 2014. Substrate stiffness-regulated matrix metalloproteinase output in myocardial cells and cardiac fibroblasts: implications for myocardial fibrosis. *Acta Biomater,* 10**,** 2463-72.

Yamada, M., Tohno, Y., Takakura, Y., Tohno, S., Moriwake, Y. & Minami, T. 2003. Age-related changes of element contents in human tendon of the iliopsoas muscle and the relationships among elements. *Biol Trace Elem Res,* 91**,** 57-66.

Yamamoto, M., Yamato, M., Aoyagi, M. & Yamamoto, K. 1995. Identification of integrins involved in cell adhesion to native and denatured type I collagens and the phenotypic transition of rabbit arterial smooth muscle cells. *Exp Cell Res,* 219**,** 249-56.

Yang, F., Williams, C. G., Wang, D. A., Lee, H., Manson, P. N. & Elisseeff, J. 2005. The effect of incorporating RGD adhesive peptide in polyethylene glycol diacrylate hydrogel on osteogenesis of bone marrow stromal cells. *Biomaterials,* 26**,** 5991-8.

Yang, G., Crawford, R. C. & Wang, J. H. 2004. Proliferation and collagen production of human patellar tendon fibroblasts in response to cyclic uniaxial stretching in serum-free conditions. *J Biomech,* 37**,** 1543-50.

Yang, Y. L., Leone, L. M. & Kaufman, L. J. 2009. Elastic moduli of collagen gels can be predicted from two-dimensional confocal microscopy. *Biophys J,* 97**,** 2051-60.

Yang, Y. L., Motte, S. & Kaufman, L. J. 2010. Pore size variable type I collagen gels and their interaction with glioma cells. *Biomaterials,* 31**,** 5678-88.

Yao, L., Bestwick, C. S., Bestwick, L. A., Maffulli, N. & Aspden, R. M. 2006. Phenotypic drift in human tenocyte culture. *Tissue Eng,* 12**,** 1843-9.

Yoon, J. H. & Halper, J. 2005. Tendon proteoglycans: biochemistry and function. *J Musculoskelet Neuronal Interact,* 5**,** 22-34.

Zhang, J. & Wang, J. H. 2010a. Characterization of differential properties of rabbit tendon stem cells and tenocytes. *BMC Musculoskelet Disord,* 11**,** 10.

Zhang, J. & Wang, J. H. 2010b. Mechanobiological response of tendon stem cells: implications of tendon homeostasis and pathogenesis of tendinopathy. *J Orthop Res,* 28**,** 639-43.

Zhang, J. & Wang, J. H. 2013. Human tendon stem cells better maintain their stemness in hypoxic culture conditions. *PLoS One,* 8**,** e61424.

Zhang, X. L., Topley, N., Ito, T. & Phillips, A. 2005. Interleukin-6 regulation of transforming growth factor (TGF)-beta receptor compartmentalization and turnover enhances TGF-beta1 signaling. *J Biol Chem,* 280**,** 12239-45.

Zhu, J. 2010. Bioactive modification of poly(ethylene glycol) hydrogels for tissue engineering. *Biomaterials,* 31**,** 4639-56.

Appendix A: Human cell source and ethics

Human tenocytes ranging from passage 2 to passage 4 were provided by Dr Graham Riley from the Biomedical Research Centre, University of East Anglia, which were originally obtained by his group under ethical approval (REC reference 09/H0302/3). As primary human tenocytes were not handled or used in the studies described in the current thesis, the cells were not considered relevant material by the Human Tissue Authority (HTA) under the Human Tissue Act 2004, and consequently a tissue storage licence was not required for use of said material at Queen Mary University of London.

Table 34: Details of the human cells and their use in the thesis.

Tenocyte Type	Tendon Source	Donor Age	Donor Sex	Use and Other Details
Healthy	Achilles Tendon	76	M	Chapter 3 – used for preliminary stable gene expression study.
Healthy	Hamstring Tendon	22	M	Chapter 4 – used for shear-tension ratio study.
Healthy	Hamstring Tendon	19	F	Chapter 4 – used for shear-tension ratio study.
Tendinopathic	Achilles Tendon	51	M	Chapter 4 – used for shear-tension ratio study. 2 year duration tendinopathy.
Tendinopathic	Achilles Tendon	45	M	Chapter 4 – used for shear-tension ratio study. More than 18 month duration tendinopathy.

Appendix B: Chemicals and Materials List

Table 35: Chemical and material list, part 1 of 2.

Chemical or Material	Abbrev.	Supplier	Product no.
1-1' Carbonyl Diimidazole	CDI	Sigma Aldrich	115533
24 well plates, Non-tissue culture treated		Sigma Aldrich	CLS3738
2-hydroxyethyl methacrylate	HEMA	Polysciences Inc.	04675
3-morpholinopropanesulfonic acid	MOPS buffer	Sigma Aldrich	PHG0007
4-(dimethylamino) pyridine		Sigma Aldrich	107700
48 well plates, Non-tissue culture treated		Fisher Scientific	08-772-52
6 well plates, sterile		Sigma Aldrich	SIAL0516
Acrylate-PEG-NHS		JenKem Technology	A5022-1
Agarose		Sigma Aldrich	A9539
Aspartic Acid-Glycine-Glutamic Acid-Alanine	DGEA	GenScript	Custom peptide
Bovine Serum Albumin	BSA	Sigma Aldrich	A3311
Calcein AM		Life Technologies	C1430
Cell Strainer, 100um		Life Technologies	431752
Chloroform		Sigma Aldrich	C2432
Collagen Type I (Rat tail)		BD Biosciences	354236
Collagenase Type 2		Worthington Biochemical Corp.	CLS-2
Conical tube, 50 mL		Sigma Aldrich	CLS430897
Corning Glass slides (75x25x1mm), Clear non-frosted		Sigma Aldrich	CLS294775X25
Cryovials, 1.2 mL		Sigma Aldrich	V4757
DAPI (4',6-Diamidino-2-Phenylindole, Dilactate)	DAPI	Life Technologies	D3571
Deoxynucleotide, 10mM	dNTPs	Promega	U1515
Dialysis membrane, MWCO 500:1000		Spectrum Laboratories Inc.	734-0549
Dichloromethane		Sigma Aldrich	D65100
Diethyl Ether		VWR International	23809.328
Diethylpyrocarbonate	DEPC	Sigma Aldrich	D5758
Dimethyl Sulfoxide	DMSO	Sigma Aldrich	276855
Dispase Solution, 1U/mL		STEMCELL technologies	07923
Disposable Pestle		Sigma Aldrich	Z359947
Dry Acetone, water-free		Sigma Aldrich	650501
Dulbecco's Modified Eagle Medium with GlutaMAX, low glucose	DMEM-G	Life Technologies	21885
Dulbecco's Modified Eagle Medium, low glucose	DMEM	Life Technologies	11880
Ethanol, 200 proof		Sigma Aldrich	E7023
Ethidium Homodimer		Life Technologies	E1169
Ethylene glycol		Sigma Aldrich	10246-6
FastStart Universal SYBR Green Master		Roche Life Science	04913850001
Fluoraldehyde O-phthalaldehyde	OPA	Thermo Scientific	PN26025
Fluorescein O-methacrylate		Sigma Aldrich	568864
Foetal Bovine Serum	FBS	Sigma Aldrich	F7524
Formaldehyde loading dye		Sigma Aldrich	R4268-5VL

Table 36: Chemical and material list, part 2 of 2.

Chemical or Material	Abbrev.	Supplier	Product no.
Glycogen		Sigma Aldrich	AM9510
HEPES, 1M		Sigma Aldrich	H0887
Hydroquinone		Sigma Aldrich	H9003
Irgacure 2959		Ciba Speciality Chemicals	Irgacure2959
Irgacure 651		Ciba Speciality Chemicals	Irgacure651
Isopropanol		Sigma Aldrich	I9516
KAPA Universal qPCR kit		Anachem	KK4702
L-Glutamine, 200mM		Sigma Aldrich	G7513
Loctite Power Flex Control Gel		RS Components	330-4018
Methacrylic Anhydride	MA	Sigma Aldrich	27668-5
MultiScribe Transcriptase Kit (including 10x sample buffer, Deoxynucleotide triphosphates, 25x RT Random Primers)		Life Technologies	4368814
N,N'-Dissucinimidyl Carbonate	DSC	Sigma Aldrich	225827
Non-essential amino acids	NEAA	Sigma Aldrich	M7145
Paraformaldehyde		Sigma Aldrich	P6148
Penicillin/Streptomycin, 10000U/10mg per mL	Pen/Strep	Sigma Aldrich	P4333
Phalloidin (Alexa Fluor 488)		Life Technologies	A12379
Phase Lock Gel Heavy		5 Prime	232830
Phosphate buffered saline	PBS	Sigma Aldrich	P5368
Polyethylene glycol (MW3000)	PEGDM	Merck Schuchardt	8.19015.1000
Primers and Probes		Life Technologies	Custom order
QIAgen MiRneasy Micro Kit (including QIAzol lysis reagent and MinElute Spin Columns)		QIAgen	217084
QIAshredder		QIAgen	79654
Random Hexomers		Life Technologies	48190-011
Rhodamine methacrylate		Polysciences Inc.	23591
RNase Free Water		Sigma Aldrich	W4502
RNasin ribonuclease inhibitor		Promega	N2511
Sodium Bicarbonate		Sigma Aldrich	S-8875
Superscript II Kit, 200U/µL (including Dithiothreitol (DTT) and 5X Sample Buffer)		Life Technologies	18064-014
Syringe filters, 0.22 µm		Merck Millipore	10497342
TaqMan Low Density Array Cards, 48 gene layout	TLDA cards	Life Technologies	4342253
TaqMan Universal PCR Master Mix		Life Technologies	4324018
Tetraethylene glycol dimethacrylate	TEGDM	Polysciences Inc.	02654
Tissue culture flasks, filter cap		Sigma Aldrich	C7481
Triton X-100		Sigma Aldrich	X100
Trizol (Tri-reagent)		Sigma Aldrich	15596-026
Trypan Blue		Sigma Aldrich	T8154
Trypsin-EDTA (1X concentration)		Sigma Aldrich	T3924
Tyrosine-Arginine-Glycine-Aspartic acid-Serine	YRGDS	GenScript	Custom peptide

Appendix C: Additional shear-tension ratio graphs (2ΔCt)

Collagens – Tendinopathic Tenocytes

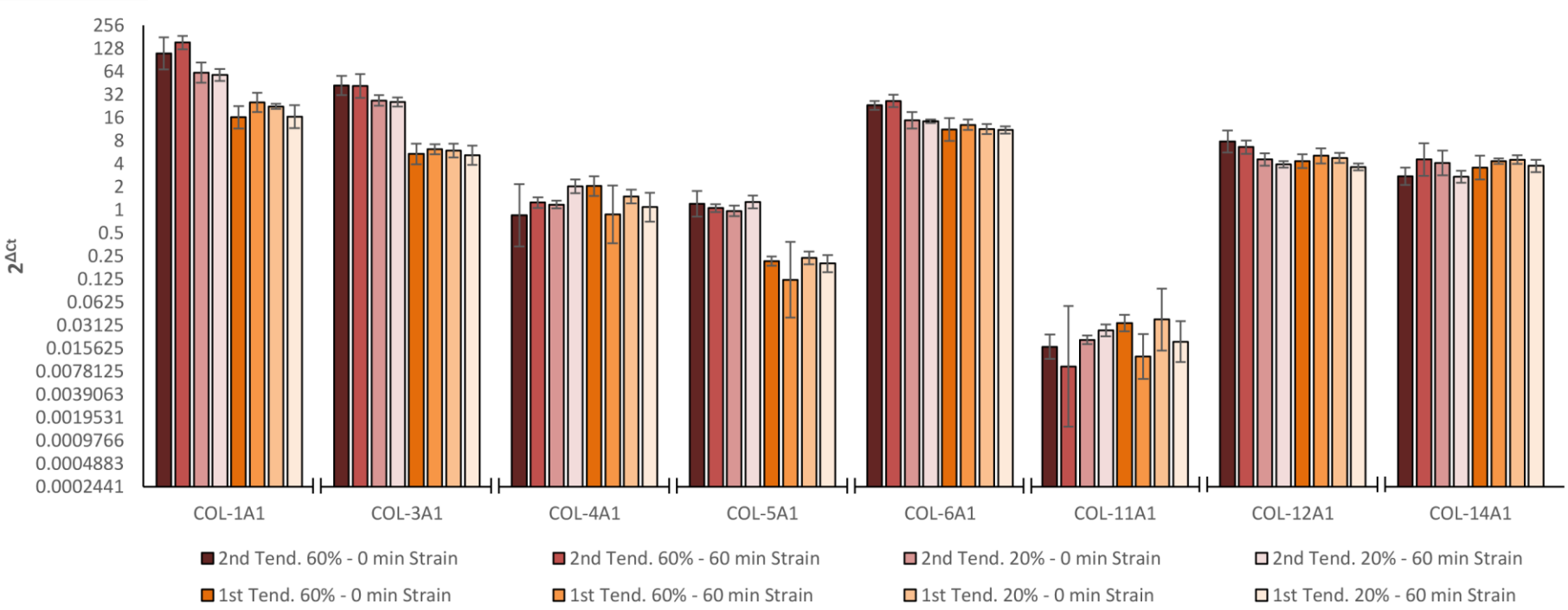

Figure 89: Average collagen gene expression for strained composites with tendinopathic tenocytes. Expression shown as $2^{\Delta Ct}$ (normalised to TOP-1) and both shown separately. Error bars represent standard deviations. Data labelled as 'XX. YY – ZZ strain', where XX is either '1st Tend.' Or '2nd Tend.' representing the donor, 'YY' indicates the fibre type and 'ZZ' indicates the soak time. n=6 per composite type.

Collagen – Healthy Tenocytes

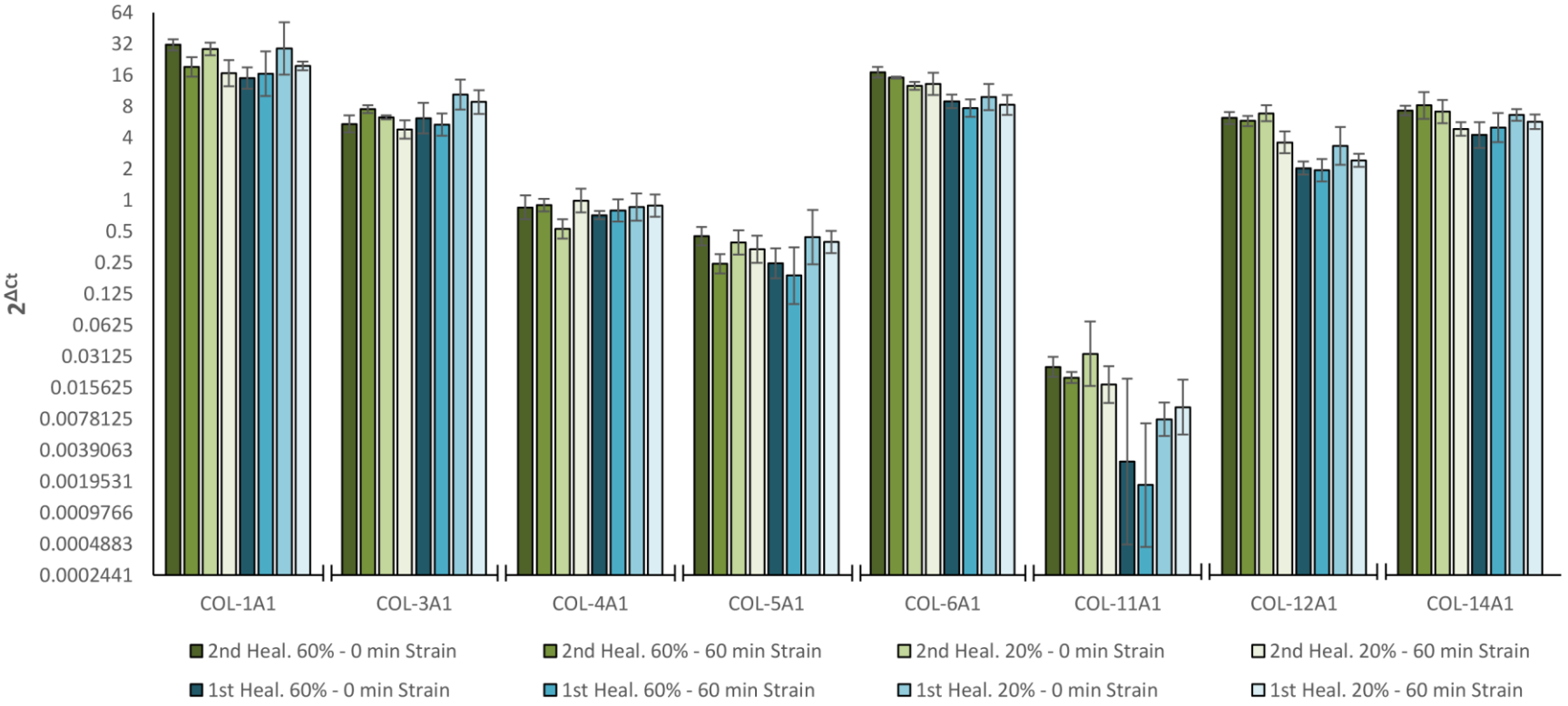

Figure 90: Average collagen gene expression for strained composites with healthy tenocytes. Expression shown as $2^{\Delta Ct}$ (normalised to TOP-1) and both shown separately. Error bars represent standard deviations. Data labelled as 'XX. YY – ZZ strain', where XX is either '1st Heal.' Or '2nd Heal.' representing the donor, 'YY' indicates the fibre type and 'ZZ' indicates the soak time. n=6 per composite type.

MMPs – Tendinopathic Tenocytes

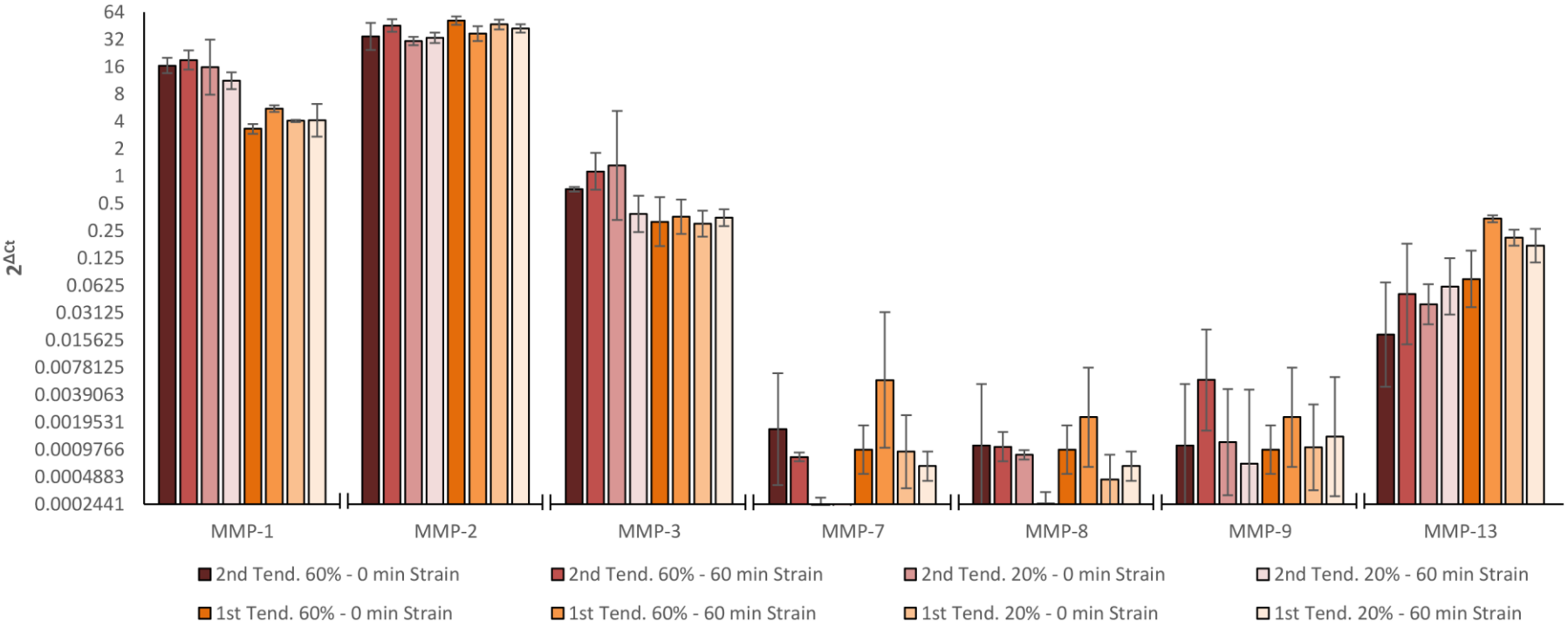

Figure 91: Average MMP gene expression for strained composites with tendinopathic tenocytes. Expression shown as $2^{\Delta Ct}$ (normalised to TOP-1) and both shown separately. Error bars represent standard deviations. Data labelled as '1st Tend.' Or '2nd Tend.' representing the donor, 'YY' indicates the fibre type and 'ZZ' indicates the soak time. n=6 per composite type.

MMPs – Healthy Tenocytes

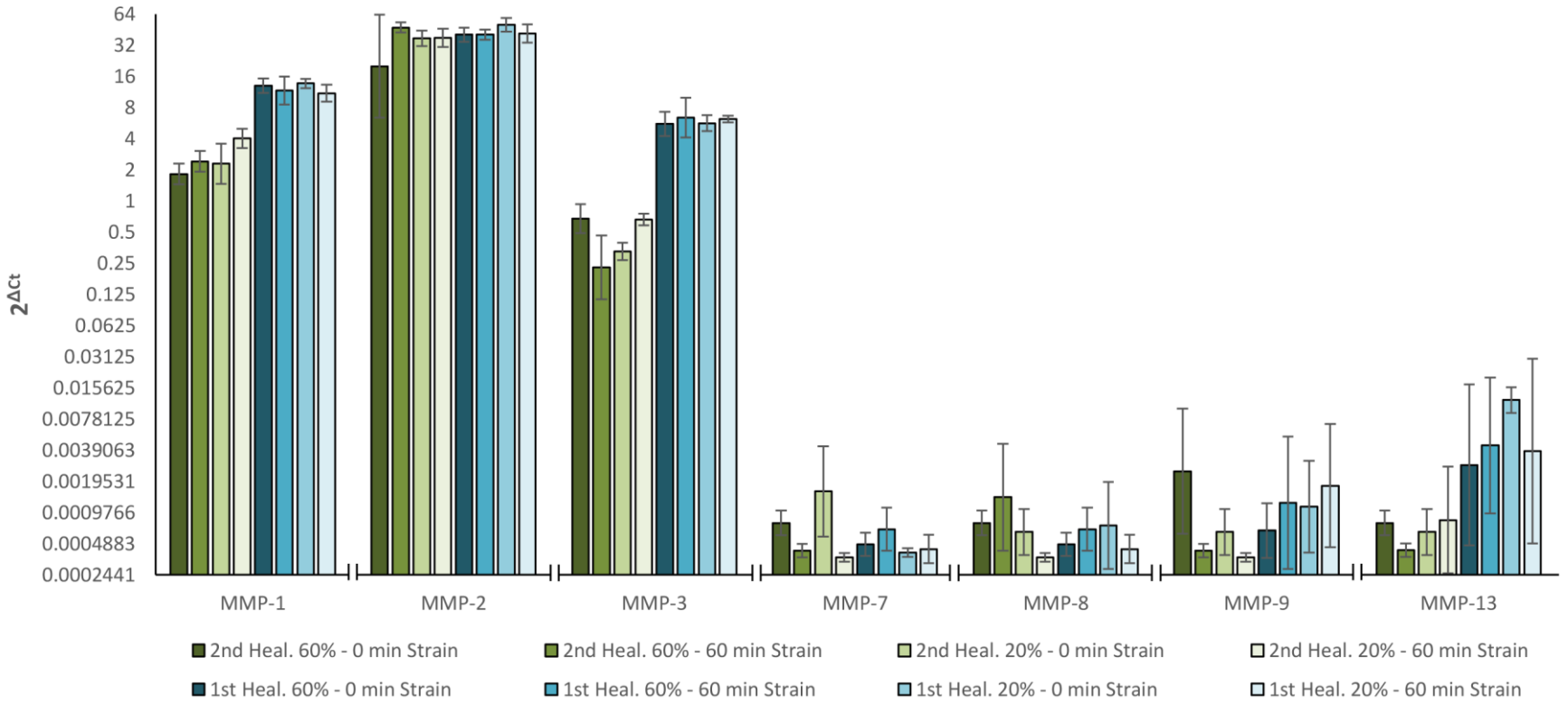

Figure 92: Average MMP gene expression for strained composites with healthy tenocytes. Expression shown as $2^{\Delta Ct}$ (normalised to TOP-1) and both shown separately. Error bars represent standard deviations. Data labelled as 'XX. YY – ZZ strain', where XX is either '1st Heal.' Or '2nd Heal.' representing the donor, 'YY' indicates the fibre type and 'ZZ' indicates the soak time. n=6 per composite type.

ADAMTSs – Tendinopathic Tenocytes

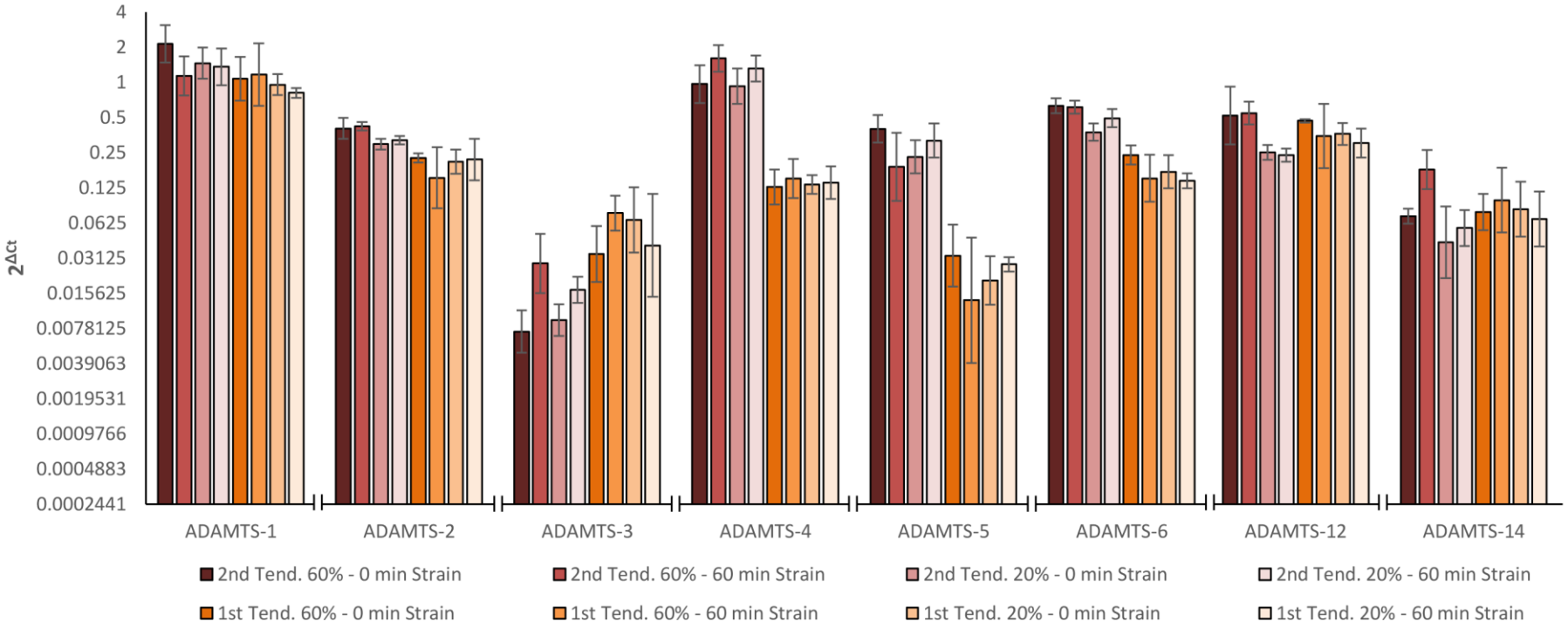

Figure 93: Average ADAMTS gene expression for strained composites with tendinopathic tenocytes. Expression shown as $2^{\Delta Ct}$ (normalised to TOP-1) and both shown separately. Error bars represent standard deviations. Data labelled as 'XX. YY – ZZ strain', where XX is either '1st Tend.' Or '2nd Tend.' representing the donor, 'YY' indicates the fibre type and 'ZZ' indicates the soak time. n=6 per composite type.

ADAMTSs – Healthy Tenocytes

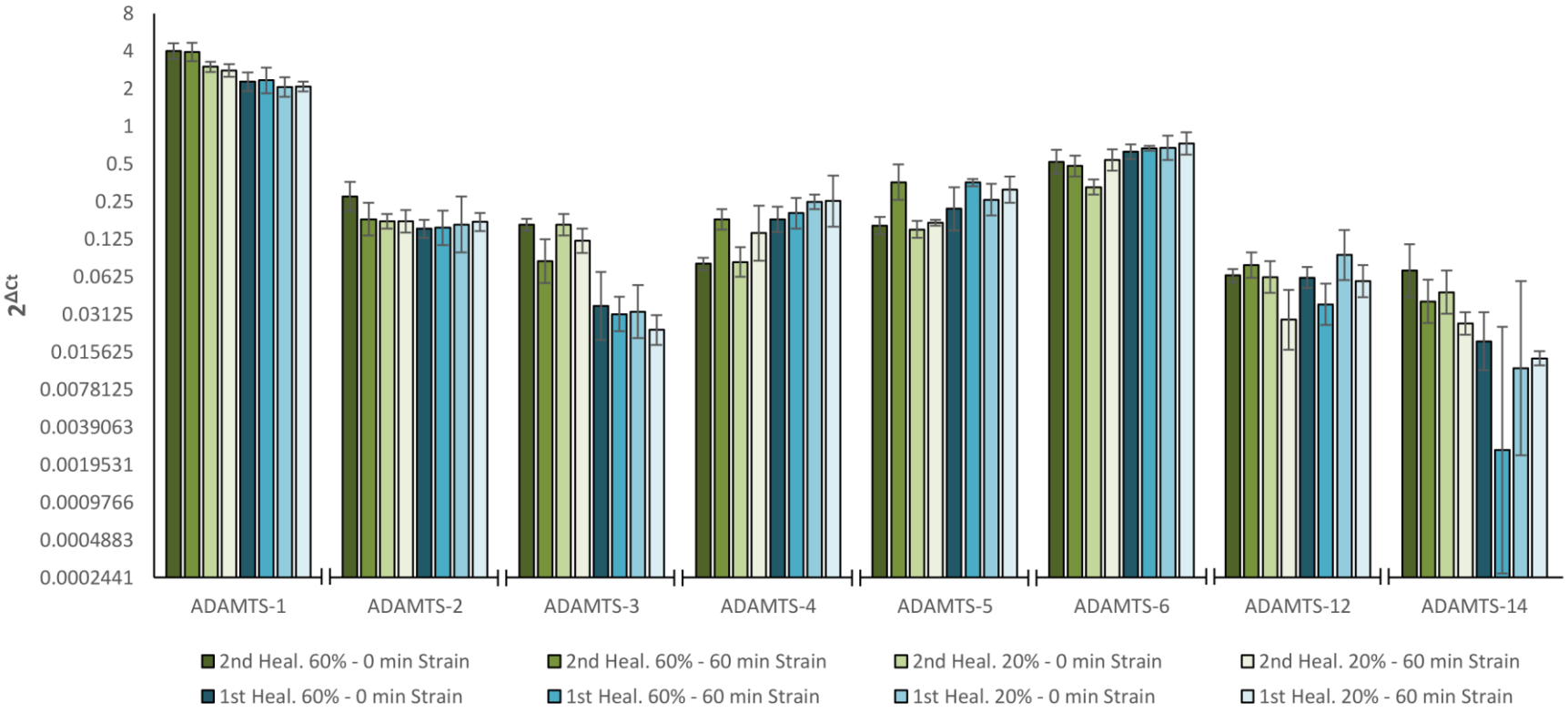

Figure 94: Average ADAMTS gene expression for strained composites with healthy tenocytes. Expression shown as $2^{\Delta Ct}$ (normalised to TOP-1) and both shown separately. Error bars represent standard deviations. Data labelled as 'XX. YY – ZZ strain', where XX is either '1st Heal.' Or '2nd Heal.' representing the donor, 'YY' indicates the fibre type and 'ZZ' indicates the soak time. n=6 per composite type.

TIMPs – Tendinopathic Tenocytes

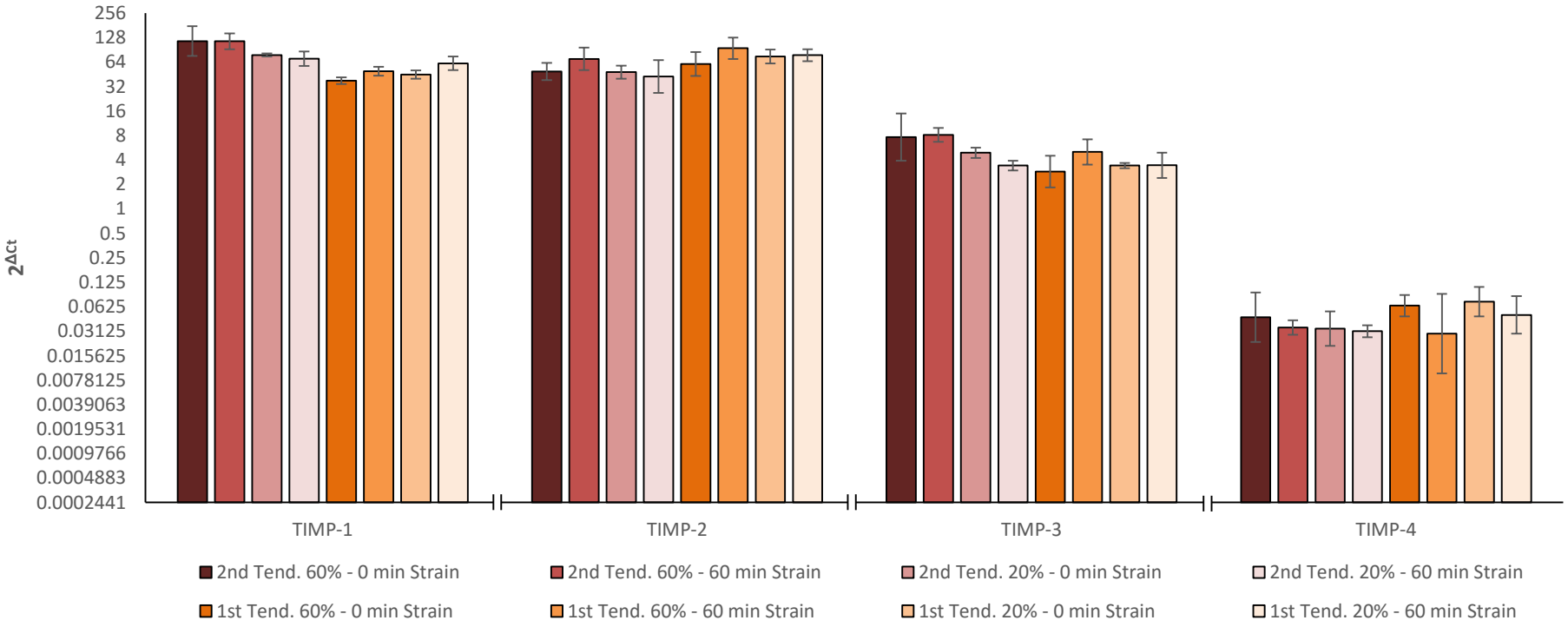

Figure 95: Average TIMP gene expression for strained composites with tendinopathic tenocytes. Expression shown as $2^{\Delta Ct}$ (normalised to TOP-1) and both shown separately. Error bars represent standard deviations. Data labelled as 'XX. YY – ZZ strain', where XX is either '1st Tend.' Or '2nd Tend.' representing the donor, 'YY' indicates the fibre type and 'ZZ' indicates the soak time. n=6 per composite type.

TIMPs – Healthy Tenocytes

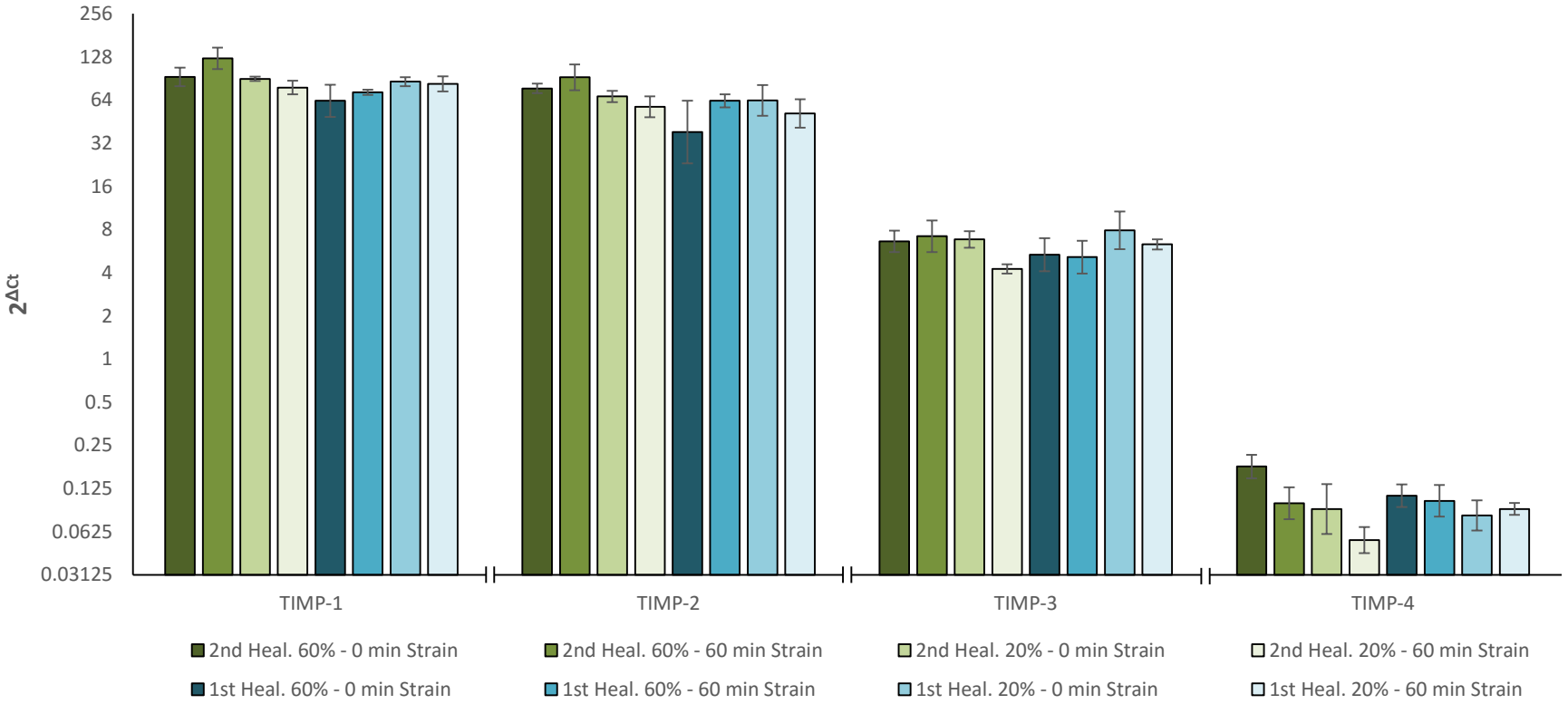

Figure 96: Average TIMP gene expression for strained composites with healthy tenocytes. Expression shown as $2^{\Delta Ct}$ (normalised to TOP-1) and both shown separately. Error bars represent standard deviations. Data labelled as 'XX. YY – ZZ strain', where XX is either '1st Heal.' Or '2nd Heal.' representing the donor, 'YY' indicates the fibre type and 'ZZ' indicates the soak time. n=6 per composite type.

Interleukins – Tendinopathic Tenocytes

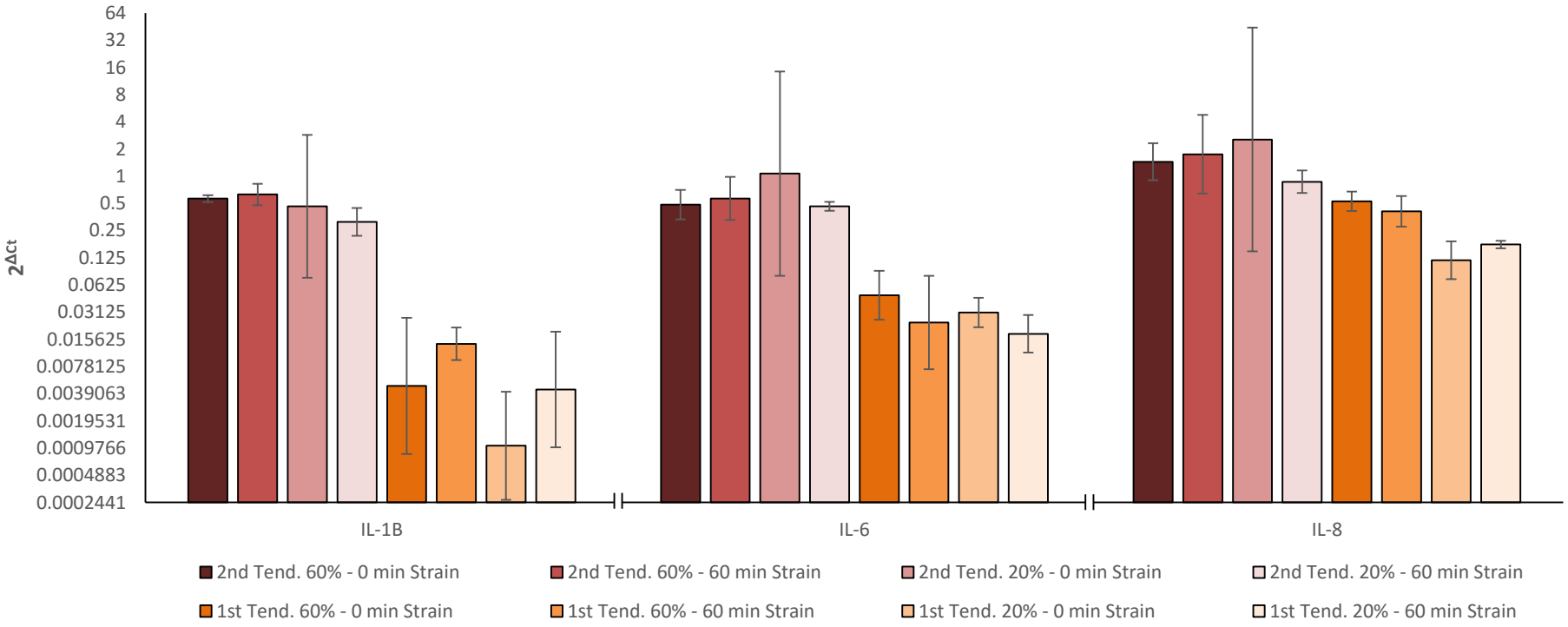

Figure 97: Average interleukin gene expression for strained composites with tendinopathic tenocytes. Expression shown as $2^{\Delta Ct}$ (normalised to TOP-1) and both shown separately. Error bars represent standard deviations. Data labelled as '1st Tend.' Or '2nd Tend.' representing the donor, 'YY' indicates the fibre type and 'ZZ' indicates the soak time. n=6 per composite type.

Interleukins – Healthy Tenocytes

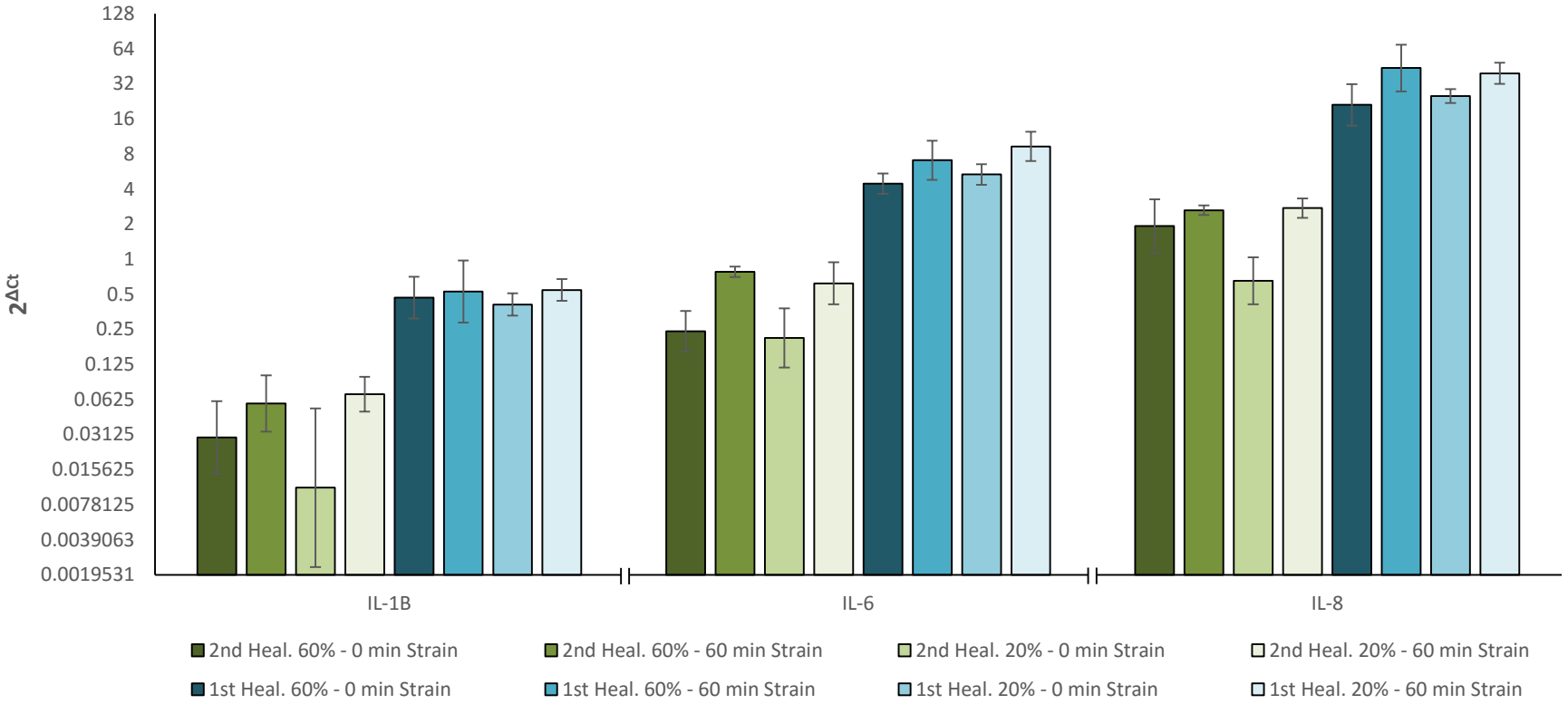

Figure 98: Average interleukin gene expression for strained composites with healthy tenocytes. Expression shown as $2^{\Delta Ct}$ (normalised to TOP-1) and both shown separately. Error bars represent standard deviations. Data labelled as 'XX. YY – ZZ strain', where XX is either '1st Heal.' Or '2nd Heal.' representing the donor, 'YY' indicates the fibre type and 'ZZ' indicates the soak time. n=6 per composite type.

Proteoglycans – Tendinopathic Tenocytes

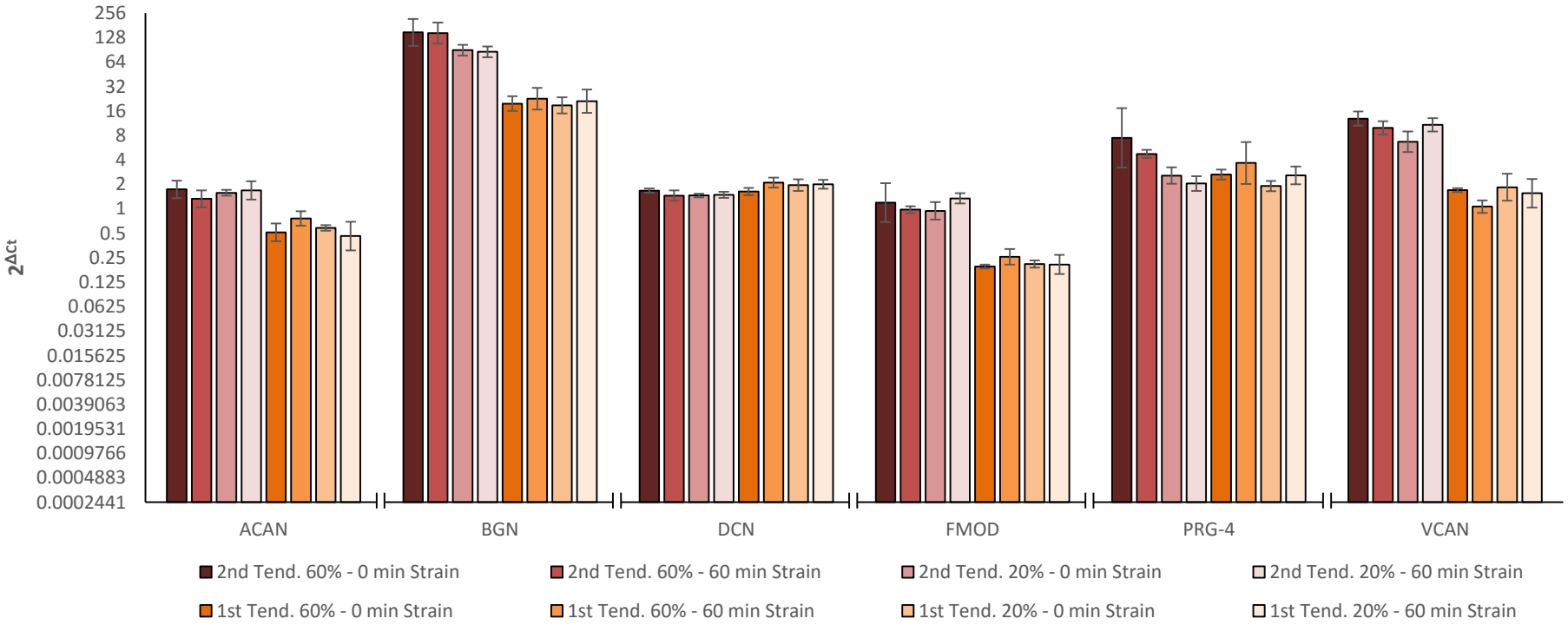

Figure 99: Average proteoglycan gene expression for strained composites with tendinopathic tenocytes. Expression shown as $2^{\Delta Ct}$ (normalised to TOP-1) and both shown separately. Error bars represent standard deviations. Data labelled as 'XX. YY – ZZ strain', where XX is either '1st Tend.' Or '2nd Tend.' representing the donor, 'YY' indicates the fibre type and 'ZZ' indicates the soak time. n=6 per composite type.

Proteoglycans – Healthy Tenocytes

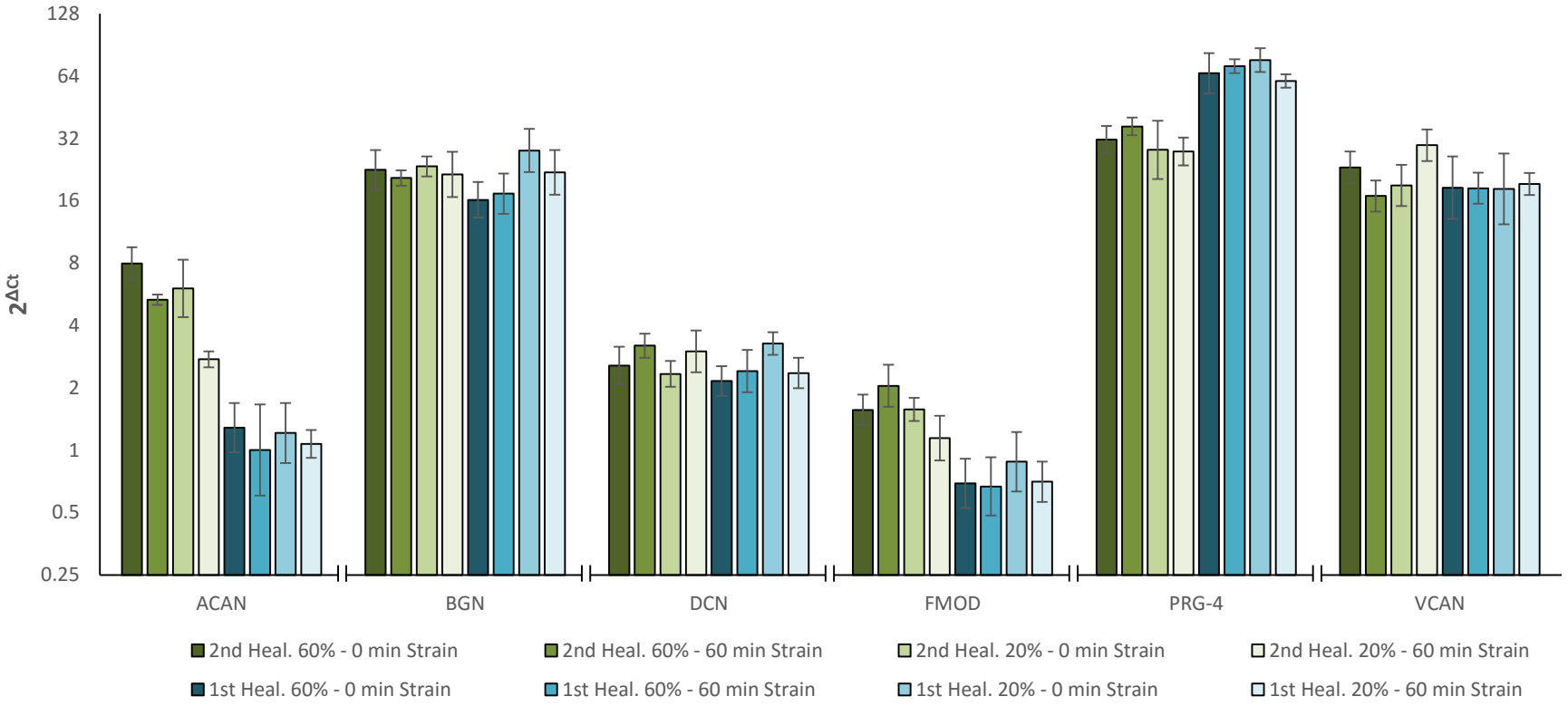

Figure 100: Average Proteoglycan gene expression for strained composites with healthy tenocytes. Expression shown as $2^{\Delta Ct}$ (normalised to TOP-1) and both shown separately. Error bars represent standard deviations. Data labelled as 'XX. YY – ZZ strain', where XX is either '1st Heal.' Or '2nd Heal.' representing the donor, 'YY' indicates the fibre type and 'ZZ' indicates the soak time. n=6 per composite type.

Other Proteins – Tendinopathic Tenocytes

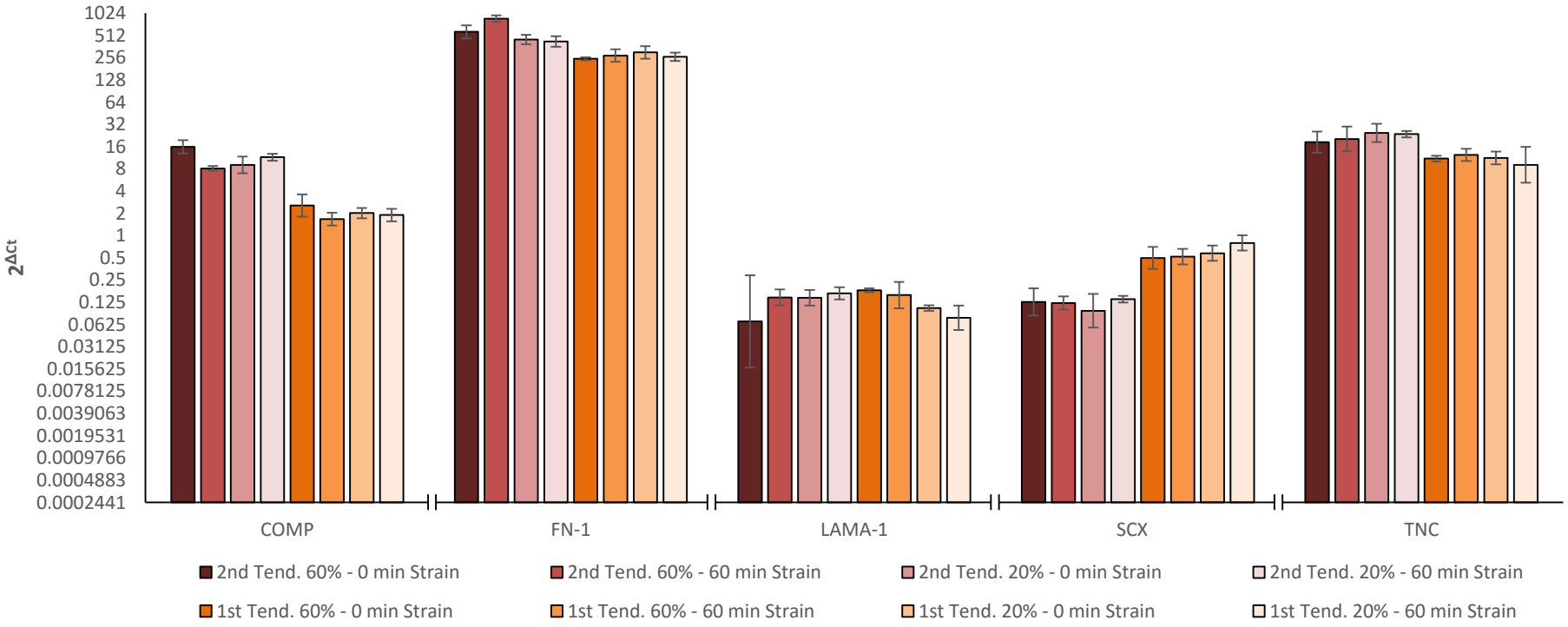

Figure 101: Average other protein gene expression for strained composites with tendinopathic tenocytes. Expression shown as $2^{\Delta Ct}$ (normalised to TOP-1) and both shown separately. Error bars represent standard deviations. Data labelled as 'XX. YY – ZZ strain', where XX is either '1st Tend.' Or '2nd Tend.' representing the donor, 'YY' indicates the fibre type and 'ZZ' indicates the soak time. n=6 per composite type.

Other Proteins – Healthy Tenocytes

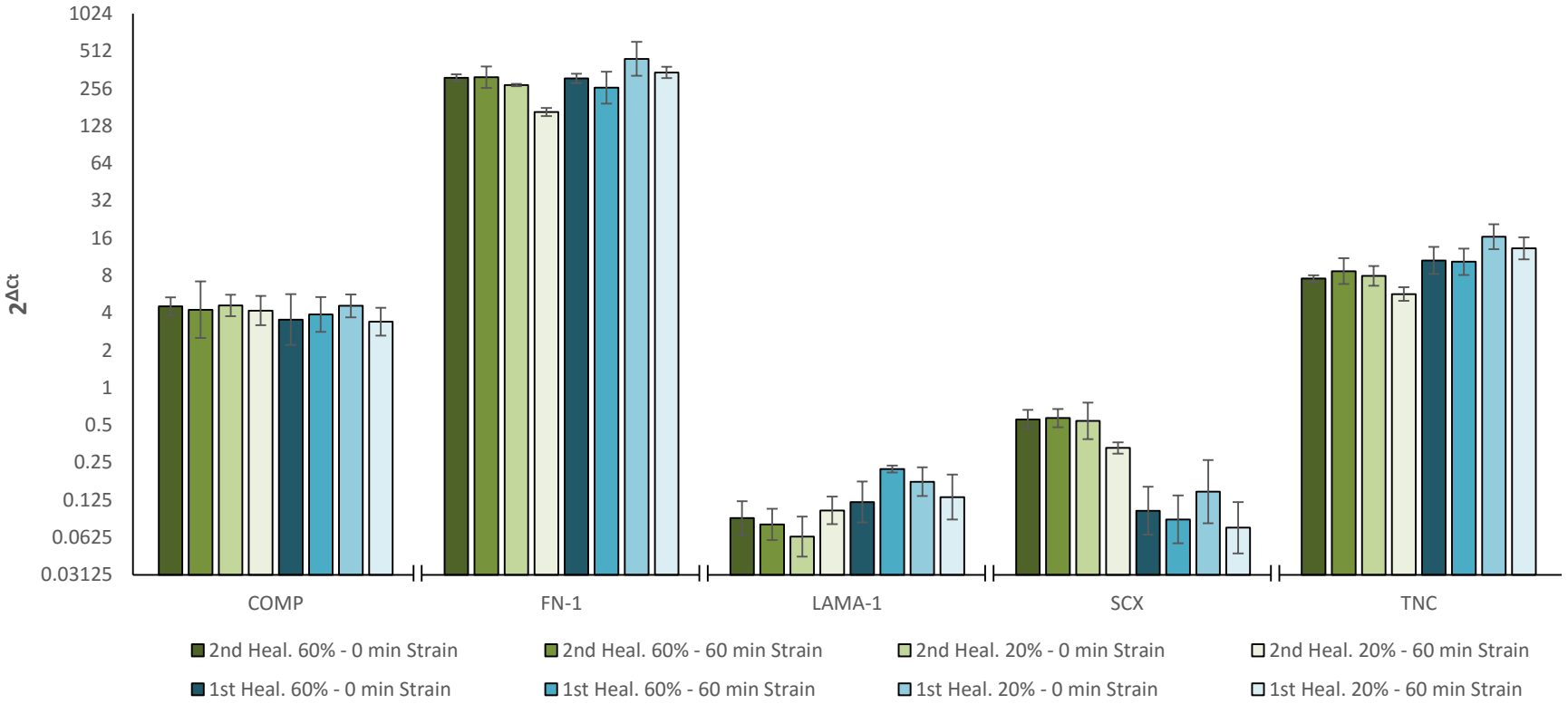

Figure 102: Average other proteins gene expression for strained composites with healthy tenocytes. Expression shown as $2^{\Delta Ct}$ (normalised to TOP-1) and both shown separately. Error bars represent standard deviations. Data labelled as 'XX. YY – ZZ strain', where XX is either '1st Heal.' Or '2nd Heal.' representing the donor, 'YY' indicates the fibre type and 'ZZ' indicates the soak time. n=6 per composite type.

Appendix D: Publications and Presentations

Papers in Draft:

- Tenocyte response to fibre composite micromechanics: Shear and tension ratios. D. Patel, S. Sharma, S.J. Bryant, and H.R.C. Screen.
- Matrix related gene expression profile of healthy and tendinopathic human tenocytes in response to shear and tension ratios. D. Patel, E. Jones, G. Riley, and H.R.C. Screen.
- Cell attachment peptides: critical factors affecting tenocyte sensitivity to shear-tension ratios. D. Patel, S. Sharma, S.J. Bryant, and H.R.C. Screen.

Abstract Publications:

- Human Tenocyte Metabolism Under Pathological And Physiological Loading Conditions. D. Patel, S.J. Bryant, G. Riley, E. Jones, and H.R.C. Screen. (2014) *British Journal of Sports Medicine 09; 48(Suppl_2)*:A51-A51.

Podium Presentations:

- Shear-Tension Ratio Effect On Healthy And Tendinopathic Human Tenocyte Metabolism. *International Symposium on Ligaments & Tendons (ISL&T) 2015, Las Vegas, USA.*
- Healthy and Tendinopathic Human Tenocyte Metabolism. *Arthritis Research UK (ARUK) Annual Fellows Meeting 2015, Loughborough, UK*
- Mechanotransduction mechanics in physiological and pathological Human tendon cells. *Oliver Bird – Arthritis Research UK PhD Conference 2014, London, UK.*

Posters Presentations:

- Mechanotransduction mechanics in physiological and pathological Human tendon cells. *Oliver Bird – Arthritis Research UK PhD Conference 2014, London, UK.*
- A Means to Investigate Human Tenocyte Metabolism Under Physiological and Pathological Loading Conditions. *Arthritis Research UK (ARUK) Annual Fellows Meeting 2013, Loughborough, UK.*
- Human tenocyte metabolism under pathological and physiological loading conditions. *International Scientific Tendinopathy Symposium (ISTS) 2014, Oxford, UK.*